Master Thesis, Department of Geosciences

Compaction and Evolution of Rock Properties and Rock Physics Diagnostics of Albatross Discovery, SW Barents Sea

Arif Naushad Butt

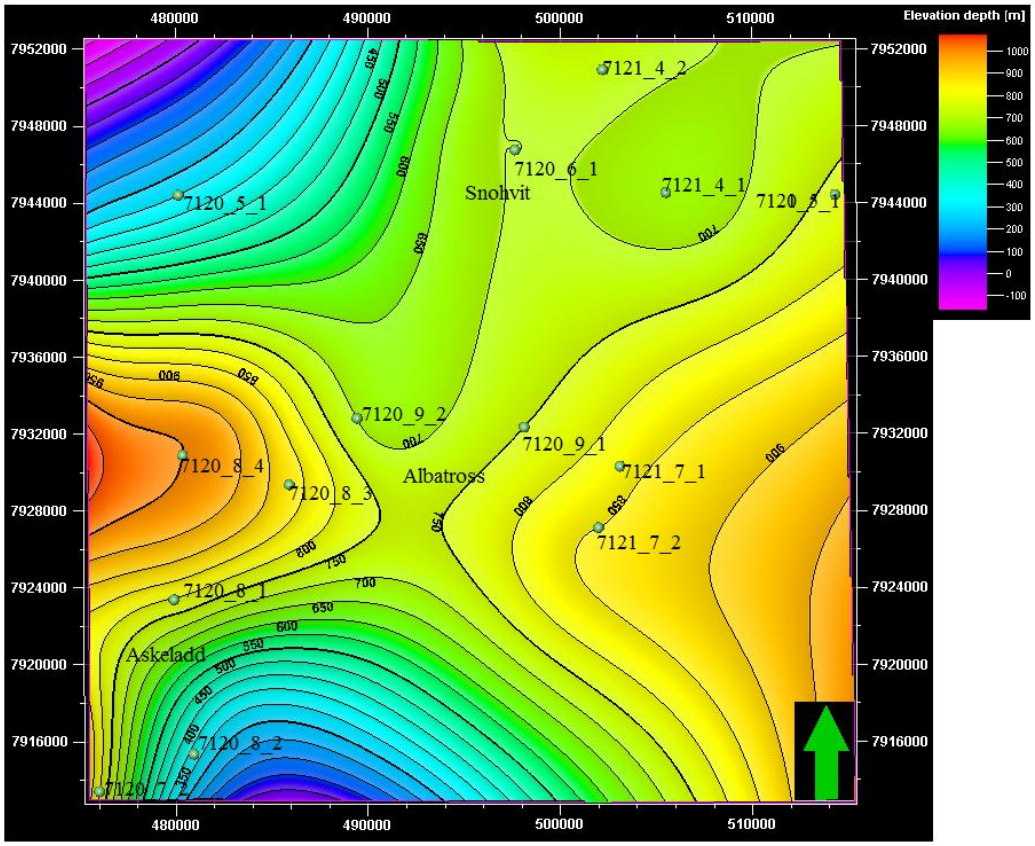

UNIVERSITY OF OSLO

FACULTY OF MATHEMATICS AND NATURAL SCIENCES

Compaction and Evolution of Rock Properties and Rock Physics Diagnostics of Albatross Discovery, SW Barents Sea

Arif Naushad Butt

Master Thesis in Geosciences

Discipline: Geology

Department of Geosciences

Faculty of Mathematics and Natural Sciences

University of Oslo

03.12.2012

Tutor: **Nazmul Haque Mondol (UiO)**

This work is published digitally through DUO – Digitale Utgivelser ved UiO

http://www.duo.uio.no

It is also catalogued in BIBSYS (http://www.bibsys.no/english)

PREFACE

This thesis is part of the ‘‘BarRock’’ (Barents Sea Rock Properties) project and is submitted to the Department of Geosciences, University of Oslo (UiO), in candidacy of the M.Sc. Degree in Geology.

This research has been performed at the Department of Geosciences, University of Oslo, during the period of January 2012- Novermber 2012 under the supervision of Nazmul Haque Mondol, Associate Professor, Department of Geosciences, University of Oslo, Oslo, Norway.

DEDICATION

To my nieces
Sahar and Maham
&
Family

ACKNOWLEDGEMENTS

It would have been impossible to write this thesis without my supervisor, Nazmul Haque Mondol, an associate professor, whose continuous help, encouragement and supervision from the scratch, has enabled me to acquire and develop new analytical techniques.

I am equally thankful to Michael Heeremans and IT staff, Department of Geosciences for their technical support and assistance in various ways during my research work whereas I am obliged to the academic and administrative members of the Department of Geosciences for their cooperation during this research work.

Special thanks are to the people, who are working on the BarRock project, especially; Mohammad Koochak Zadeh, Mohsin Kalani, Sirikarn Narongsirikul and Oluwakemi Yetunde Ogebule, for their constructive guideline in achieving this goal.

Moreover, I am indebted to my study group mates, Danial Farvardini, Jamilur Rahman Mohsin Fardi and Muhammad Jamil who remained a consistent source of motivation for me. Their team spirit, qualitative discussion and the social life will never be overlooked.

My family, whose prayers and continuous support throughout this period, has always strengthened my devotion into the work and brought me to this level.

Lastly, I pay my heartfelt thanks to my course mates, who make up a significant diversity from different continents to enable me to develop alternative models of thinking and an open-minded culture.

A.Butt

ABSTRACT

The Albatross discovery is located approximately 140 km northwest of Hammerfest (city of midnight sun), Norway in the central part of Hammerfest Basin, SW Barents Sea. The Albatross discovery included within Snøhvit field development project (the first gas development project in the Barents Sea) with two other discoveries, Snøhvit and Askeladd, in the area. The reservoirs contain gas and condensate in the Lower and Middle Jurassic sandstones of the Stø Formation. The study focuses compaction and rock perperties evolution of the whole sedimentary package penetrated by six exploration wells and to investigate physical and acoustic behavior of the reservoir sandstones applying rock physics diagnostics tool. In addition, an uplift estimation of the greater Snøhvit area (Snøhvit, Askeladd and Albatross) has also been performed.

An integrated approach using well log data, published compaction trends and rock physics diagnostics methodology has been utilized in order to understand the evolution of rock properties with increasing burial and to investigate physical and acoustic behavior of reservoir sandstones of the Stø Formation. Bottom hole temperature has been used to infer the transition zone temperature from mechanical to chemical compaction. On the basis of transition from mechanical to chemical compaction, an estimation of eshumation is investigated. The sandstones of Nordmela, Tubåen and Fruholmen Formations, other possible reservoir rocks in the area, have also been investigated by rock physics diagnostics techniques.

Results from this study clearly show that due to the combine effect of mechanical and chemical compaction, the rock properties such as velocity, density and porosity altered significantly as a function of depth. On the basis of abrupt velocity increase within a narrow depth interval the transition from mechanical to chemical compaction has established. The transition from mechanical to chemical compaction occurred within the Knurr Formation at varying depth and temperature depending upon geothermal gradient and structural configuration. The abrupt velocity change reflects stiffening of grain framework due to quartz cementation. The quartz cementation increases with depth as long as the surface area is available for precipitation of quartz and temperature is higher than 70ºC. The detail investigation suggested that the present day transition zone temperature is far bellow the temperature usually for the transition zone from mechanical to chemical compaction reflecting the study area as an exhumed basin. It can be stated that the transition zone temperature, before exhumation, was sufficient enough to initiate the chemical compaction.

When observed Vp versus depth trends of all wells have been compared with published compaction trends, there was a clear mismatch observed. On the basis of difference between compaction published trends for normally compacted basin and trends observed in studied wells a rough exhumation was estimated. The exhumation estimates differ for Snøhvit, Albatross and Askeladd discoveries depending upon the structural configuration. The exhumation of Snøhvit field is in between 300 to 800 m increasing from west to east whereas in the Albatross discovery it increases in opposite direction ranging from 700 to 1000 m. In the Askeladd discovery it ranges from 300 to 1000 m and decreasing from south to north. This exhumation estimation is in accordance with the published literature

The reservoir quality of Stø sandstones, investigated by rock physics diagnostics, decrease from eastern wells to western wells with different depth levels. This change in the quality of sandstones is due to the lithological variations within the Stø Formation. The depositional history suggested that the eastern wells are close to the shoreline (proximal zone) than the western wells (distal zone), controlling the deposition of coarser and well sorted sediments causing decrease in velocity. Hence, the impact of compaction (mechanical and chemical compaction) of Stø sandstones is lower in the east compared to west. Due to different deposition history resulted the grain sorting and variable geothermal gradient, the composition may different that also reflects different degree of cementation and, hence, different rock physical properties. Over-consolidation of reservoir rocks due to quartz cementation resulted in high impedance sandstones difficult to discriminate the effect of pore fluids.

The study demonstrates that the complex burial history of Hammerfest basin uplift, erosion and renewed burial during Cenozoic time has influenced the distribution of hydrocarbons in the reservoirs and the position of fluids contacts. Exhumation suggested in this study can be used to calibrate the porosity/density/velocity versus depth relationships used in reservoir characterization work flows and also in assessing the degree of tertiary migration from traps due to exsolution of gas.

NOMENCLATURE

AI: Acoustic Impedance

AVO: Amplitude versus Offset

BHT: Bottom Hole Temperature

BSF: Below Sea Floor

CC: Chemical Compaction

EI: Elastic Impedance

FRM: Fluid Replacement Modeling

HC: Hydrocarbon

HR: Hampson Russell

I_{GR}: Gamma Ray Index

IP: Interactive Petrophysics

K: Bulk Modulus

MC: Mechanical Compaction

MD: Measured Depth

N/G: Net to Gross Ratio

PR: Poisson's Ratio

RKB: Relative to Kelly Bushing

RPT: Rock Physics Template

R_2: Correlation Coefficient

SI: Shear Impedance

S_w: Water Saturation

TVD: Total Vertical Depth

Vp: P-Wave Velocity

V_{sh}: Volume of Shale

Vs: S-Wave Velocity

μ: Shear Modulus

Table of Contents

LIST OF FIGURES

LIST OF TABLE

CHAPTER 1
Introduction

1.1 Background and motivation

Globally, the demand of hydrocarbon is increasing with the passage of time but, on the other hand, the hydrocarbon discoveries are continuously decreasing. The potential to find commercial hydrocarbon reserves may there in many world hydrocarbon provinces but there is a need to extract or locate them more efficiently with modern techniques, infused with the integration of different disciplines.

Nowadays, the focus of Barents Sea in terms of hydrocarbon potentiality has been the subject of increased scientific and economic interest. Geologically, young passive continental margins in the north and west bound the large epicontinental sea of the greater Barents Sea. Svalbard archipelago and Franz Josef Land lie in the north. Novaya Zemlya makes the eastern boundary of the Barents Sea which extends south to the Kola Peninsula and Norwegian coast (Fig. 1.1).

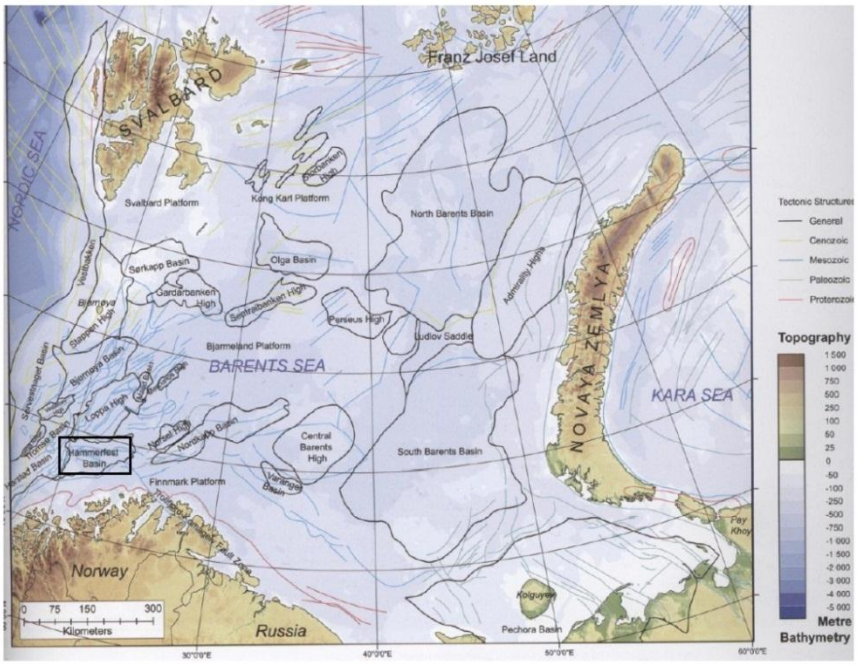

Figure 1.1: Map of the greater Barents Sea showing the main structural elements. The study area is highlighted with black rectangle (Modified from Smelror et al., 2009).

Although, there is success to find hydrocarbon in the Norwegian Barents Sea region yet three main episodes of uplift, roughly 60 Ma (Paleocene), 33 Ma (Oligocene) and 5 Ma (Pliocene-Pleistocene), have made the site more difficult to find commercial accumulation. Dore and Jensen (1996) discussed in detail the causes of uplift and failure to find commercial petroleum accumulation can be listed briefly as following:

- The release of pressure due to uplift and erosion resulted in the two phases oil accumulations, which, with the release of further pressure, causes the gas expansion that, forced the oil below spill points.
- The spillage from hydrocarbon accumulation due to the tilting governed by differential uplift and may cause failure the seals.
- Lower reservoir quality than expected because of buried deeper than the present day burial.
- Due to the uplift and decrease in temperature, the cooling of the source rock ceased the hydrocarbon generation.

To understand the backup processes causing vertical movement, subsidence and uplift, the region has caught attention of the world. A vast amount of seismic acquisition has been carried out in this area with respect to petroleum exploration. Extensive knowledge of the opened and unopened areas already exist in the Barents Sea region, we need to focus on how to bridge up the gap of the findings between these two areas. Approximately, until now, 96 exploration wells (18 Appraisal, 78 Wildcat) have been drilled and 25 discoveries have been made in which most of them are in or around the Hammerfest basin (Fig. 1.2). The remaining wells are spread across the shelf and have tested several plays.

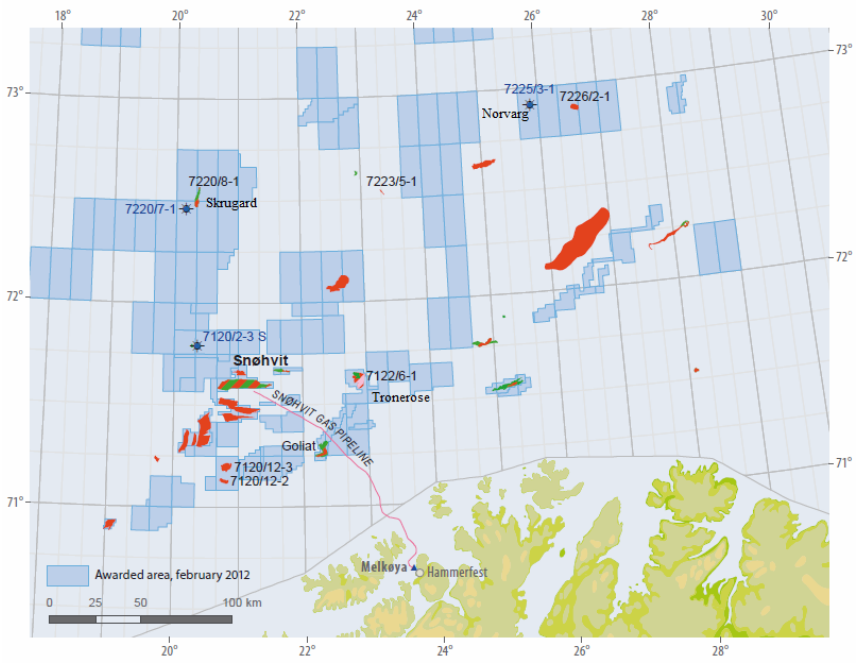

Figure 1.2: Number of fields and discoveries in the Barents Sea (Source: NPD).

According to Ohm et al. (2008), roughly one in three wells has been successful in the Norwegian Barents Sea. Multiple source rock intervals at different stratigraphic levels from the Carboniferous to the Cretaceous make the Barents Sea more attractive. As compared to the North Sea, there is one major source rock (Kimmeridge shale) that equivalent to the Hekkingen Formation in the Barents Sea region. Formerly, the most common play models involved mainly gas prospects, such as, Snøhvit in the Barents Sea region. After the drilling campaigns in the 1980s, the Norwegian Barents Sea area has been considered as a gas prone. The Snøhvit gas field was discovered in 1984, started development in 2005 being the first development project in the Barents Sea and was the stepping stone for the exploration

activities in the Arctic. The discoveries of Skrugard and Havis in 2011-2012 proved this area as oil prone, providing a gate way for future exploration activities in the Barents Sea Region.

1.2 Research objectives

The study investigates compaction and evolution of rock properties of different sedimentary packages in the Albatross discovery penetrated by six exploration wells. It also focuses qualitative and quantitative study of lithologies and fluid properties of several reservoir rocks present in the uplifted Hammerfest basin. The overall objectives of this research can be highlighted as follow:

- To analyze the compaction (mechanical and chemical) and evolution of rock properties of the thick sedimentary packages in the Albatross discovery by using available well log data.
- To investigate general compaction trends of sands and shales.
- To identify the transition from mechanical to chemical compaction and its effects on dynamic rock properties.
- To give a rough estimates of Cenozoic exhumation of the Snøhvit development.
- To apply several rock physics diagnostics methods to examine porosity, saturation, shale volume (net-to-gross), cementation, and pore fluid discrimination of four reservoir rocks (Stø, Nordmela, Tubåen and Fruholmen Formations) in the Albatross discovery. The special emphasis is given to Stø Formation, the main reservoir in the area.

1.3 Study area

Albatross, one of the discoveries along with Snøhvit and Askeladd within the Snøhvit development, is located in the central part of the Hammerfest basin, SW Barents Sea. It is situated about 140 km NW of the city Hammerfest, at a water depth of 310-340 m (Fig. 1.2). The Hammerfest basin is an elongated east-northeast striking graben and about 150 km long and 70 km wide (Fig. 1.3). Towards south it is bounded by Troms-Finnmark fault complex (TFFC). The Asterias Fault Complex (AFC) separates this basin from the Loppa High to the north. Its western border towards the Tromsø Basin is delineated by southern-most part of the Rignvassoy-Loppa Fault Complex (RLFC), while towards east it forms a flexure against the Bjarmeland Platform.

Albatross was discovered by the exploration well 7120/9-1 in 1982. Albatross discovery has two parts Albatross and Albatross Sør. The study area contains four wells, which are 7120/9-1, 7120/9-2, 7121/7-1 and 7121/7-2.Two more exploration wells 7120/8-3 and 7120/8-4 (Fig. 1.3), which are the part of Askeladd gas field (Askeladd Nord), have been included in this research to get better overview in and around the study area. The well 7120/8-3 contains traces of hydrocarbon (NPD Fact pages) whereas the well 7120/8-4 is dry. The three other wells 7120/9-1, 7120/9-2 and 7121/7-2 contain gas whereas the well 7121/7-1 contains both gas and condensate (Source: NPD Fact pages).

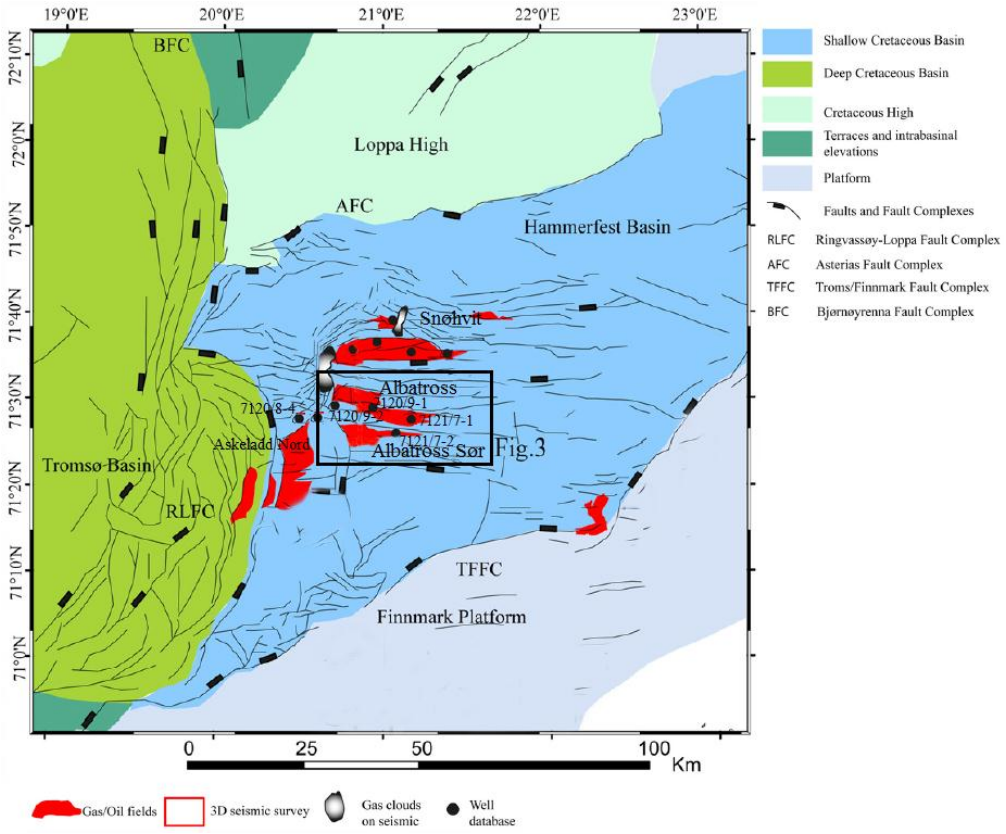

Figure 1.3: Structural elements of the Hammerfest basin (Modified from Ostanin et al., 2012). The Albatross discovery is highlighted with a rectangle within which location of the studied wells are shown.

The Snøhvit development was split into four phases. First phase of development include remotely operated subsea development, 143 km multiphase pipeline to shore and an LNG liquefaction plant at Melkoya (Fig. 1.2). After the Snøhvit gas is cooled and converted into LNG, it is transported to markets in the US and Europe. Snøhvit will be developed by a total of 21 wells. In the first phase of development, 10 wells have been drilled, nine production wells and one CO2 injection well of which six production wells and one CO2 injection well are in the Snøhvit and the three production wells in the Albatross discovery. The production wells were drilled on Albatross in 2005-06 and Gas production in the Snøhvit and Albatross Discovery has started in 2007. The first CO2 was injected into the reservoir in April 2008. The other three phases of development on Snøhvit, include another 10 wells on the fields as well as related flow line and umbilicals, will be completed until 2032 (Source: Statoil).

1.4 Database and methodology

A total 15 exploration wells from the Snøhvit development have been used in this study (Table 1.1). Most of these wells are wildcat (W) and appraisal (A). The well 7120/8-4 is dry and the well 7120/8-3 shows trace of gas. The remaining four wells 7120/9-1, 7120/9-2, 7121/7-1 and 7121/7-2 from the Albatross area contain hydrocarbon (mostly gas). The deepest well in the Albatross discovery is 7120/9-2 with the total depth of 5072 m (RKB) and Røye Formation of Permian age is the deepest penetrated formation. The status of all the wells used in this research has been given in the Table 1.1.

Table 1.1: Number of wells used and its purpose along with entry and completion date (Source: NPD Factpages).

Fields	Wells	Entry date	Completion date	Temp. gradient (^{0}C/km)	BHT (^{0}C)	Purpose	Content
Askeladd	7120/7-2	26.05.1983	21.08.1983	35.7	97	W	Gas/Condensate
	7120/8-1	28.06.1981	10.09.1981	34.86	95	W	Gas/Condensate
	7120/8-2	15.04.1982	29.07.1982	33.59	91	W/A	Gas
Albartoss	7120/8-3	07.04.1983	24.05.1983	23.12	58	A	Gas
	7120/8-4	14.11.2007	10.12.2007	34.85	98	W	Shows
	7120/9-1	25.07.1982	26.09.1982	30	73	W	Gas
	7120/9-2	18.04.1984	20.10.1984	30.95	161	W/A	Gas/Condensate
	7121/7-1	11.06.1984	05.08.1984	31.48	72	W/A	Gas
	7121/7-2	07.07.1986	12.08.1986	32.46	74	W	Dry
Snøhvit	7120/5-1	17.04.1985	06.06.1985	23	66	W	Shows
	7120/6-1	02.02.1985	02.05.1985	35.46	102	W/A	Oil/Gas
	7120/6-2S	14.06.2007	22.07.2007	35.25	111	A	Oil/Gas
	7121/4-1	06.08.1984	27.10.1984	32	88	W	Oil/Gas
	7121/4-2	29.01.1985	14.04.1985	32.5	95	W	Gas/Condensate
	7121/5-1	07.06.1985	28.09.1985	34.68	115	W/A	Oil/Gas

The 9 wells from Askeladd and Snøhvit discoveries have been taken into account in order to analyze the exhumation of the area (Snøhvit, Albatross and Askeladd) as a whole. The well data from both the fields (Askeladd & Snøhvit) has been considered only for comparison purpose. For that purpose, the Askeladd and Snøhvit well data has been taken from two previous master theses (Fardi, 2012 and Rahman, 2012).

For the interpretation and analysis of the well data, different softwares have been used like Petrel, Hampson Russell (HR), Interactive Petrophysics (IP) and Microsoft Excel. For compaction and evolution of rock properties analysis to carry out, IP and Excel have been used. For well correlation and interpretation as well as for depth/temperature contour mapping of the transition zone (TZ), help has been taken from Petrel 2011 by Schlumberger. Two of the rock physics cement models; (a) contact cement model and (b) constant cement model have been digitized using plot digitizer. Fluid substitution modeling (FRM) has been done in elog which is one of the Hampson Russell packages.

In addition to well logs data, published compaction trends have been used for compaction study.

1.5 Chapter descriptions

This study has been divided into six different chapters on the basis of thesis title in which chapter 1 is the general introduction of the study area along with the motivation, research objective and limitations. The overview of the Albatross discovery, SW Barents Sea is also covered in the chapter 1.

Chapter 2 considers the regional tectonic and geological evolution incorporating structural elements of the Barents Sea with special emphasis on source, reservoir and cap rocks with respect to stratigraphy of the Hammerfest basin. Stratigraphic correlation of the source, reservoir rocks of different geological age and the reservoir geometry of the Hammerfest basin have also been included in the second chapter.

Research methodology together with theoretical background is explained in chapter 3. The different dataset and the methodologies, which are used during this research work for the analysis of the different reservoir and the source rocks, are explained in details in this chapter. Similarly, the theoretical background of compaction and rock physics are explained briefly under the chapter 3.

Chapter 4 accentuate on compaction, rock properties evoluation and exhumation estimation in the study area. Important results regarding different rock parameters like velocity, porosity, density, gamma ray etc. exhumation and compaction trends (mechanical to chemical), the effects of pore fluid, pore pressure discussed in detail in the chapter. The results of correlation of source and reservoir rocks are also included in this chapter.

The outcomes related to rock physics diagnostics of the reservoir rocks are explained in detail in the chapter 5. A summary of the present research along with concluding remarks have been given in the last chapter 6.

1.6 Limitations and future works

Being time limited research, mineralogical analysis of reservoir, source and cap rocks has not been included. Thin section has not been utilized in this study either. As we know provenance and depositional environments effect the distribution of mineralogical composition and textural properties (e.g. grain size and sorting) of reservoir and source rocks. Hence, unavailability of thin section was a great limitation.

The shear velocity is of high importance for rock physics diagnostic. Most of the wells do not have Vs measurements. One (7120/8-4), out of six wells in the Albatross discovery, contains shear wave log. Due to that reason, empirical relations given by various authors have been used for other wells for rock physics analysis. These empirical relations may not be described exact behavior of the rocks where actual shear wave log can do.

Rock physics dignostics routinely done with the help of effective porosity and this porosity get directly from neutron and calculated from density and sonic logs is not quite certain because of over and under-estimation of matrix density (density of solid grains). The average

porosities have been calculated from neutron and density porosity logs but these may also not give us the accurate effective porosity.

The rock physics templates (RPT's) have successfully been used for unconsolidated sand reservoirs but there is no such standard rock physics templates for cemented rocks. Rock properties change due to uplift add further uncertanities to perform rock physics diagnostics of over-consolidated reservoirs rocks in the Hammerfest Basin.
Because of time limitation, AVO modeling or analysis have not been performed. Someone can extend this work by utilizing output to incorporate AVO analysis on different reservoir rock units.

CHAPTER 2

Geology of the Albatross Area

Due to different stages of tectonic uplift, which has influenced the petroleum system of the area, the geological history of Barents Sea is more complex as compared to North Sea. Although the Norwegian Barents Sea with multiple source rock intervals represents the important example of overfilled petroleum system but exhumation has caused the depletion of the hydrocarbon accumulation of the region. There is a need to understand the geological framework of an area providing qualitative and quantitative characteristics of the source, reservoir and cap rocks which help to evaluate the hydrocarbon prospects of the region.

2.1 Regional tectonic and geological evolution

The Barents Sea is fragmented into two main geological provinces i.e. eastern and western province with different tectonic history. The eastern province was influenced by late Paleozoic tectonism and the mineral deformation has been occurred in the Post Jurassic times while Mesozoic and Cenozoic tectonic activity affected the western province (Gabrielsen et al., 1990) (Fig. 2.1). The geological evolution has been stated in Early Palaeozoic time due to which the Barents Sea and the area around it, have suffered four stages of evolution (Fig. 2.1).

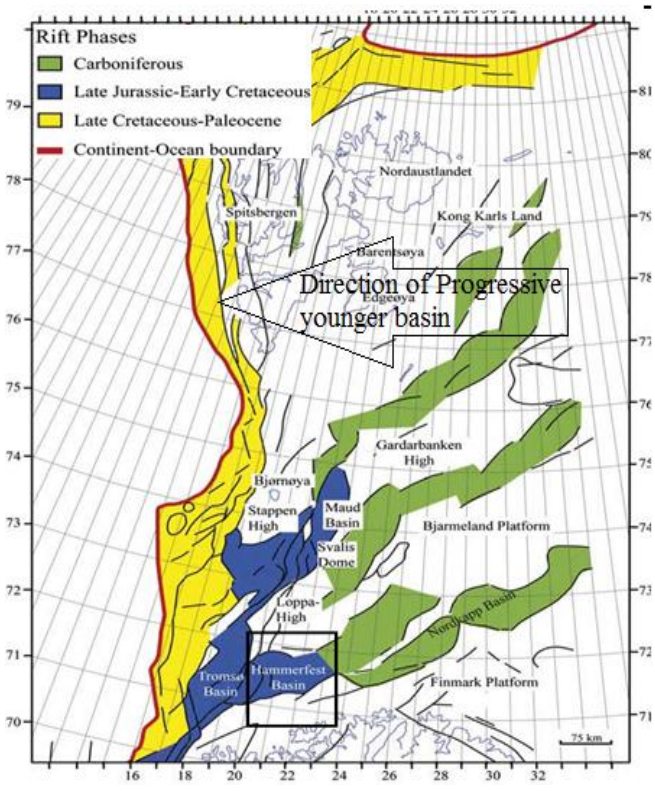

Figure 2.1: Main structural elements in the Barents Sea (Gabrielsen et al., 1990; Gudlaugsson et al., 1998; Faleide et al., 2008). Different colors are showing the focus of tectonic activity through time. Study area is shown by black rectangle (Modified from Glorstad-Clark et al., 2010).

The Early Paleozoic Caledonian Orogeny which was the result of the closure of the Iapetus Ocean and the suturing of Greenland to Norway and Spitsbergen formed the metamorphic basement of the Barents Sea (Fig. 2.2a) (Dengo and Rossland 1992). The trend of the Caledonian structures in Northern Norway is north-east (Dengo and Rossland 1992; Sturt et al., 1978; Townsend, 1987), which is quite similar with the trend of many of the younger extensional basins which give a clue that Caledonian structures control the geometric configuration of north-east and north-west trending basin bounding normal faults (Dengo and Rossland 1992). The Post Caledonain geological history of the Barents Sea is controlled mainly by three rifts episodes (Fig. 2.1) documented by several authors, which are as follow:

- Late Devonian Early Carboniferous
- Middle Jurassic- Early Cretaceous and
- Tertiary rift phase

The oldest tectonic event in the western Barents Sea that can be mapped regionally occurred in Late Devonian-Early Carboniferous as the initial rifting between Norway and Greenland started (Fig. 2.2). This event created a fundamental basement shape of the half-grabens and intervening highs that effected the location of younger basin and hydrocarbon traps, the depositional environment of source, reservoir and cap rocks and timing of hydrocarbon maturation and migration (Dengo and Rossland 1992; Gabrielsen et al., 1990; Lippard and Roberts, 1987; Breivik et al., 1995). During this stage the Tromsø, Bjørnøya, Nordkapp, Fingerdjupet, Maudand Ottar basins have been formed. Along with these, Hammerfest basin was also started to form (Dengo and Røssland, 1992; Breivik et al., 1995; Gudlaugsson et al., 1998).

There was quiet tectonic period, during middle Carboniferous to lower Permian, but some of the basement involved normal faults were reactivated which were the results of Uralian Orogeny and loading by westward prograding clastic sediments (Dengo and Rossland 1992; Roberts and Sturt, 1980). Because of the uplift in the south and east, the late Permain sediments were deposited on the shelf sequence and the depocenters at the time of Permian were in the north eastern and south western part of the present Hammerfest basin (Berglund et al., 1986).

During the Late Permian-Early Triassic, closure of Uralian Sea took place and Barents shelf assumed the form of distal foreland basin to Uralian Mountain receiving bulk of sediment influx which caused the reactivation of certain basement involved normal faults (Dengo and Rossland, 1992). In the early to middle Triassic the subsidence rate was higher in the eastern part, compared to west side (Faleide et al., 1984). The westerly prograding sequences were coarser and proximal into the eastern part of the Hammerfest basin probably related to Uralian Orogeny far to the east (Berglund et al., 1986). The middle and upper Triassic interval is composed of repetition of upward coarsening clastic sequences, indicating cyclic changes from open marine to continental deposits giving rise to mixed lithologies of clay stones, siltstones, sandstones and shales with thin lenses of coal (Berglund et al., 1986). A regional unconformity was formed at the end of middle Triassic because of the relative uplift in the eastern side shifting the area of maximum sedimentation to the west (Faleide et al., 1984). The alternating sequences of continental shaley sediments and shallow marine sandy sediments during late Triassic to middle Jurassic were controlled by complex interaction of

tectonic subsidence, eustatic sea level changes and local sediments supply (Berglund et al., 1986).

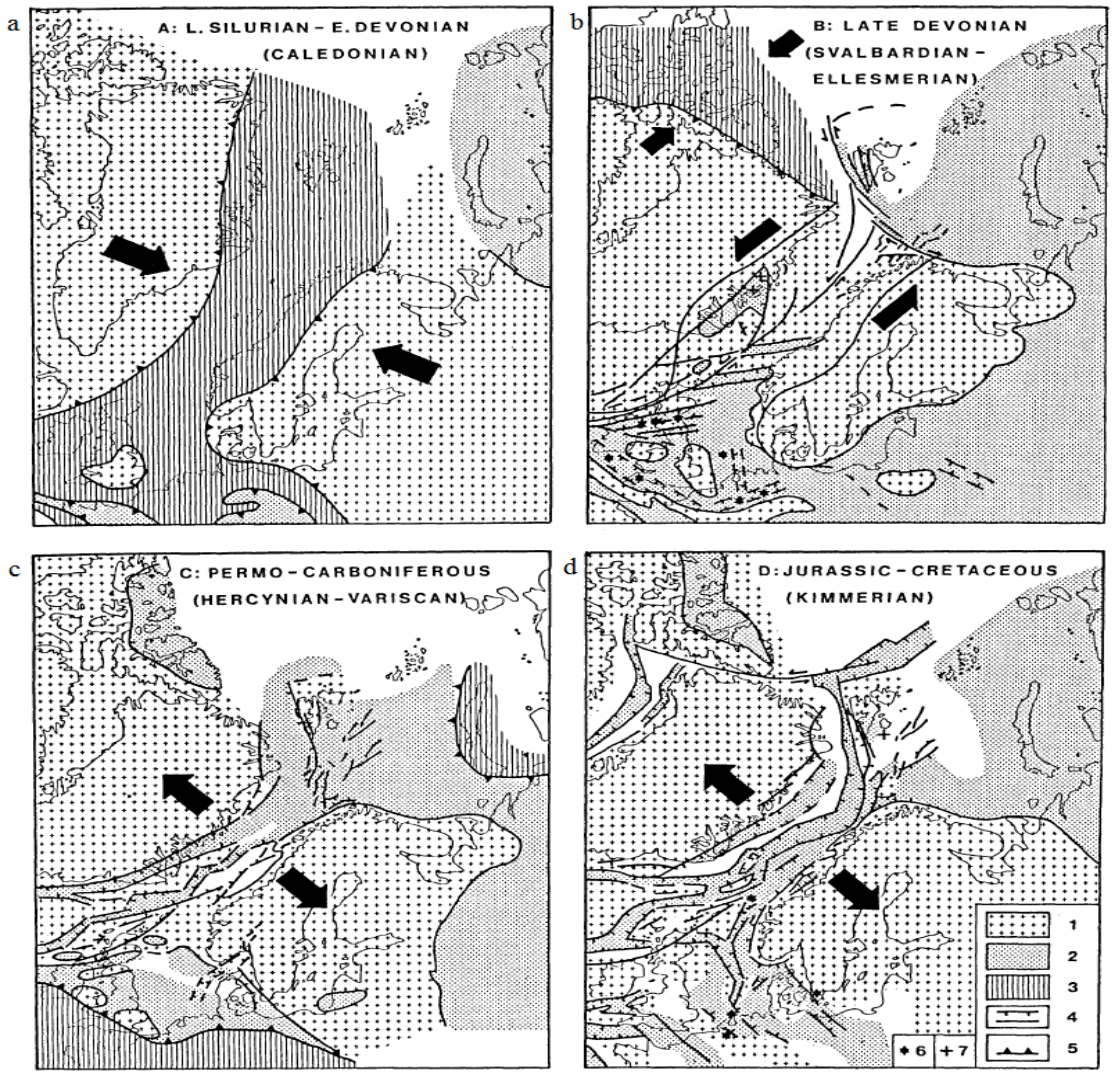

Figure 2.2: Main stages in the evolution of western Barents Sea and surrounding area. (Modified from Faleide et al., 1984). 1, stable elements – continental cratons and intrabasinal highs; 2, sedimentary basins; 3, active foldbelts; 4, normal and wrench fautls; 5, deformation front of active foldbelts; 6, intrusions; 7, volcanics.

The general relative rise in sea level caused the deposition of the Stø formation in the middle Jurassic, the main reservoir rocks in the SW Barents Sea region (Berglund et al., 1986). The lower and middle Jurassic sequences have been deposited before the onset of tectonic movements that lead to the formation of Hammerfest basin indicating pre-rift sediments (Berglund et al., 1986). During the late Jurassic, a relatively thin transgressive layer was syn-tectonically deposited within these rift basins and because of stagnant and reducing conditions, these upper Jurassic clays (Fuglen and Hekkingen Formations) are rich in organic matter, which makes it an excellent source rocks in the Barents Sea region.

During Teriary, the tectonic activity is related to the opening of North Atlantic and Arctic Oceans in Late Paleocene time while in Early to Mid-Miocene times the spreading ridges

were established names as Knipovich and Mohns Ridges (Dengo and Rossland, 1992). Along the pre-existing zone of weakness, west of Loppa High and Senja Ridge most of the deformation occurred whereas stable conditions exists towards east of Loppa High (Dengo and Rossland, 1992). In Eocene time, the western margin of the Barents Sea developed as a sheared margin, following the sea floor spreading with upto 550km of dextral strike-slip movement on the Hornsund Fault (Myhre et al., 1982; Dengo and Rossland, 1992). Norwegian Barents Sea experienced the main continental break-up in the middle of Cenozoic (Oligocene). Geological history of western Barents Sea ends up with an extensive uplift event in the Late Cenozoic and the subsequent erosion of approximately 3km of sediments in the some region (Nyland et al., 1992). From Mid-Miocene to present, the western Barents Sea is experiencing a regional uplift (Dengo and Rossland, 1992).

Rønnevik et al. (1975) identified the Hammerfest basin situated between 70º50′N, 20ºE, 71º15′N, 20ºE, 72º15′N, 23º15′E and 71º40′N, 24º10′E. The Hammerfest basin is located in southwestern part of the Barents Shelf. It is a composite sedimentary basin and its general shape is an elongated east-northeast striking graben, which is 150 km long and 70 km wide, formed during the second rift phase (Fig. 2.1) (Berglund et al., 1986). Towards south it is bounded by Troms-Finnmark fault complex (TFFC) and the Asterias Fault Complex (AFC) separates this basin from the Loppa High to the north. Its western border towards the Tromso Basin is delineated by southern-most part of the Rignvassoy-Loppa Fault Complex (RLFC), while towards east it forms a flexure against the Bjarmeland Platform (Ziegler et al., 1986, Gabrielsen & Farseth 1989; as cited in Gabrielsen et al., 1990). The Hammerfest basin is subdivided into western and eastern subbasins (Ziegler et al., 1986; Gabrielsen et al., 1990) which is separated by the extension of the Trollfjord-Komagelv fault trend (Gabrielsen and Farseth 1989). The western part dips westwards towards Tromsø Basin, with internal fault system comprised of E-W, ENE-WSW and WNW-ESE trending faults informally called the Hammerfest basin fault system by Gabrielsen (1984).

2.2 Structural elements

According to Faleide et al. (1993b), three main geological provinces separated by major fault zones have been recognized based on tectonic and sedimentary architecture (Fig. 2.1), which are as follow:

1- The oceanic Lofoten Basin, which formed during the Cenozoic opening of the Norwegian- Greenland Sea and the Vestbakken volcanic Province.
2- The south-western Barents Sea of late Cretaceous and Early Tertiary basins such as Harstad, Tromso, Bjornoya and Sorvestsnaget basin which are separated by intrabasinal highs such as Senja Ridge, Veslemoy High and Stappen High.
3- Mesozoic basins and highs between 20^0&25^0 East, which have not experienced pronounced Cretaceous/Tertiary subsidence, these include Finnmark Platform, Hammerfest basin, Loppa high, Fingerdjupet Subbasin (Faleide et al., 1993b).

The Hammerfest basin made up of both deep, high angle faults along the basin margins, listric normal faults existed centrally in the basin, and these faults are detached above the Permian sequence (Berglund et al., 1986; Gabrielsen et al., 1990). The eastern part of the basin is less affected by faulting characterizing sag basin (Gabrielsen et al., 1990). 6-7 km depth of the basement has been calculated in the Hammerfest basin (Roufosse, 1987, as cited in Gabrielsen

et al., 1990). The central part of the Hammerfest basin is occupied by Snøhvit field, which is late Kimmerian trough, an ENE trending graben feature in the eastern part of the Troms I area, flanked by platforms to the north and south (Stewart et al., 1995). Loppa High towards north, Tromsø basin to the west and Troms Finnmark platform to the south are the boundaries of Snøhvit field (Fig. 2.3). Seismic survays indicated that the Hammerfest basin had a thick sequence of the Mesozoic strata which to the west descended into the still deeper Tromsø Basin (Stewart et al., 1995 and the doming parallel to the basin axis that was active from the Middle Jurassic to early Barremian (Linjordet et al., 1992) affected it.

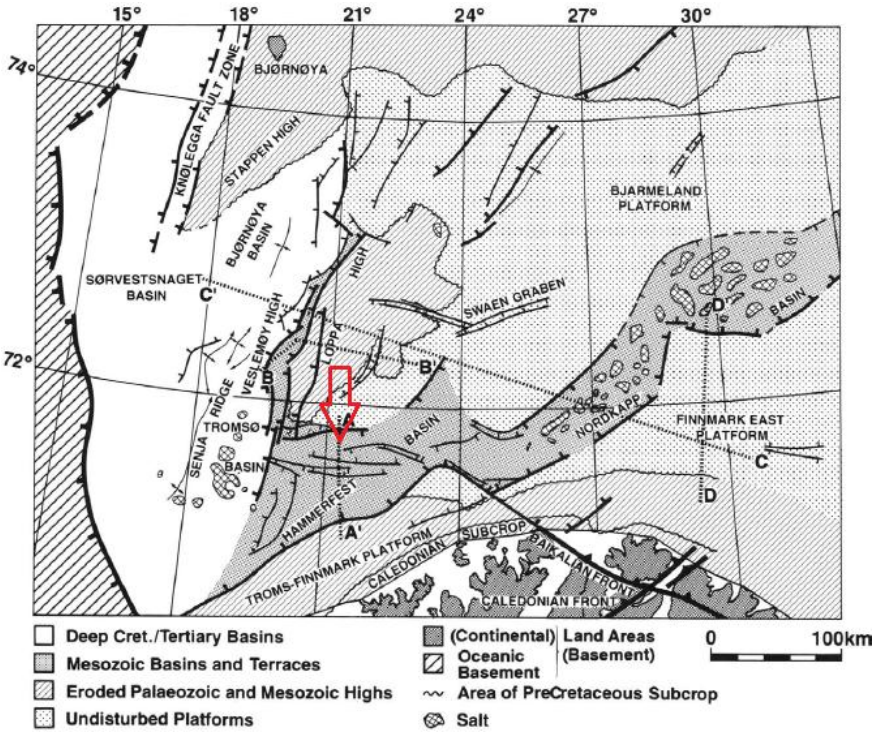

Figure 2.3: Structural elements of the Hammerfest basin. Location of Hammerfest basin is indicated by red arrow (Modified from Stewart et al., 1995).

Main structural framework with respect to the lower Cretaceous hydrocarbon discoveries and key wells are showin in the Figure 2.4a. The lower Cretaceous sandstone play along the margin of the Hammerfest basin is highlighted by the key wells south of Loppa High and North of the Troms-Finnmark Platform (Fig. 2.4b). The SW-NE trending Hammerfest basin between Loppa High and the Troms-Finnmark Platform is the most tectonic element (Seldal, 2005). These structural elements existed in the Early Permian based on the information from the drilled wells (Gabrielsen et al., 1984, 1990). Basinal salt structures are present have been drilled in the Tromsø and Nordkapp basins. In these half grabens thin salt layers and anhydrite may have been deposited in the Permian. Marginal Permian carbonates have been drilled on the Loppa High and on the Troms-Finnmark Platform on the horst structure in the Hammerfest basin. The main faults follow the northest-southwest Caledonian trend and formed along the old weakness zones which have been reactive through time (Seldal, 2005, Berglund et al., 1986). Tectonic activity was on its peak in the Jurassic as the result of Cimmerian movements. These movements sustained until Early Cretaceous and due to the sea level changes, caused the deposition of Lower Cretaceous sandstone reservoirs along the basin margin in the Hammerfest basin (Seldal, 2005).

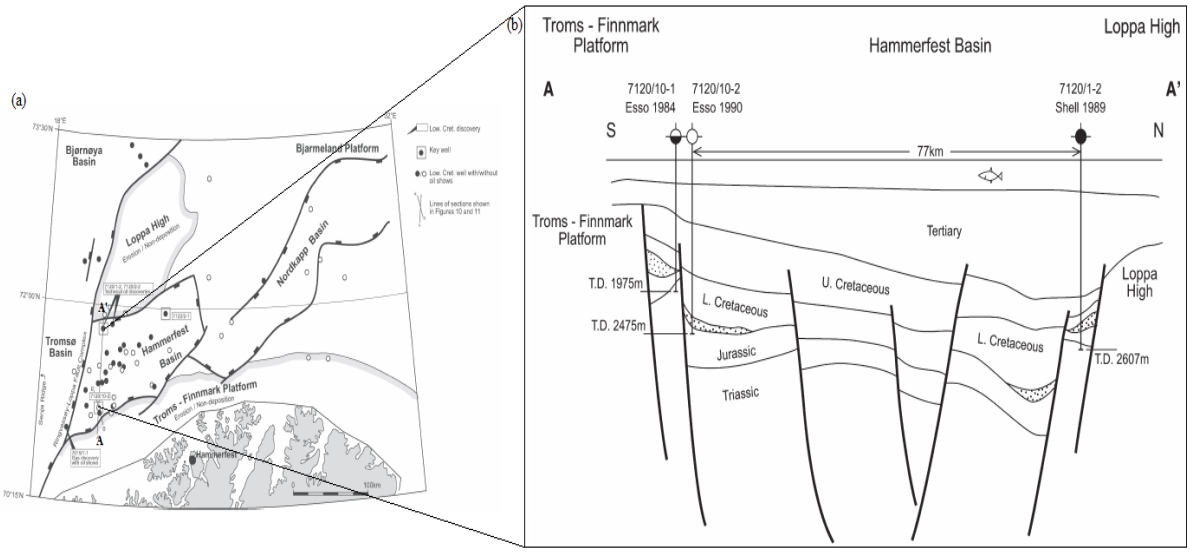

Figure 2.4: (a) Tectonic elements and Lower Cretaceous hydrocarbon discoveries (b) Lower Cretaceous sandstone play along the section. Red arrow is showing the study area (Modified from Seldal, 2005).

During Albian/Aptian times, Tromsø Basin experienced a major regional subsidence; this became the main depocentre through the Cretaceous and Tertiary. The area east of Hammerfest basin experienced severe erosion due to major regional uplift in the Late Tertiary which influences the reservoir and source rocks in the Snøhvit area (Faleide et al., 1996). The maximum depth experienced by these rocks was greater than the present day burial depth, which changes the source and reservoir rocks meaningfully. In the Miocene, maximum regional uplift with erosion and truncation was reached and this continued through the middle Pliocene before the Tromsø Basin again experienced the deposition and subsidence in the Late Pliocene. In the Late Pliocene/Pleistocene times a colder climate and the onset of glacial periods prevailed due to the lower of the temperature (Seldal, 2005).

The major subsidence of the basin occurred along the north and south margin (Fig. 2.5b). In the central part of the basin, the prevailing east-west trending fault system is the result of flexural extension related to the doming. The dip direction of these major faults is towards basin axis, where horsts and grabens formed along the crest of the dome. Because of the unique geometry of the Hammerfest basin, it can be classified into northern and southern provinces with respect to hydrocarbon generation and migration (Linjordet et al., 1992). The updoming of the central part of the basin formed a series of east-west oriented normal faults in the Hammerfest basin. The Snøhvit is situated in three of these fault blocks with the major portion in the east west oriented horst with dip gently towards west (Linjordet et al., 1992).

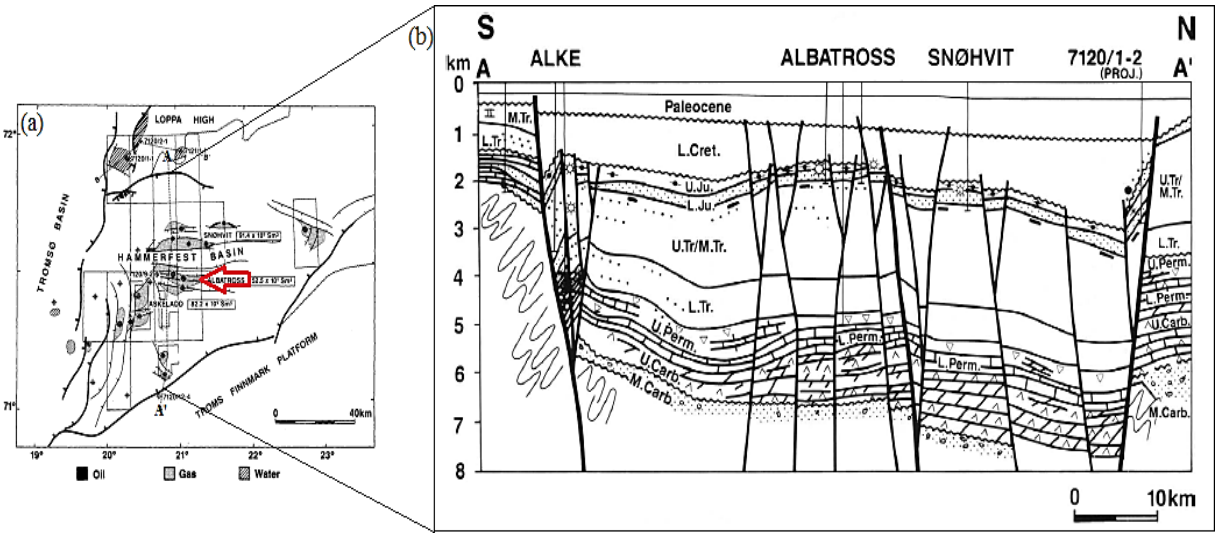

Figure 2.5: (a) Map of hydrocarbon occurrences in the Hammerfest basin (b) Geoseismic cross-section showing the main fields. Red arrow is showing the location of the study area (Modified from Stewart et al., 1995).

2.3 Stratigraphy

The Barents Shelf boreholes data have depth coverage down to Permian strata while Permo-Carboniferous rocks of this region are believed to be analogous as those of Svalbard, Bjørnøya nd Northeast Greenland (Faleide et al., 1993b). The late Paleozoic strata in the SW Barents Sea are thought to be present on the basis of boreholes and seismic reflection/refraction data (Jackson et al., 1990; Faleide et al., 1993; Faleide et al., 1991). The Devonian, Carboniferous and Permian succession is dominated by carbonates with, to some extent, evaporates.

The lower-middle Jurassic interval in the Hammerfest basin is represented by sandstones which is extended throughout the area, the thickness of which increases towards the Tromsø Basin and also covered the Loppa High and Finnmark Platform but has suffered exhumation and erosion during later tectonic events (Fig. 2.5b) (Glørstad-Clark et al., 2010; Faleide et al., 1993b). The middle-late Jurassic rifting event is the key factor for different lithologies (shales and clay stones with subordinate marly dolomitic limestone and rarely occurring siltstone and sandstone) in the Barents Sea representing paleo-depositional environments, deltaic and shallow marine conditions was prevailed before rifting and deep sea conditions were exist after rifting (Worsley et al., 1988; Faleide et al., 1993).

In the early Cretaceous, the depositional environment was marine, leading to the deposition of shales and clay stones (Faleide et al., 1993). Whereas the late Cretaceous was the period of clastic sedimentation mainly clay stones in the Tromsø Basin, which is the indication of open marine, deep shelf environment, on the other hand, the western part of the Hammerfest basin changed into more calcareous dominated towards the east showing the shallow detritus straved shelf environment (Worsley et al., 1988; Faleide et al., 1993).

Paleogene was the period of open to deep marine environment with the sedimentation dominated by claystones with thin interbedded siltstones, tuffaceous material and carbonates

(Faleide et al., 1993). Lower Paleogene sequence show lateral variation in lithology and is present throughout the SW Barents Shelf while the younger sequence is preserved only in the Tromsø, Harstad and Sørvestsnaget basins (Faleide et al., 1993). Neogene and Quaternary stratigraphic sequence have unconfirmable contact with the underlying Paleogene and Mesozoic sequence (Faleide et al., 1993). A brief description of the stratigraphic units (Fig. 2.6), described as groups, encountered in the studied wells is given below:

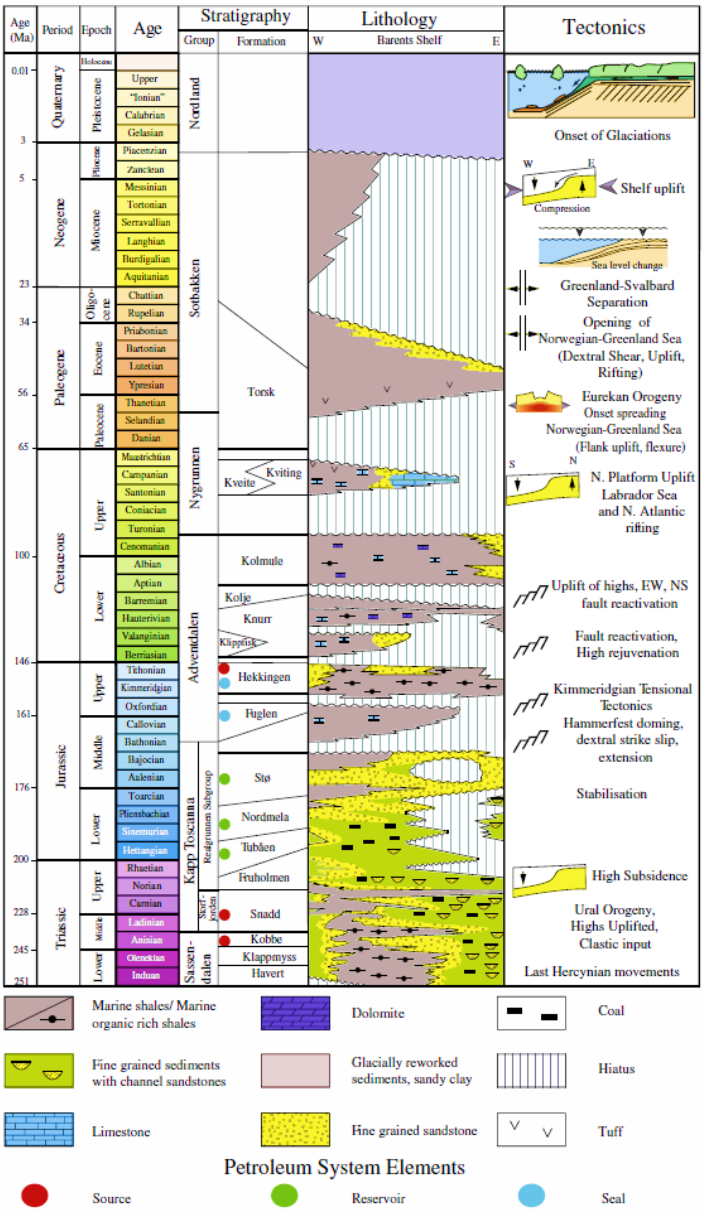

Figure 2.6: Generalized stratigraphy of Barents Shelf, accompanying tectonic events, megasequences and petroleum system of the study area is also shown in the figure (Modified from Ostanin et al., 2012).

The detail of stratigraphic groups and its formations which have been encountered in the studied wells in given below:

The Ladinian-Bathonian age of Kapp Toscana Group have different sandstones units of different sources containing significant oil and gas reservoir potential in the lower part. Shale dominancy increases upwards. This group is divided into two subgroups Realgrunnen and Storfjorden subgroups. Stø and Snadd formations belong to Storfjorden subgroup and other subdivisions are Fruholmen, Tubåen and Nordmela formations (Fig. 2.6) (Worsley, 2008). The sands of coastal and channel area were extracted from mature province areas on the Baltic Shield and Novaya Zemlya as a significant provenance area and their reservoir primary quality was increased by marine reworking at the time of high stand (Worsley, 2008). Sandstone of this area reflects overlapping of lithologies upwards, showing increase marine reworking and mixing of the components from different provenance areas (Worsley, 2008). Triassic deposition in the region, which is characterized by synchronous transgressive-regressive sequences, was disturbed by tectonic activity (Worsley, 2008, Mørk et al,. 1989; Mørk and Smelror 2001). The Stø Formation represents the main reservoir interval in the Hammerfest basin, lower to middle Jurassic in age whereas the Triassic and late Jurassic organic rich shales are the possible source rocks of the area (Fig. 2.6). The formations which have been encountered in studied wells along with total depth are given in the Table 2.1.

Table 2.1: Formation tops in the study area which have been utilized, to delineate source (Hekkingen) and reservoir (Stø, Nordmela & Tubåen Formations) rocks (Source: NPD).

Age		Group(Gr.)/ Formation (Fm.)	7120_9_2	7120_8_4	7120_8_3	7120_9_1	7121_7_1	7121_7_2
Era	Period		Top MD (m)	Top MD (m)	Top MD (m)	Top MD (m)	Top MD (m)	Top MD (m)
Cenozoic	Quaternary	Nordland Gp.	316	298	303	343	351	347
	Paleogene	Stobakken Gp.	380	376	605	590	442	430
		Torsk Fm.	380	376	605	590	442	430
Mesozoic	Cretaceous	Nygrunnen Gp.	1072	1186	1067	965	894	889
		Kveite/Kviting Fm.	1072	1186	1067	965	894	889
		Adventdalen Gp.	1097	1279	1200	984	931	923
		Kolmule Fm.	1097	1279	1200	984	931	923
		Kolje	1847	1798	1962	1607	1588	1578
		Knurr Fm.	1871	2142	2055	1761	1732	1728
	Jurassic	Hekkingen Fm.	1906	2179	2104	1813	1796	1806
		Fuglen Fm.	1965	2250	2187	ABSENT	1848	1880
		Kapp toscana Gp.	1971	2264	2192	1840	1849	1882
		Stø Fm.	1971	2264	2192	1840	1849	1882
		Nordmela Fm.	2048	2360	2277	1896	1908	1938
		Tubåen Fm.	2156	2496	Not Penetrated	1986	2001	2028
	Triassic	Fruholmen Fm.	2290	2643		2077	2045	2073
		Snadd Fm.	2552	Not Penetrated		2173	Not Penetrated	Not Penetrated
		Sassendalen Gp.	3962			Not Penetrated		
		Kobbe Fm.	3962					
		Klappmyss Fm.	4245					
		Havert Fm.	4806					
Paleozoic	Permian	Templefjorden Gp.	4844					
		Ørret Fm.	4844					
		Røye Fm.	4956					

Well known regional transgression of Bathonian age disrupted the supply of coarser clastics and marine calcareous mudstones and caused the deposition of anoxic black shales of Hekkingen Formation, which is the subdivision of Adventdalen group during Callovian/ Oxfordian time. Other subdivisions are Kolmule, Kolje, Knurr and Fuglen formations. The

Hekkingen Formation is the excellent source rock with marine dominated kerogens and upto 20 % of organic content in the upper Jurassic units (Worsley, 2008).

The entire section thins eastward across the Hammerfest basin. Greenish grey to grey clay stones with thin limestone pass into more sandy or calcareous condensed sequence. Clay stone represents Kveite Formation and the condensed sequences are assigned to the Kviting Formation. These formations are two sub members of Nygrunnen group. The condensed calcareous sandy unit shows the time of maximum transgression. The depositional environment of this group is open marine deep shelf in the western area that passed into shallower starved shelf regime in the eastern region. The age of this group is from Cenomian to Maastrichtian (Dalland et al., 1988).

There is increase in thickness of sediments approximately 300 m near the southern margin upto 1 km in the northwestern basin. Clay stone dominates in this group with minor siltstone, tuffaceous and carbonate zones. Large area of Barents Shelf east of Senja Rift was uplifted and exposed to erosion due to the shift in tectonic regime and these erosional products were deposited in the west of the ridge. Due to that post depositional erosion, the upper part of Sotbakken Group is not preserved in the eastern part but we can see well preserved lower part throughout the Barents Shelf. Late Paleocene to early/middle Eocene age is well documented by preserved sequences. Mid Paleocene was the period of transgression for Barents Shelf and in this transgressional environment outer sublittoral to deep shelf clay stone was deposited. The Torsk Formation is the only subdivision within this group (Dalland et al., 1988).

The depositional environment for this group is bathyal to glacial marine and the age of sediments is Late Pliocene to Pleistocene/Holocene. The upper boundary is marked by Seabed. Sands and clays convert into sandstones, clay stones, and the sandy content increases upward (Dalland et al., 1988).

2.4 Petroleum system

The petroleum system can be defined as a system, which includes a pod of active source rock and all related oil and gas and includes all the important elements and processes required for oil and gas accumulation to exist. The important elements are the source rock, reservoir rock, seal (cap) and overburden rock and the processes include trap formation and generation migration and accumulation of petroleum (Magoon et al., 1994). All the events and processes should be placed correctly in time and space for the availability of the occurrence of the working petroleum system.

In the Barents Sea three different petroleum systems; Paleozoic, Early-Mid Triassic and Late Jurassic can be found and the Hammerfest basin belongs to Late Jurassic to mixed petroleum system (Fig. 2.7) (Henriksen et al., 2011). The late Jurassic to early Cretaceous rifting originated the later subsidence which results in the maturity of the Jurassic source rocks. This rifting has created the tilted fault blocks and has produced the restricted marine conditions for the deposition of principal source rock (Fig. 2.8).

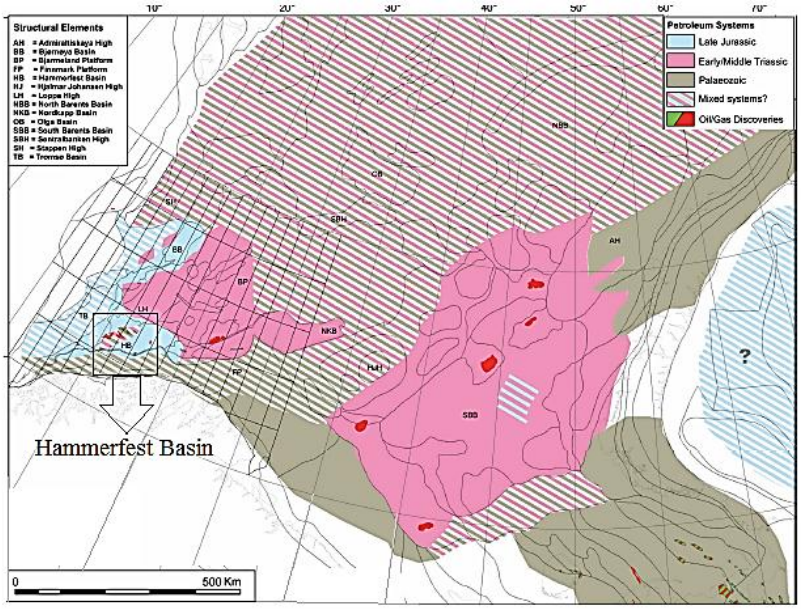

Figure 2.7: Petroleum system of the greater Barents Sea. This map is based on inferred presence of source rocks and modeled maturity and is calibrated to the distribution and geochemistry of the hydrocarbons in wells in the Norwegian Barents Sea. Hammerfest basin is highlighted with black rectangle (Modified from Henriksen et al., 2011).

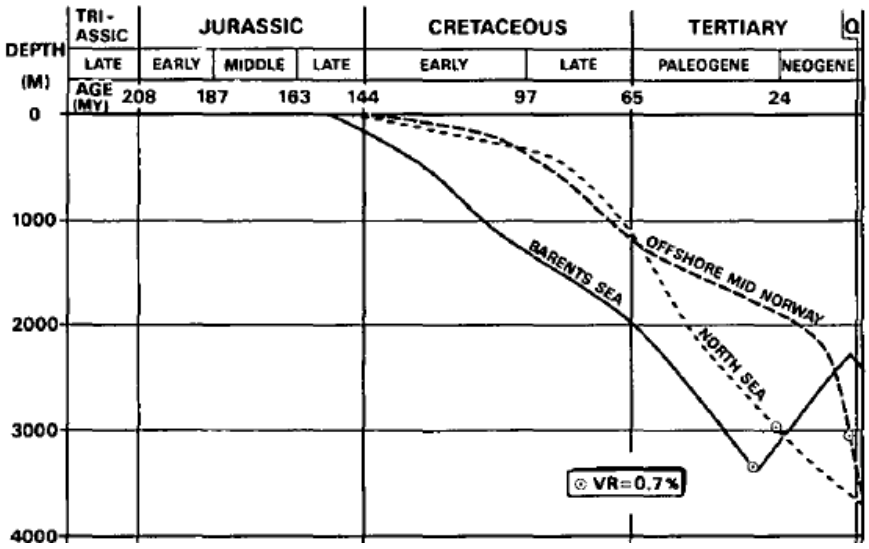

Figure 2.8: Generalized burial history graphs for the upper Jurassic shales in the North Sea, offshore mid Norway and in the SW Barents Sea. The vitrinite reflectance values of the 0.7% show entry into the mature zone for oil generation (Modified from Spencer et al., 1993).

The petroleum system in the Barents Shelf has experienced different stages of Cenozoic exhumation due to which the tertiary migration has been occurred from the available traps.

An overview of the different source rock and reservoir intervals in the Norwegian Barents Sea is given in the Figure 2.9.

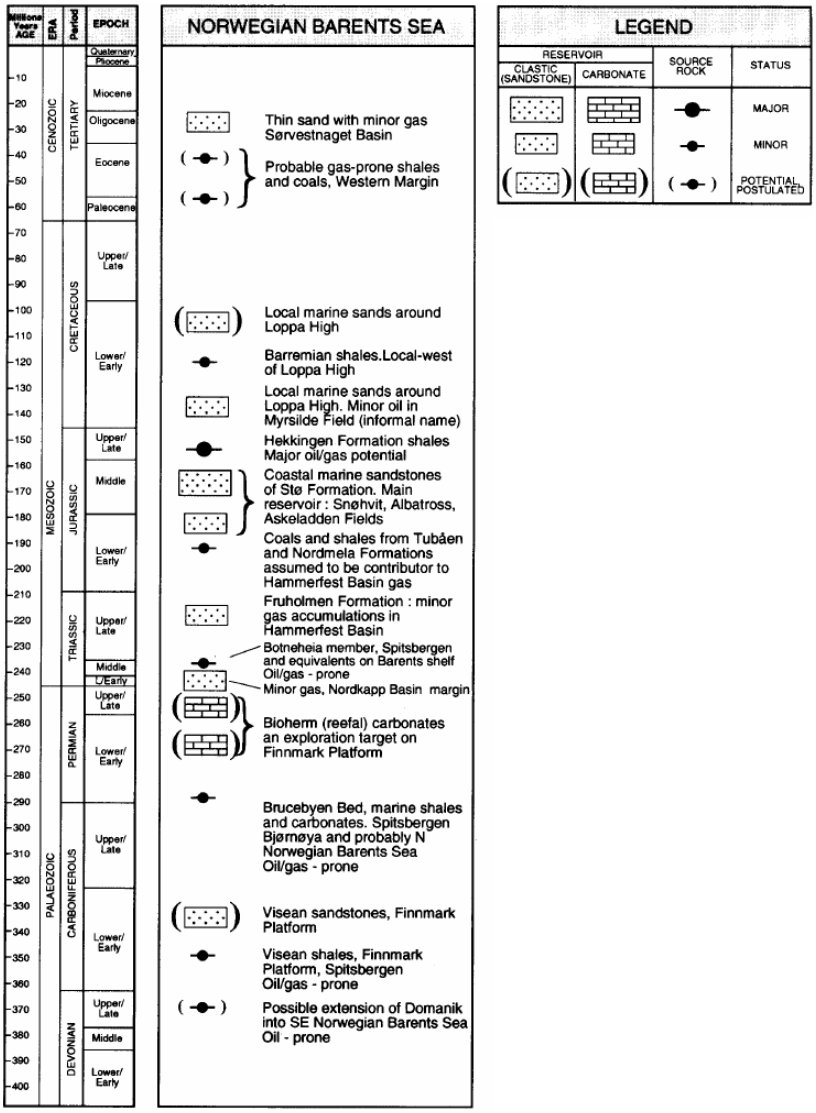

Figure 2.9: Major source and reservoir rocks of the Norwegian Barents Sea (Modified from Dore, 1995).

2.4.1 Source rocks

The term "source rock" represents a sedimentary unit, which is capable of producing the hydrocarbons, and after being formed, migrates into a reservoir. A typical source rock contains greater than usual organic matter (> 1% TOC in the clastic rocks) which remains preserved in the oxidation environment (Dore, 1995). Oil formation occurs at lower temperature than gas during burial and continuous heating due to creaking of kerogen takes place. Terrestrial kerogen generates gas while marine kerogen (algal material) produces oil (Dore, 1995).

The major source rocks in different geological regions are shown in the Figure 2.10 and Table 2.2 represents summary of these source rocks with additional information on organic geochemical properties.

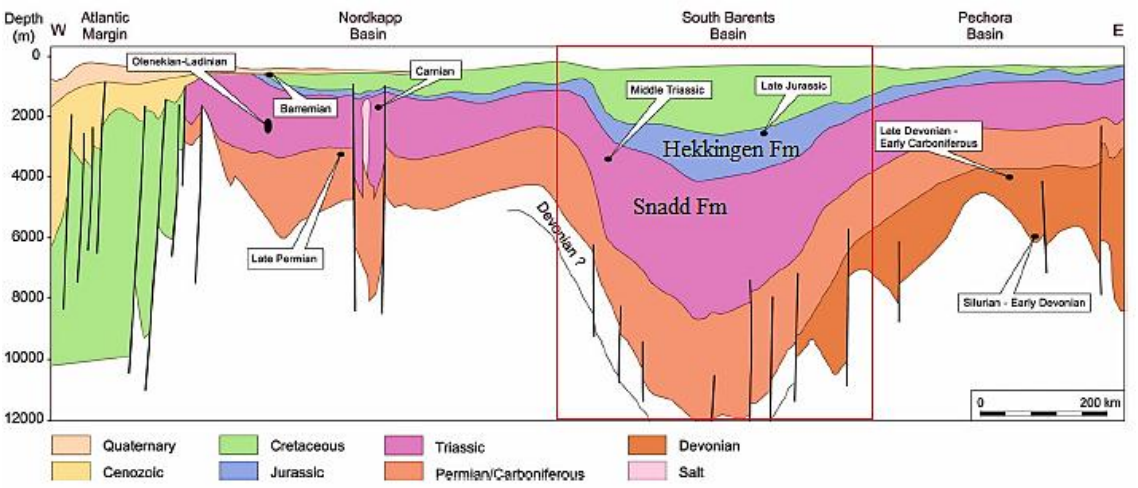

Figure 2.10: Stratigraphic occurrence of major source rocks in the Barents Sea is show by regional seismic profile. Study area is highlighted by red rectangular (Modified from Henriksen et al., 2011).

Table 2.2: Summary of petroleum source rocks in the Barents Sea (Modified from Henriksen et al., 2011).

Age	Formation	Thickness (m)	Kerogen Type	TOC (%)	HI (mg/g TOC)
Barremian	Kolje	<30	II-II/III	1-7	130
Kimmeridgian	Hekkingen	10-250	II/III	<20	300
Carnian-Norian	Snadd		III-I	<5	<600
Ladinian	Snadd	1-15	II	6	300-500
Anisian	Kobbe	5-20	II-II/III	2-8	200-590
Olenekian	Klappmyss	<100	III/II	3.5	180-350
Late Permian	Ørret	80-350	II/III	<3.5	200-330

The southwestern Barents Sea contains Permian to Early Cretaceous multi-sourced system making this area as an over-filled petroleum basin (Ohm et al., 2008). Three possible source rocks are present in the Studied area; the late Jurassic-Early Cretaceous shales of Hekkingen Formation, the Early Jurassic Nordmela Formation and the Triassic Shales (Linjordet et al., 1992; Stewart et al., 1995). The Hekkingen Formation is organic rich shale and supposed to be widely distributed hydrocarbon source rock in the Barents Sea region with the potential to produce light oil, condensate and gas (Leith et al., 1993, Bugge et al., 2002) whereas the terrestrial Nordmela Formation and over-matured Triassic shales have generated gas and condensates (Ohm et al., 2008). The Hekkingen Formation is a black shale having tendency to split into sheets called as paper shale (Bugge et al., 2002) and this formation is equivalent to the Kimmeridge clay in the North Sea with anoxic deep marine restricted basin depositional conditions (Dalland et al., 1988). The Hekkingen Formation is the most prolific because of its high total organic carbon (TOC) (Table 2.2) and the hydrocarbon generation potential (Fig. 2.11).

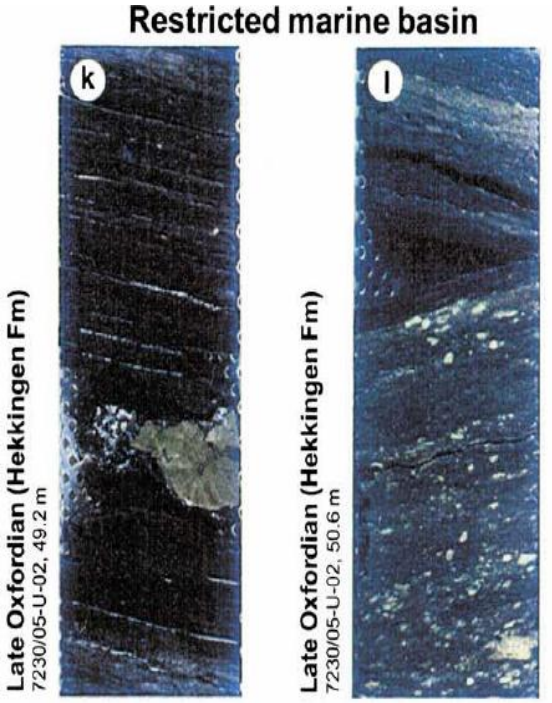

Type II and II/III kerogen and high gamma radiation. 7–23% TOC in lower part (paper shales), 4–14% in the upper part. Thin siltstone to skeletal laminae. Cone-in cone and septarian type calcite concretions/beds often in high gamma radiation zones. Pyrite concretions/laminae. Bioturbation absent to very rare. Benthic fauna suggesting restricted (?dysoxic) conditions together with high planctonic fossil content suggests stratified water body with anoxic to dysoxic bottom conditions.

Figure 2.11: Core description of the Hekkingen Formation (Modified from Bugge et al., 2002).

But the effects of uplift is that it placed the source rock to the shallow depth thus preventing source rock potential for generating more hydrocarbons as well as influencing the reservoir quality and seal strength (Fig. 2.12). In the Hammerfest basin, Triassic source rocks entered in the gas window whereas Hekkingen Formation is in the oil window (Fig. 2.12). Therefore, it is important to understand the geological evolution as well as the exhumation history of any area before the interpretation of the petroleum system. In the Hammerfest basin, Triassic source rocks entered in the gas window whereas Hekkingen Formation is in the oil window (Fig. 2.12). During exhumation and erosion, the temperature required to generate hydrocarbon for the Hekkingen Formation has dropped thus preventing further hydrocarbon generation, the main negative consequence of hydrocarbon generation in the uplifted area like Hammerfest basin.

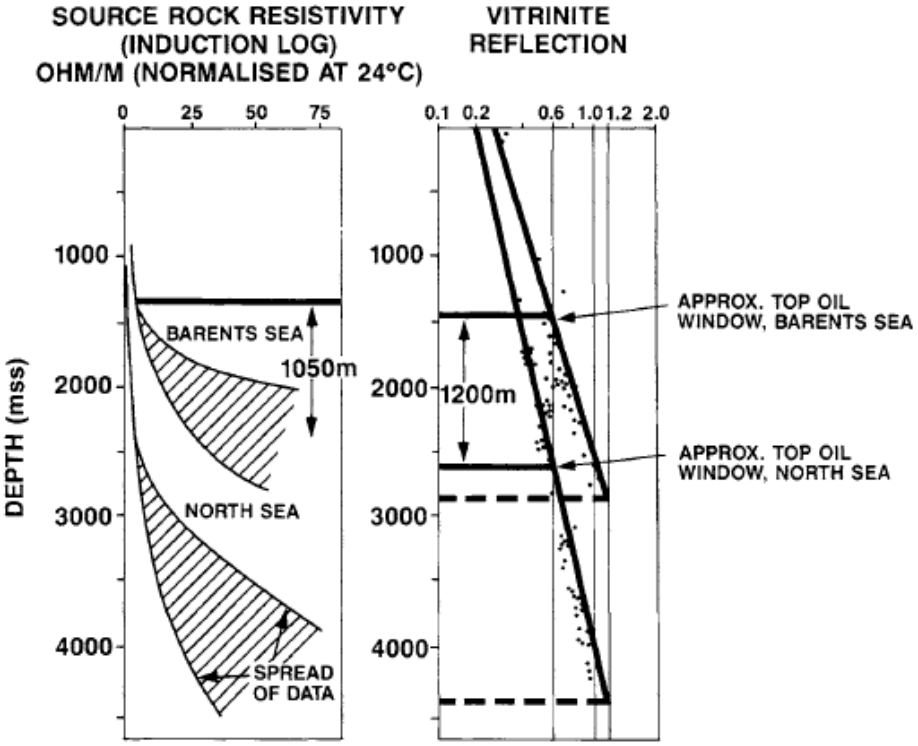

Figure 2.12: Comparison of the source rock resistivity and vitrinite reflectance depth plots for the North Sea and Barents Sea (Modified from Stewart et al., 1995).

2.4.1.1 Stratigraphic correlation of source rocks

Depositional environment of any formation in any area can cause in the change of petrophysical properties of the rock unit. That is why it is important to interpret the depositional environment as well as the provenance area of the sedimentary succession. Moreover, this kind of investigation can help in conducting compaction (Ch. 4) and rock physical diagnostics (Ch. 5) of the particular area. For this purpose four wells (7120/8-4, 7120/9-2, 7120/9-1 & 7121/7-2) from the study area have been selected using gamma ray log response and the wells have been flattened at a depth of 1800 (m) MD. The stratigraphic correlation is done only for source rock Hekkingen Formation of the study area (Fig. 2.13).

The Hekkingen Formation in the Hammerfest basin is, undoubtedly, main source rock and the thickness of this formation decreases from east to west (Fig. 2.13). The depositional environment of this formation is deep marine, which is caused by the renewed regional transgression in the Bathonian, which limits the supply of coarse clastic sediments, and marine calcareous mudstones gave way to the anoxic black shales of the Hekkingen Formation during Callovian/Oxfordian (Worsley, 2008). Also due to the different rate of subsidence and uplift caused the formation of deep basins bordered by exposed platforms and highs in the western area (Fig. 2.4) (Henriksen et al., 2011). Perhaps due to these reasons, the thinkness of the Hekkingen Formation towards west is less as compared to the eastern side and paleo depositional environment could be the reason for different gamma ray reading within the same formation.

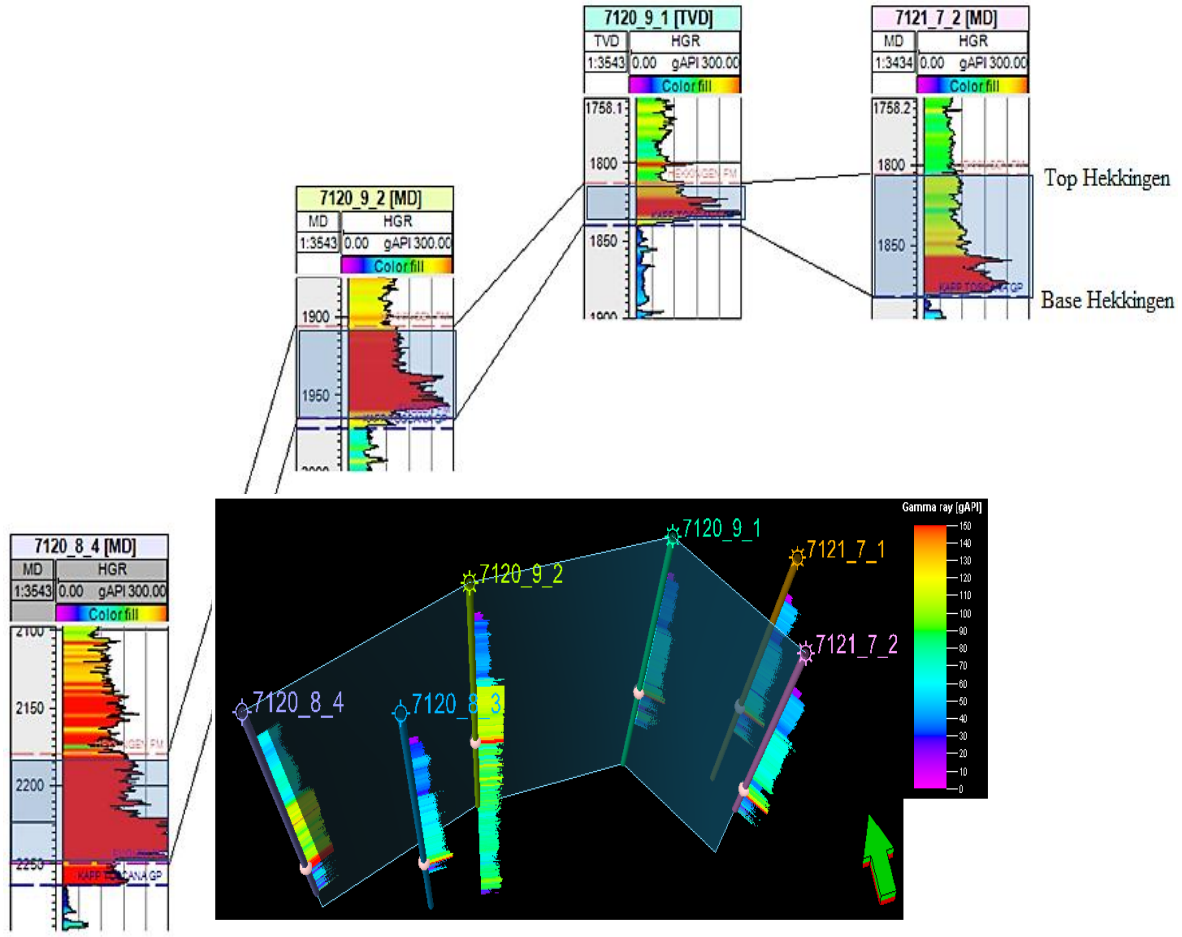

Figure 2.13: Stratigraphic correlation of the source rock Hekkingen Formation of the study area, well fencing, along with gamma ray log, is showing the wells used for correlation.

2.4.2 Reservoir rocks

In the Hammerfest basin, the most important reservoir rock lie in the units of Jurassic age. Major discoveries, which have been made in the area, have been found in the lower to middle Jurassic Stø Formation (Dore, 1995). It is believed that 85% of the reserves in the Norwegian Barents Sea lie within the Stø Formation, most of which is expected to be in the form of natural gas (Dore, 1995). The other reservoir rocks are lower Jurassic Nordmela and Tubåen Formations containing good reservoir quality. The depositional environments of these formations are coastal, deltaic, and marine to shoreface settings (Fig. 2.14).

The Stø reservoir rock consists predominantly of mature sandstones with thin beds of shale and siltstone (Dalland et al., 1988). The depositional environment for Stø Formation is of prograding coastal areas and shales and siltstone patches depicts regional transgressive episodes (Dalland et al., 1988). The thickness of the formation varies within the basin but the formation is the thickest in the southwestern wells thinning towards east. It can be defined by 3 sequences on the basis of transgression. The basal part is only present in the western part of the Hammerfest basin. Maximum transgression shown by middle part and the uppermost part is highly variable represents syndepositional uplift and differential erosion (Dalland et al., 1988). In general, it shows shoreline and near shore environment, which is strongly affected

by storm wave process and bioturbation (Berglund et al., 1986). The Stø Formation can be differentiated into two subunits (Fig. 2.15a). The upper part of this formation is poorly sorted as compared to the lower part, which represents good quality reservoir. Due to the influence of the low energy conditions and high bioturbation, the lower part of the Stø Formation has poor quality and bad sorting.

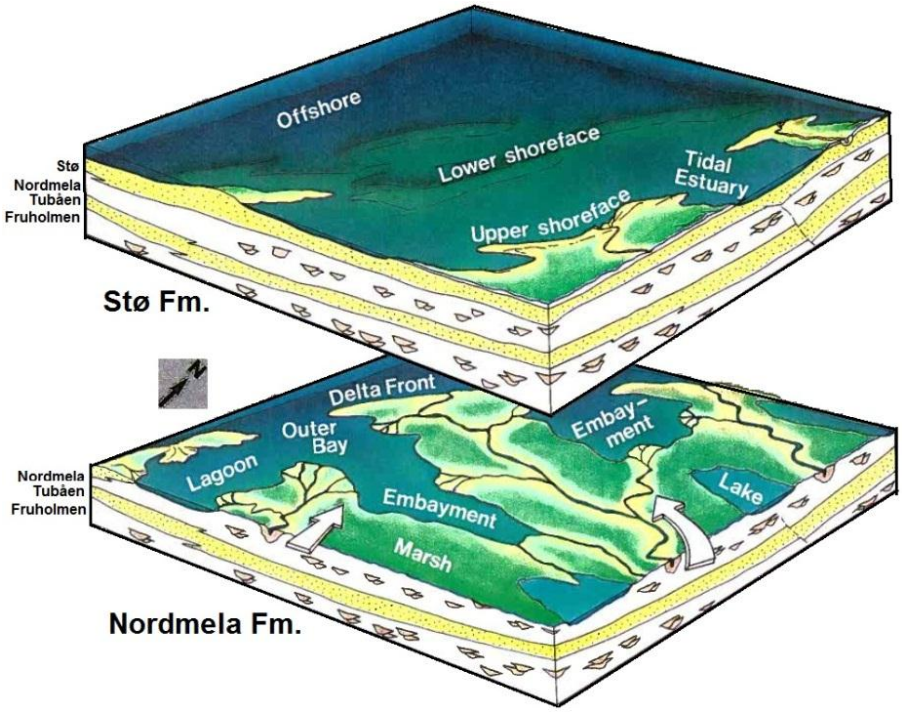

Figure 2.14: Paleogeography and depositional environments model for Stø and Nordmela Formations (modified from Berglund et al., 1986).

The depositional environment for Nordmela Formation is subtidal or tidal channel, which reflects lenticular, and flaser bedding (Fig. 2.15b). Channel sands believe to have vertical fluid flow restriction. However, good connectivity with horizontally distributed channels is produced good quality reservoirs.

Another reservoir rock belongs to Kapp Toscana Group is Tubåen Formation which is dominated by sandstones with subordinate shales and minor coals and will be used for CO2 re-injection (Spencer et al., 2008). The development of this formation is tripartite with a shales interval sandwiched between two sandstones rich intervals. The base of this formation is of late Rhaetian to early Hettangian. The sands intervals in the Tubåen Formation is believed to represents stacked series of high-energy marginal marine (tidal inlet dominated barrier complex and/or esturies) environments. In comparison fine to medium-grained, Tubåen Formation has better reservoir quality than Nordmela Formation. Because of greater burial depth, digenetic history destroys the reservoir quality more in the Tubåen Formation than Stø Formation.

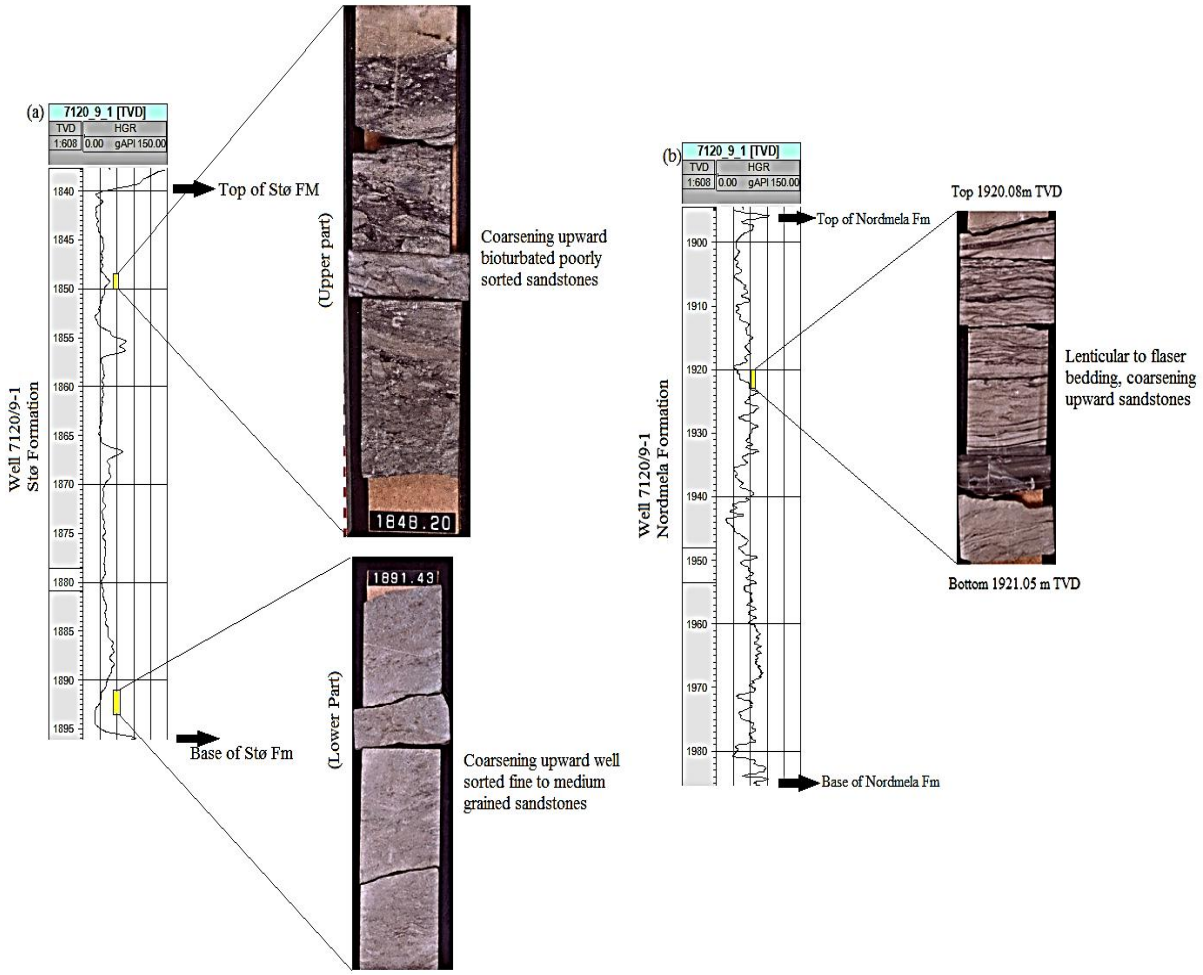

Figure 2.15: Core photographs of the (a) Stø and (b) Nordmela Formations from the well 7120/9-1 showing different sedimentary structure reflecting varying depositional environments (Source: NPD).

2.4.2.1 Stratigraphic correlation of different reservoir units

Complex interplay of tectonic subsidence, eustatic sea level changes and local sediment input are the controlling factors for the cyclic changes in the shale continental and sandy shallow marine sediments in Late Triassic to Middle Jurassic sedimentary sequences (Bergland et al., 1986). The general relative sea level rise, which was started in Middle Jurassic times, caused the deposition of the Stø Formation, which is the main reservoir rock of the study area. The maximum thick of the Stø Formation (96 m) is observed to the west side whereas the minimum thickness (56 m) is towards east (Fig. 2.16).

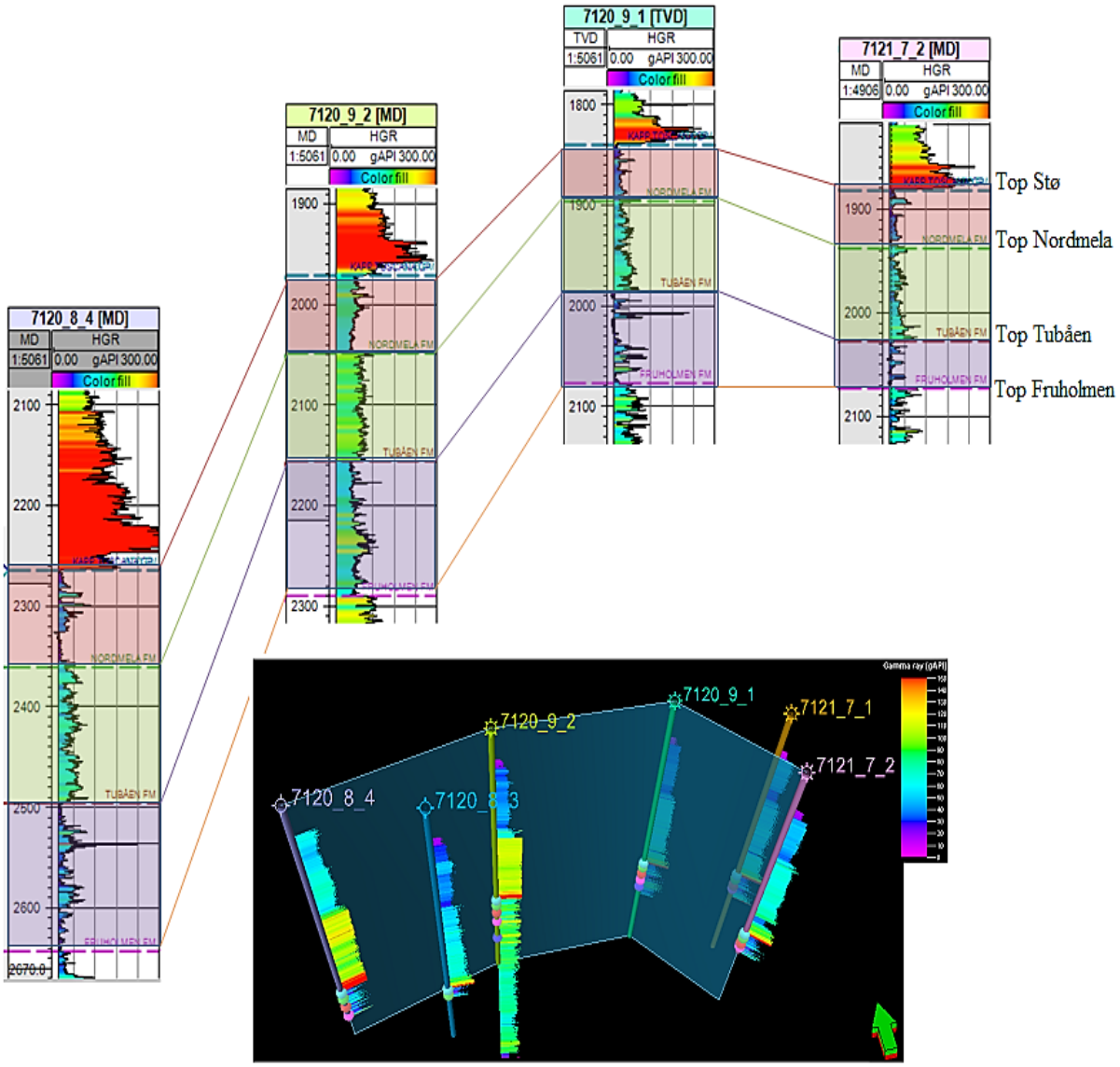

Figure 2.16: Stratigraphic correlation of different reservoir rocks using gamma ray log response from west to east, well fencing is showing the wells used for correlation with gamma ray log.

The sandstones of the Stø Formation are of better quality than the underlying Nordmela Formation along with this they have homogeneous lateral reservoir continuity. It is inferred that these sequences passes into more distal low energy marine environment westwards (Fig. 2.17) (Stewart et al., 1995).

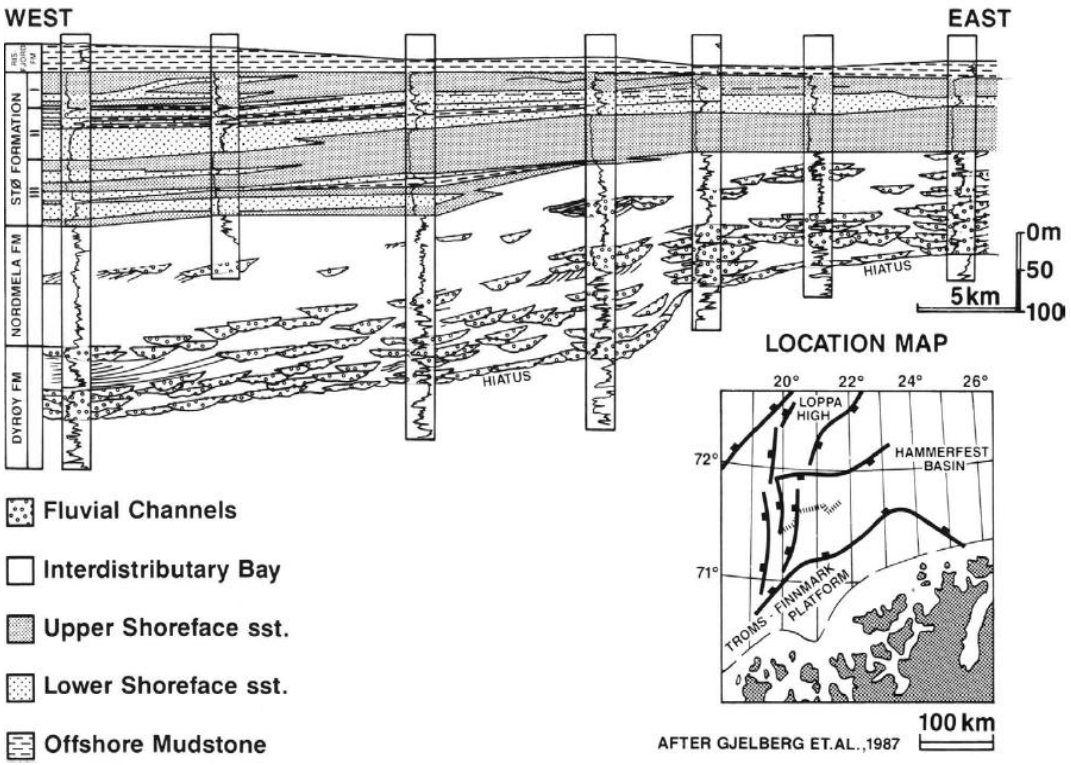

Figure 2.17: East-west regional well correlation of the late Triassic to Jurassic succession in the Hammerfest basin showing lateral variation in the depositional facies (Modified from Stewart et al., 1995).

The other reservoir rocks are Nordmela and Tubåen Formations. The Nordmela Formation reflects deltaic environment along sub environments, which were lagoon, marsh, embayment lakes, channels etc. representing broad alternation of fine grained sandstones, siltstones, mudstones and thin coal beds. The overall depositional environment of the Nordmela Formation reflects lower delta plain where dominating river system was anastomosing fluvial origin of thicker and coarser sandstones tends to be concentrated in the central part of the formation, although this unit represents only 20 % of the total lithology (Berglund et al., 1986). There was an active source to the south of the present Troms-Finnmark Fault Complex (TFFC) along with easterly sourced sediments was active, which caused the fluvial drainage towards west due to which fine to medium grained sandstones deposit over a large area. This could reflect the fact of thickening of strata west side. The lagoonal facies commonly occur at the top of the Nordmela Formation is the evidence of minor transgression before the beginning of major transgression and this lagoonal facies is mainly restricted to the south western part of the area and decreases in thickness towards east.

With the start of rise in regional sea level, the Stø Formation was deposited in the shoreline and near shore depositional environments. Due to shoreline environment, this formation is severely affected by storm-wave processes and bioturbation. The whole formation represents many episodes of sea level fluctuation but the upper part of the formation represents more distal marine facies compare to the lower part (Berglund et al., 1986). It is also proposed that the wide distribution of the Stø Formation is the result of these fluctuations, which reasoned rapid lateral switching of the coastline and reworking of the sediments of a wide area. The sandstones of the Stø Formation are of better quality as compared to the underlying Nordmela

Formation and in addition to that, they have more homogeneous lateral reservoir continuity. It is suggested that these sequences passes into more distal low energy marine environment westwards (Fig. 2.17) (Stewart et al., 1995). The changes in the facies from east to west show proximal to distal setting within similar formation (Fig. 2.14).

The overall depositional trend of Early-Middle Jurassic in the Hammerfest basin reflects upward transgression from upper delta plain (Tubåen Fm.) through lower delta plain (Nordmela Fm.) to delta front or shore face (Stø Fm.) to deep sea (Hekkingen Fm.) environments. The continuous proximal facies onlaping on the east/south-east with gradual thinning eastward suggest a basin margin in the same direction (Berglund et al., 1986).

2.4.2.2 Reservoir geometry

The main reservoir rock of the Hammerfest basin is the Stø Formation consists of thick sandstones with alteration of thin shales and mudstones. The Stø Formation depth in the Snøhvit development varies due to structural complexities (Fig. 2.18). The depositional environment of the Stø Formation is overall shallow marine whereas as the presence of the shales represents the transgressive events in an offshore environment (Stewart et al., 1995). The reservoir sandstones of the lower to middle Jurassic Nordmela and Stø Formations are considered to be well sorted. It range in size from fine to medium grain and reflects various degrees of roundness. Some of the sandstones units are poorly sorted ranging in size from fine to coarse.

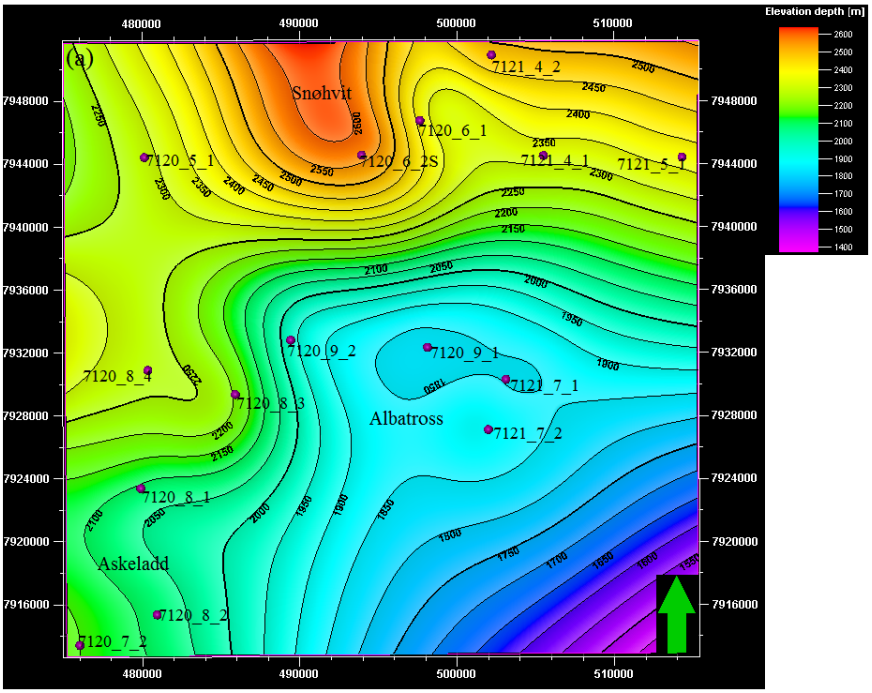

Figure 2.18: Contour map, for Stø Formation in the Snøhvit development, Hammerfest basin, is showing the depth variation.

The Nordmela sandstones are finer in size as compared to the Stø Formation sandstones. The monocrystalline quartz is the detrital mineralogy of the Stø and Nordmela Formations. Other minerals found in theses sandstones are polycrystalline quartz, mica, chert, potassium

feldspar, plagioclase, metamorphic and sedimentary rock fragments and to some extent, heavy minerals are also present. Quartz is the main cement. Due to the pressure solution overgrowth, the intergranular porosity has been reduced in the Stø Formation. Due to the compaction of the Stø Formation, the stylolites have been developed in the lower part of the formation (Linjordet and Olsen, 1992). The reservoir summery of the Snøhvit field is given in the Table 2.3.

Table 2.3: Snøhvit field reservoir summary (Modified from Linjordet and Olsen, 1992).

Pay zone	
Formation	Stø and Nordmela
Age	Early/Middle Jurassic
Gross thickness	130-200 m
Net/Gross ratio, average (range)	0.89 (0.23-1.0)
Porosity, average (range)	15% (10-18%)
Water saturation, average (range)	10% (3-26%)
Permeability, average (range)	200md (20-500md)

2.4.3 Traps/Seals

Tectonically active Hammerfest basin has experienced several phases of uplift, which caused the development of many fault related traps like hanging wall rollover anticlines, antithetic faults or sealing faults. In the Hammerfest basin, the traps that form the Jurassic fields are related to fault bounded positive blocks traps (Sec. 2.2, Fig. 2.5) (Dore, 1995).

In the Snøhvit area, two excellent seals Fuglen Formation and Hekkingen Formation are present causing the entrapment of the hydrocarbon (Fig. 2.19). Lower part of the Hekkingen Formation showed very high gamma ray response as compared to the upper part along with very low P-wave velocity. The reason for this could be interpreted as the combine effects of high gas content as well as high pore pressure. Due to that reason, the lower part of the Hekkingen Formation acts as a seal in the study area. One more point, which is in favor of the Hekkingen Formation with respect to its sealing property, is the mechanical strength and less brittleness of the formation (Linjordet et al., 1992).

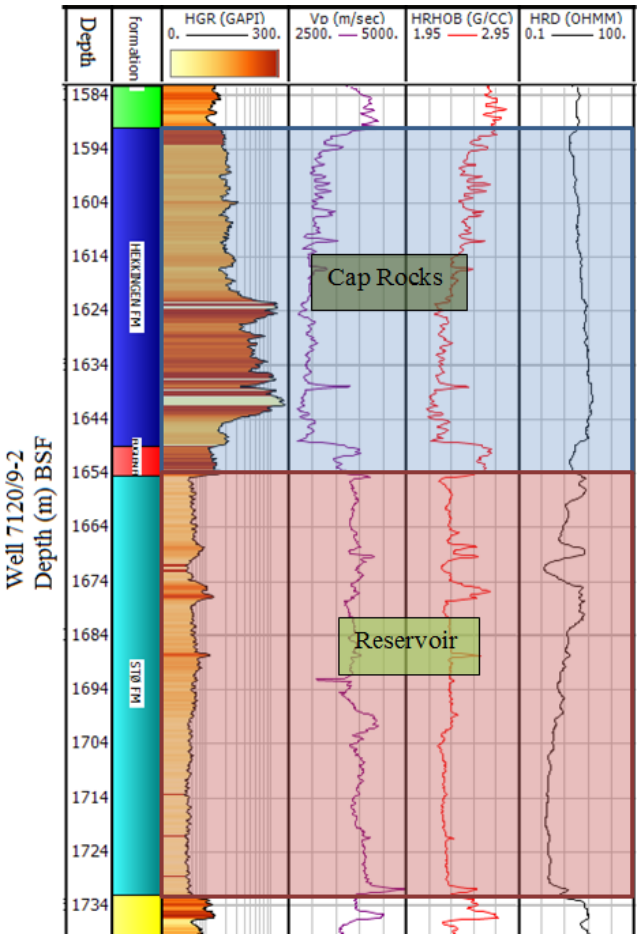

Figure 2.19: The main cap/seal rock Hekkingen and Fuglen Formations of the study area along with gamma ray, Vp, density and resistivity log response.

2.5 Hydrocarbon fluid flow

The fluid flow in the vertical direction through sediments is a widespread and dynamic geological process occurs on passive and active continental margins worldwide (Vadakkepuliyambatta et al., 2012). Fluid flow is linked with excess pore fluid pressure and attributed to temporally and spatially varying processes such as rapid sediment loading, uplift and erosion, dissociation of gas hydrate, polygonal faulting and hydrocarbon generation and leakage from deep and shallow reservoirs (Vadakkepuliyambatta et al., 2012). Fluid flow is a long term and complex geological process, belonging to the system where generation, migration, accumulation and seabed seepage of the fluid flow all occur at different times (Selley, 1998).

Vadakkepuliyambatta et al., 2012 suggested the importance of the shallow gas accumulation linked to the fluid leakage in the following ways:

Shear strength of the sediments can be reduced by shallow gas accumulations and can be hazardous to hydrocarbon exploration and development.
The shallow gas occurrence and underlying indications of fluid flow may be the indication of deeper prospective erservoirs.

Shallow gas reserves could be of great interest in the future.

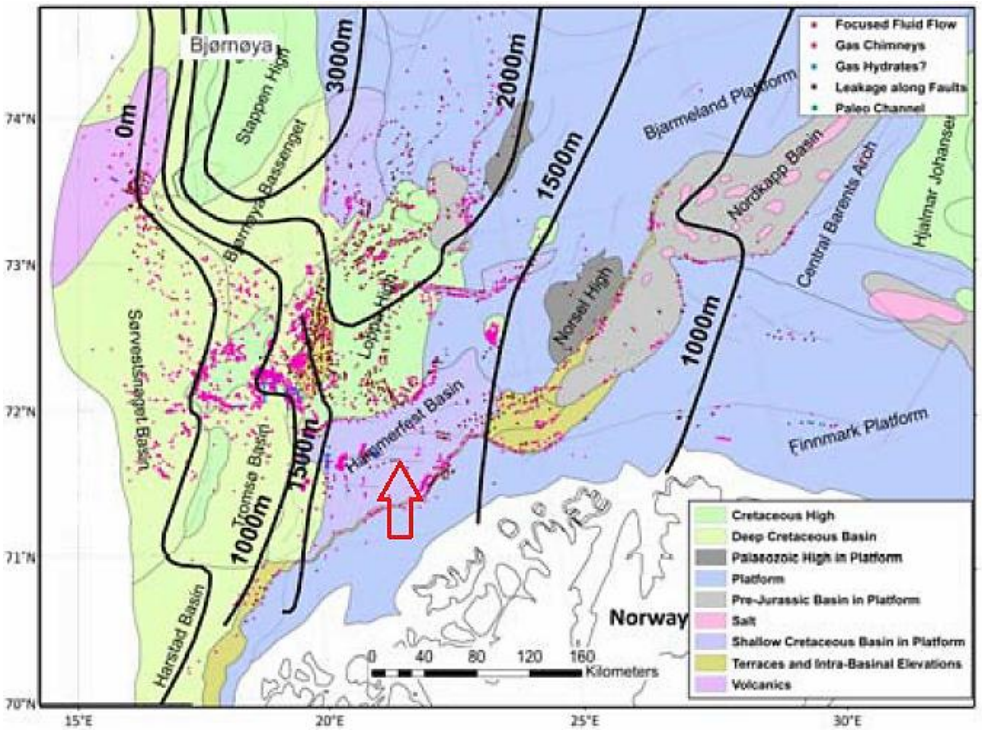

Figure 2.20: Distribution of fluid flow features (shaded in pink) in the SW Barents Sea, most of it located on top of major faults in the area. The amount of erosion (black lines) shows no direct relation to the distribution of fluid flow (Source: Vadakkepuliyambatta et al., 2012).

A total of 93 large gas chimeys with varying sizes in the study area have been mapped (Fig. 2.20). The distribution of these chimneys is densly populated on the western part of the study area. The Hekkingen Formation is the major source rock of the area whereas Triassic shales prevail in the eastern part (Ohm et al., 2008, Vadakkepuliyambatta et al., 2012). Presence of structural traps, especially faults, increases the probabilities of fluid flow since the fault reactivation during glacial periods could negatively affect the sealing ability. Triassic source rocks are over mature or gas mature in the western part of the SW Barents Sea (Ohm et al., 2008; Vadakkepuliyambatta et al., 2012).

Fluid flow features are spatially related with the structural elements in the area (Fig. 2.20) with major faults. Most of the fluid flows are above the major deep seated faults located in the hydrocarbon rich cource/reservoir rocks in the area (Fig. 2.20) suggesting the inavility of the faults to seal hydrocarbon successfully. Reactivation of these faults during uplift and glaciation has triggered these fluid flows from the faults. Isostatic uplift and associated erosion affected the hydrocarbon accumulation and migration in the SW Barents Sea (Vadakkepuliyambatta et al., 2012).

CHAPTER 3
Research Methodology and Theoretical background

3.1 Sediment compaction and exhumation estimation

The physical properties of sedimentary basin change continuously during burial due to the increase in stress and temperature. These physical properties can also be altered during uplift and cooling. This all leads to the decrease in the porosity and increase in velocity and density with increasing burial depth. Overburden or tectonic stress caused in the increase of the effective stress, which originates compaction (strain). During 0-2 km burial depth, generally, well-sorted sand is loose and mechanical compaction play an important role; below this depth temperature play its role for compaction of the sediments (chemical compaction).

Depositional trends are important in compaction and rock properties evaluation depending on the geology of the basins. Depositional trends can affect the digenetic trends. Due to the change in local geology from basin to basin or due to the different depositional environment within the same formation, the responses from the digenesis is different. The varying tectonic setting gives different kind of digenetic trends.

In order to investigate the digenetic trends and to calculate the exhumation in the study area, 15 wells have been used in this research from the Snøhvit development (Ch. 1, Table 1.1).

3.1.1 Define compaction

The rocks properties are in the state of continuous modification from the time of sediments deposition to burial at deeper level or in the time of subsequent uplift (Bjørlekke, 2010). The porosity loss due to the reduction in bulk sediments volume, and increase in the bulk density as a function of burial depth is generally called as compaction (Storvoll et al., 2005). Compaction of sediments depends upon the initial composition, effective stress and the time-temperature history (Marcussen et al., 2009). The compaction phenomenon can be difined in two terms; mechanical compaction and chemical compaction. The changing reservoir properties, therefore, is the combined function of mechanical and chemical compaction with increasing depth (Bjørlykke, 2010; Mondol et al., 2007, Oelkers et al., 1992, 1996). Compaction processes are sensitive to variation in mineralogical, textural relationship and grain size and cause to change the rock physical properties like velocity, bulk density and compressibility (bulk modulus). The changing rock physical properties as a response to burial depth, temperature and mineralogy is essential to predict for a input to basin modeling, exhumation studies, seismic interpretation and depth conversion (Marcussen et al., 2009).

The purpose of this section is to give an insight into mechanical and chemical compaction and their effects on the rock physical properties with burial depth and with temperature.

3.1.1.1 Mechanical compaction

Mechanical compaction of sediments starts immediately after deposition, causes increased stress at the point of grain contact, and due to which it increases rigidity (Storvoll et al., 2005). Mechanical compaction, which causes the porosity reduction (Fig. 3.1) by packing of

grains closer enough and by grain deformation, reorientation and fracturing, enhance the mechanical stability (Bjørlykke, 2010).

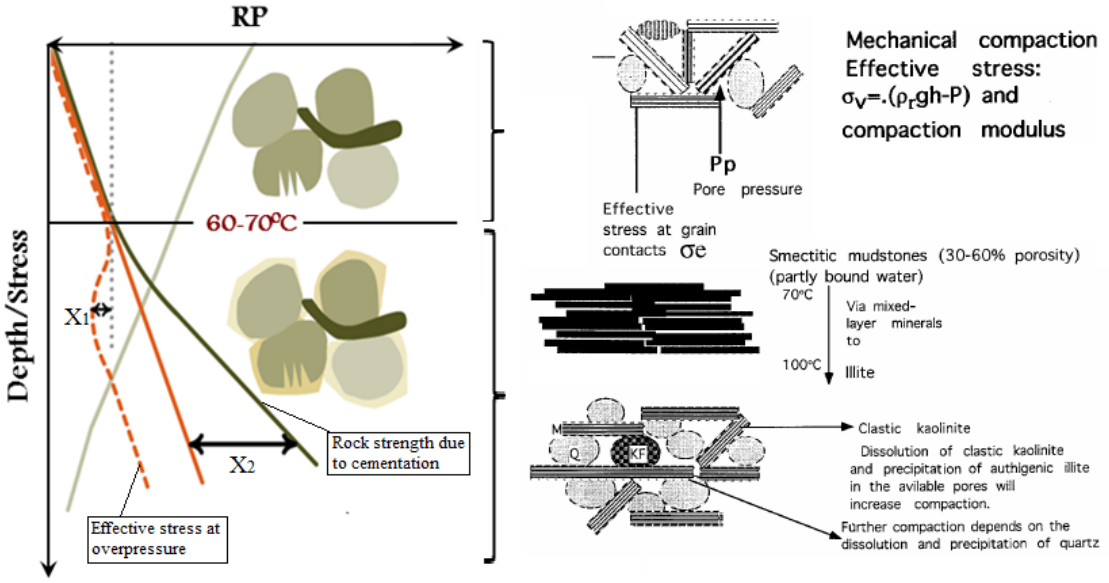

Figure 3.1: Schematic representation of mechanical and chemical compaction of mudstones (Modified from Bjørlykke and Jahren, 2010).

Mechanical compaction is the result of increased effective stresses during burial following the laws of soil mechanics and dominates in the shallow part of the basin down to 2-4 km depth temperature range 80- 100 ºC depending upon the geothermal gradient (Fig. 3.1) (Bjørlykke, 2010; Mondol et al., 2007).

The factors which affect the mechanical compaction i.e. mineralogy, grain size, shape and sorting are the function of the rocks eroded (provenance), duration and mechanism of transport of the sediments into the deposition site (Mondol et al., 2007; Bjørlykke and Jahren, 2010).

The mechanical compaction of fine-grained clayey sediments is different from that of sands and carbonates (Mondol et al., 2007; Athy 1930; Weller 1959; Magara 1980; Chuhan et al., 2003). The higher porosity of mudstones at the time of deposition is affected more by the mechanical compaction than any other sediment which resulted in the change of physical properties with the increase of stress or burial depth (Fig. 3.2) (Mondol et al., 2007). The primary composition of mudstones consists of various types of clay minerals in which smectite and kaolinite are the important one. These constituents are referred as end members in comparison with other clay minerals such as illite, chlorite etc, with respect to grain size, surface area and cation exchange capacity. Smectite is considered to be the most abundant fine grained clay found in the nature having high cation exchange capability and large surface area (700 m^2/g) whereas kaolinite is the course grained having lower cation exchange capacity and smaller surface area (10 m^2/g) (Mondol et al., 2007, 2008). Due to that reason, the kaolinite experiences more compaction due to crushing of larger grains as compared to smectite. This is also true for sandstone (Fig. 3.3). Small amount of detrital clay in sand will affect more than clean sand (Bjørlykke and Jahren, 2010).

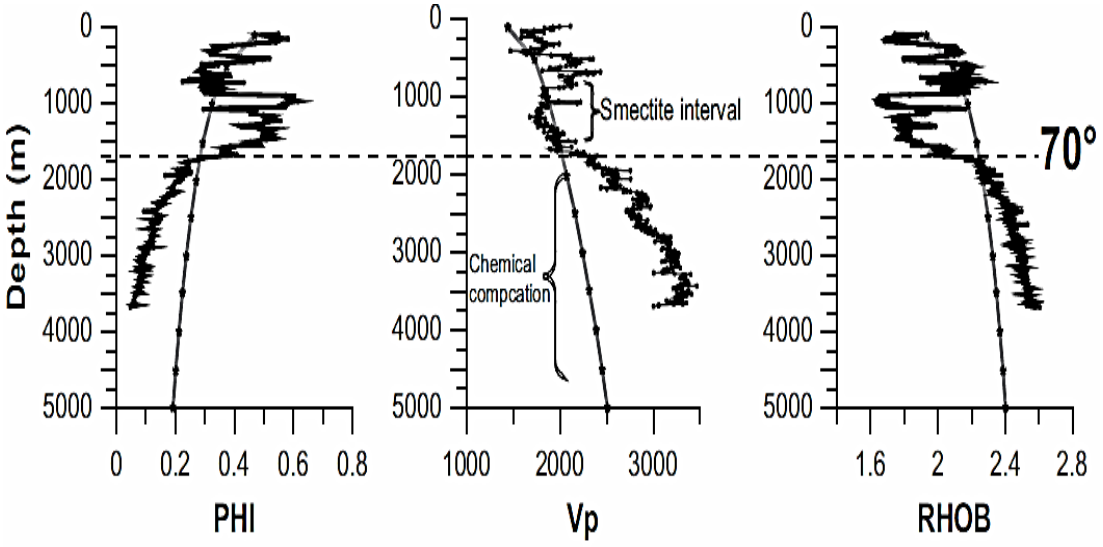

Figure 3.2: Experimental compaction of synthetic mudstone (20 % smectite/80% kaolinite: Mondol et al., 2007) compared with log values from natural occurring mudstones with same composition (Source: Peltonen et al., 2009).

3.1.1.2 Chemical compaction

Chemical compaction includes dissolution of minerals or amorphous material and precipitation of mineral cement at higher temperature greater than 80-100ºC which is dominates in the deeper part of the basin where temperature, time, mineral composition and pore fluid composition are the principle controlling factors (Fig. 3.1) (Mondol et al., 2007; Bjørlykke and Jahren, 2010; Peltonen el al., 2009; Bjørlykke, 1998).

Chemical compaction must be thermodynamically controlled so that unstable mineral can dissolve and precipitation of new and stable minerals with respect to composition of pore water and temperature. Higher temperature causes minerals with lower water content like the dissolution of smectite and kaolinite and precipitation of illite (Fig. 3.1). These reactions are kinetic controlled like activation energy and temperature (Bjørlykke et al., 2010). Unstable clay mineral smectite will dissolve at temperature above 70- 100ºC to form mixed layer mineral and illite. The silica that is released in this process must therefore be precipitated for the continuation of this reaction. This released silica causes stiffening of grain framework and higher velocities (Fig. 3.1). If the smectite is rich in iron, chlorite can be precipitated as well but the released silica must be precipitated as quartz (Bjørlykke, 2010). The stability of smectite is related to the high concentration of silica. Amorphous silica from volcanic sediments and Opal A from fossils like diatoms and siliceous sponges are the silica source for the precipitation of quartz cementation. Amorphous silica (Opal A) will be replaced by Opal CT when dissolved, at a temperature around 50-70 ºC which, at average geothermal gradient, correspond to 1.5- 2 km overburden. Opal CT is then converted into quartz in the temperature range of 60- 80 ºC (Ch. 4, Fig. 4.16).

Smectite + K-feldspar = illite + quartz……. (Eq. 3.1)

At greater burial and higher temperature the kaolinite will become unstable in the presence of K-feldspar which causes silica to precipitate as quartz.

Kaolinite + K-feldspar = Illite + quartz + water…… (Eq. 3.2)

This reaction is the cause of increased density i.e lower water content. In the absence of K-feldspar or other available source of potassium in the rock, the kaolinite is stable upto 200 ºC (Bjørlykke, 2010; Bjørlykke 1983; Bjørlykke 1986).

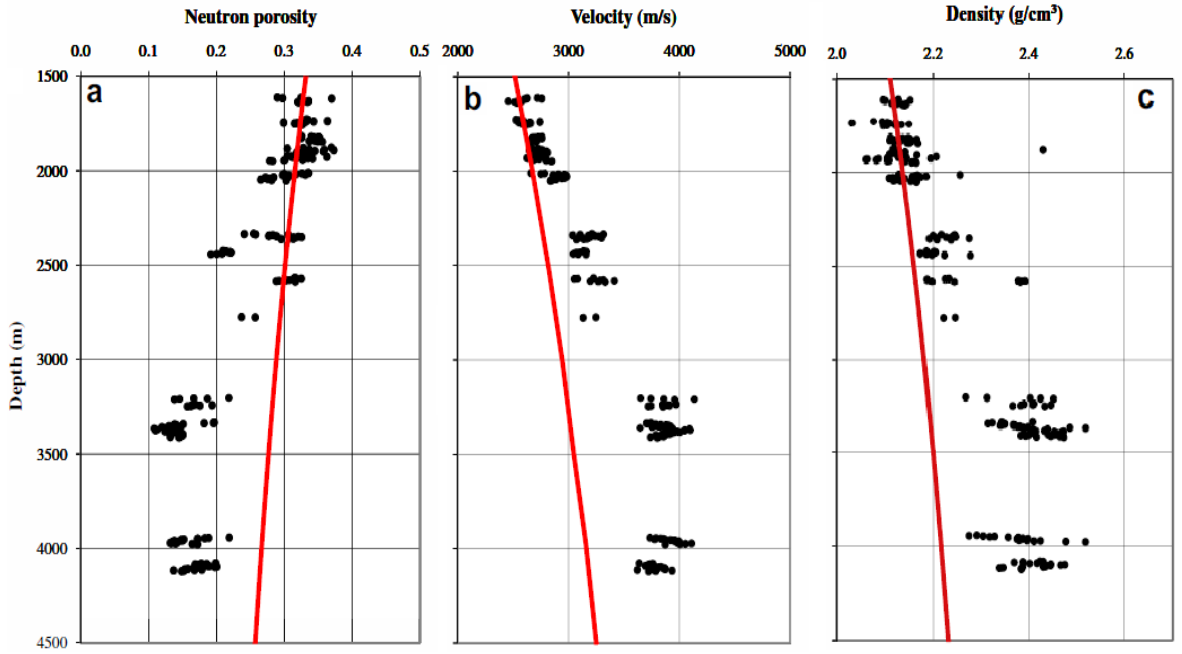

Figure 3.3: Black points showing the comparison between logs data and experimental compaction of loose sandstone (red curve) (Modified after Marcussen et al., 2010).

The above figure is showing that velocity, density and porosity depths trends in a relatively uniform lithology (loose sand) dependent on different temperature and stress controlled compaction processes.

3.1.1.3 Transition zone

Diagenetic reactions are driven towards higher mechanical and chemical stability. Reactions in the sand and shales are driven by effective vertical stress due to the overburden which results in the reduction of porosity (volume) at temperature below 70-80^{0}C. But at greater depth compaction is mostly chemical and the reactions are controlled by thermodynamics and kinetics (Bjørlykke and Jahren, 2010). Hence the transition from mechanical to chemical compaction is important because these two compaction phenomenon change the rock properties in different ways. In order to evaluate the rock properties it is necessary to know the behavior of the rock as a function of compaction. The range for mechanical compaction is in the first few km depending upon the geothermal gradient then chemical compaction domain starts. In a particular range of temperature chemical compaction stiffens the rock by precipitation of the quartz cement.

An example of transition zone in the studied well is shown in the Figure 3.4 where velocity increases abruptly as a function of depth but the density remains constant. This change is not due to lithological variation but the onset of quartz cement (Fig. 3.4).

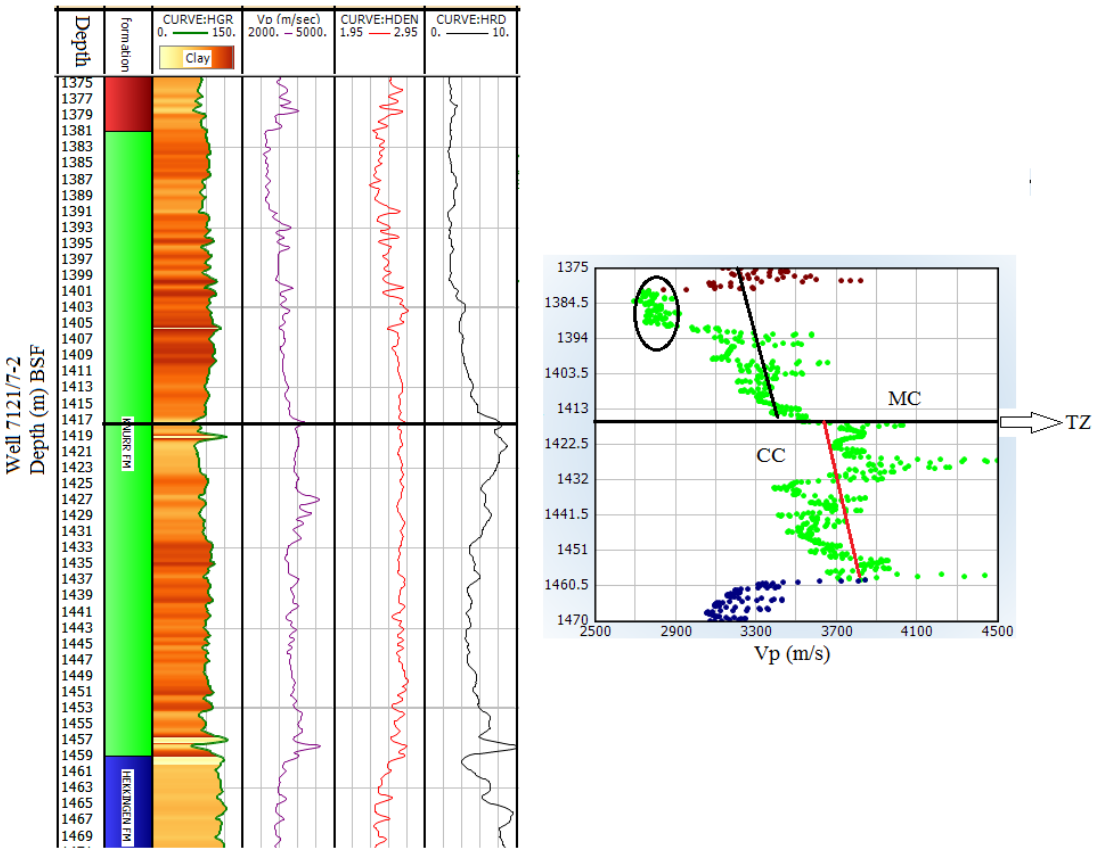

Figure 3.4: The transition zone in the Knurr Formation (black line) in wells 7121/7-2. To find TZ gamma ray, Vp, bulk density and deep resistivity logs are compared for the Knurr Formation.

3.1.2 Transition zone identification

Overconsolidation due to uplift and grain framework stiffening due to cementation give reservoir rocks higher bulk and shear modulus. Normally they don't have higher bulk and shear modulus at the same depth in the absence of these factors. Due to these factors the rock properties change and the quality of the reservoir will be different than expected. Hence the delineation, at which depth the rock properties are changing due to cementation, will assist future development of the drilled prospect.

The Vp, density and neutron porosity logs have been used to investigate the change in the rock properties due to cementation with increasing burial. The gamma ray log, published regional data and well completion reports have been used as the main lithologic control with depth for the different logs under investigation. The delineation of transition zone is based on Vp-depth trends in all the studied wells. The transition zone identification is done on the basis of abrupt increase in the velocity (Fig. 3.4). In order to examine transition zone temperature and to correlate with the published literature, it is essential to calculated geothermal gradient which is based on bottom hole temperature.

3.1.3 Temperature gradient

Quartz cementation has a profound effect in strengthening the rock frame at a faster rate as compared to the vertical stress from the overburden at a greater depth. Only 2-4 % of quartz cement is more than sufficient to halt further mechanical compaction in the sandstones, and then the compaction is chemically controlled due to the rate of mineral dissolution and precipitation. Therefore, it is essential to know the temperature gradient of the basin in order to correctly identify the transition zone from mechanical to chemical compaction. The temperature which is used during this research work, has been calculated from bottom hole temperature (BHT). The equation, which is used for measuring temperature gradient, is:

$$m = \frac{y-c}{x} \quad \text{..... (3.3)}$$

Where, m is the geothermal gradient, y is the bottom hole temperature (BHT), c is the mean annual surface temperature and x is the total depth. The 4^0C mean annual surface temperature has been used in this study and the geothermal gradient calculated for the study area is given in the Ch. 1, Table 1.1. The bottom hole temperature (BHT) for two of the wells 7120/8-4 and 7121/7-2 in the study area has been asked through personnel communication with NPD.

On the basis of geothermal gradient, the transition zone temperature was calculated and compared with the published literature. There was found a divergence on the basis of which it was assumed to calculate exhumation in the study area.

3.1.4 Exhumation estimation

The several stages of uplift and erosion, together called as exhumation, making the Norwegian Barents Sea more complex with geological point of view. To understand the rock properties, to estimate maximum burial depth and the maximum temperature experienced by the source and reservoir rocks, it is essential to make correction for exhumation. By calculating the correct exhumation, the maturation history of the source and reservoir rocks as well as the timing of migration from the source rock can be calculated accurately.

When present day transition zone temperature was compared with the actual temperature, there was found a mismatch reflecting Hammerfest basin as an exhumed basin. In order to estimate the exhumation, a composite data from the 15 wells (Snøhvit, Albatross and Askeladd) was compared with published compaction curves; a first order linear velocity-depth trend based on Storvoll et al. (2005), a kaolinite-silt (50:50) kaolinite-smectite (80:20) and kaolinite (100%) curves from experimental laboratory compaction trends based on Mondol et al. (2009) Mondol et al. (2007) and a Cenozoic shale velocity depth trend line based on Japsen (1999). These published compaction curves based mainly on shale data points from several wells in the North Sea but can be used to calibrate exhumation estimation in Barents Sea even though the data from the Barents Sea show higher velocity-depth gradient due to extensive Cenozoic exhumation and thermal exposure of sediments over time leading to higher chances of quartz cementation.

The experimental compaction curve of brine saturated kaolinite-silt (50:50) mixture was used as a base for exhumation estimation. The choice of this compaction trend rather than end

members sand, silt or clay is due to the fact that mudrock in nature exist as a mixture of sand, silt and clay with varying fractions. The formations (Kolmule, Kolje and Knurr) in the wells under investigation are rich in shale and silt beds and are in the mechanical compaction domain.

Number of simple approaches has been used in estimating exhumation:

- The transition zone from mechanical to chemical compaction at present day burial depth is deciphered using rock physics cross plots.
- Volumetric shale fraction (Vsh) corresponding to mechanical compaction at present day burial depth is calculated across the entire area and cross-plotted as a function of depth with experimentally compacted kaolinite-silt (50:50) mixture curve.
- The difference along the depth (m) axis gives an estimate of the magnitude of exhumation, which natural samples have undergone, in that area.

3.1.5 Vsh calculation

The corrected exhumation are then, used to explain the digenetic effects on the rock properties in the Hammerfest basin. Moreover, all the published compaction trends which have been used, established on shale data points. Hence it is necessary to calculate shale volume in the studied wells.

All the published compaction trends which have been used to estimate exhumation based only on shale data points. Hence, it's necessary to calculate shale volume in the studied well to account for exhumation. In order to estimate shale volume (Vsh), the gamma ray curve has been used and for this purpose the gamma ray index (IGR) has been calculated by following equation:

$$I_{GR} = \frac{GR_{log} - GR_{min}}{GR_{max} - GR_{min}} \quad \text{(3.4)}$$

Where, I_{GR} is the gamma ray index, GR_{log} is the gamma ray reading of formation, GR_{min} is the minimum gamma ray (clean sand or carbonate) and GR_{max} is the maximum gamma ray (shales) (Asquith and Krygowski, 2004).

The linear relation of I_{GR} with shale volume (Vsh) is the first order estimation of shale volume. Different authors have given different nonlinear equations. In this study, there have been used two equations (Larionov, 1969).
The equation for unconsolidated rocks:

$$V_{sh} = 0.083(2^{3.7.I_{GR}} - 1) \quad \text{(3.5)}$$

And,

For consolidated older rocks:

$$V_{sh} = 0.33(2^{2.I_{GR}} - 1) \quad \text{(3.6)}$$

For shale volume calculation, cutoff 0.25≤shale≥0.75 has been applied as sand and shale data points respectively in the gamma ray log of all the studied wells (Fig. 3.5). This calculated Vsh has been then compared with published compaction trends in order to estimate exhumation in the study area.

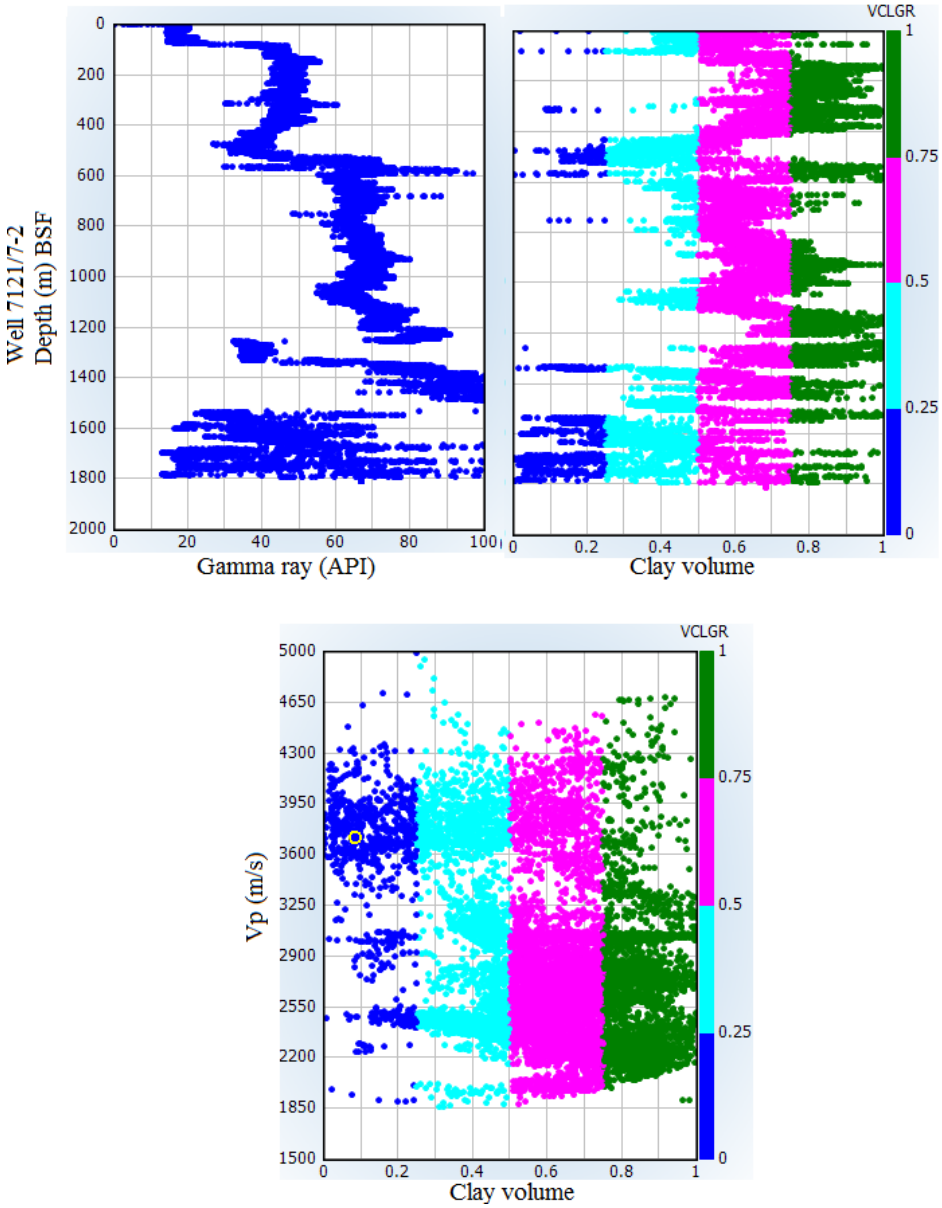

Figure 3.5: Vertical distribution of Vsh considering (0.25≤shale≥0.75) parameters for sand and shale contents in the 7121/7-2 well. The variation in the Vp represents the heterogeneity of shale volume.

3.2 Rock physics diagnostics

Rock physics is used to bridge the geological properties (porosity, mineralogy, grain sorting and fluid contents) with the seismic properties (elastic moduli, P-wave impedance and Vp/Vs ratio) (Storvoll and Brevik, 2008). The link between rock physics and different geological parameters that include cement volume, clay volume and degree of sorting, permits to

perform lithology substitution from the observed rock types at a particular well location to the rock types assumed to be present in the vicinity (Avseth et al., 2005). Out of the six wells, 7120/8-4 is the dry well and all others contain hydrocarbon mostly gas. Mineralogy of the grains and degree of sorting of the grains from east to west in the study area is changed due to the paleo-depositional environment (Sec, 2.4.2.1, Fig. 2.17). To compare the fluid and mineralogical effect on the rock physical properties, suits of six wells have been used to find the rock physics relation among the wells in the study area (Fig. 3.6).

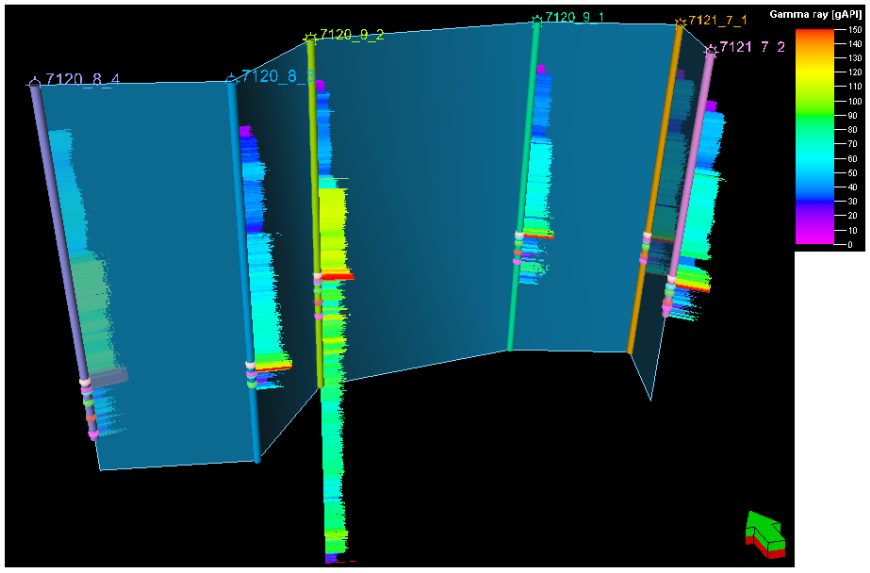

Figure 3.6: The number of wells in the study area (Albatross) used for rock physics analysis.

3.2.1 Porosity and density estimation

Due to the missing density log in the well logs, there was a need for calculating density and for that purpose the Gardner equation (Eq. 3.7 a) (Gardner et al., 1974) and Lindseth equation (3.7 b) (Lindseth, 1979) have been used involving Vp velocity.

$$\rho_b = 1.741 * V_p^{0.25} \ldots\ldots\ldots\ldots\ldots\ldots \text{(3.7 a)}$$

$$\rho_b = (Vp - 3460)/(0.308 * Vp) \ldots\ldots \text{(3.7 b)}$$

Where Vp is in km/s and ρ_b is in g/cc. The measured Vp has been used for calculating density.

And for the calculation of density porosity the following equation has been used

$$\emptyset_{Density} = \frac{\rho_{matrix} - \rho_{bulk(\log)}}{\rho_{matrix} - \rho_{fluid}} \ldots\ldots\ldots\ldots\ldots \text{(3.8)}$$

In the equation (3.8) the matrix density is quartz density assumed to be 2.65 g/cc whereas the fluid density is 1.1 g/cc assumed for brine density.

Neutron logs are porosity logs, which are used to measure the concentration of hydrogen in a formation. Since it measures the concentration of hydrogen in the formation, due to the gas

affect it measure less porosity of the formation as compared to the actual porosity. Moreover, due to the shale effect, it measures the higher porosity than normal.

Due to the uncertainties in the porosity and density logs, the average of the logs has been used during rock physics analysis with the help of Equation 3.9.

$$\emptyset_{Avg} = \sqrt{\frac{\emptyset^2_{density} + \emptyset^2_{neutron}}{2}} \quad \ldots\ldots\ldots\ldots\ldots\ldots (3.9)$$

A comparison of densities calculated from Vp using Gardner et al. (1974) and Lindseth (1979) equations and the measured density of the Stø Formation, in the well 7120/8-4 has been performed (Fig. 3.7).

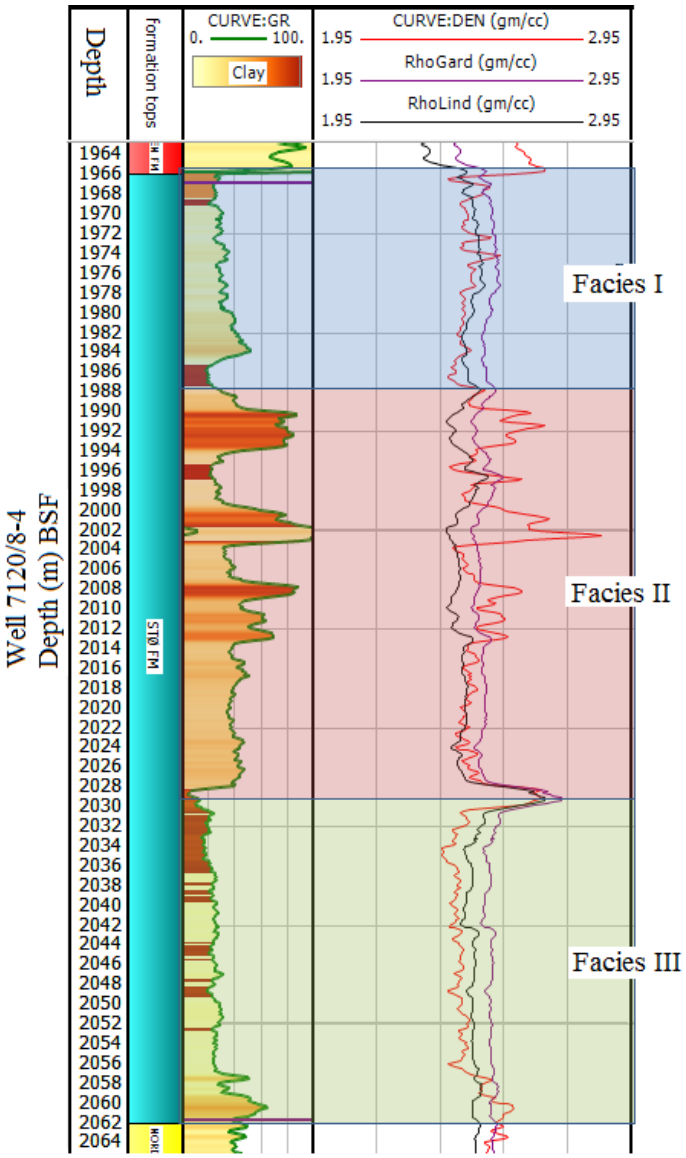

Figure 3.7: Comparison among measured and calculated Gardner et al. (1974) and Lindseth. (1979) densities for three different facies in the Stø Formation in well 7120/8-4.

3.2.2 Estimation of net-to-gross

There is a great focus on the hydrocarbon prediction from the heterogeneous reservoirs. One of the useful parameter in quantifying the heterogeneity of sandstones is net-to-gross ratio (Avseth, 2009). The net-to-gross ratio, which could be defined as the ratio of clean, permeable sand to that of reservoir thickness including intercalating impermeable shale as a whole, is an important factor in the reservoir characterization (Avseth, 2009). Avseth (2009) concluded that with the decrease in the N/G will be resulted in the increase in Vp/Vs regardless of the porosity, even though there is high gas saturation in the sands. There would be a dramatic decrease in the acoustic impedence with low porosities (i.e. decreasing N/G) but increase slightly when the sands have higher porosities values.

The Stø Formation is the main reservoir of the study area (Albatross discovery). The depositional environment and the quality of the Stø Formation are described in detail in Sec. 2.4.2. Assuming volume of clay <30% as a clean sand, N/G ratio of the Stø Formation for six studied wells has been given in the Table 3.1.

Table 3.1: Reservoir parameters of the Stø Formation in six studied wells.

Wells	Gross	Net	Net/Gross	Gas Saturation	Porosity
7120/8-3	86	73.87	0.86	Shows	17-15%
7120/8-4	94.90	75.17	0.79	Dry	15-14%
7120/9-1	55.80	52.70	0.94	80-90%	20%
7120/9-2	77.50	71.86	0.92	70-80%	20-18%
7121/7-1	57.50	54.51	0.95	70-80%	17-15%
7121/7-2	56.10	49.29	0.88	80-90%	20-18%

3.2.3 Saturation estimation

Pore fluid sensitivity in the reservoir can be affected by sandstone heterogeneity and microstructure. Hence, it is important to include these geological factors in the rock physcis analysis (Avseth, 2009). The onset of quartz cementation tends to occur at a depth which corresponds to 70-80^{0}C, changing the reservoir rock properties and reducing the pressure and fluid sensitivity of the sandstone (Avseth, 2009). This onset of quartz cementation will move the brine saturated sandstone data in Vp/Vs versus AI crossplot to an area of very low Vp/Vs where it is expected to plot hydrocarbon saturated sandstone data points. Before ploting such rock physics cross plot, it is recommended to know the initial saturation and fluid type to avoid ambiguities.

The theory behind the calculation of saturation is based on Archie's equation which is explained as below:

The water saturation (S_w) is determined from the resistivity of the rock partly saturated with formation water (R_t) and the resistivity of the rock fully saturated with water (R_0).

$$Sw = \sqrt[n]{R0/Rt} \quad \text{(3.10)}$$

Where n is the saturation exponent falls between 1.8 and 2.5. Since $R_0 = (F.\ R_w)$ we can obtain

$$Sw = \sqrt[n]{F.\,Rw/Rt} \quad \text{..... (3.11)}$$

The equation 3.11 equation is called as Archie's equation.

Water saturation has been calculated for the reservoir rock Stø Formation in the eastern and western well. The eastern well (7121/7-2) is gas saturated and the western well (7120/8-4) is a dry well (Fig. 3.8). Estimation of gas saturation in the six studied wells is given in the Table 3.1.

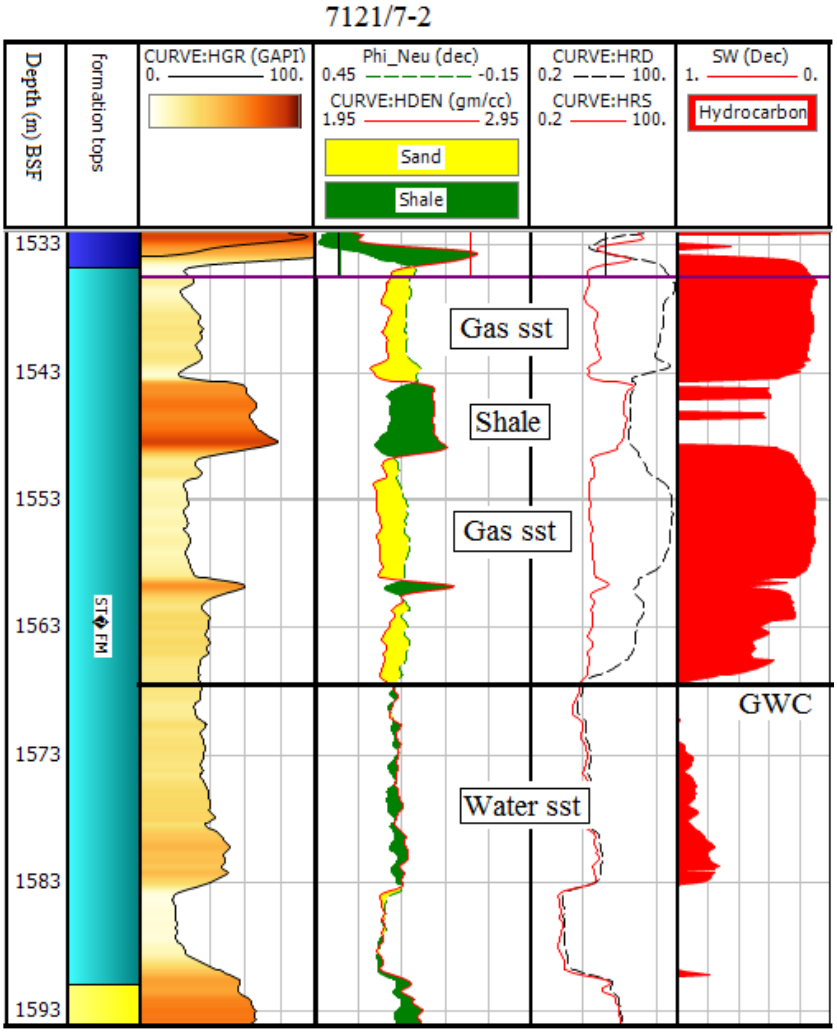

Figure 3.8: The estimation of saturation in the reservoir Stø Formation for the wells 7120/8-4 and 7121/7-2 with the help of resistivity log. The gamma log and neutron density crossover is also displayed.

3.2.4 Vs prediction

Biot-Gassmann model fails when applied to fine grained clastic rocks like mudstones due to the limitation, Castagna et al., (1985) derived an empirical relation between Vp and Vs velocity called mudrock line:

$$V_P = 1.16V_S + 1.36 \quad \text{(3.12)}$$

Castagna et al. (1993) introduced another least square fit relation between Vp and Vs velocities for the estimation of Vs from the P-wave velocity

$$Vs = 0.804Vp + 0.856 \quad \text{(3.13)}$$

Based on laboratory data, Hans (1986) introduced another empirical relation:

$$V_S = 0.794V_p - 0.787 \quad \text{(3.14)}$$

Where, velocity is in km/s.

Krief et al. (1990) suggested an excellent linear fit equation using square of the two velocities using following equation:

$$V_P{}^2 = aV_S{}^2 + b \quad \text{(3.15)}$$

Where velocities are in km/s and the constants a and b are determined by Krief et al. (1990) can be summarized in Table 3.2:

Table 3.2: The constant 'a' and 'b' contain values in different conditions.

Lithology	a	b
Sandstone (wet)	2.213	3.857
Sandstone (gas)	2.282	0.902
Sandstone (Shaley)	2.033	4.894
Limestone	2.872	2.755

The purpose of calculating Vs by using different equations is to approximate which of the calculated Vs closely fits the measured Vs and could be used for rock physics analysis in the area (Fig. 3.9).

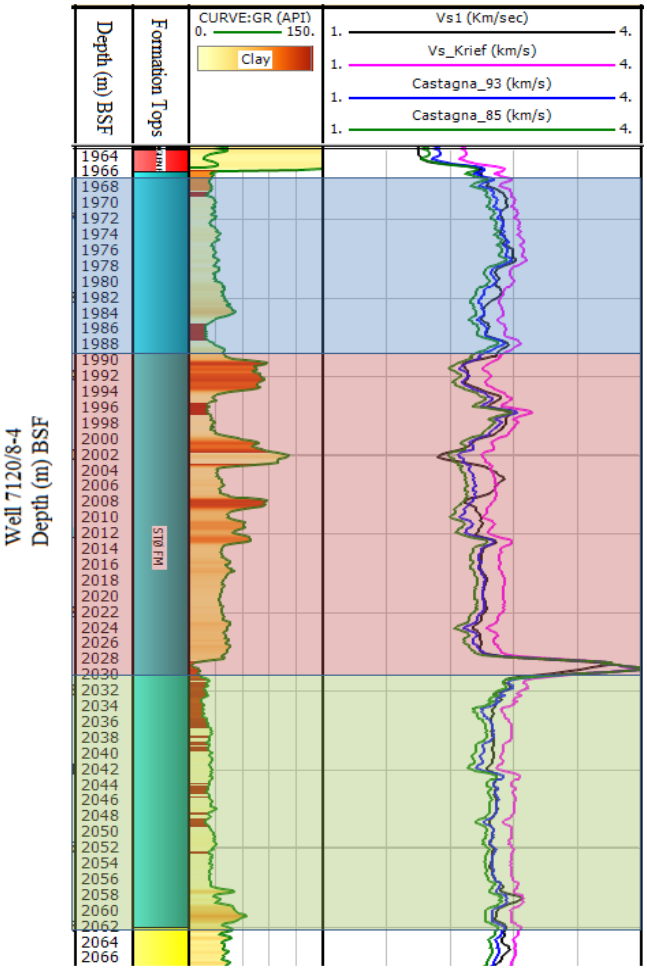

Figure 3.9: Vs comparison in the Stø Formation of 7120/8-4 well.

Shear wave velocity (Vs) is an integrated tool to analysis the rock physics properties; also it is, along with shear modulus (μ), very sensitive for cementation and fluid discriminator. So with the help of Vs / μ, the transition zone could also be identified. Only one well 7120/8-4, out of six wells, contains shear velocity measurement within the reservoir zone, which is below the transition zone from mechanical to chemical compaction. By using measured Vp-Vs data points from the well 7120/8-4, the empirical equation have been derived which is used to calculate Vs for other wells (Fig. 3.10) (Eq. 3.16). The equation is given below:

$$Vs = 0.80Vp - 0.916 \quad \text{(3.16)}$$

Where Vp and Vs are given in km/s and $R^2 = 0.92$. The calculated Vs has been used to calculate shear modulus (μ) for other wells by using following equation:

$$\mu = \rho V_s^2 \quad \text{(3.17)}$$

Where, Mu (μ) is in GPa, ρ is kg/m^3 and V_s is m/s. After calculating shear modulus, it was used to identify the transition zone of different wells in the study area.

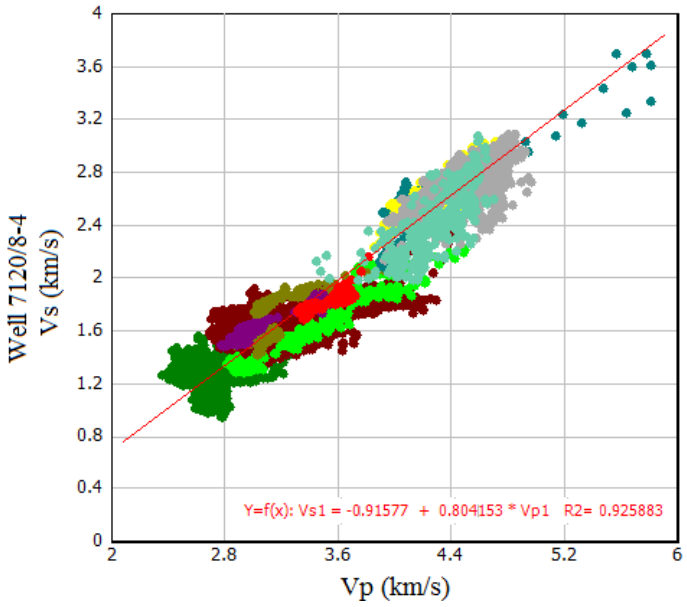

Figure 3.10: Vp-Vs cross-plot of all the data points from the well 7120/8-4, empirical equation along with R2 is also given.

3.2.5 Construction of RPTs

Ødegaard and Avseth (2004) first introduced the technology of rock physics templates (RPT's). By combining depositional and diagenetic trends with Gassmann fluid substitution, charts or templates of rock physics can be generated for the prediction of lithology and hydrocarbons by using well logs and seismic data. The RPT's are basin specific and depends on the local geological factors and these factors include lithology, mineralogy, burial depth, diagenesis, pressure and temperature. These factors should be in mind while generating RPT's for the local basin (Avseth et al., 2005). The commonly used RPT is the acoustic impedance and Vp/Vs ratio cross-plot used for lithology and fluid indicator (Fig. 3.11) (Avseth et al., 2005), others include shear impedance and AI, elastic impedance (EI) and AI, Lame's parameter and shear modulus (μ), etc. (Avseth et al., 2005).

Figure 3.11 comprises a background shale-trend line, a brine-sand-trend line, and curves for increasing gas saturation as a function of porosity on a rock physics template of Vp/Vs versus AI cross-plot domain. The black arrows are showing (conceptually) the effects of various geologic trends:

1) Increasing shaliness,
2) Increasing cement volume,
3) Increasing porosity,
4) Decreasing effective pressure,
5) Increasing gas saturation.

The ambiguity of interpretation is noticeable. For example, increase in shale content can be misinterpreted with decrease in effective pressure or nature do not follow the increasing or decreasing trend exactly like these trend lines etc.

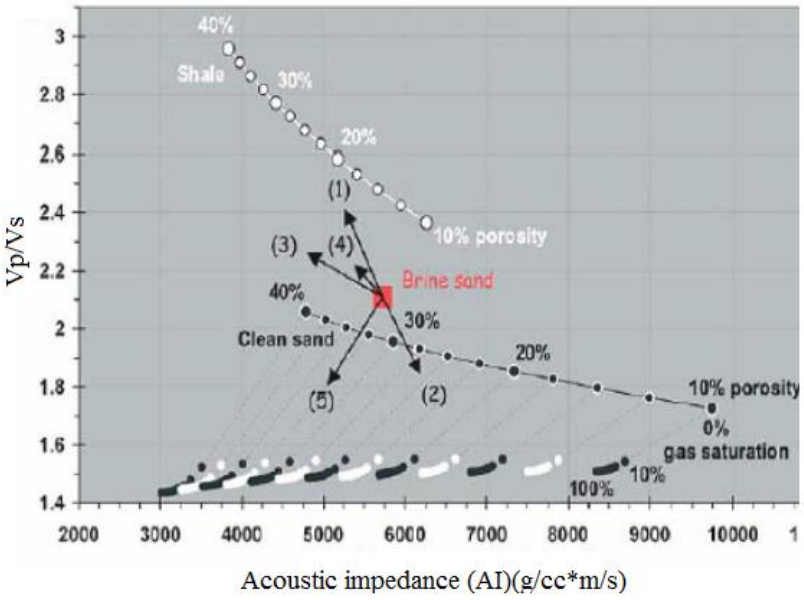

Figure 3.11: Rock physics template (RPT) cross plot between AI and Vp/Vs ratio (Modified by Avseth et al., 2005).

The initial step in creating a template is to determine the appropriate rock physics model. Theoretical rock physics models are calibrated and validated using the local rock parameters considering local geology and well log data. Well log data are analyzed to define the reservoir and source rock and evaluate reservoir properties. Then the lithology and fluid content of the rock is diagnosed by superimposing theoretical rock physics curve. It is important to map the data to a common fluid during creating templates, otherwise the effect of pore fluid and rock frame become mixed (Milovak, 2009).

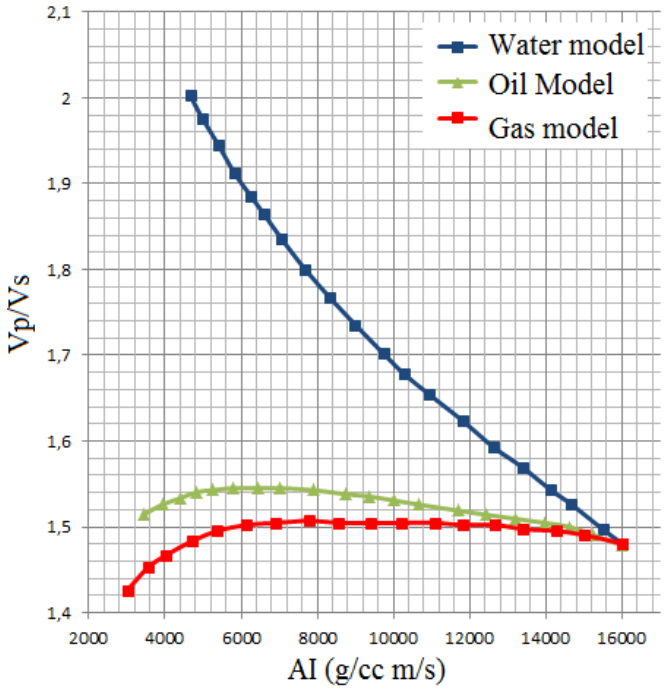

Figure 3.12: Rock physics template (RPT) cross plot between AI and Vp/Vs ratio.

The following steps are used to build a template for the study area (Fig. 3.12):

- Estimate dry bulk and shear moduli at the initial porosity (φ_c = 40%), applying Hertz-Mindlin theory.
- Used Carmichael (1989) quartz bulk and shear modulus as a zero porosity mineral point.
- Interpolate between the two-end members using modified Hashin-Shtrikman upper bound at different porosities.
- Perform Gassmann fluid substitution to calculate effective moduli at different fluid saturations.
- From calculated moduli and density at different saturations and porosities, calculate Vp and Vs which later use for analysis in different cross-plots to emphasize fluid and lithology component.

3.2.5.1 Gassmann fluid substitution theory

The applications of fluid substitution are widespread from seismic monitoring to AVO analysis and modeling. The basic function of this technique is to estimate the insitu fluid scenario and the model 'what-if' scenario. The Gassmann-Biot (Gassmann, 1951; Biot, 1956) theory calculates the resulting increase in effective bulk modulus, K_{sat} of the saturated rock using the following equation:

$$\frac{K_{sat}}{K_0 - K_{sat}} = \frac{K_{dry}}{K_0 - K_{dry}} + \frac{K_{fl}}{\emptyset(K_0 - K_{fl})} \quad \text{..... (3.18)}$$

$$\mu_{sat} = \mu_{dry} \quad \text{..... (3.19)}$$

where K_{dry}, $K_{sat}$are the effective bulk modulus of dry rock and the rock with pore fluid, K_0 is the bulk modulus of mineral material making up rock, K_{fl} is the effective bulk modulus of pore fluid, Φ is the porosity, μ_{dry}, μ_{sat} are the effective shear modulus of dry and of the rock with pore fluid. Gassmann fluid substitution model give the opportunity to estimate the seismic P-wave, S-wave velocities and density of the target horizons under different set of conditions such as porosity, pressure, mineralogy and pore fluid saturation etc.

Gassmann's equation assumes a homogeneous mineral modulus and statistical isotropy of the pore space but is free of assumptions related to the pore geometry. The basic assumptions about the porous fluid-filled rock are:

- All pores are connected (i.e. open porosity), as a result of this, the fluid offers no resistance to shear deformation and therefore, the effective dry shaer modulus is same as that of effective wet shear modulus.
- All grains have the same physical properties (effective mineral grains)
- The pore fluid is homogenous and fully saturates the pore volume (effective fluid)
- Gassmann equation is only valid at sufficiently low frequencies because there is dispersion effects associated with high frequencies.

The one most common problem in using the Gassmann's relations to predict saturated rock moduli from dry-rock moduli or vice versa is that to predict the change that result when one

fluid is replaced with another. We can solve this problem simply use this equation twice like from initial to dry state and from dry state to any new fluid saturated state. We can algebraically eliminate the dry-rock moduli from the equation and relate the saturated-rock moduli K_{sat1} and K_{sat2} in terms of the two fluid bulk moduli K_{fl1} and K_{fl2} as follows:

$$\frac{K_{sat1}}{K_0 - K_{sat1}} - \frac{K_{fl1}}{\emptyset(K_0 - K_{fl1})} = \frac{K_{sat2}}{K_0 - K_{sat2}} + \frac{K_{fl2}}{\emptyset(K_0 - K_{fl2})} \quad \text{..... (3.20)}$$

3.2.5.2 FRM parameters

Pore fluids have the ability to change of the rock properties (Vp, Vs & density) as well as seismic properties. In order to check the change in fluid properties with varying pore fluid saturation, Hampsson Russell calculator has been used using different parameters by utilizing well 71208/4 (Fig. 3.13).

Biot-Gassmann method has been applied by using Fluid Replacement Modeling (FRM) in Hampsson Russell in order to investigate 'what if' scenario for different fluid type and saturation. Because of 0.79 N/G ratio in the well 7120/8-4, both quartz (79%) and clay (21%) used for mineral matrix. The matrix properties used in this study are shown in the Table 3.3. Pressure effect has not been considered due to which the input porosity is set equal to output fluid substituted model.

Table 3.3: Quartz and clay parameters according to Carmichael (1989) (Source: Mavko et al., 2009).

Mineral	Bulk modulus (GPa)	Shear modulus (GPa)	Density (g/cc)	Vp (km/s)	Vs (km/s)
Quartz	37	44	2.65	6.05	4.09
Clay	6.90	20.90	2.58		

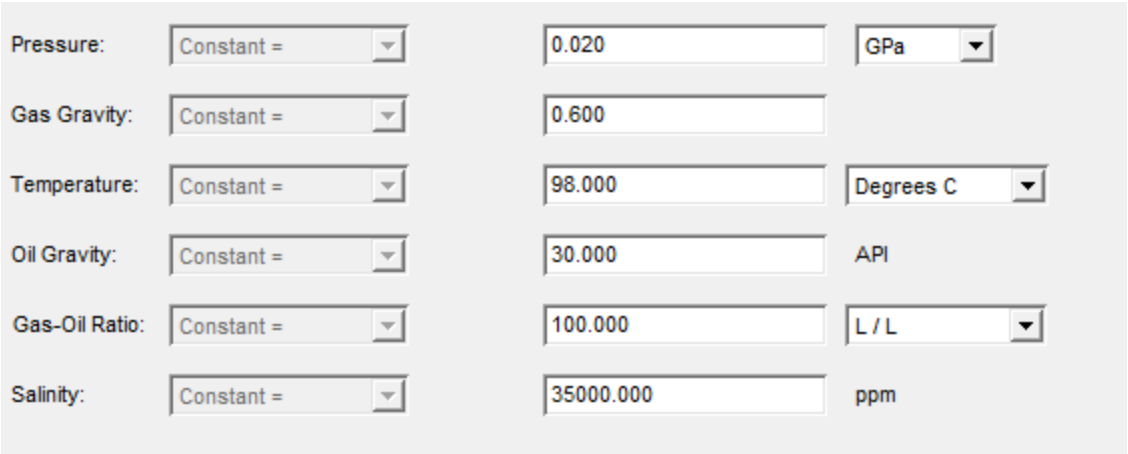

Figure 3.13: Values at reservoir conditions in the well 7120/8-4.

	Oil	Gas	Brine	Pore Fluid	
Calculated Density:	0.7610	0.1204	0.9948	0.9948	(g/cc)
Calculated Modulus:	0.7436	0.0403	2.5933	2.5933	(GPa)
Saturation:	0.00	0.00	1.00	[frac]	

Figure 3.14: Fluid properties used for fluid replacement modeling (FRM).

The fluid properties (Fig. 3.14) represent the default values in the HR software based on Batzle and Wang (1992). For simplification, homogeneous saturation method has been used for the calculation of fluid properties in the HR. These parameters are set to be constant and used for different fluid saturations.

3.2.6 The rock physics cement models

Rock physics cement models can be used to interpret sonic and seismic velocities in terms of reservoir parameters (Fig. 3.15). Figure 3.15 shows an example of such cross plot between porosity versus elastic modulus i.e. bulk or shear modulus (Avseth, 2010). Sandstone microstructure and reservoir heterogeneity due to cementation can affect the pore fluid and stress. Due to this reason, it is important to include these geological factors in the rock physics analysis. We can infer (diagnose) the rock texture with the known values of porosity and corresponding elastic modulus.

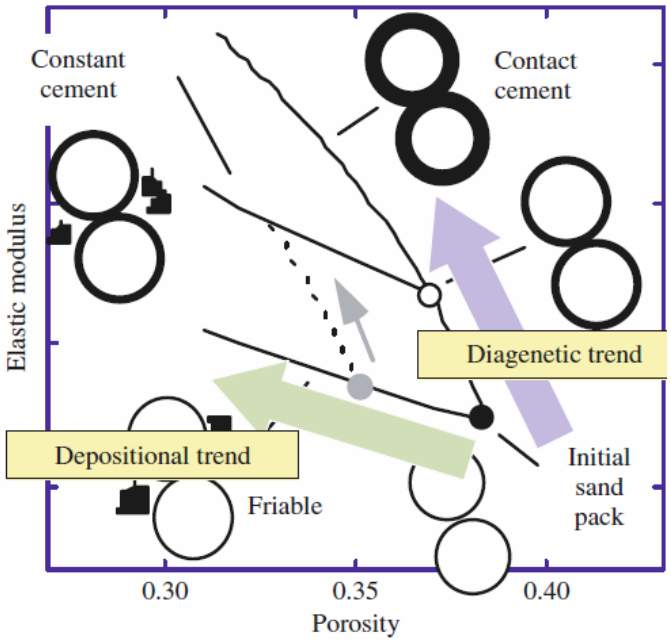

Figure 3.15: Linkage of rock microstructure to elastic properties through rock physics (Avseth, 2010).

There are several models that explain the microstructure and the texture of the rock, i.e. to predict the type of the rock and microstructure from the seismic velocities. Dvorkin and Nur (1996) introduce the cement models. This diagnostic can be performed by selecting an effective medium theoretical model curve to trend in the data, with the assumption that the microstructure of the sediments matches best with the theoretical model used. The effective

way to do this is to define the elastic properties of the end members. The rock has the properties of the minerals at zero porosity but at the high porosity limit, elastic contact theory defines the elastic properties of the rocks. Then there is need to interpolate the data between these two end members by using either upper or lower Hashin-Shtrikman bounds (Fig. 3.14). The upper bound used to explain the theoretical stiffest way to the mix lithology grains which are load bearing along with pore filling materials whereas theoretical softest way can be explained by the lower bound to these mix lithology. In other words, the contact cement is the good representative for upper bound while the lower bound describes the frible sand model explain mostly sorting of sand composits.

The following Figure 3.16 is showing the three cement models used for rock physics analysis. For mineral points, Carmichael (1989) pure quartz grain velocity and modulus have been used (Table 3.3). Constant and contact cement lines have been digitized from Avseth et al., (2010) and interpolate it upto mineral points (φc = 0) using quartz bulk and shear modulus.

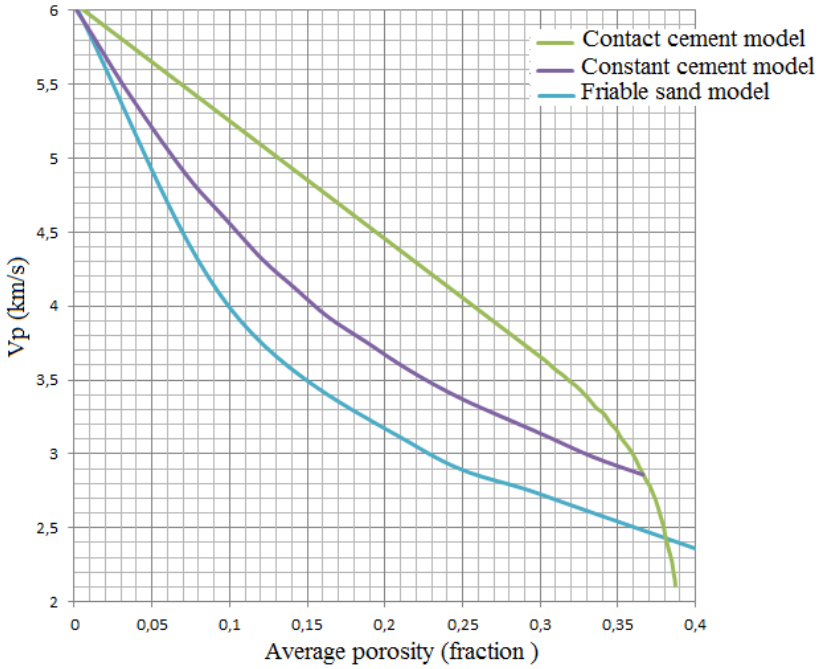

Figure 3.16: Cement models of pure quartz at water saturated conditions. The cement fraction is 2% in the constant cement model.

3.2.6.1 The friable-sand model

For high porosity sands Dvorkin and Nur (1996) introduced the friable sand model or unconsolidated sand model, which describes the velocity-porosity relation with the degree of sorting. This model describes how the well-sorted end member, which is the representation of well-sorted packing of similar grains whose elastic properties can be determined by the elasticity at the grain contacts, modified with additional smaller grains filled the pore space. The typical critical porosity Φ_C for well-sorted end member is around 40 %. The poorly sorted sands are represented by friable-sand model. Addition of smaller grains deposited in the pore spaces for well-sorted end member can disturb the degree of sorting by decreasing the porosity, there would only be slight increase in the stiffness of the rock (Avseth et al., 2005).

3.2.6.2 The contact cement model

With increasing burial depth, the sandstones will become cemented and this cement could be diagenetic quartz, calcite, albite or other minerals. Cementation increases the stiffness affects because of glued grains contacts. In this model, it is assumed that the porosity reduces from the initial porosity of a sand pack because of the uniform cementation on the surface of the grains. The contact cement increases the stiffness of the grains by strengthening of the grains contacts. There would be large velocity increase along with minor porosity decrease due to initial cementation effects (Avseth et al., 2005).

3.2.6.3 The constant cement model

This model is introduced by Avseth et al. (2000), assuming that the sands with varying sorting can have same amount of contact cement. Non-contact pore-filling materials are basically the cause of porosity reduction. This model is the combination of the contact cement model in which porosity decreases from the initial sand pack porosity to porosity $\emptyset b$ because of the contact cement deposition and the friable sand model where the porosity reduces from $\emptyset b$ due to the deposition of solid grains away from the grains contacts. The amount of cementation depends often on the depth while the sorting is associated to lateral variation in the flow energy during the deposition of the sediments. In accordance with these cases, we can refer to this model as a constant depth model for the clean sand, although there could be lateral variation in the velocity due to the local cementation source (Avseth et al., 2005).

3.2.7 Cement volume estimation

Changes in the physical properties with the increasing depth are because of diagenetic processes which mainly depend on the primary sediment composition (Bjørlykke et al., 2004). Quartz cement is the main diagenetic mineral which controls the reservoir quality in the deeply buried quartz rich sandstones in many basins (Walderhaug and Bjørkum, 2003). The initial cement dramatically changes the AVO properties of the reservoir and causes in reduction of pressure and fluid sensitivityof the sandstones (Avseth et al., 2008). The change in the gradient of velocity is due to the rapid grain framework stiffening because of small amount of quartz cement at the grain contacts (Marcussen et al., 2010). At tempertarue higher than 70-80ºC, the velocity shows correlation with small amount of quartz cement. The relatively small amounts of cement (1–5%) that may increase the velocity due to grain framework stiffening, will not affect the density and porosity much because the rock volume is not changed considerably. The porosity in quartz-rich sandstones is mainly controlled by quartz cementation at large burial depths (Marcussen et al. 2010). The volume of quartz precipitated in a given volume of rock is mainly controlled by two factors (Walderhaug, 1996) (i) the precipitation rate integrated over time and (ii) the surface area of detrital quartz grains that are exposed to the formation brine such that silica may precipitate.

The quartz cement is obtained mainly from dissolution at stylolites and available specific surface area. These stylolites are the only internal source quartz cement with a clay poor unit which developed from clay rich or seldomly micaceous or organic matter rich laminae (Walderhaug and Bjørkum, 2003). There is also a correlation between distance to nearest stylolite and the quartz cement volume. Therefore, quartz cement shows 10-20% (Blue eclipse) volume for the samples which are located a centimeter or less from a stylolite which

with the increasing distance 3-20cm, quartz contents would be 4-10%. The quartz volume will be decreased to 5% (red eclipse)as the distance from the nearest stylolite increases to 25 cm and then remain constant as the distance to nearest stylolite increases to almost 2 m (Fig. 3.17) (Walderhaug and Bjørkum, 2003).

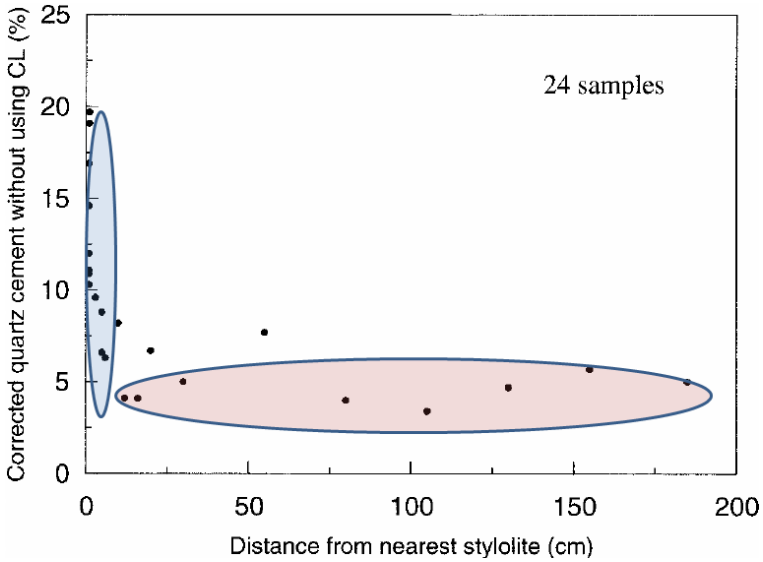

Figure 3.17: Relationship between quartz cement volume and the distance from nearest stylolite (Modified from Walderhaug and Bjørkum, 2003).

CHAPTER 4
Compaction and Evolution of Rock Properties

It is important to understand that the rocks are controlled by compaction during burial, when establishing a link between geology and rock physics. Effect of compactional process on sediments will vary depending upon the original mineralogical composition and texture of the sediments (grain size, shape, sorting, and clay type/amount) which will be different significantly in different depositional environments (fluvial, shallow marine, deep marine) (Sec. 2.4.1, 2.4.2). Rate of sediment burial, temperature variation with depth and time, overpressure, exhumation (uplift and erosion) and types of pore fluid in the sediments are the factors should be taken into account while discussing compaction.

In this chapter, an attempt has been made to understand the changing rock properties as a function of burial depth under the effect of compaction (both mechanical and chemical) using well logs and several published depth trends (e.g. velocity-porosity, density-depth and porosity-depth) for pure (sand and shale) and mixed (sand-clay, silt-clay mixtures) lithologies.

4.1 Results

4.1.1 Rock properties versus depth trends

As we discussed earlier, compaction of sediments can be divided into two types; mechanical compaction (MC) which if stress dependent and chemical compaction (CC) dependent on temperature and time. Due to combine effect of MC and CC rock properties such as velocity, density and porosity change as a function of burial depth. The general trend observed in all six wells in the study area, is the increase in the velocity and density with burial depth and there is reduction in porosity accordingly with some exceptions at different zones may due to lithologic variations, pore fluid and overpressure (Fig. 4.1). The Vsh estimated from the gamma ray logs is used, as a lithology control to explain the deviation of velocity, porosity and bulk density versus depth compared to published trends.

The demarcation of transition zone (TZ) for all the wells is based on the Vp-depth trend. The transition zone is identified in the Knurr Formation for all the wells with varying depth. In correlation with gamma ray log it is assured that the change in the Vp within the Knurr Formation is not due to the change in the lithology. A zone of low Vp (velocity inversion), just beneath the transition zone, is observed with low bulk density and very high gamma ray value corresponds to the major source rock (Hekkingen Formation) of the study area in all six wells (Fig. 4.1). The Kviting Formation in the wells 7120/8-3, 7121/7-1 and 7121/7-2 reflects high Vp value of upto 4200 m/s within a shallow depth of 1000 m. The density and resistivity logs response is also high for this formation. The lower part of the Kolmule Formation in the well 7120/9-2 has a higher Vp compared to the formations above it with high density and high deep resistivity. The Vp log response of Kolje Formation in the well 7120/8-4 is unique in that sense it reflects high Vp of 4400 m/s in the upper part of the formation at a depth of 1500 m BSF, then the middle part of the formation follows the normal Vp trend and lower part of the formation again has higher Vp. The general porosity trend of the Kolje Formation is decreasing with increasing depth.

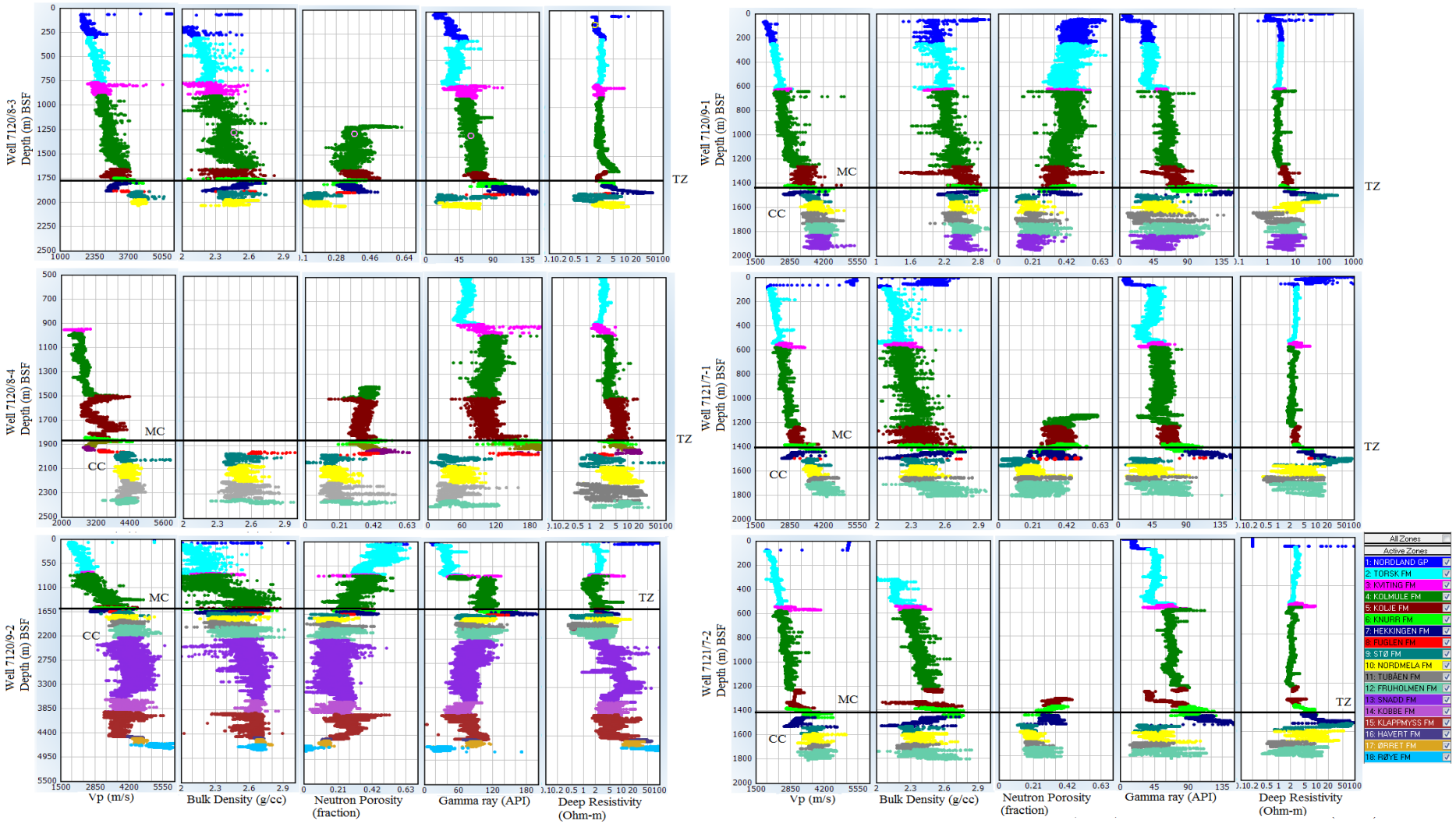

Figure 4.1: Compaction trends observed in all the six wells.

The well 7120/9-2 is selected as a reference well for the detail investigation of compaction and its influences on rock properties. The reference well 7120/9-2 has most data coverage in terms of depth (deepest penetration within the six studied wells) data (Ch. 2, Table 2.1).

4.1.2 Vp-depth trend in reference well 7120/9-2

The Vp response versus depth in the reference well 7120/9-2 shows a general increasing trend (Fig. 4.2) but at the end approximately 3300 (m) BSF velocity inversion can be observed. Transition zone between MC and CC can be marked based on abrupt change in Vp-depth trend at depth 1562 (m) BSF. Two trends have been marked (shown as solid black and red lines) for mechanical and chemical compactions (Fig. 4.2). The solid black line representing mechanical compaction zone ranging approximately from 0 (m) BSF to a depth of 1600 (m) BSF, on the other hand chemical compaction zone ranging from approximately 1700 (m) BSF to a total depth of 4640 (m) BSF.

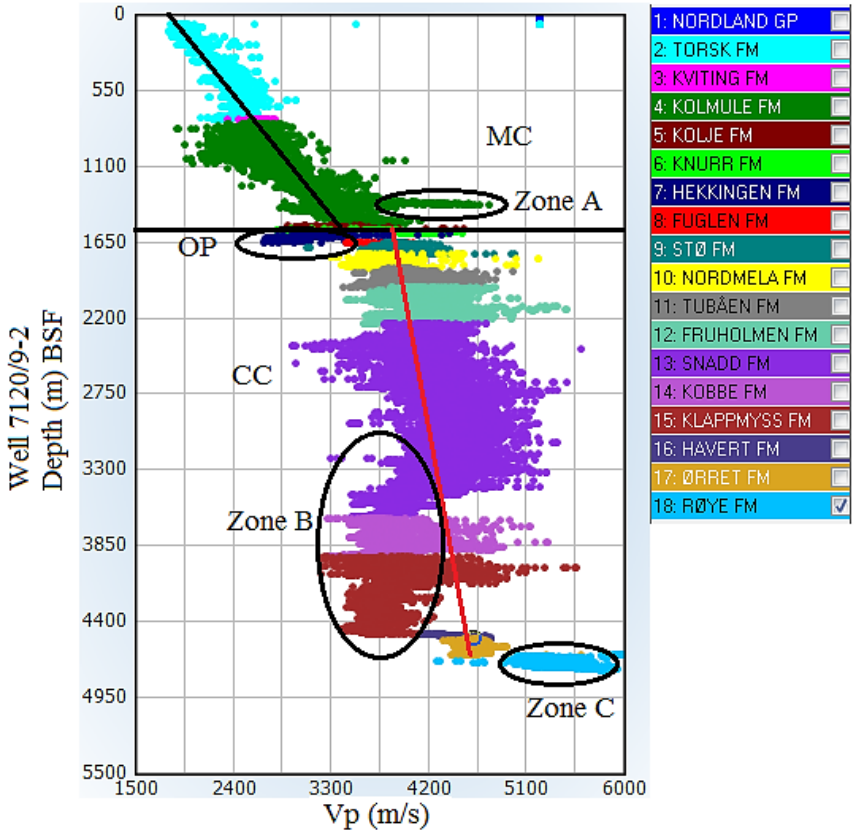

Figure 4.2: Vp-depth trend for the reference well along with anomalous zones.

Vp-depth trend in the mechanical compaction zone is less than 3500 m/s but there are some zones in the mechanical compaction which show higher velocity than normal at a shallow burial depth of approximately 1400 (m) BSF in the Kolmule Formation, marked by a zone A may represents carbonate. An overpressured (OP) zone is also observed in the reference well just below the transition zone which indicates the major source rock (Hekkingen Formation) in the study area. In the chemical compaction zone, there is initially increase in Vp-depth trend but velocity reversal indicated by zone B, is also observed whereas zone C again showing increase in the Vp-depth trend (Fig 4.2).

4.1.3 Transition zone between MC and CC

In order to understand the transition from mechanical to chemical compaction, Vp and density logs from all the six wells were plotted against depth (BSF) (Fig. 4.3). An experimental compaction trend (50:50 silt-clay mixture) published by Mondol (2011) has been taken into account as areference curve represents normal compaction incorporated in the VP-depth and density-depth crossplot for comparison. Only shale data points sorted by Vsh≥0.75 have only been considered for compaction analysis to find a generalized compaction trend for shallow mechanically compacted shale dominated sediments. In well 7120/8-4 density log available only in the deeper part that represents chemical compaction (Fig. 4.3). All the remaining five wells (7120/8-3, 7120/9-1, 7120/9-2, 7121/7-1 and 7121/7-2) have full density log coverage. Vp is available in all the six studied wells.

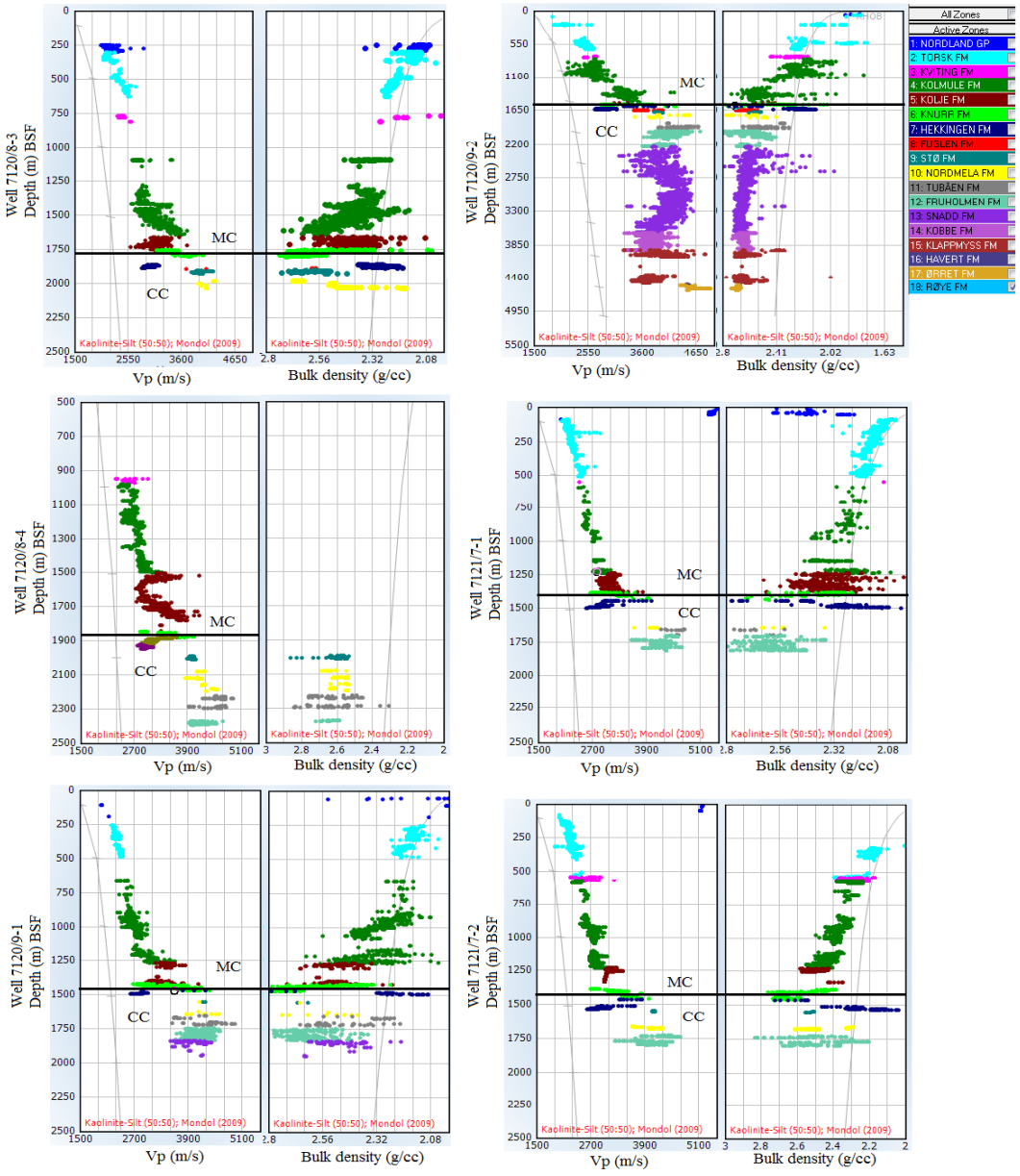

Figure 4.3: Depth versus Vp and density cross plots containing only shale data points along with kaolinite-silt (50:50) (Mondol, 2011) experimental curve in all the wells.

The transition from MC to CC zone has been marked on the basis of Vp-depth trends of the study area. The transition has been made based on sharp increase in the Vp for a given lithology at present burial depth (Fig. 4.3). The transition zone varies with respect to each other depending upon the structural configuration and geometry of the Hammerfest basin. The transition from MC to CC in all six wells observed within the Knurr Formation. Above and below the TZ, a significant change in the Vp can be observed (Fig. 4.3). The TZ can be marked clearly on the basis of abrupt change in Vp-depth trends in all the wells (Fig. 4.3).

Table 4.1: The depth of TZ in the Knurr Formation within the six studied wells.

Wells	TZ depth (m) BSF	Formation
7120/8-3	1772	Knurr Formation
7120/8-4	1864	Knurr Formation
7120/9-1	1443	Knurr Formation
7120/9-2	1562	Knurr Formation
7121/7-1	1416	Knurr Formation
7121/7-2	1417	Knurr Formation

The Knurr Formation has been zoomed carefully to measure accurate depth of the transition zones in the six wells (Fig. 4.4, 4.5, 4.6). The gamma ray, Vp, bulk density and deep resistivity logs have been taken into account to identify TZ (Fig. 4.4, 4.5, 4.6). Gamma ray log has been used as a purpose to check the lithological variation within the Knurr Formation as well as to investigate the change in Vp-depth trends due to lithologic change or initiation of quartz cement in the transition zone among all the wells. Deep resistivity log has also been analysed to check the presence of organic matter in the Knurr Formation. The top of the Knurr Formation (marked by vertical black eclipe) in most of the wells show very high gamma ray reading with low velocity and density may represent organic rich shale (Fig. 4.4, 4.5, 4.6) except in the well 7120/8-3.

Gamma ray log showing more or less similar lithological variation in the Knurr Formation among all the wells but the velocity variation in this formation is rapid at the transition zone. The Vp-depth gradient in the mechanical compaction zone marked by black line in all the wells is analogous (Fig. 4.4, 4.5, 4.6). This Vp-depth trend changes suddenly after crossing TZ marked by a new trend (red line). The transition zone depth is measured from BSF and is different for different wells except in two wells 7121/7-1 & 7121/7-2 where we observed almost similar depth (Table 4.1). The maximum transition zone depth is observed to be 1864 (m) BSF in the western most well 7120/8-4 and the minimum TZ depth values 1416 and 1417 (m) BSF are observed in the two eastern most wells 7121/7-1 and 7121/7-2.

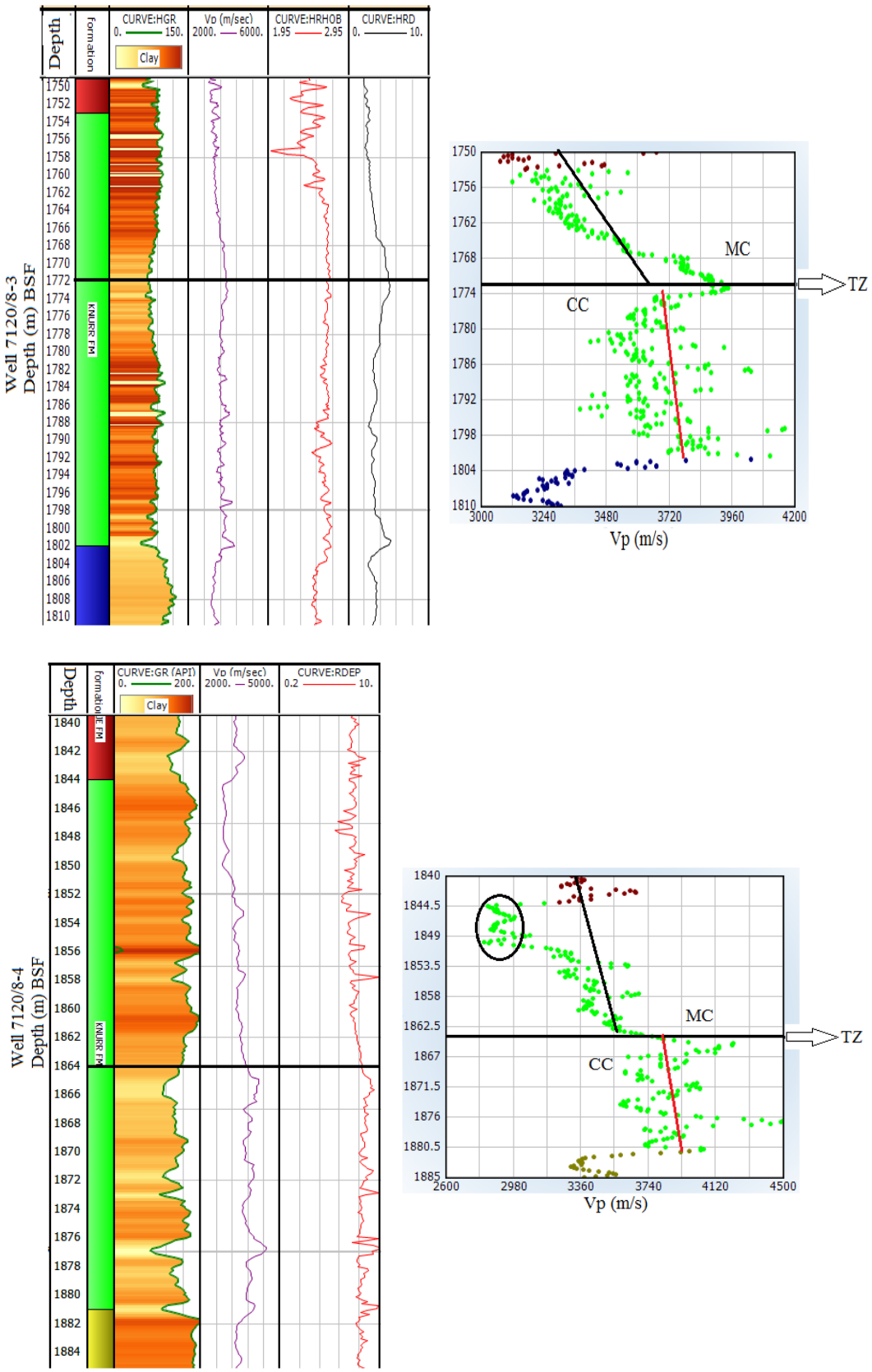

Figure 4.4: The transition zone in the Knurr Formation (black line) in wells 7120/8-3 and 7120/8-4. To find TZ gamma ray, Vp, bulk density and deep resistivity logs are compared for the Knurr Formation.

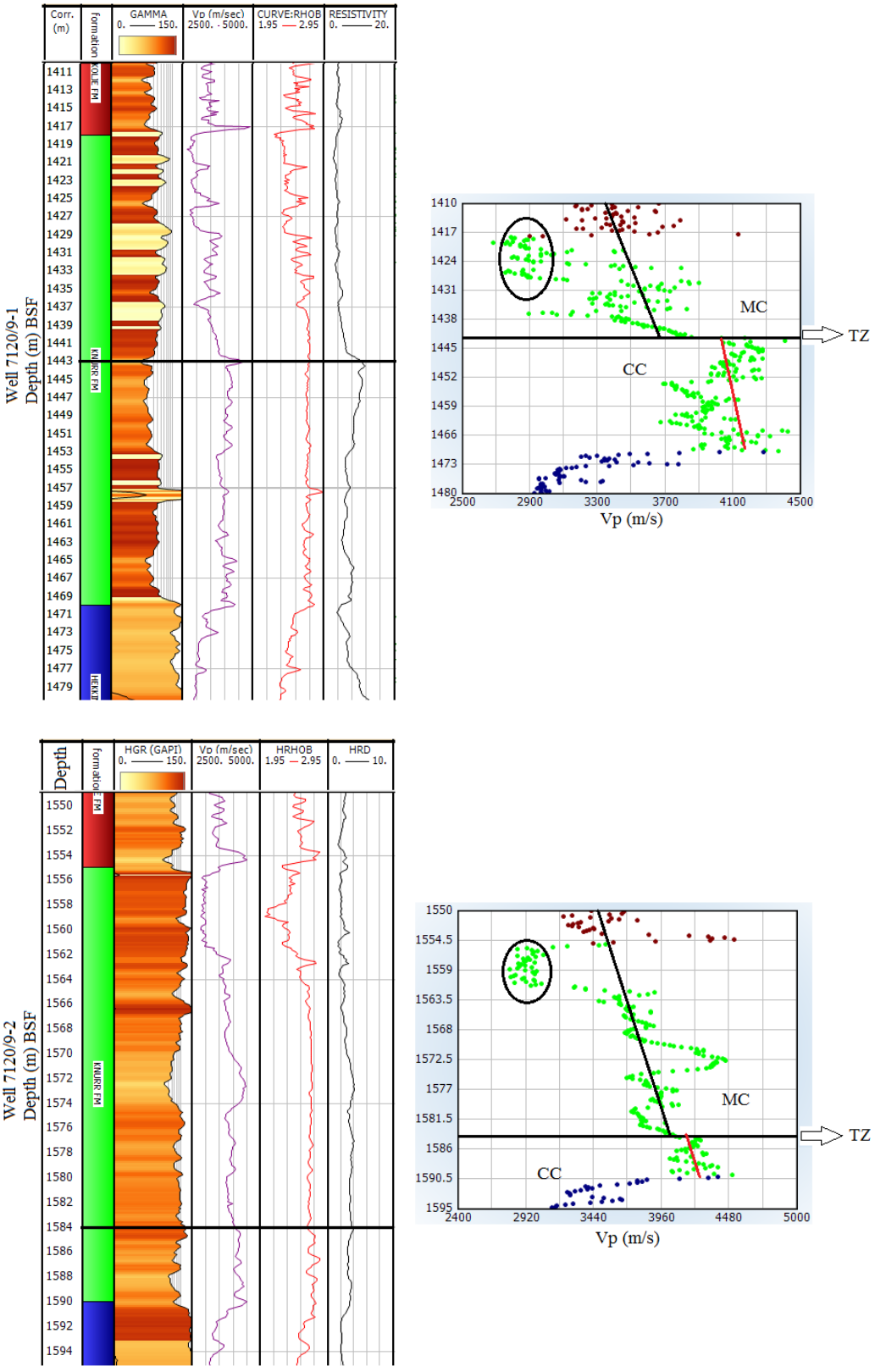

Figure 4.5: The transition zone in the Knurr Formation (black line) in wells 7120/9-1 and 7120/9-2. To find TZ gamma ray, Vp, bulk density and deep resistivity logs are compared for the Knurr Formation.

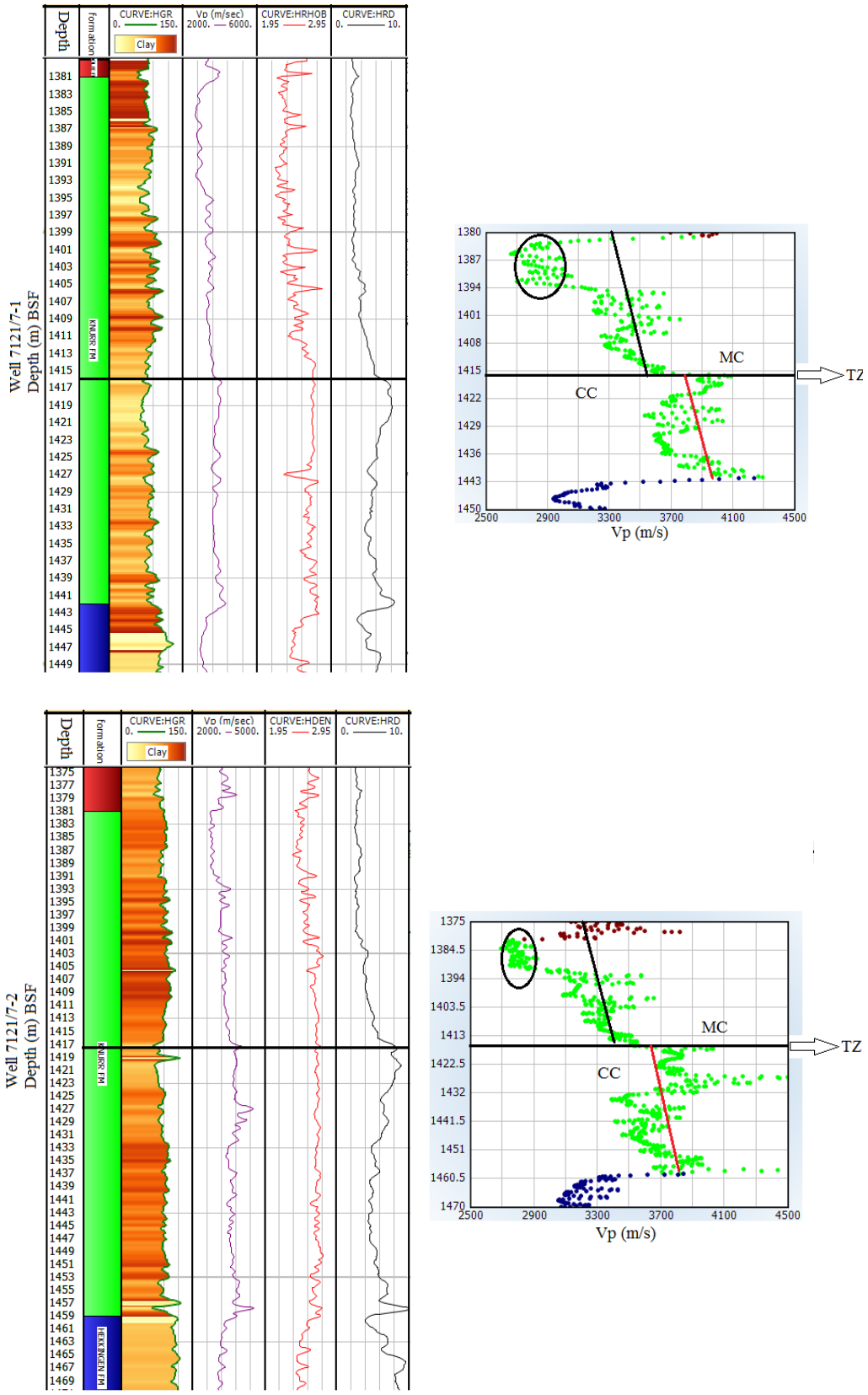

Figure 4.6: The transition zone in the Knurr Formation (black line) in wells 7121/7-1and 7121/7-2. To find TZ gamma ray, Vp, bulk density and deep resistivity logs are compared for the Knurr Formation.

Velocity-density crossplot, being a good discriminator for mechanical to chemical compaction zones, has been plotted in the Figure. 4.7. Two distinct clusters can be seen based on Vp-density cross plots representing mechanical and chemical compaction zones whereas a vertical eclipse marks the transition between these two zones. Different formations are being shown by different colors. Five out of six wells have been used for these cross plots because the well 7120/8-4 does not contain density data related to mechanical compaction zone. The cluster belongs to mechanical compaction zone is showing low Vp and density values whereas the cluster representing chemical compaction zone is displaying high Vp and density values. The TZ is observed within the Knurr Formation. The green data points in the Figure 4.7 are showing the transition from MC to CC. After the transition there is almost no density variation (green data points), but the velocity is increasing dramatically within this narrow range of density data points.

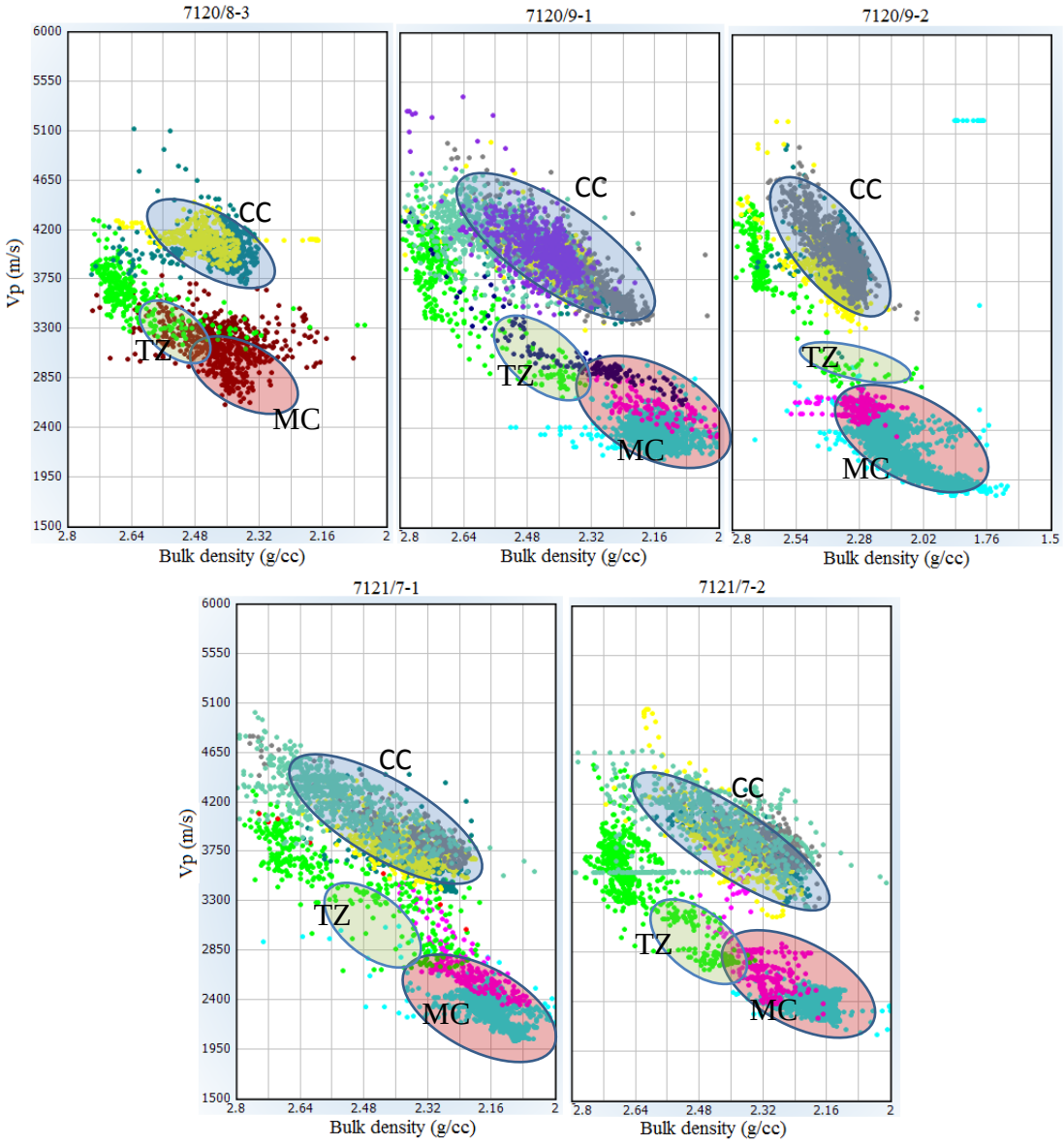

Figure 4.7: Vp-bulk density crossplots, for all six wells, are showing two different clusters of all the data points where, the green data points represent the data from different wells identified by the transition zone.

4.1.4 Effect of temperature on chemical compaction

It is important to comprehend how geologic properties of the rocks are controlled by compaction (both MC and CC) during burial. As stated earlier, the compaction process affected the sediments depending upon the original composition and texture (grain size, shape, sorting, clay type etc) which is different in different depositional environments.other factors should also be taken into account in compaction study are burial rate, temperature variation as a function of depth and time, overpressure, exhumation (uplift and erosion) and the types of pore fluid in the sediments. Time and temperature are the exponentially related to quartz cementation, the most important process in the chemical compaction. The transition from mechanical to chemical compaction usually starts at 70-80^{0}C in the normally subsiding basins (Storvoll and Brevik, 2008).

Sediments, at the time of deposition, are loose, unconsolidated, and transformed into stiff cemented rock with increasing depth and temperature (Anders, 2011). Various studies show that the temperature is the most important factor which dissolves and precipitates the minerals in both sands and shales (Mackenzie, 2005; Thyberg et al., 2010). Thus, temperature can be used as a parameter to understand the rock physics model that can explain the rock properties from the site of deposition to a greater burial depth (Anders, 2011).

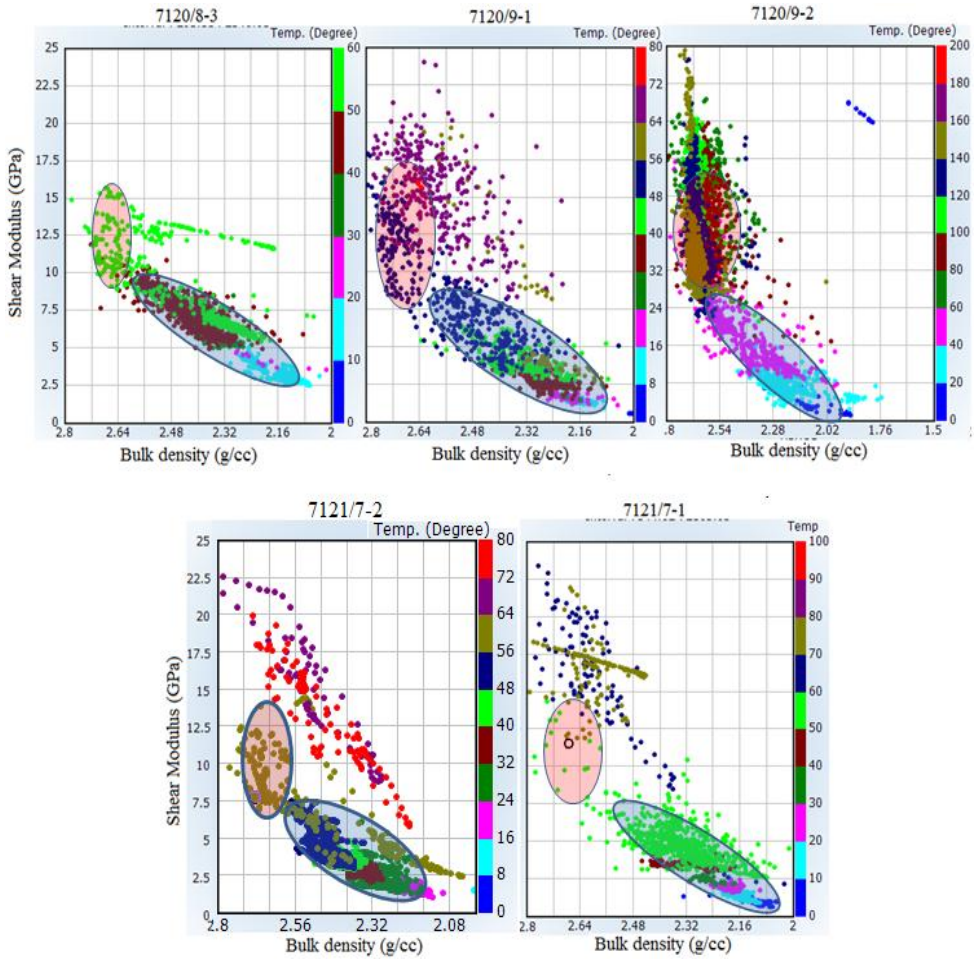

Figure 4.8: Bulk density versus shear modulus (shales only) color coded by temperature showing the transition from mechanical to chemical compaction in five wells.

The transition zone temperature ranges in the study area lies between 48 to 51^{0}C for the wells 7120/8-3, 7120/9-1, 7120/9-2, 7121/7-1 & 7121/7-2. However, the transition zone temperature for the well 7120/8-4 is anomalously high (73^{0}C).

The shear modulus is very much sensitive to identify quartz cement and can change significantly with the onset of small amount of quartz cementation which intern helps in finding the transition zone (TZ) from mechanical to chemical compaction. The calculated shear modulus versus density cross plots color coded by temperature is showing two clusters of data points (Fig. 4.8). All the wells except 7120/8-4 show knee points where shear modulus increase considerably at almost similar density values. The knee points in different cross plots representing the transition zones (TZ) from mechanical to chemical compaction and the temperature index giving the idea about the temperature range along the transition zone, which is almost similar to that temperature, calculated on the basis of BHT.

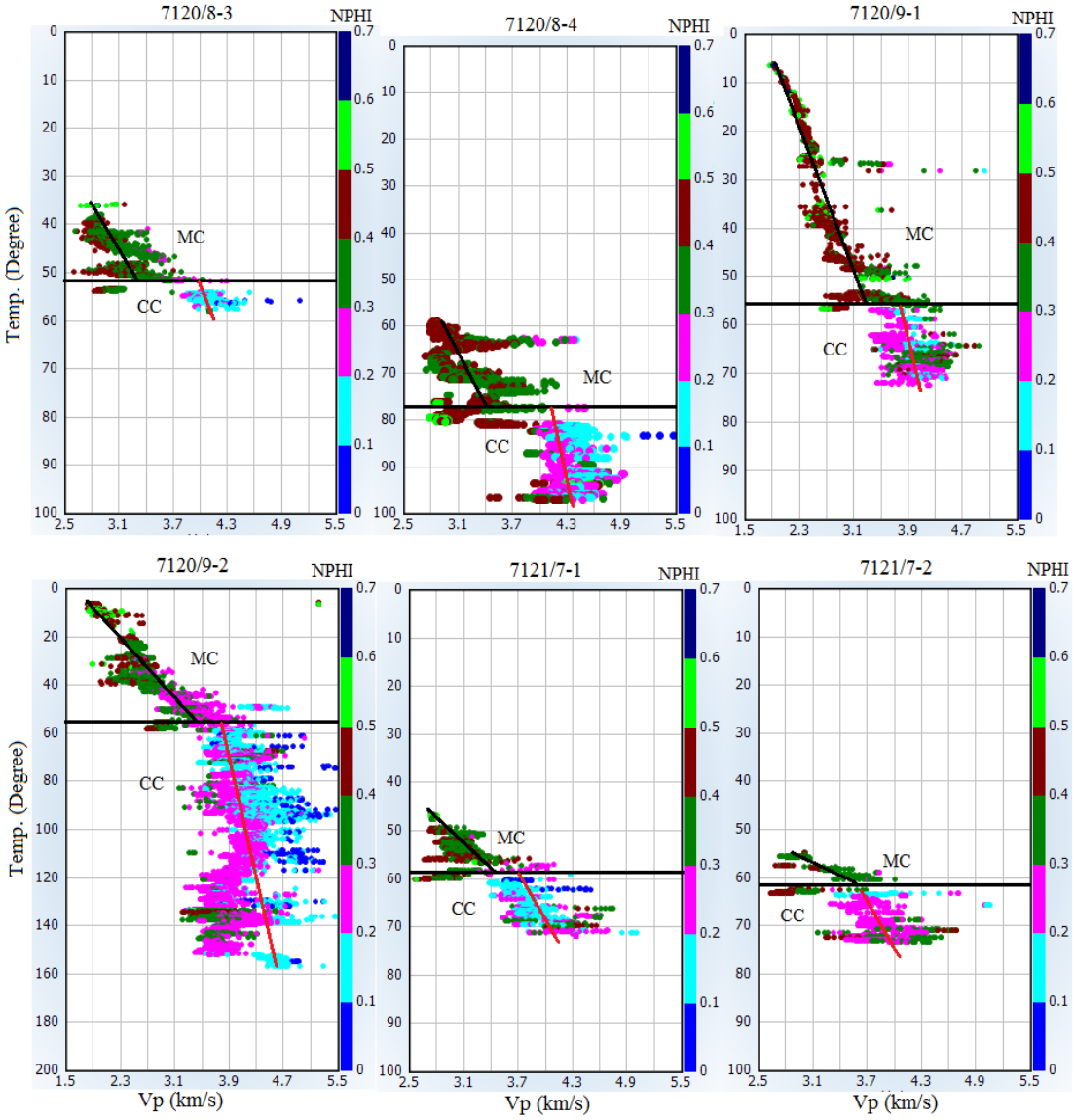

Figure 4.9: Crossplot of bottom hole temperature versus Vp color coded by neutron porosity (NPHI).

The bottom hole temperature versus Vp color coded by NPHI also plotted in the Figure 4.9. For this kind of cross plot, only data points related to 0.75≥ Vsh ≤0.25, represent pure shale and pure sand, have taken into account. At a given porosity values, large velocity variation can be observed. The transition zone from mechanical compaction to chemical compaction can be marked on the basis of abrupt change in velocity data color coded by porosity and the temperature at the transition zone more or less similar to that temperature calculated earlier.

4.1.5 Uplift estimation

Exhumation correction is important for accurate time temperature measurement and this intern is significant for quality of reservoir rock and source rock maturation. The transition zone in the study area at a present burial depth is showing divergence from the standard temperature reflecting Hammerfest basin as an uplifted area. Estimation of exhumation is done considering only shale data points sorted by Vsh≥.75. Complete Vp log has been used for accurate analysis of velocity variation with depth. Three published compaction trends of known lithologies (50:50 kaolinite-silt mixture, 80:20 kaolinite-smectite and pure kaolinite) have been taken into account as reference curves (Mondol et al. 2007, Mondol, 2009) for exhumation study, along with other published compaction trends to avoid any misinterpretation. When the Vp-depth trend was compared with the published curves, there was found a clear mismatch between published trends and the trends observed in the studied wells in mechanical zone, even greater mismatch in chemical compaction zone. After correcting exhumation, the data points related to velocity-depth trend match with the reference curves (Fig. 4.10).

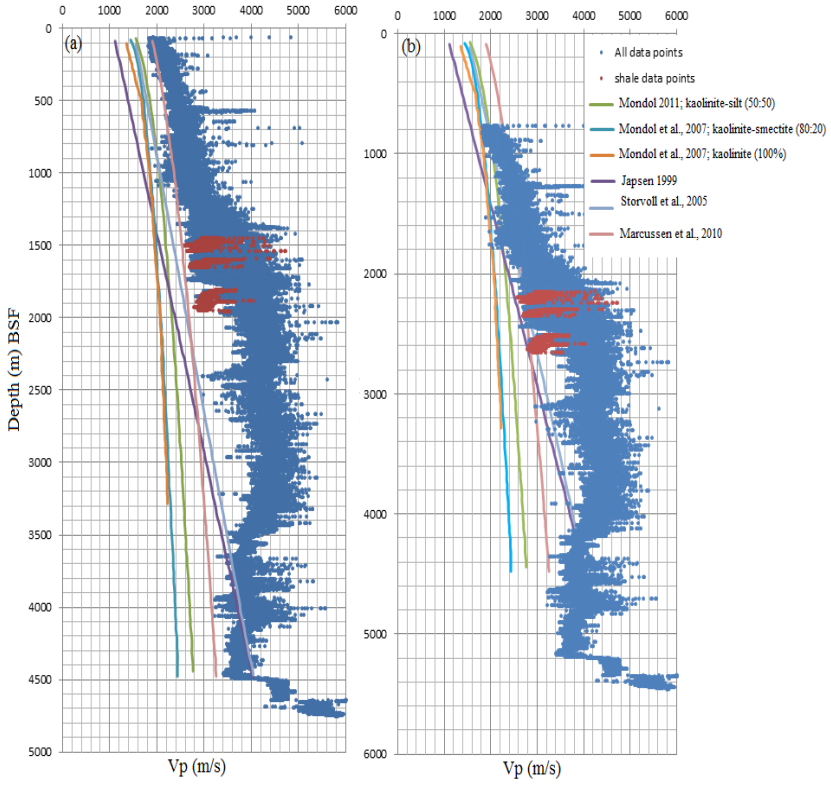

Figure 4.10: Vp-depth crossplot of all data of all the wells (a) before and (b) after exhumation correction.

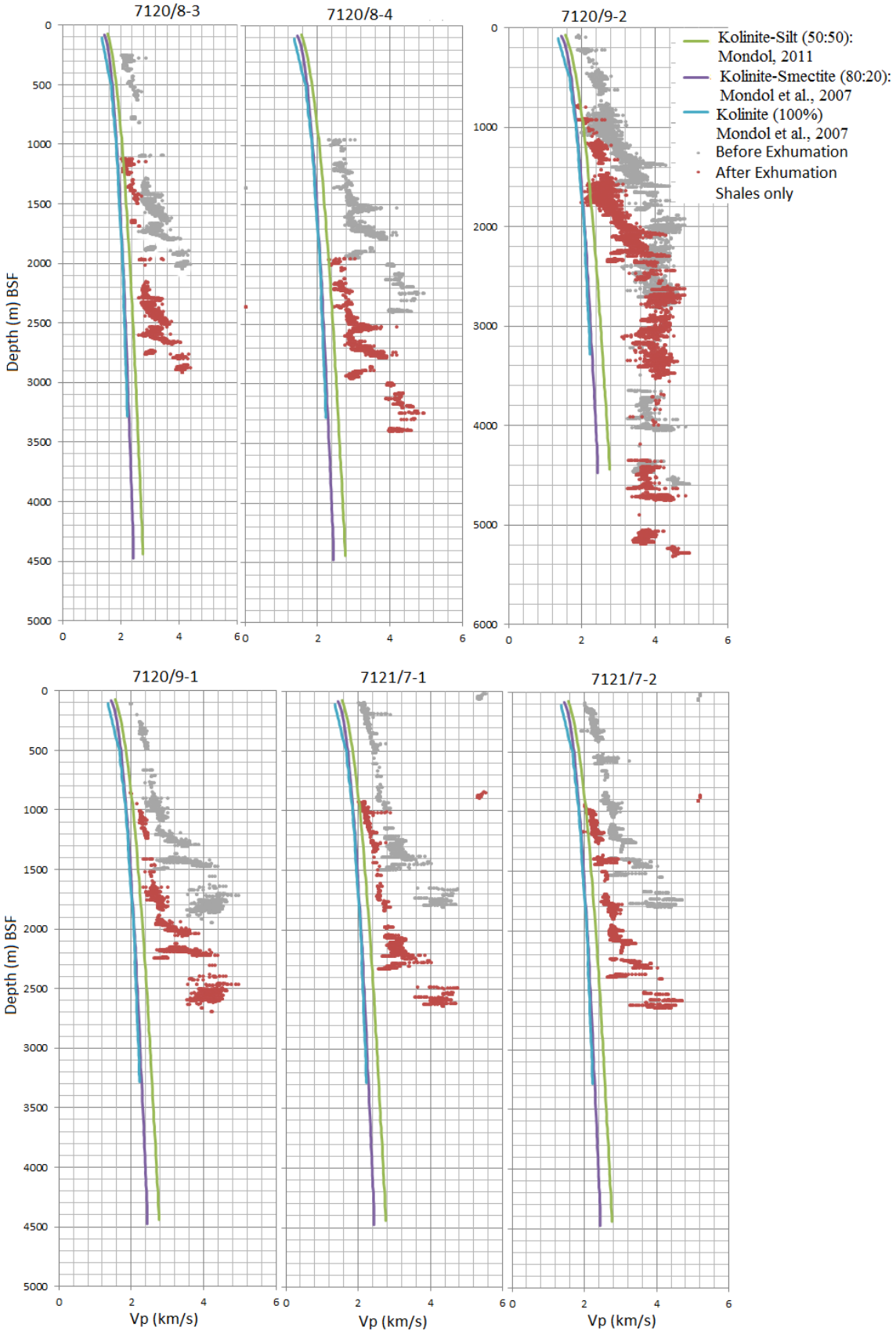

Figure 4.11: Vp-depth cross plot of shale data points with experimental reference curve showing exhumation estimation in all the wells.

When Vp-depth trends, sorted by Vsh before exhumation, were compared to the published compaction trends, the studied well log Vp is much higher than the published compaction curves at shallow depth (Fig. 4.11). When correction for exhumation was applied to all the wells, it is evident that the compaction of shale in the mechanical compaction zone depicts a similar compaction trend with the published trends (Fig. 4.11).

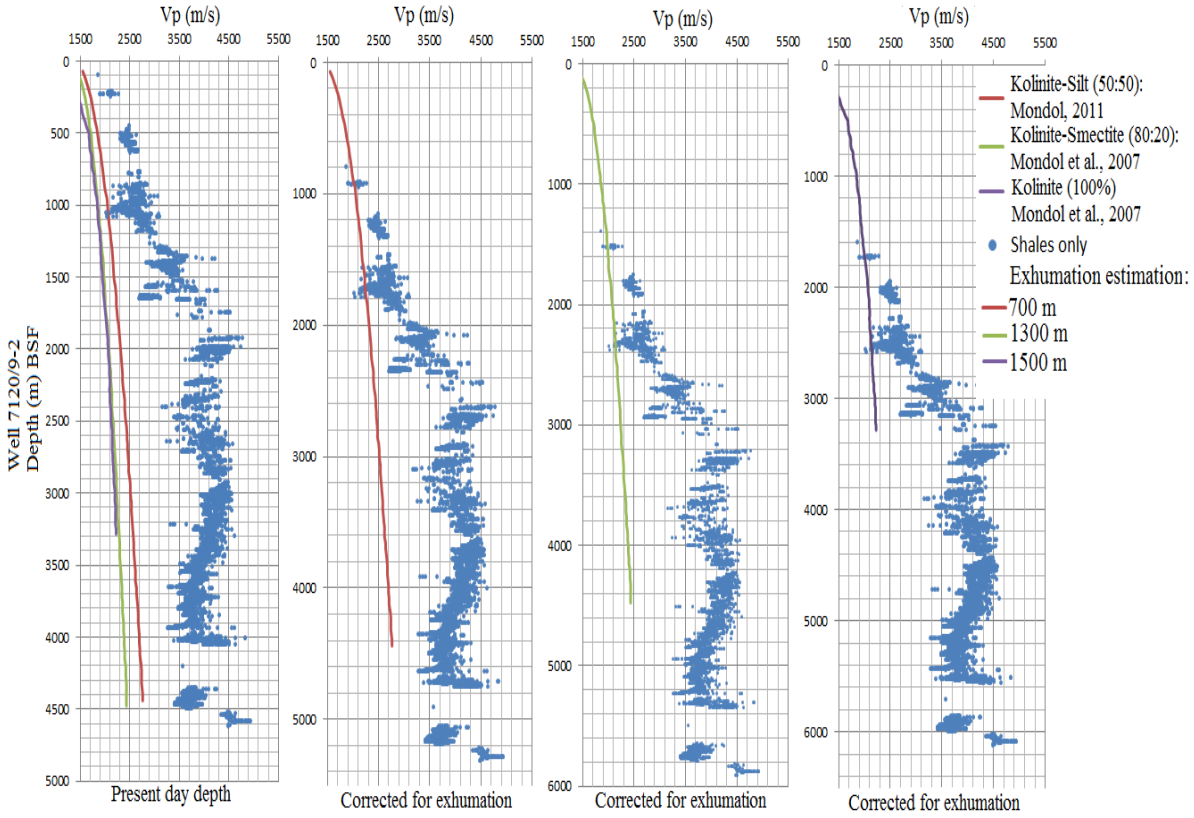

Figure 4.12: Exhumation estimation based on only shale data points for the well 7120/9-2 using different reference curves.

The well 7120/9-2, is the deepest well in the study area having complete suits of well logs, was taken as the reference well for analysing exhumation. Only shale data points (Vsh≥.75) were considered during this analysis. When exhumation correction was applied to the data using Kaolinite-silt (50:50) (Mondol, 2009), kaolinite-smectite (80:20) (Mondol et al., 2007) and kaolinite (100%) (Mondol et al., 2007) it is found to be 700, 1300 & 1500 m exhumation respectively (Fig. 4.12). When the comparison has been made between Vp-depth trends and published compaction curve 50:50 kaolinite-silt, the exhumation estimation has been calculated for Snøhvit development which is given in the Table 4.2.

The reason for using, 50:50 kaolinite-silt published compaction trend, as a reference trend has been explained in Ch. 3, Sec. 3.1.4 along with other published trends.

Table 4.2: The table is showing exhumation estimation based on published compaction trend kaolinite-silt (50:50) in the Snøhvit development.

Fields	Well Names	Total depth (m)	TZ at present depth (m) BSF	TZ temp. at present depth (^{0}C)	Exhumation (m) BSF	TZ depth before exhumation (m) BSF	TZ temp. before exhumation (^{0}C)
Askeladd	7120/7-2	2523	1741	69.11	800	2541	100.87
	7120/8-1	2610	1670	64.89	795	2465	95.78
	7120/8-2	2590	1640	61.64	330	1970	74.05
Albatross	7120/8-3	2335	1772	48.05	870	2642	71.65
	7120/8-4	2697	1864	72.41	1000	2864	111
	7120/9-1	2300	1443	49.06	750	2193	74.46
	7120/9-2	5072	1584	54.59	700	2284	79.82
	7121/7-1	2160	1416	50.23	830	2246	79.68
	7121/7-2	2156	1417	51.66	850	2267	82.65
Snøhvit	7120/5-1	2699	1907	43.85	300	2207	50.76
	7120/6-1	2820	1888	66.95	700	2588	91.77
	7120/6-2S	3035	1860	65.56			
	7121/4-1	2609	1827	58.81	680	2507	80.7
	7121/4-2	2799	1944	69.01	720	2664	86.58
	7121/5-1	3197	1922	66.67	760	2682	93.04

4.1.6 Compaction trends of two pure lithologies in the reference well 7120/9-2

The Albatross discovery in the Hammerfest basin, being a clastic sedimentary basin, contains sandstone and shale in abundance. The compaction trends of two pure lithologies (sandstome and shale) are carefully studied. The compaction trends of sands and shales are investigated in the reference well 7120/9-2, taking into consideration only the Vsh≥.75 for pure shale Vsh ≤0.25 for pure sand computed from the gamma ray log. Vp-depth trends in the figure given below showing (a) all data points (b) only shale data points (c) only sand data points. A general compaction trend in the mechanical compaction zone is represented by a black line whereas the general compaction trend in the chemical compaction zone is represented by a red line. The sands data points are showing more mechanical compaction than shales data points in the mechanical compaction domain whereas this is the opposite case in the chemical compaction domian (Fig. 4.13). Anomalous zone marked by the black circle is showing low values of Vp compared to the formations above it.

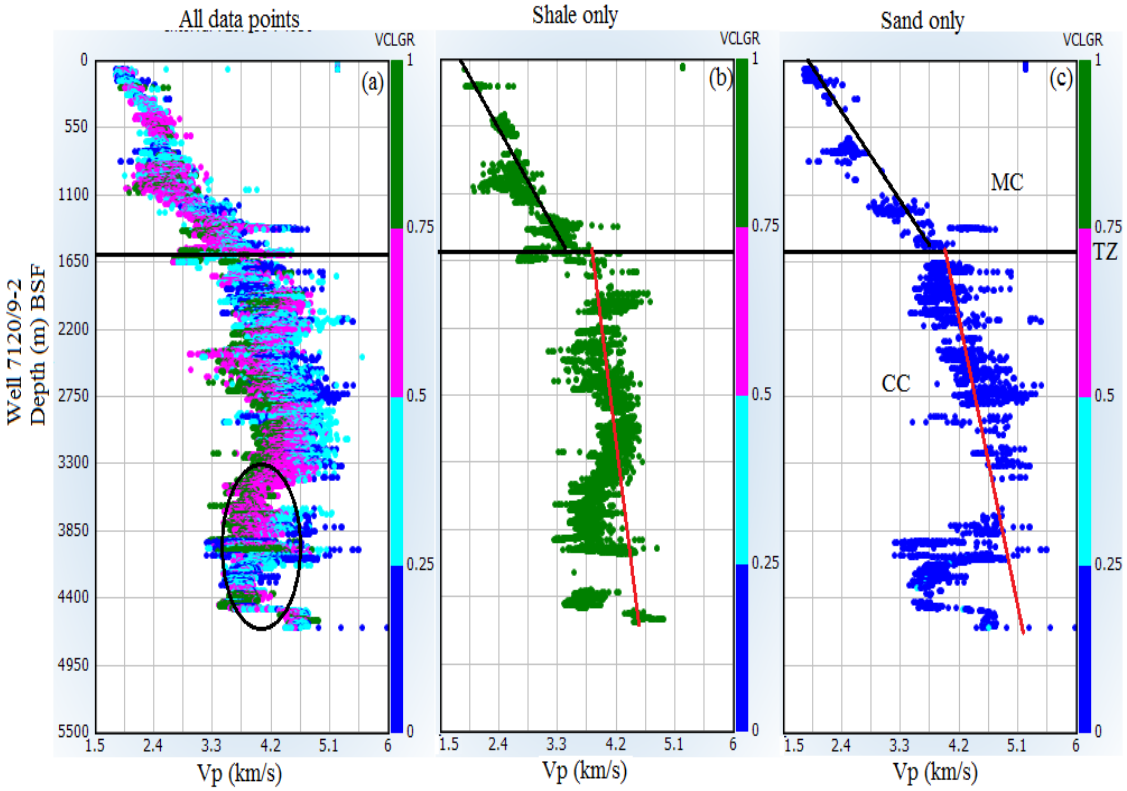

Figure 4.13: Sand and shale compaction trends variation for the well 7120/9-2.

The Figure 4.14 is showing data points related to shale (Vsh≥0.75) in the well 7120/8-4. The density porosity (DPHI) was computed by using a bulk density of clay 2.57 g/cc. The density and velocity tends to increase with burial depth whereas the porosity shows inverse relation. All three parameters are varying with depth because of burial diagenesis. The data points related to Vp, bulk density and porosity depth trends deviate from the experimental compaction curve kaolinite-silt (50:50) (Mondol, 2009). This is because of exhumation as cleared from the plots beneath showing a much closer fit to experimental compaction curve after correcting for exhumation of 700 m uplift to the data (Fig. 4.14).

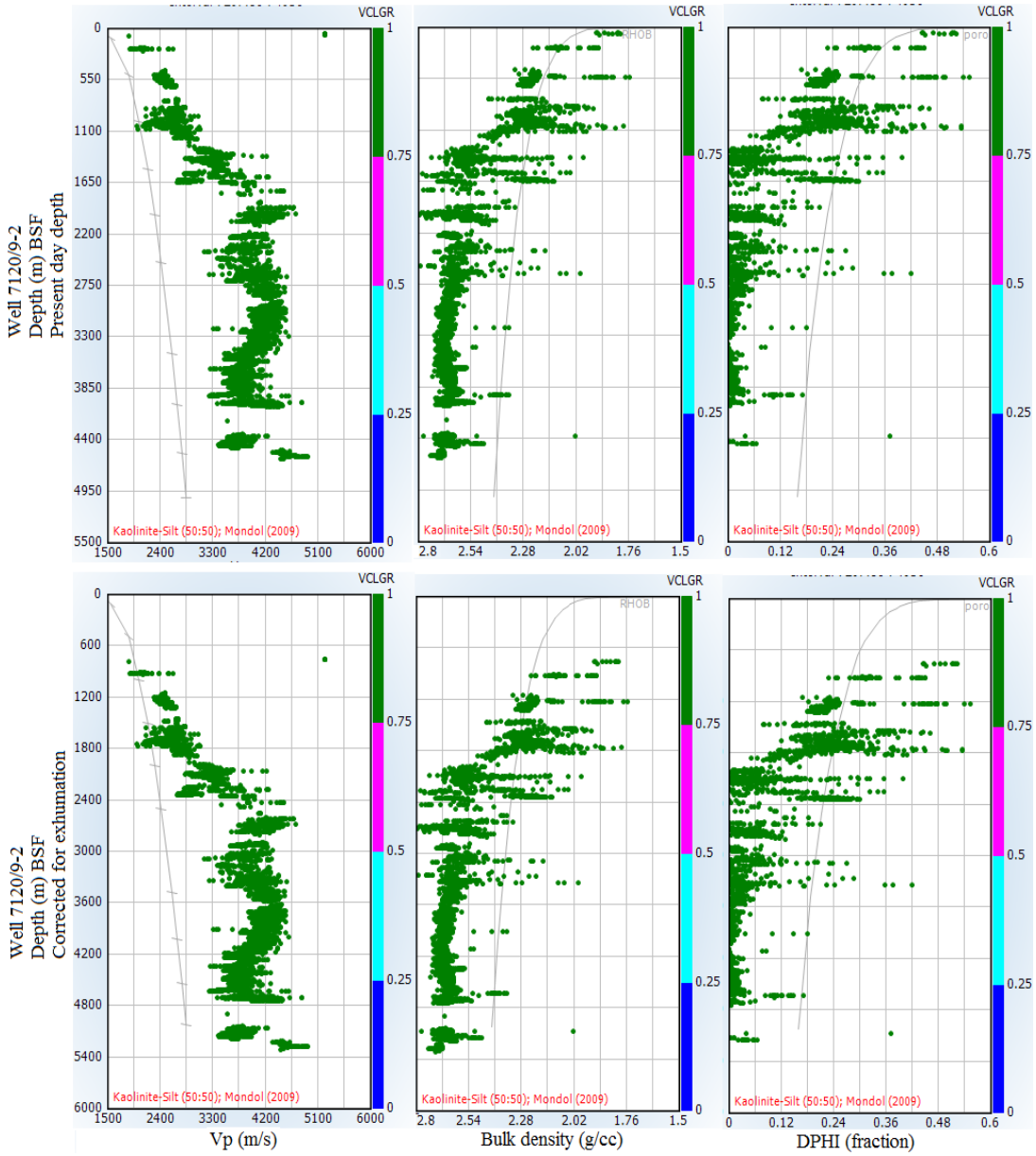

Figure 4.14: Vp/ bulk density/ porosity depth trends for shale in the reference well 7120/9-2 before (above) and after (below) exhumation correction.

4.1.7 Source rock affect on rock properties and Opal A/Opal CT conversion

The source rock of the Barents Sea which is widely distributed through out the Hammerfest basin is the marine shales of Upper Jurassic–Lower Cretaceous Hekkingen Formation indicated by very high gamma ray reading (Fig. 4.15). The basal part of the Hekkingen Formation represented by Alge Member is coarsening upward with very high gamma ray reading compared to the Krill Member and the Fuglen Formation below. High gamma ray reading of the basal part reflects high organic contents compared to Krill Member. The velocity reversal in the Hekkingen Formation can be observed in all the wells (Sec. 4.1.5, Fig. 4.10).

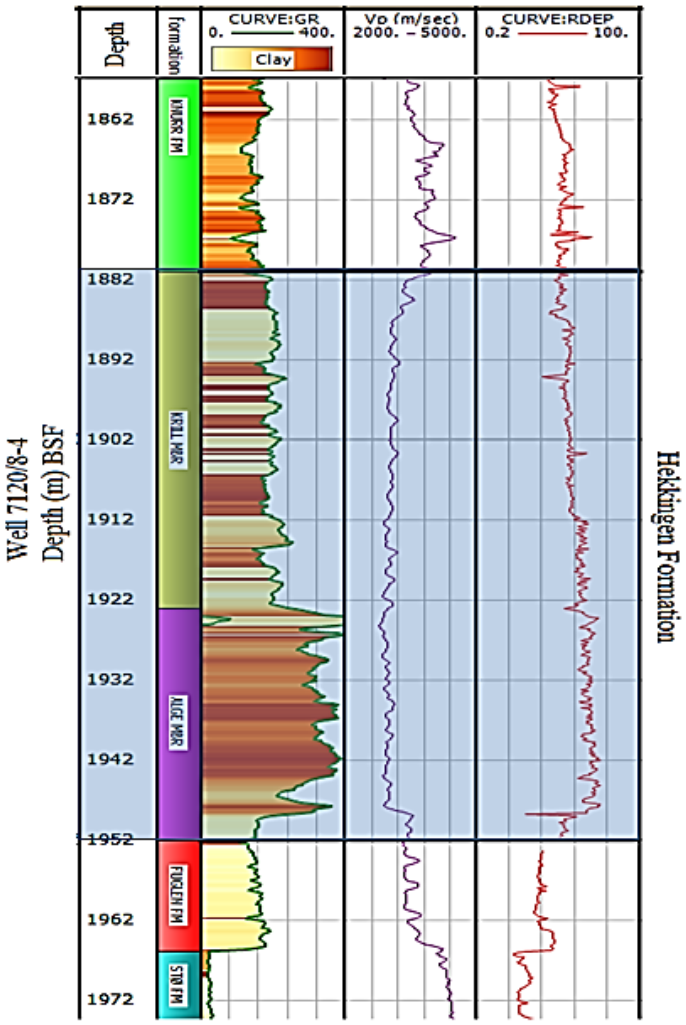

Figure 4.15: Gamma Ray, Vp and deep resistivity versus depth crossplot of the Hekkingen Formation, the main source rock in the well 7120/8-4.

The well 7120/8-4 was chosen to check the compaction trend of source rock. Being dry well it contains only brine neglecting the effects of hydrocarbon in pore fluid in the underlying Kapp Toscana Group. The velocity reversal is observed immediately below the transition zone (TZ) in the chemical compaction (CC) domain from 1880 (m) BSF to 1925 (m) BSF depth in the Hekkingen Formation shown by 'F' in Figure. 4.16. Along with the low velocity, it has high resistivity compared to the formations above and below due to the effects of high organic contents in the basal part Alge Member (Fig. 4.15).

The data point represented by red color (Fig. 4.16) in the well 7120/8-4 belongs to Kolje Formation in the well 7120/8-4. Vp-depth trend for Kolje Formation is different from the rest of the log trend. Due to that reason Kolje Formation has been zoomed out to check the possible anomaly in gamma ray, velocity, porosity and resistivity against depth (Fig. 4.17). The Kolje Formation has been divided into three zones (C, D & E). Zone G which is in the chemical compaction (CC) zone belongs to lower part of Tubåen and Fruholmen Formations of Kapp Toscana Group. The Zone G showing velocity reversal compared to the rest of Kapp Toscana Group (Fig. 4.16).

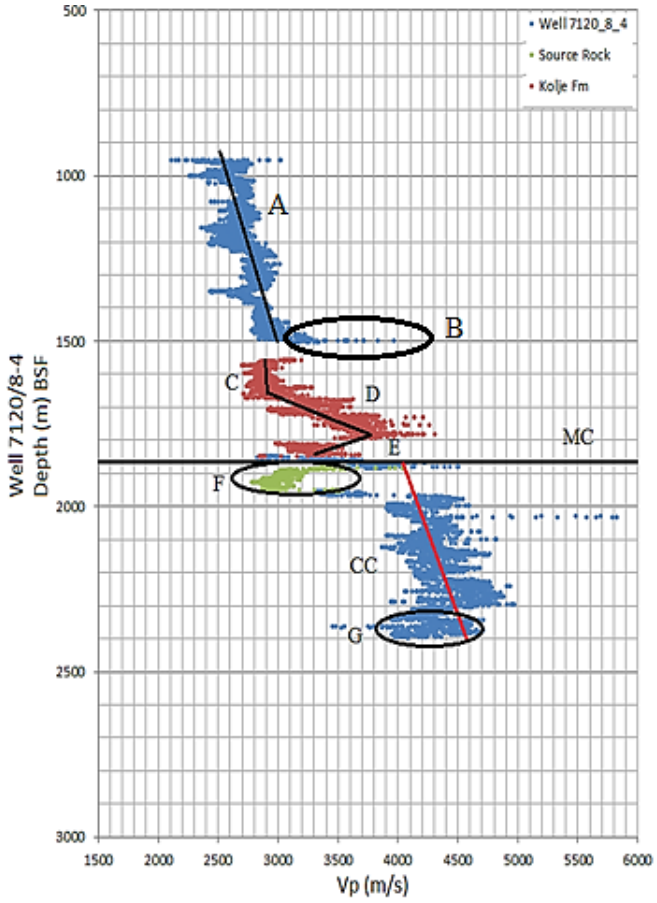

Figure 4.16: All the data points of the well 7120/8-4, showing source rock (green color) velocity inversion.

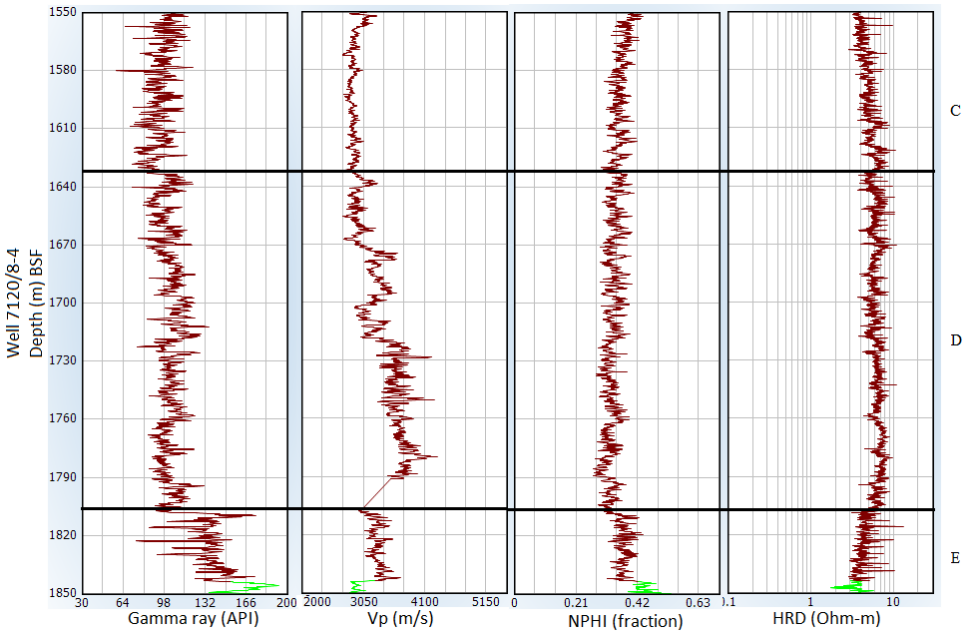

Figure 4.17: Gamma ray, Vp, porosity and deep resistivity logs for Kolje Formation in the well 7120/8-4.

The zone A and B have already explained in the previous sections in details. The 100 m thick interval is represented by the interval 'C' showing nearly constant velocity with depth which is the Kolje Formation of middle Cretaceous age (Dalland et al., 1988). The Kolje Formation composed dominantly of dark brown to dark grey shale and claystone with minor inter beds of pale limestone and dolomite. The depositional environment of this formation is of distal open marine conditions with good water circulation but periodic restricted environment was also experienced. The interval 'D' and 'E' also belongs to Kolje Formation. A sharp increase in the Vp can be observed in the interval 'D' whereas the basal part of the Kolje Formation is showing velocity reversal (Fig.4.17).

The Upper Jurassic source rock of the Barents Sea represented by the interval 'F' consists of brownish grey to very dark grey shale and claystone with thin interbeds of limestone, dolomite, siltstone and sandstone. Theses minor clastic components are most common towards basin margins (Dalland et al., 1988). The lower part of the formation is showing very high gamma ray reading. This can be used to differentiate the lower Alge member from the upper Krill member in the formation (Fig. 4.15) (Dalland et al., 1988). The interval 'F' showing anomalously low Vp value compared to the upper Knurr Formation and the Fuglen Formation below it.

The interval 'G' from 1844 m to 2344 m BSF depth consists of lower part of Tubåen and Fruholmen formations of the well 7120/8-4. This interval represents Late Cretaceous to Upper Jurassic age formations. The whole Kapp Toscana Group was zoomed in, in order to better analyze the changing rock physical properties with depth (Fig. 4.18).

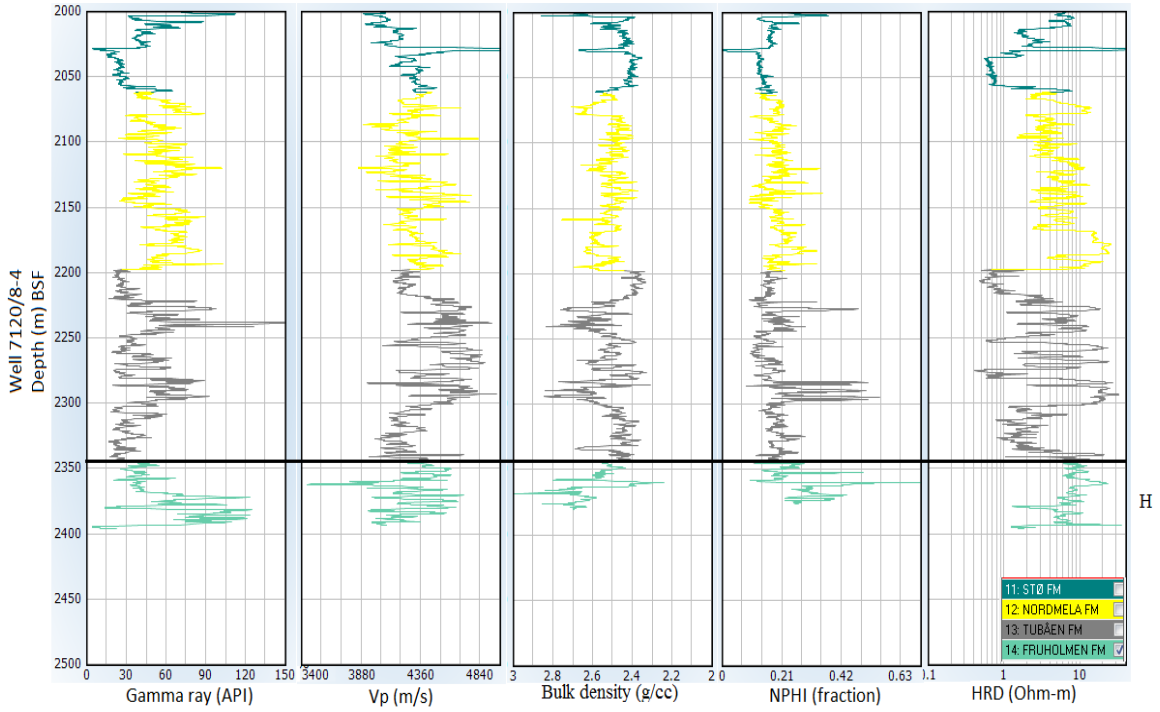

Figure 4.18: Gamma ray, Vp, porosity and deep resistivity logs for Kapp Toscana group in the well 7120/8-4.

The oldest penetrated formation of the well 7120/8-4 is the Fruholmen Formation (Upper Triassic) represented by the interval 'H' (Fig. 4.18). The Fruholmen Formation consists of

basal gray shale which passes upwards into interbedded sandstones, shales and coals. The thickest sequence (262 m) is found in the well 7120/9-2 of the study area (Dalland et al., 1988). The Vp-depth trend for the interval 'H' is decreasing as compared to the formations above it (Fig. 4.18). The lower part of this formation shows higher gamma ray and NPHI values but the deep resistivity value is lower.

4.2 Discussion

4.2.1 Rock properties versus depth trends

Because of general velocity depth trends for all the wells of the study area, two kinds of patterns can be observed with anomalous zones showing low velocities. These similar velocity depth trends are related to mechanical compaction (MC) and chemical compaction (CC) zones. The Vp-depth trend for mechanical compaction zone indicates that there are no major lateral lithological variations and the effective stress was homogeneously distributed in the mechanical compaction zone through out the study area (Fig. 4.1). Close observation of the gamma ray logs from all the wells in the study area reveals that there is no significant lithological variation around the transition from mechanical to chemical compaction and also predicts that these mudstones are, to some extent, homogeneous (Fig. 4.1).

The Kviting Formation which is thickest (93 m) in the well 7120/8-4 pinches out towards East with a thickness of 25m in the well 7120/9-2 and passes into Kveite Formation of the same group which become thicker towards East and pinches out towards West. The maximum thickness of 37 m of the Kveite Formation was encountered in the 7121/7-1. The Fuglen Formation of the study area is absent in the 7120/9-1 and in the eastern part of the study area, the thickness of this formation is less than 2 m. (Ch.2, Table 2.1). Paleo-depositional environment with respect to well location and basin configuration could be the cause of such scenario (Ch. 2, Sec. 2.3).

The clay stone of the Kviting Formation of all the wells falls into mechanical compaction regime, was deposited during late Cretaceous and formed during periods of uplift (Ch. 2, Sec. 2.1). This late Cretaceous unit consists of clay stones, interbeded limestone and calcareous sand units (Worsley, 2008). Calcite cementation at a shallow burial depth is the cause of reduction in primary porosity but on the other hand, it strengthens the grain framework. The carbonates of this formation are responsible for high velocities of upto 4500 m/s at a shallow in the wells (7120/8-3, 7121/7-1 & 7121/7-2) (Fig. 4.1). The reason for high velocity could be explained by Bjørlykke and Jahren (2010).

- Meteoric water leaching and precipitation of kaolinite
- Presence of biogenic carbonate and silica
- Precipitation of authigenic minerals on the sea floor

Meteoric water is sourced by rainwater and for mineral dissolution and precipitation; continuous source of meteoric water is needed. The wells 7121/7-1 & 7121/7-2 are the eastern most wells whereas the well 7120/8-3 is towards west and the paleo-coast line was exist towards east and small tributary towards west (Fig. 4.20). The flow of meteoric water is higher in the western side than eastern which could cause more precipitation in the shallow depth and could explain the reason for higher Vp in the 7120/8-3 wells compared to eastern wells.

On the basis of gamma ray log reading two distinct lithology trends (sandstones & shales) can be marked. Delineation can be marked between these two trends in the Fuglen and Stø formations boundary. These trends are similar in all the wells but the gamma ray readings are

different. Different gamma ray readings within the same formation could be caused by the location of wells with respect to paleo-depositional environments.

The thickness of main reservoir Stø Formation in the study area increases from east to west however, the thickness of Hekkingen Formation, which is the main source rock, decreases from eastern well 7121/7-2 to western well 7120/9-2. The thickness of Hekkingen Formation in the wells 7120/8-3 & 7120/8-4 is more or less similar with that of eastern well (7121/7-2) (Fig. 4.19).

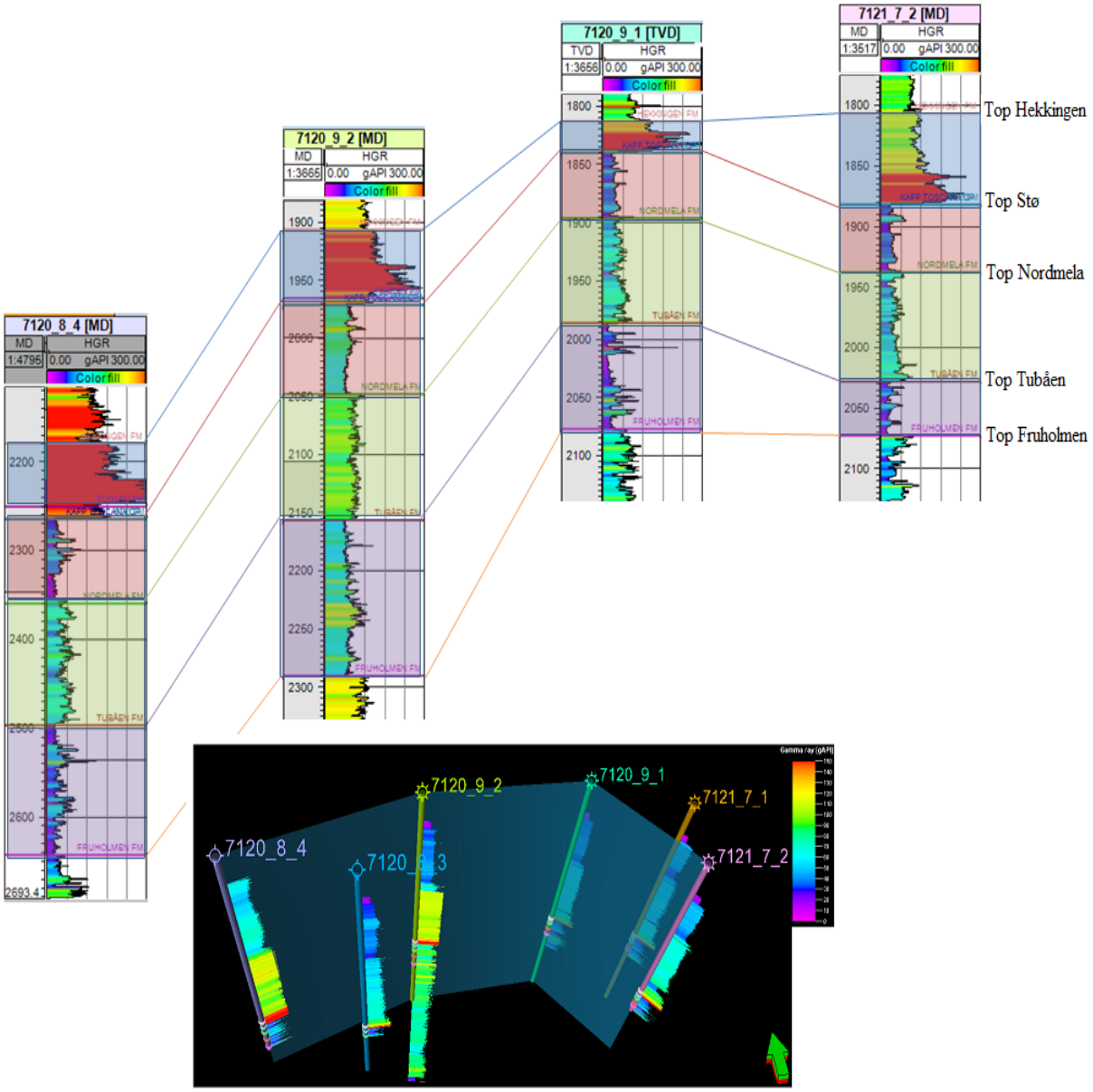

Figure 4.19: Stratigraphic correlation of the source and different reservoir rocks using gamma ray log response from west to east, well fencing is showing the location of wells used for correlation.

As the Stø Formation depositional environment is delta to shoreface, the provenance at that time was in the south west direction bringing bulk of sediments. That's why western wells (7120/8-3, 7120/8-4) being closer to the shoreline receiving huge amount of sediments than eastern wells (7121/7-1, 7121/7-2) (Fig. 4.20). On the other hand the thickness variation of the source rock Hekkingen Formation could be explained by structural geometry and paleo-depositional environment of the Hammerfest basin.

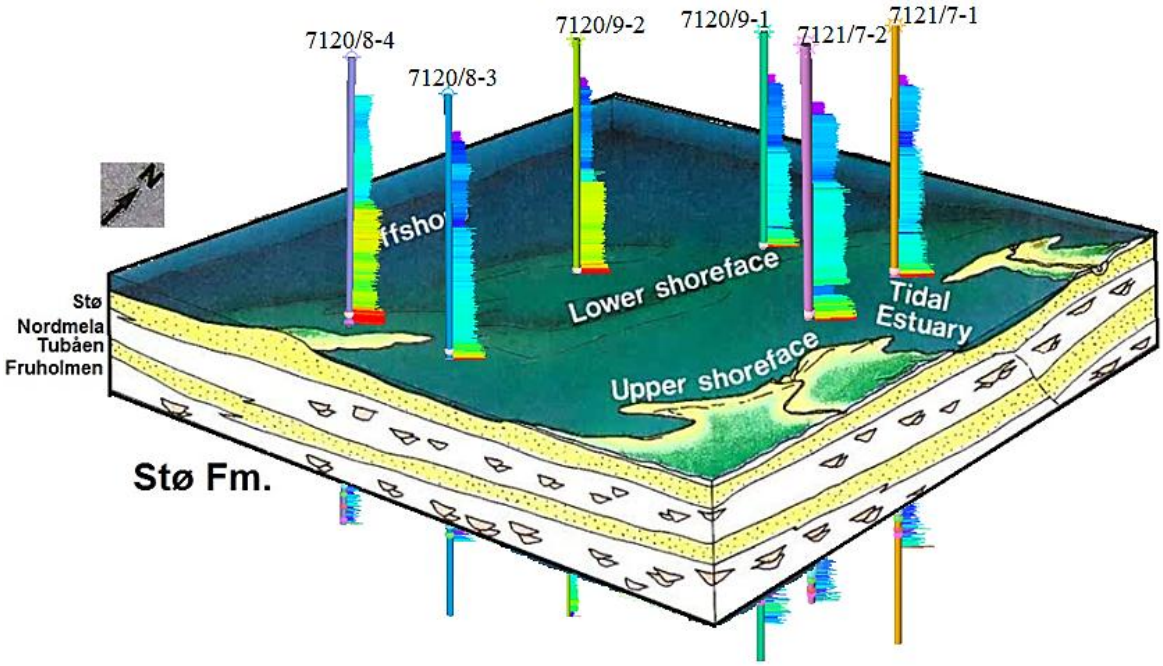

Figure 4.20: The possible location of wells in the Albatross discovery according to depositional environment of the Stø Formation based on gamma ray log response explained by Berglund et al. (1986).

Lower velocities in the overpressured rocks have been related to the reduction in the effective vertical stress which results in less mechanical compaction and preservation of the primary porosity. But at greater depth (>3km) it is the temperature and quartz cementation that controls the porosity not the vertical stress. This implies that if higher porosities are found in deeply buried over pressured sediments, the over pressure must have been started to build at a shallow depth (<2km) when the sediments were still under the effects of mechanical compaction. This phenomenon could be the cause of lower velocities of the Triassic formations in the well 7120/9-2 (Sec. 4.1.2, Fig. 4.2, 4.21).

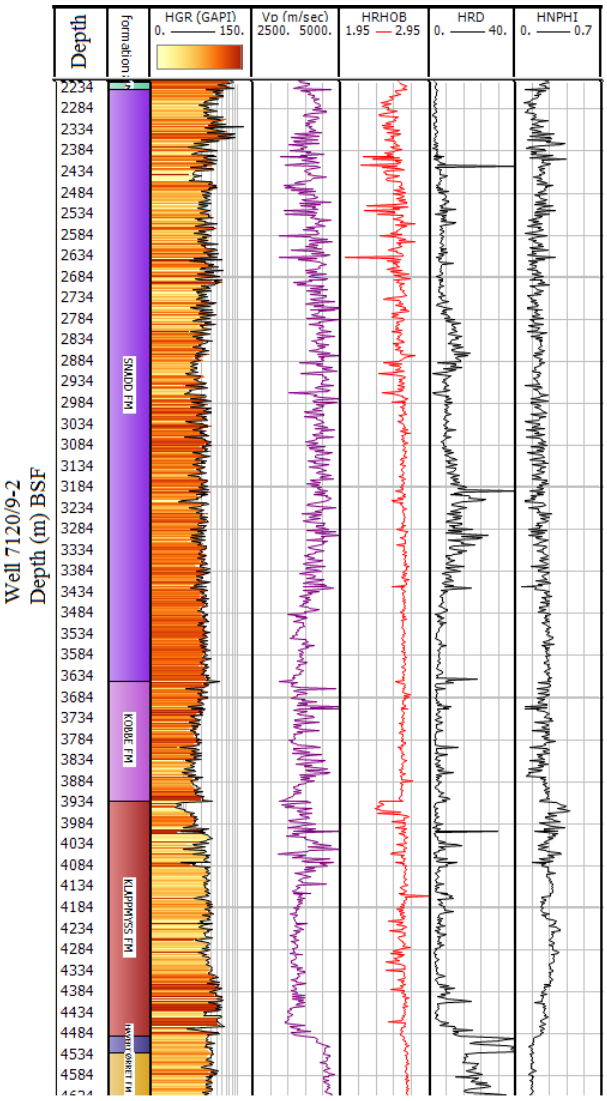

Figure 4.21: Anomalous zones and corresponding petrophysical logs in the well 7120/9-2.

4.2.2 Transition zone between MC and CC

The upper part (10-15 m) of the Knurr Formation in all the wells except 7120/8-3 is showing anomalously lowers velocity and density (Fig. 4.4, 4.5, 4.6). As far as the lithology is concerned, the Knurr Formation composed dominantly of clay stone (NPD Fact pages) deposited in open and generally distal marine environments with local restricted bottom conditions (Worsley et al., 2008) during Early Cretaceous time (Barremian). This was the time of extensive megmatism along with northern margin upliftment (Ch. 2, Sec. 2.1). Volcanic ash deposited during this time, consists of smectite rich clay minerals. Smectite rich clays show a substantial reduction in velocity with increasing depth (Thyberg, 2000). Due to the low permeability in smectite rich clay, the phenomenon of overpressure could also be happened (Storvoll et al., 2005). Smectite clays are also difficult to compact because of the presence of bound water in their mineral structure and because of their high specific surface area (Storvoll et al., 2005). Over pressure could be the cause in the reduction of velocity and density in the upper part of Knurr Formation.

The Present day transition zone depth (Fig. 4.23) from mechanical to chemical compaction occur in the Knurr Formation of the study area which is obviously marked on the basis of sharp increase in the Vp-depth trends (Fig. 4.4, 4.5, 4.6). There is overall decrease in the depth of transition zone from north to south but in the study area (Albatross discovery), the transition zone depth increases from east to west (Fig. 4.23). The present day complex structural configuration of the Hammerfest basin described the variation in the transition zone depth from well to well. Moreover, temperature plays a vital role in changing the compactional processes from mechanical to chemical compaction. There is overall tendency in increase of TZ temperature from east to west which could be explained by spatial variation in the thermal history within the basin (local heating events or different subsidence/uplift histories). Present day geothermal gradient (23^0C/km) is very low for the well 7120/8-3 (Fig. 4.22) as compared to other wells though the transition zone depth of this well is more or less similar with other wells in the study area. When present day transition zone depth is compared with the present day transition zone temperature gradient, it gives the clue about paleo-temperature gradient in the study area. Hence, the transition zone depth of the well 7120/8-3 suggests that the paleo-temperature was similar with other wells in the area.

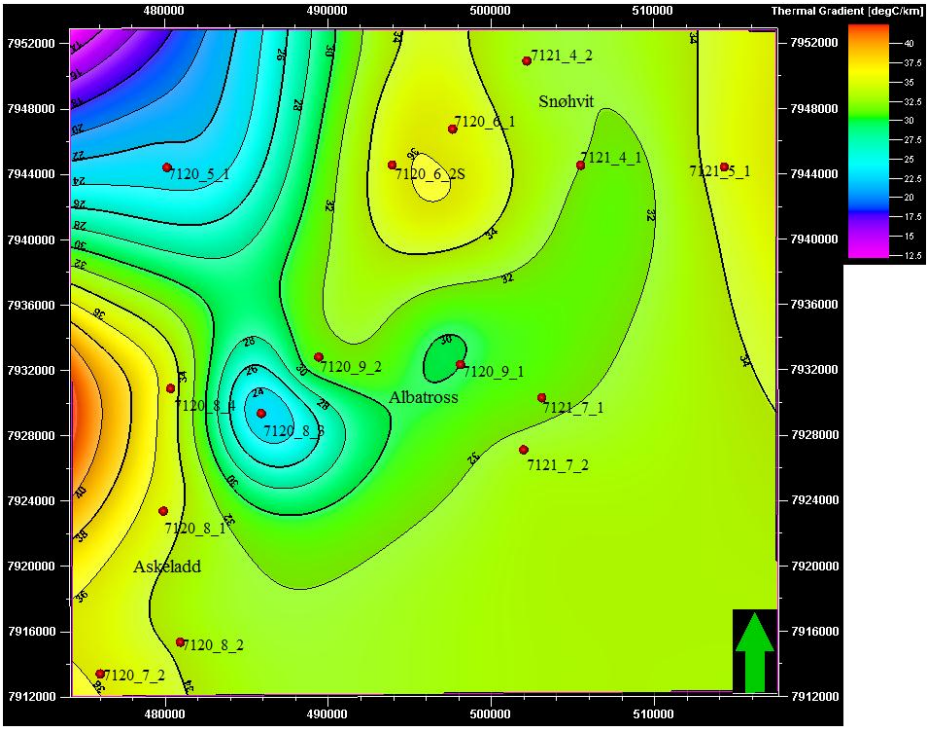

Figure 4.22: Present day geothermal gradient calculated on the basis of bottom hole temperature (BHT) in the Snøhvit development.

Transition from mechanical to chemical compaction is indicated by increase in Vp and shear modulus within Knurr Formaion (Fig. 4.4 to 4.9). All the formations above Knurr Formation are mudstones units. Hence, all the formations in the mechanical compaction (MC) zone are composed of mudstones and mudstone compaction is controlled by the mineralogy and micro-fabric of the grains (Fawad et al., 2011). Gamma ray log does not show much variation within Knurr Formation in the study area (Fig. 4.4, 4.5, 4.6). This indicates a uniform lithology distribution throughout study area. Thus, onset of quart cementation as a function of temperature is accountable for the increase in velocity.

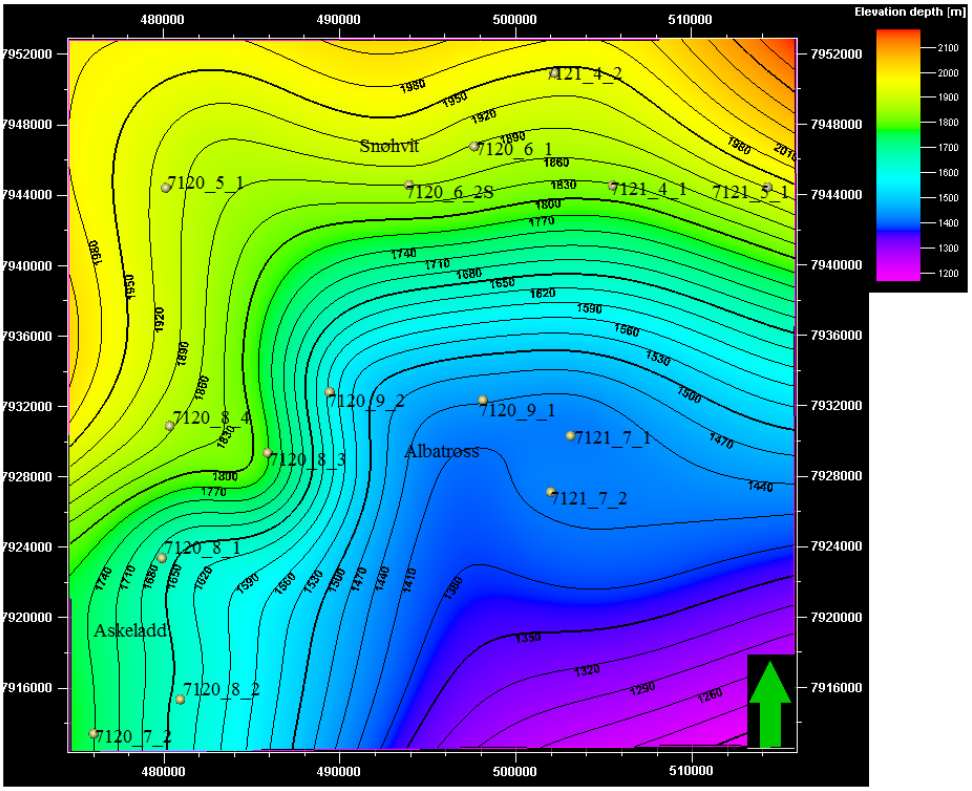

Figure 4.23: Present day transition zone depth contour map with location of wells in the Snøhvit development.

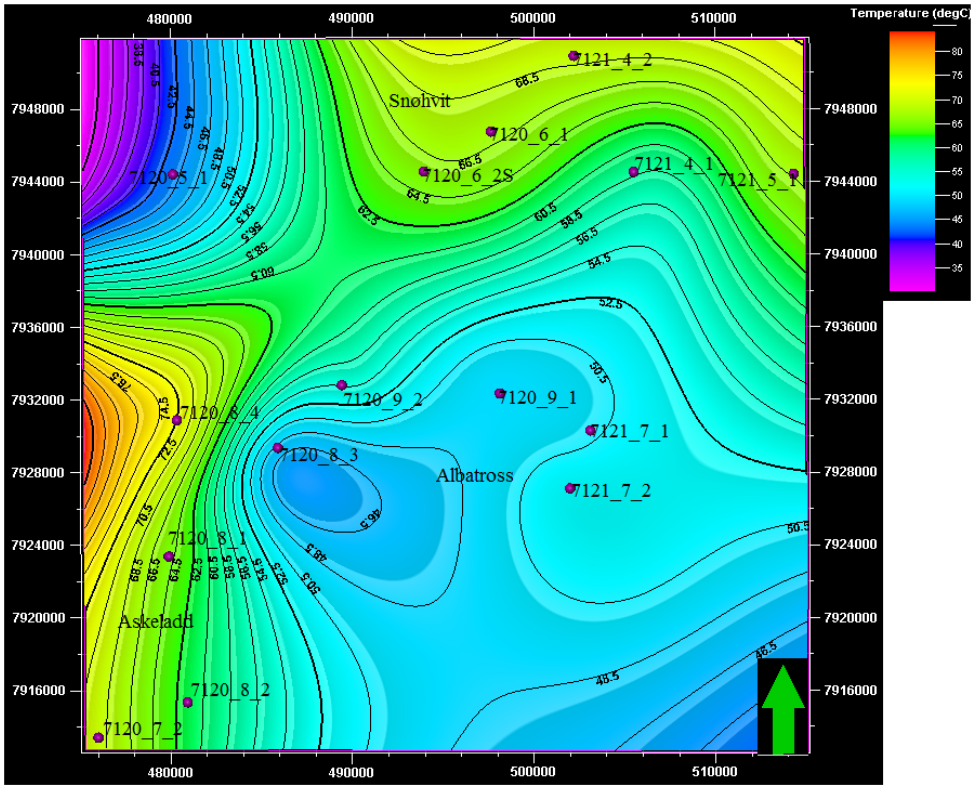

Figure 4.24: Transition zone present day temperature contour map with location of wells in the Snøhvit development.

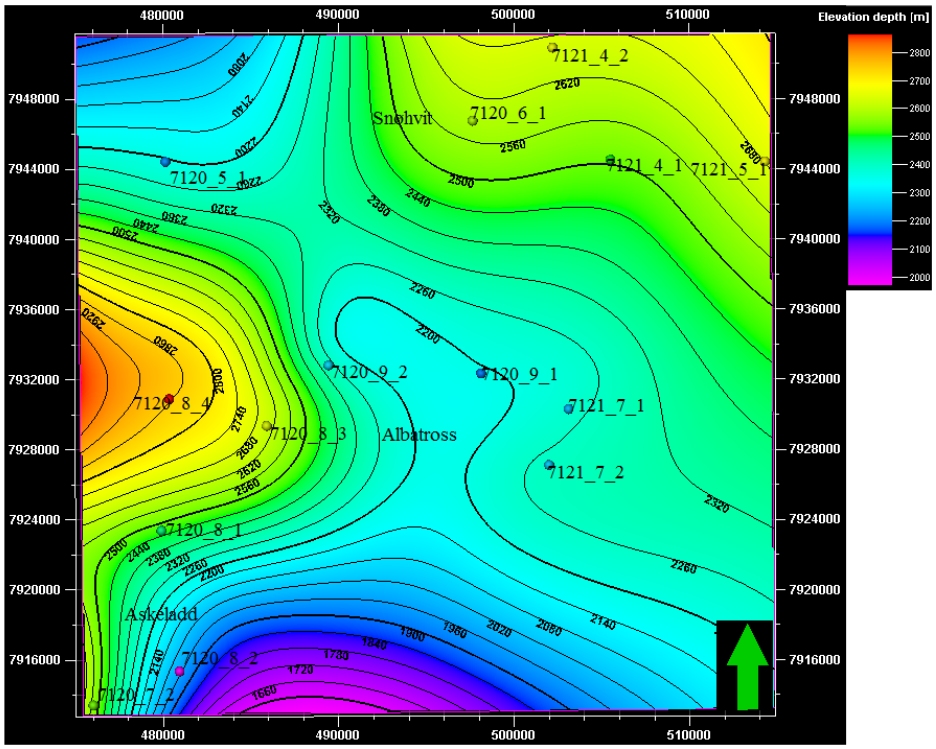

Figure 4.25: Contour map of transition zone depth before exhumation with location of wells in the Snøhvit development.

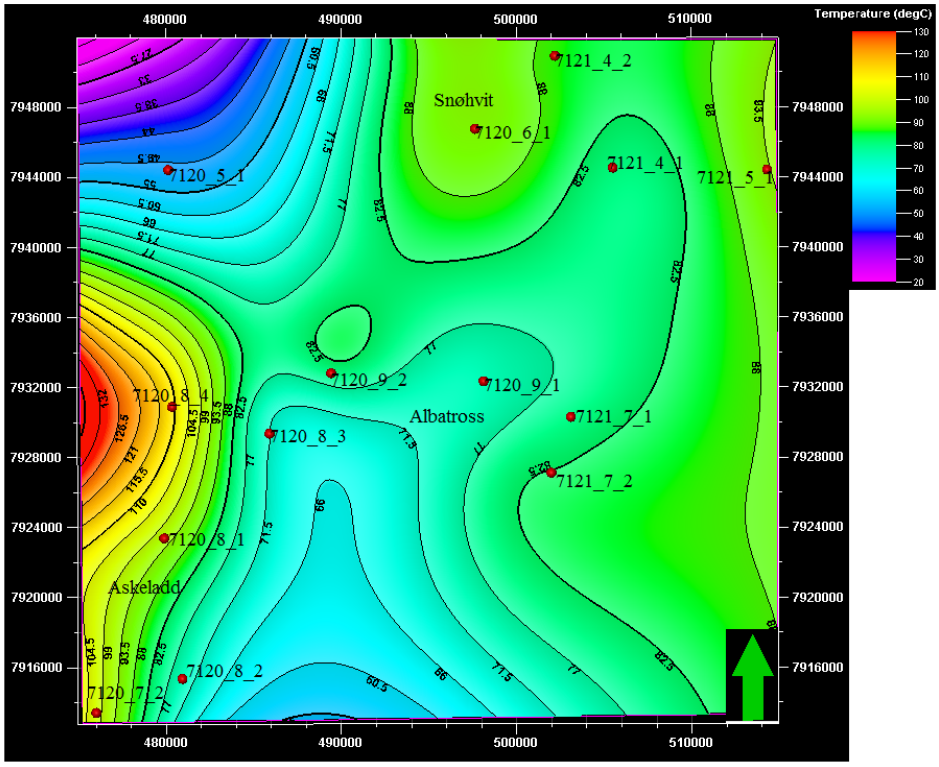

Figure 4.26: Contour map of transition zone temperature before exhumation with location of wells in the Snøhvit development.

Present day temperature of the transition zone (Table 4.2, Fig. 4.24) in the Snøhvit development is not sufficient to start a transition from mechanical to chemical compaction. It is lower than the standard temperature (70-80^{0}C), giving indication of exhumation. When correction for exhumation was applied to present day transition zone depth, it shows that at a shallow burial depth of 2-2.5 km, mechanical compaction is the main controlling factor and it is controlled by effective stress, whereas, the higher temperature 70-80^{0}C bring about the chemical compaction to the sediments at a deeper level (Fig. 4.25, 4.26). Transition zone depth for all the wells in the Snøhvit develpomene in given in the Table 4.2 whereas botthom hole temperature and the geothermal gradient of all the wells is given in the Ch. 1, Table 1.1.

4.2.3 Uplift estimation

Temperature is the important factor, which controls the transition from mechanical to chemical compaction, diagenesis of sediments, source rock maturation, cap rock quality and hydrocarbon migration. Temperature also gives a clue about exhumation according to this research work. Exhumation estimation gives us temperature history experienced by source and reservoir rocks. In order to estimate the total exhumation, compaction based well log data was compared with laboratory experimental curves. It is revealed that the shales in the mechanical compaction zones are more compacted than the published compaction trend at the same effective stress level (Fig. 4.11). These high velocity intervals in the mechanical compaction zone could disclose the fact that these have been subjected to higher pressure before exhumation.

Mineralogical composition of the shales in the study area for uplift estimation has not been analyzed through thin section. Due to that fact, different mixtures of clay-clay and clay-silt have been used to estimate the amount of exhumation in the study area. Different experimental curves, in the well 7120/9-2, estimate different exhumation results which reflect the importance of mineralogical composition during exhumation calculation (Fig. 4.12). Hence, compositional variations between experimental and natural data effect the exhumation estimation.

On the basis of comparison between Vp-depth trends and published compaction trends, the calculated exhumation estimates differs for Snøhvit, Albatross and Askeladd discoveries depending upon the structural configuration. The exhumation for Snøhvit field is from 300 to 800 m increasing from west to east whereas in the Albatross discovery it increases in opposite direction ranging from 700 to 1000 m. In the Askeladd discovery it ranges from 300 to 1000 m and decreasing from south to north.

In spite of the uncertainties in the shale volume calculation, overlapping of natural data with experimental curves, the results of this research work reveals that the exhumation estimation has followed the result published by Ohm et al. (2008) based on vitrinite reflectance data (Fig. 4.27 & 4.28). The work done by Ohm et al. (2008) suggests 500-1500 m exhumation in the Hammerfest basin. There is a need to emphasis that the technique they have followed was based on vitrinite reflectance and temperature data whereas Vp-depth trends as a function of compaction processes has been applied in this research work.

The western side of the Hammerfest basin is more affected by the faulting (Ch. 2, Sec. 2.1) and maximum exhumation is experienced by the western wells (Table 4.2) in the Albatross

discovery, moreover gas leakage is also more in the western side of the Albatross discovery (Ch. 2, Sec. 2.5, Fig. 2.20). All these factors together could explain the reason of dry wells in the western side of the Albatross discovery. It is clear from the investigation that a complex burial history of Hammerfest basin involving uplift, erosion and renewed burial during Cenozoic time has influenced the integrity of the seal rock due to which the distribution of oil and gas in the reservoirs and the position of fluid contacts has been affected.

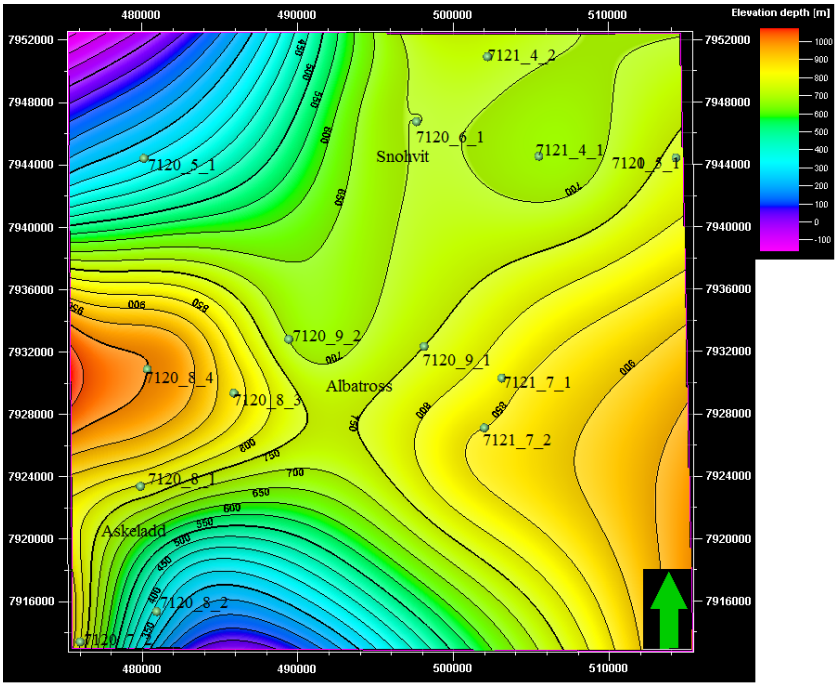

Figure 4.27: Contour map showing exhumation based on the experimental curve kaolinite-silt (50:50) in the Snøhvit development.

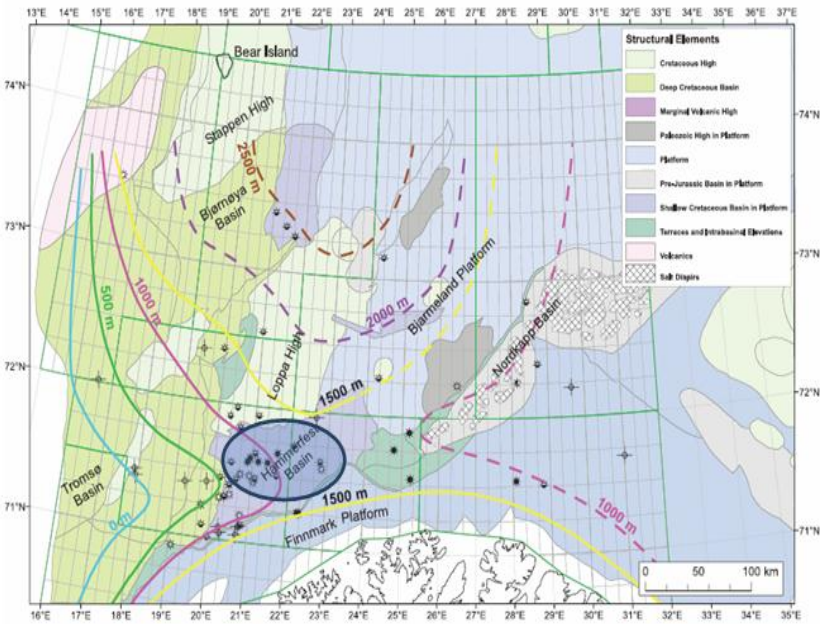

Figure 4.28: Tentative uplift map based on Vitrinite reflectance data (Modified after Ohm et al., 2008).

4.2.4 Source rock affect on rock properties and Opal A and Opal CT conversion

The presence of the source rock of the study area has a dramatic effect on the rock physical properties in the form of reduction in P-wave velocity and density with increasing depth for all the wells. The velocity reversal is observed in the Hekkingen Formation of the study area marked by 'F' (black circle) (Fig. 4.16) just beneath the transition zone from mechanical to chemical compaction. The Hekkingen Formation is one of the major source rocks of the Barents Sea deposited in the marine, deeper water with anoxic environment containing TOC 20 % approximately (Worsley, 2008; Dalland et al., 1988). Density/velocity inversion in the Hekkingen Formation could be the results from the physical properties of karogen and the overpressure. Pore pressure greater than hydrostatic stress causes over pressuring in the source rock is generated during rapidly subsiding basin with low permeability sediments and at that time anoxic conditions was prevailing. Due to which pore pressure could not be able to attain hydrostatic equilibrium. This could be related to under-compaction of the source rock Hekkingen Formation of the study area due to the decrease in the effective vertical stress.

Several factors can be the reason of reduction in Vp with depth in the source rock Hekkingen Formation of the study area. 3D network of the kerogen mainly occur as a laminae in the source rock having preferably parallel orientation to the bedding causing anisotropy in the velocity measurement in such a way that the velocity recorded parallel to the bedding is higher than perpendicular to the bedding (Stainforth and Reinders, 1990; Philippi and Cordell, 1974). Elastic properties and anisotropy of mudstones and shales are highly affected by the degree of the alignment of the grain scale texture (Fawad et al., 2011; Johansen et al., 2004). Bedding oriented velocity measurement is greater in the mature source rocks like Hekkingen Formation during generation and expulsion of hydrocarbons because of adsorption of HC on the insoluble kerogens. Low aspect pore ration parallel to bedding with low compressibility due to the conversion of kerogen to liquid and gaseous HC result in the destruction of kerogen network (Pepper and Corvi, 1995; Vernik and Liu, 1997). However, kerogen is relatively soft as compared to the mineral matrix; it is basically a load bearing organic matter (Palciauskas, 1991). Oil and gas generated due to the thermal cracking of kerogen, become the part of fluid phase thus decreasing the solid phase volume. This increment in the fluid phase of the organic rich source rock like Hekkingen Formation can affect the rate of compaction as well as the rock physical properties.

Smectite will become unstable with increasing temperature greater than 60-80 ℃ (Marcussen et al., 2009; Hower et al., 1976) depending upon the burial history along with time and temperature (Bjørlykke, 1998). The dissolution of smectite and precipitation of illite and quartz can cause the dewatering of upto 30 % by volume (Marcussen et al., 2009; Srodon, 1999). The quartz released during this reaction causes the grain framework stiffening due to quartz cementation (Peltonen et al., 2009). This illitization of smectite also releases crystalline water (Abercrombie et al., 1994). This released crystalline water has the ability to reduce the salinity of the pore water. Thus low salinity pore water will not conduct the electric current largely (Marcussen et al., 2009). This phenomenon of high resistivity in the source rock like Hekkingen Formation of the study area could explain the reason (Fig. 4.15) (Marcussen et al., 2009).

The depositional environments for the clastic sediments have some organism which can produce organic matter which then, at later stage, could be included within the sediments. Both sandstones and mudstones always consists of significant amount of biogenic material from calcareous, siliceous organism and this may provide an important source of carbonate and silica cement at greater burial depth. Another major source of silica is the diatoms and radiolarians which are precipitated as quartz. During the Cretaceous, diatoms were in abundance and have been the major source of silica during Cainozoic (Ch. 2, Sec. 2.1) (Bjørlykke and Jahren, 2010).

In the Mesozoic, the evolution of pelagic planktonic calcareous organisms is caused in the increase of the supply of carbonate on the sea floor, including in the deeper water sediments (Bjørlykke and Jahren, 2010). Amorphous silica (Opal A) is the basic constituent of the structure of the organisms like siliceous sponges which could be dissolved and replaced by Opal CT at higher temperatures and this transition occur at temperature around 50-70ºC corresponding to the depth of 1.5-2 km at average geothermal gradient (Bjørlekke, 2010). This statement is in agreement with the transition of Opal A to Opal CT in the well 7120/8-4 with a geothermal gradient of 34.85ºC (NPD, personal communication). The Opal A/Opal CT transition occurs at a depth of 1667 (m) BSF at temperature 62.08ºC represented by the zones C and D (Fig. 4.16). This transition caused in the increase of velocity from approximately 2700 m/s to 4300 m/s within the thickness of 300 m. This transition from Opal A to Opal CT and then to quartz can cause the change in the acoustic impendence. These reactions are temperature dependent and they tend to occur as a horizontal zones that could be mistakenly understood as a fluid contact (G/W or O/W) (Bjørlykke, 2010).

During transformation from Opal A to Opal C then to quartz, each phase is less disordered and progressive silica diagenesis is accompanied by increased grain density and there could be porosity reduction (Fig. 4.17) and this transition is accompanied by a sharp change in the Vp-depth trend (Fig. 4.16) (Nobes et al., 1992). A separation between Opal A and Opal CT can be observed while cross plotting Vp-porosity together (Fig. 4.29).

The zone E has a high gamma ray and porosity values, low sonic velocity, and deep resistivity values compared to the upper part of the formation (Fig. 4.16, 4.17). The basal part of the formation is related to the log break towards west of the Hammerfest basin which is considered to be the condensed intervals (Dalland et al., 1998). Lower half of the formation contains 0.9-5.5 wt% TOC in which upto 1.5 wt% is represented by bitumen staining resulting in the increased value of HI (hydrogen index) (Smelror et al., 2001).

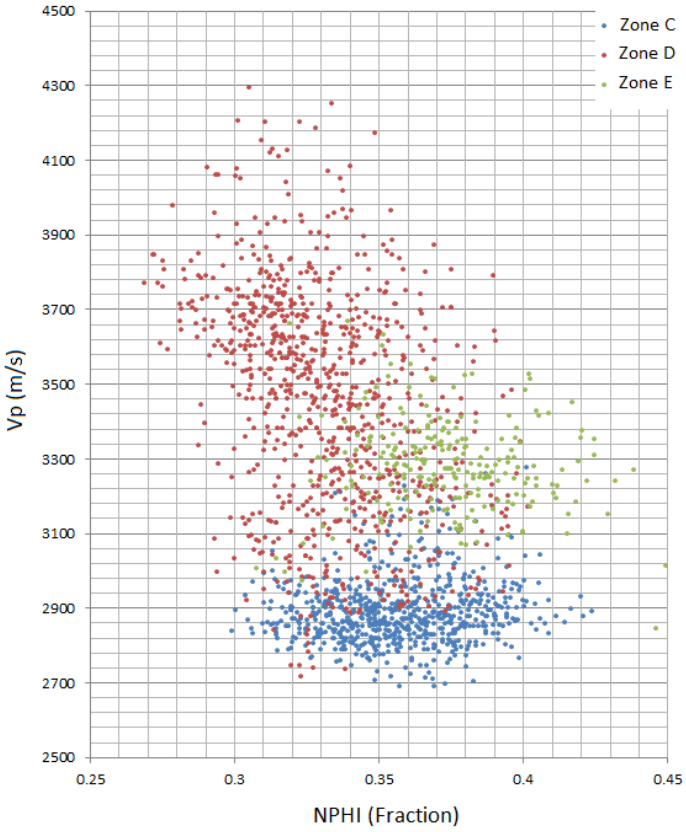

Figure 4.29: The separation between Opal A (Zone C) and Opal CT (Zone D) sonic velocities is clear when the sonic velocity is plotted against the porosity. A distinct gap between the sediments above and below the Opal A/Opal CT boundary appears (Nobes et al., 1992).

CHAPTER 5
Rock Physics Diagnostics

For an efficient interpretation, rock physics is an essential tool which provides the basic relationship between lithology, pore fluid and geological depositional parameters of reservoir rocks. In order to analyze the elastic properties (velocity, density, impedance and Vp/Vs), rock physics act as a bridge to link these elastic properties of rocks to the reservoir properties (water saturation, porosity and shale volume (Chi, X. 2009). Rock physics models can also be used to build a template for efficient reservoir characterization (Ødegaard and Avseth, 2004; Avseth et al., 2005).

In this chapter, the emphasis has been given to Stø reservoir being the main reservoir in the Albatross discovery by using different rock physics templats (e.g. density/porosity versus Vp, porosity-Vp-clay content and Vp/Vs ratio versus IP) a series of rock physics diagnostics. Rock physics diagnostics were also performed on other reservoir rocks (Nordmela, Tubåen and Fruholmen) in the Kapp Toscana Group.

5.1 Results

5.1.1 Vp-density/porosity relationship of Stø Formation

A comparison of densities calculated from Vp using Gardner et al. (1974) and Lindseth (1979) equations and the measured density of the Stø Formation, in the well 7120/8-4 has been performed (Fig. 5.1).

The Stø Formation, depending upon its lithological difference, has been divided into three sub-facies. The Facies I is shaley sandstones, in the Facies II, the percentage of shale is higher than the other two sub facies and the Facies III represents more or less clean sandstones (Fig. 5.4). The depth-density curve reflects the fact that the Lindseth (1979) calculated density is in good agreement to the measured density as compared to the density calculated by Gardner et al. (1974) equation. However, for the Facies III, a difference among the measured, Gardner and Lindseth densities can be seen. Density could be an important parameter to differentiate lithologies and other petrophysical properties (porosity and fluid content) and the velocity, which have been used to calculate density, could be different in various mineralogical composition and fluid contents of the rock. Hence, it could be hard to calculate absolute density by using empirical relations where Vp is the input parameter. It is important to keep in mind that Vp also changes with different parameters and so may change calculated density.

Density porosity has been cross-plotted against sonic velocity for the well 7121/7-2. For that purpose, Stø Formation data points have been split into two units based on different fluid saturation. Purple data points are representing hydrocarbon-saturated sandstones whereas aqua color showing water saturated sandstone (Fig. 5.2). Three reference curves have also been plotted; Wyllie et al. (1956), Gardner et al. (1974) and Raymer et al. (1980). Most of the Stø Formation data points follow the Raymer and Wyllie reference curves. Hydrocarbon saturated data points follow Raymer reference curve whereas Wyllie reference curve is followed by water saturated data points for the Stø Formation.

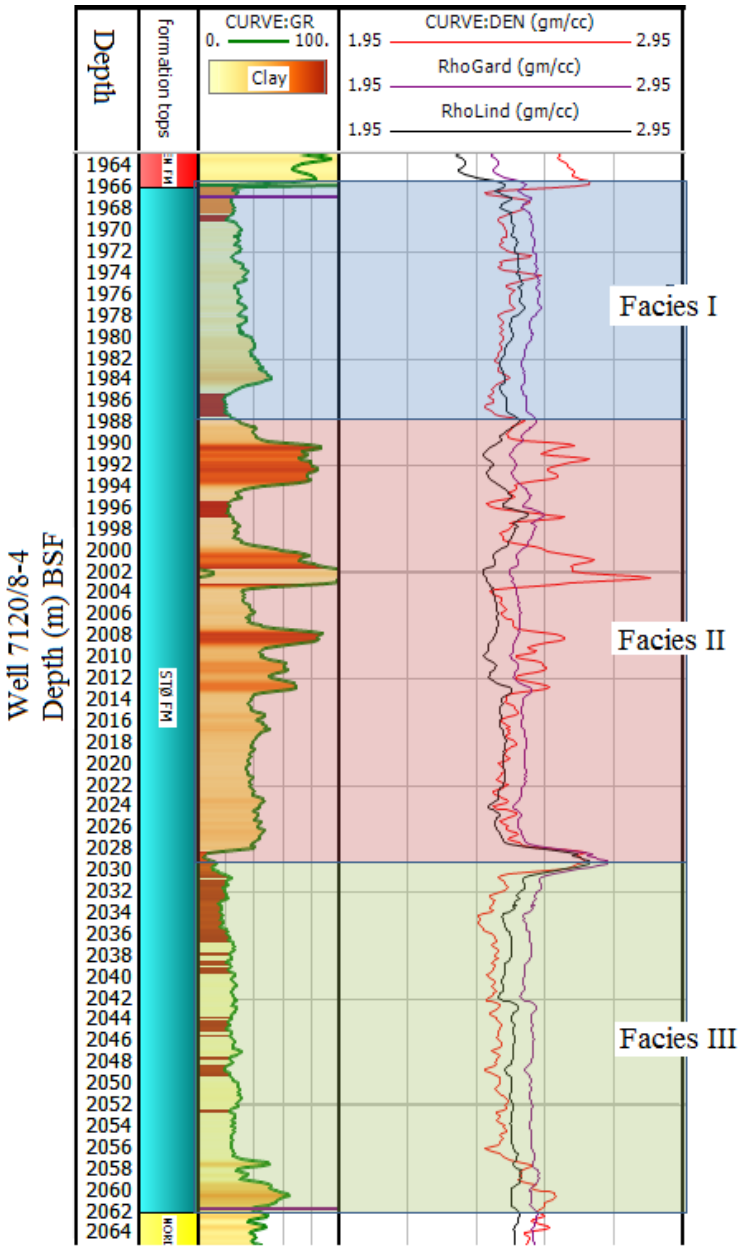

Figure 5.1: Comparison among measured and calculated Gardner et al. (1974) and Lindseth. (1979) density for three different facies in the Stø Formation in well 7120/8-4.

The assumptions behind the three models (Raymer et al., 1980, Wyllie et al., 1956 and Gardner et al., 1974) are to use clay free data points, mono mineralic (Quartz), isotropic rock should have same velocities. The data points included in the analysis from the Stø Formation may not be clay free due to error associated with V_{sh} estimation. Moreover, the uncertainties in calculating the density porosity make this data spreading indefinite to some extent.

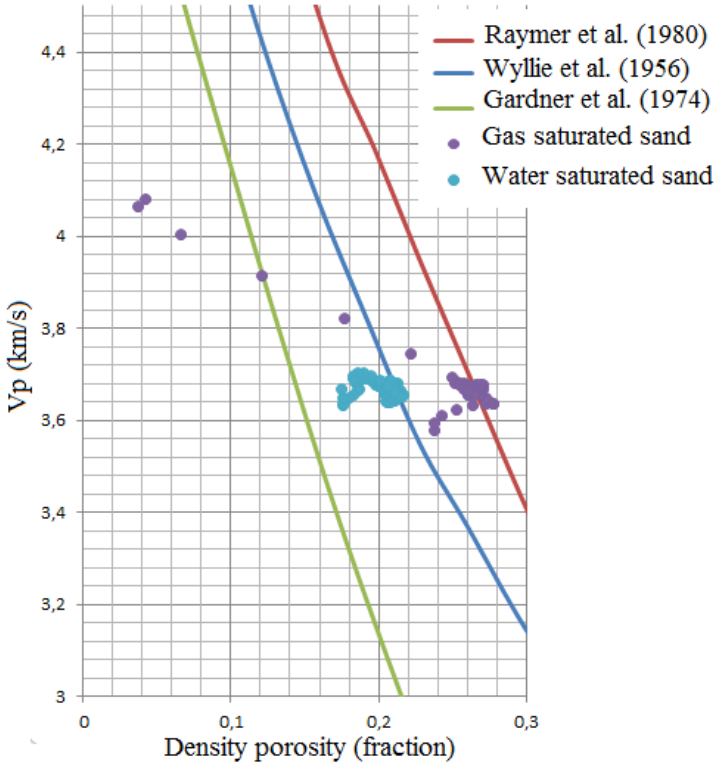

Figure 5.2: Velocity versus porosity cross plot in hydrocarbon and water saturated clay free sandstone in the well 7121/7-2 with Raymer et al. (1980), wyllie et al. (1956) & Gardner et al. (1974) curves.

5.1.2 Velocity-porosity-clay behavior

Several authors (e.g Avseth et al., 2005; Dvorkin and Nur, 1996) have proposed that in sandstones, the slope of velocity-porosity trend is highly inconsistant and depends largely on the geologic processes that control porosity. Usually steep velocity porosity trends in the sandstones are representative of porosity variation controlled by diagenesis, i.e., porosity reduction from pressure solution, compaction and cementation (Avseth et al., 2010). Whereas, the flatten trends reflect the depositional changes.

Wyllie et al. (1956), Gardner et al. (1974) and Raymer et al. (1980) equations, which have been used for calculation different relations for pure quartz sandstones but the assumptions, are to use clay free sandstone. Although, the clay minerals are the most abundant materials in the sedimentary basins and their presence change the elastic behavior of the reservoir rocks as a function of mineral type, volume and distribution. Thus, two sandstones with the same amount of clay can have different elastic properties due to the differences in volumetric percentage of clays. The clay minerals elastic properties vary significantly for different clays and are important in the rock physics modeling to comprehend the seismic and sonic log responses of shaley units and reservoir rocks with clay (Mondol et al., 2008).

Han (1986) specified an empirical relation combining velocity porosity and clay volume fraction. The cross-plot of Vp-porosity in the Stø Formation from well 7120/8-3 is plotted with Han's model, which is calculated at 40 MPa effective pressure (Fig. 5.3). The data points in this cross plot have been divided into four different parts depending on clay volume

fraction. It is clear from the observation that the decrease in velocity at same porosity influenced by clay contents. The data points of 0-20% clay contents ranges between 5-25% Han's line, whereas the data points with 20-40% clay fractions follow the Han's 15 to 25 % line.

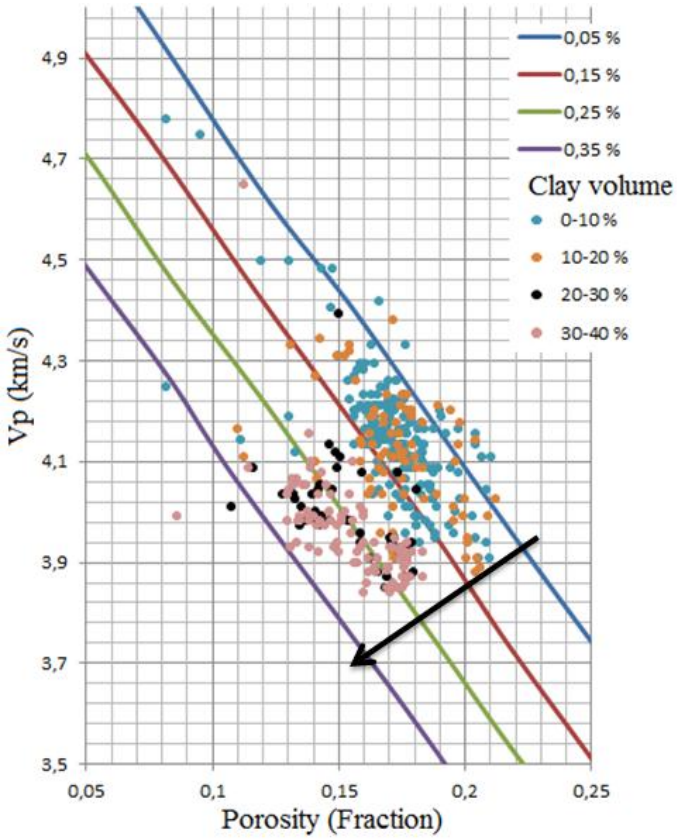

Figure 5.3: Vp-porosity cross plot of the Stø Formation in the well 7120/8-3 has been compared to Han's empirical relation with different clay volume at 40 MPa stress.

Effective stress conditions are important to calculate in the normally subsiding basin to account for such kind of crossplot. Hammerfest basin is an uplifted basin and the rocks are stiffer than expected keeping in view the present effective stress conditions. The velocities of the rocks are higher than the rocks located at similar depth in the normally subsiding sedimentary basins. All the empirical equations assume stiffness of rock corresponding to the same effective stress. For that reason, it is always important to know the actual depth of the rocks to correctly ascertain the rock stiffness when considering such kind of equations. Another point which could affect the result is the calculation of clay volume which is based on gamma ray log. Due to the variation of the density in the fluid and mineral phases, the density porosity is also uncertain. Hence, the deviation could be expected in the result from the Han's data point.

5.1.3 Compressional velocity and porosity in sand-clay mixture

Data points from Tubåen and Fruholmen Formations have been taken from the well 7120/9-1, in order to understand the dependence of velocity, porosity and clay content (Fig. 5.4). It is considered that the clay particles may locate within pore space in sand particales due to which

the porosity will decrease linearly with increasing clay content (Avseth et al., 2005). These clay particles cause in the increase in the sand lattice. This expension of the sand lattice will tend to increase the porosity of the shaley sand. In addition to that, additional pore space is created by expension of the sand lattice to be filled with clay which shifts the porosity minimum data points towards higher clay contect (Marion et al., 1992). Marion (1990) introduced V-shaped behavior of sand-shale mixture in case of porosity and clay content and inverted V-shaped in case of velocity and clay content. According to Marion et al. (1992) with the decrease of porosity, the velocity increases with increasing clay content to the critical clay point (Fig. 5.4a). This point is the transition point between shaley sand and sandy shale. Above this point porosity increases and velocity decreases with increasing clay contents.

The Fruholmen Formation is plotted in the Vp and clay volume (Vshale) plot which is showing the inverted V-shaped behavior (Fig. 5.4b). The velocity increases from sandstone to shaley sandstones because the finer particles are pore filling. When velocity increases upto 40% clay content then it starts decreasing with the increase in the clay content. This point is called as critical clay point where the velocity decreases with increasing clay content (Fig. 5.4b). This is also the transition point from shaley sand to sandy shale. After that point, the velocity decreases further towards pure shale. Whereas, the V-shaped behavior was found in the Tubåen Formation of the same well. The porosity of the sand-shale mixture decreases with increase in the clay content. At the certain point (critical clay point), the porosity of the sand-shale mixture start to increase with increasing clay content because of the clay porosity (Fig. 5.4a). Different porosities values for critical clay points (Fig. 5.4a, b) could be explained with the fact that the Fruholmen Formation has more shale content reflecting higher porosity values compared to the Tubåen Formation contains more sand hence showing lower values of porosity (Fig. 5.4c).

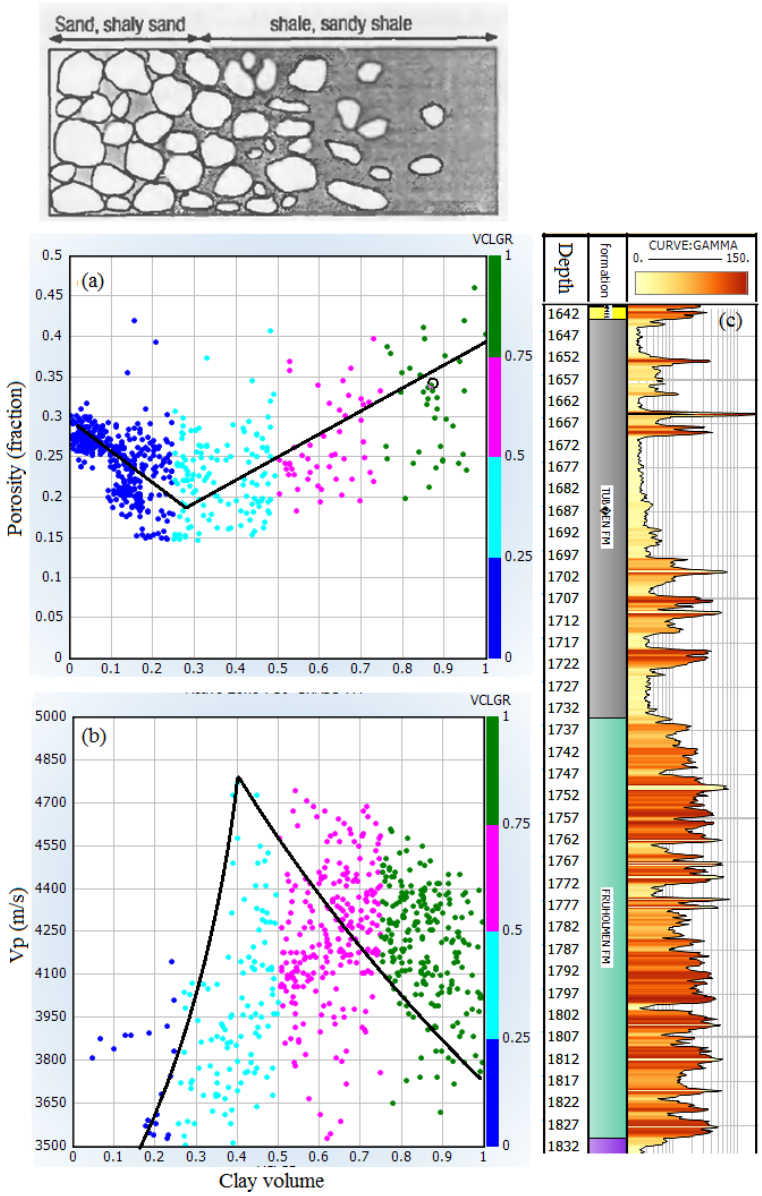

Figure 5.4: Porosity and P-wave velocity versus clay volume are showing the inverted V and V shaped behavior along with gamma ray log response (explained by Marion et al, 1992) in the 7120/9-1 well.

5.1.4 Rock physics analysis of lithofacies

In order to perform rock physics analysis on the seismic lithofacies, data points related to Stø Formation from the well 7120/8-4 has been divided into three sub-units based on the nature of gamma ray curve (Fig. 5.5). All the facies are saturated with water but due to the availability of shear log, this well has been chosen for rock physics analysis. As stated earlier the Stø Formation is encountered at a depth of 1965 (m) BSF in the well which is also the start depth of facies I upto 1989 (m) BSF while the top and bottom depth of facies II and III are 1989-2028 and 2028-2061 respectively. The facies II contain small-scale sea level fluctuation (transgression-regression cycle) due to which there is an alteration of sands and shales. There exists a variation in different log responses within the facies II. The Facies I is shaley

sandstones, in the Facies II, the percentage of shale is higher than the other two sub facies and Facies III represents more or less clean sandstones (Fig. 5.5).

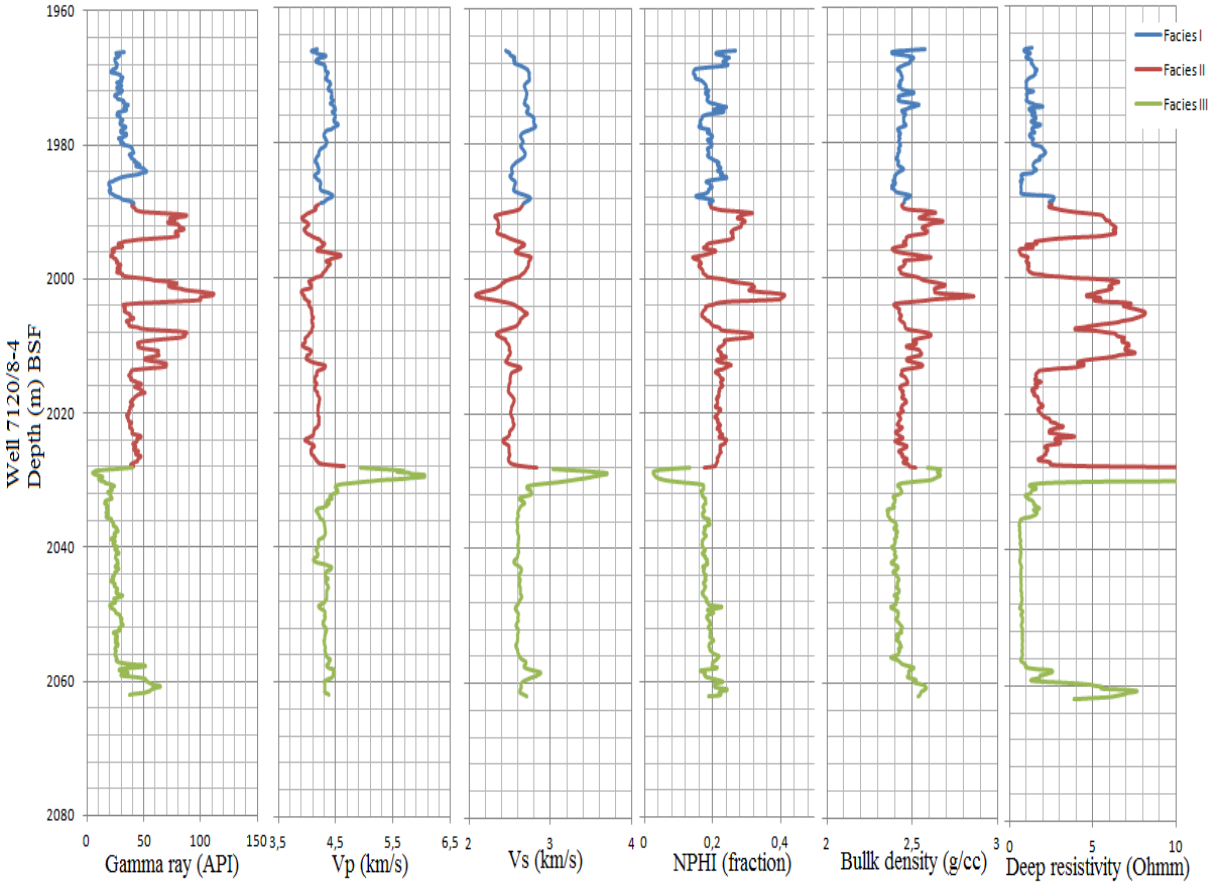

Figure 5.5: Petrophysical log responses of water saturated Stø Formation in the well 7120/8-4 with three distinct facies.

Porosity of Stø Formation has been cross-plotted against Vs, Vp/Vs ratio, bulk and shear modulus, in order to check the rock physics behavior of these three facies (Fig. 5.6). Due to the lithological differences within the Stø Formation, the facies distributions are different in these plots. The facies II has higher porosity as compared to the Facies I and III along with this, the shear modulus and Vs value for facies II is less than the rest of the facies (Fig. 5.6a, d). However, the bulk modulus of the clean sandstone is higher than that of facies I and II (Fig. 5.6c). Due to the higher Vp and lower Vs values in the Facies III, the Vp/Vs ratio is higher which is clear in the Vp/Vs-porosity crossplot. Nevertheless, the Vp/Vs ratio is expected to be higher in the shales (Facies II) (Avseth et al., 2005).

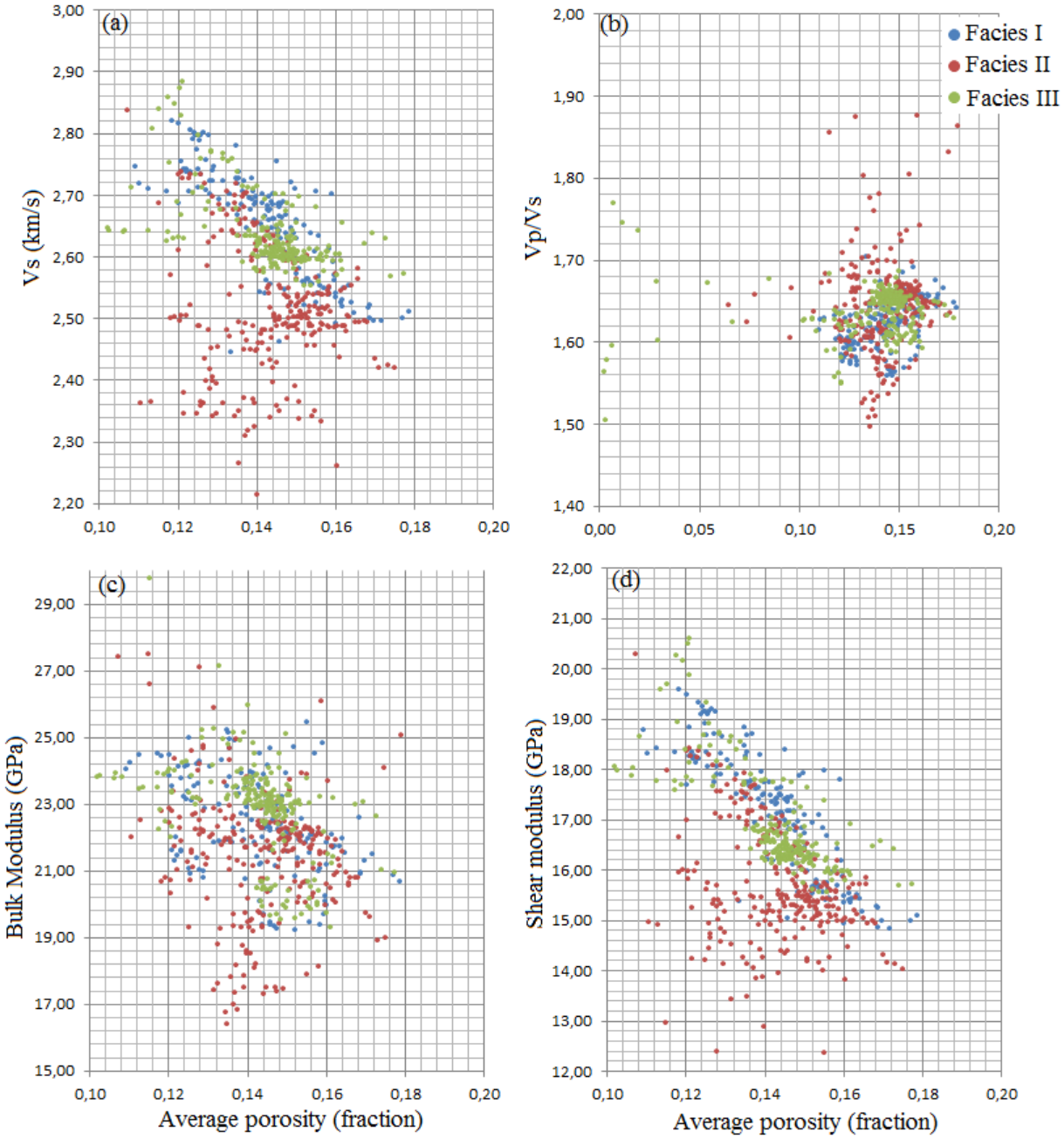

Figure 5.6: Porosity versus Vs, Vp/Vs, bulk and shear modulus of the Stø sandstones separated by three distinct facies in the well 7120/8-4.

The higher values of Vp and density for the Facies II corresponding to higher value of AI as compared to Facies III which is cleaner sandstones (Fig. 5.7c). For sand when porosity is reduced, the Poisson's ratio should be reduced as a response but here PR increases with decreasing porosity which could be explained by the effect of clays presence in the Stø Formation (Facies II) (Fig.5.7a). Poisson's ratio-AI and Vp/Vs-AI crossplots being lithology indicator (Avseth et al., 2009) show here a good lithology separator (Fig.5.7b, d).

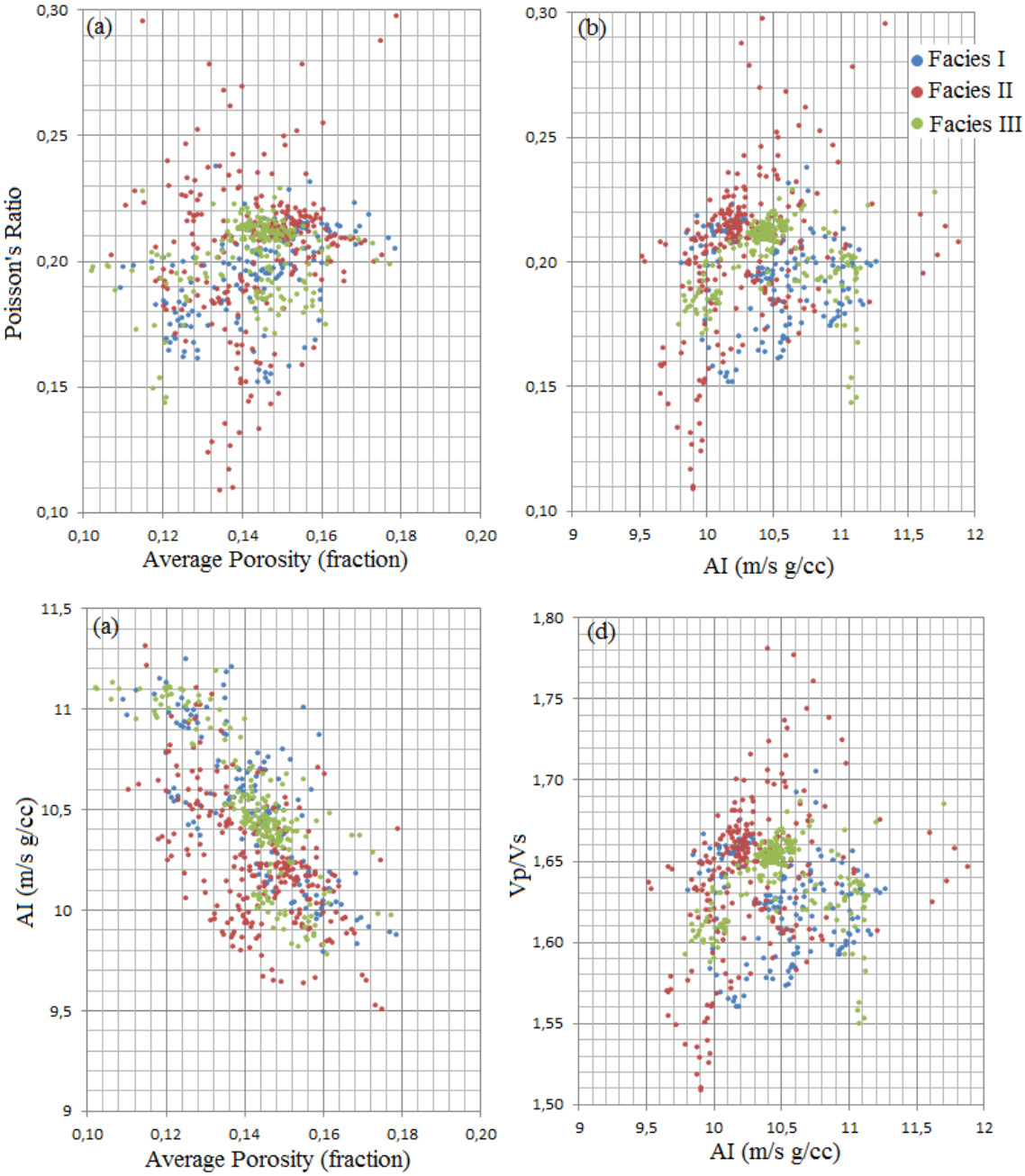

Figure 5.7: Stø Formation facies from the well 7120/8-4 in the (a) Poisson's ratio-porosity (b) Poisson's ratio-AI (c) AI-porosity (d) Vp/Vs-AI.

5.1.5 Porosity variation in Stø Formation

During burial, the porosity of sediments changes dramatically due to diagenesis. Diagenesis, here, represents all the mechanical and chemical alterations of rocks after deposition. Diagenetic processes change with depth, time and temperature. In the early diagenesis, the process damaging porosity in sands and shales is the packing and grain deformation.

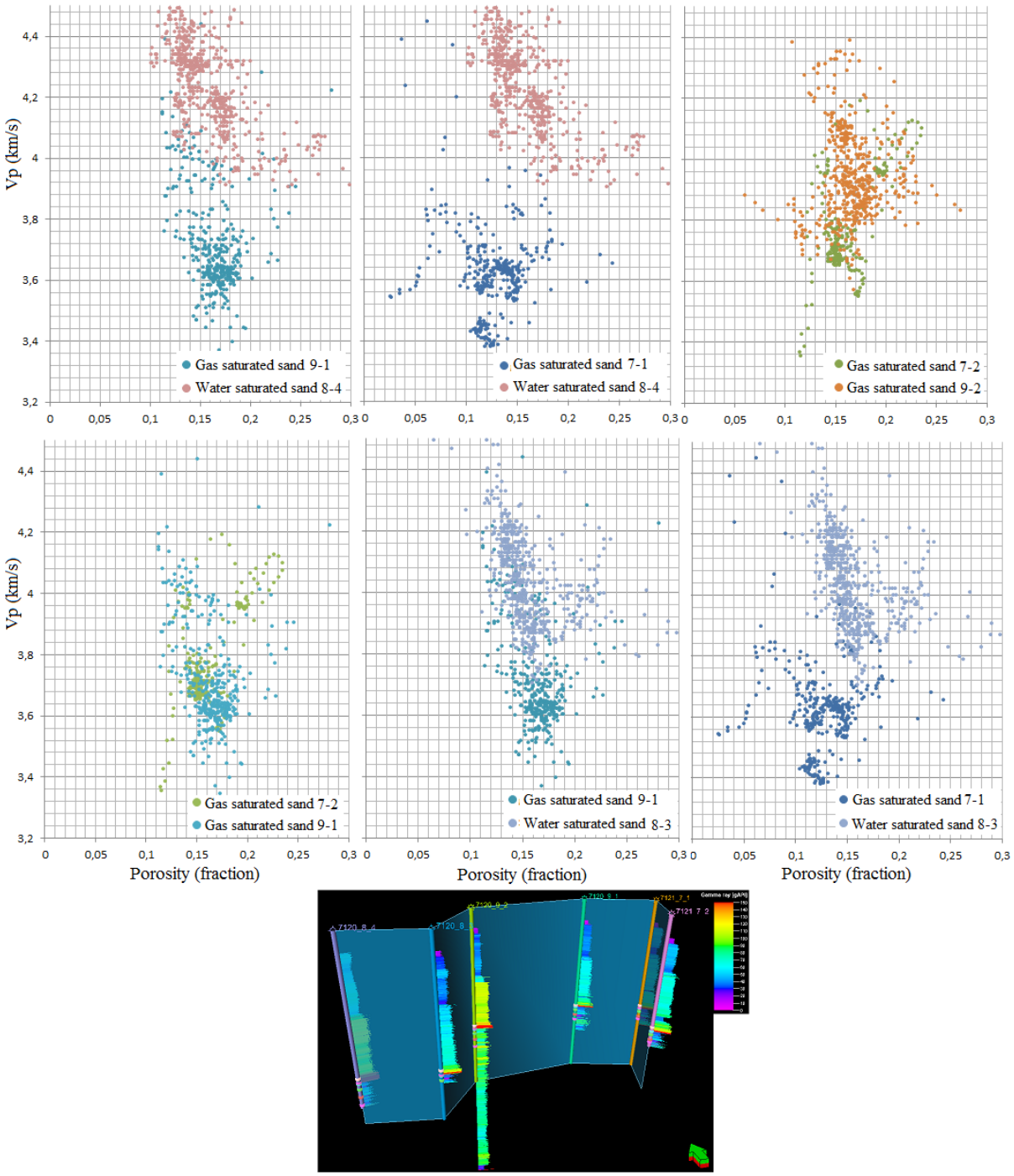

Figure 5.8: Vp-porosity variation in in the Stø Formation of all studied wells. Well fencing is showing the location of wells used.

In the deeper parts chemical compaction affects porosity. More particularly, quartz cementation is the important factor decreasing porosity in quartz rich sandstone and it's associated with pressure solution (Avseth et al., 2001). Ramm and Bjørlykke, (1994) suggested that porosity lose in the clean sandstone is mostly due to pressure solution and quartz cementation.

In order to analyze porosity variation in the Albatross discovery, Vp-porosity data points of all six wells have been cross plotted (Fig. 5.8). The Stø Formation being main reservoir has been considered for this purpose. Compaction analysis reveals that the Stø formation is in the chemical compaction domain (Ch. 4, Fig. 4.1). The porosity variation in the Stø Formation from eastern wells to western wells ranges from 14% to 20% at different depth level. The western wells have lower porosity range compared to that of eastern wells. Whereas the velocity difference in the eastern and western wells is 3400 m/s to 4200 m/s and 3800 m/s to 4500 m/s respectively (Fig. 5.8). The western water saturated wells (7120/8-3 and 7120/8-4) have lower porosity and higher Vp values compared to remaining gas saturated eastern wells.

Due to higher Vp differences within narrow range of porosity change need to be confirmed by different cement models. Porosity variation in all six wells for the Kapp Toscana group has been given in the Table 5.1. So that it could be concluded either this change is due to quartz cementation or it is the effect of mineralogical variation?

5.1.5.1 Pore fluid saturation and net-to-gross (N/G)

Pore fluid saturation in the sandstone reservoir is highly affected by sandstone heterogeneity and sandstone microstructure. Hence, in the rock physics analysis, it is important to include these geological factors. We know that the onset of quartz starts in association with smectite to illite transition at a depth which corresponds to 70-80^{0}C. This initial cement will tend to reduce the pressure and fluid sensitivity of the sandstone (Avseth, 2009).

One useful parameter of quantification of heterogeneity of sandstone reservoir is net-to-gross (N/G). A reservoir zone could have higher N/G at well log scale but low N/G at seismic scale. With the decrease in the N/G, there would be increase of Vp/Vs irrespective of porosity, even for high gas saturation in the sands. The sands with higher N/G could have dramatic affect in lower the AI but there is increase in AI with high porosities. This is all due to the varying fraction of shale in the sandstones reservoirs.

The Stø Formation in the eastern wells shows higher N/G compared to western wells (7120/8-3 and 7120/8-4). Whereas other formations in the Kapp Toscana group show lower N/G values. The gas saturation in the Stø Formation ranges from 70-90%. Remaining formations in the Kapp Toscana group show lower saturation values. The pore fluid saturation and net-to-gross of the formations in the kapp Toscana group have been given in the Table 5.1. In order to avoid any discrepancies in the rock physics templates while doing reservoir characterization, it is necessary to know the saturation, porosity as well as net-to-gross in the reservoir sandstone.

Table 5.1: Reservoir properties of the formations in the Kapp Toscana group in all six studied wells.

Wells	Gross	Net	Net/Gross	Gas Saturation %	Porosity %	Formations
7120/8-3	86	73.87	0.86	Shows	17-15	Stø Formation
7120/8-4	94.90	75.17	0.79	Dry	15-14	
7120/9-1	55.80	52.70	0.94	80-90	20	
7120/9-2	77.50	71.86	0.92	70-80	20-18	
7121/7-1	57.50	54.51	0.95	70-80	17-15	
7121/7-2	56.10	49.29	0.88	80-90	20-18	
7120/8-3	52	24.89	0.47	0		Nordmela Formation
7120/8-4	136	44.67	0.33	0	22-18	
7120/9-1	90	48.04	0.53	Traces	24-22	
7120/9-2	108	57.87	0.54	60-70	22-20	
7121/7-1	94.40	79.92	0.85	10-20	22-20	
7121/7-2	90	56.13	0.62		24-22	
7120/8-3	Not Penetrated					Tubåen Formation
7120/8-4	147	75.27	0.51	0	18-16	
7120/9-1	91	70.42	0.77	0	22-18	
7120/9-2	134	100.78	0.75	60-70	25-22	
7121/7-1	44	37.17	0.85	10-20	24-22	
7121/7-2	45	40	0.87	Traces	25-23	
7120/8-3	Not Penetrated					Fruholmen Formation
7120/8-4	31	6.86	0.22	0	22-20	
7120/9-1	96	13.32	0.14	0	28-25	
7120/9-2	262	84.85	0.32	50-60	22-20	
7121/7-1	104	27.28	0.26	30-40	22-20	
7121/7-2	65	34.06	0.52	Traces	24-22	

5.1.6 The cement models

A number of authors have given different cement models. The following three models are important with respect to rock physics diagnostic which are;

- The contact cement model (Dvorkin et al., 1994).
- The friable or unconsolidated sand model (Dvorkin and Nur, 1996).
- The constant cement model (Avseth et al., 2000).

The friable sand model of Albatross discovery has been cconstructed, while the other two models have been digitized from the Avseth et al. (2005). The cement fraction in the constant cement model is about 2%. This model has been used further for different rock physics analysis (Ch. 3, Sec. 3.2.6, Fig. 3.16).

P-wave velocity of the Stø Formation from all six wells has been plotted against porosity which shows different fraction of cement distribution within all the wells (Fig. 5.9, 5.10, 5.11). The thickness of the Stø Formation is different from east to west with varying mineralogical composition (Ch. 2, Sec. 2.4.2.1, Fig. 2.16). Due to which the Stø Formation response with respect to different cement models is unique. The Stø Formation from the western wells (7120/8-4 & 7120/8-3) follows the constant cement line, the well 7120/8-4 having slightly higher cement value compared to the well 7120/8-3 (Fig. 5.9). On the other hands, the Stø Formation data points from the eastern wells (7121/7-1 & 7121/7-2) falls between constant and friable cement models (Fig. 5.11). The velocity variation is higher in the western wells, which is 3.7 to 4.5 km/sec as compared to the eastern wells, which is 3.4 to 4.2 km/sec.

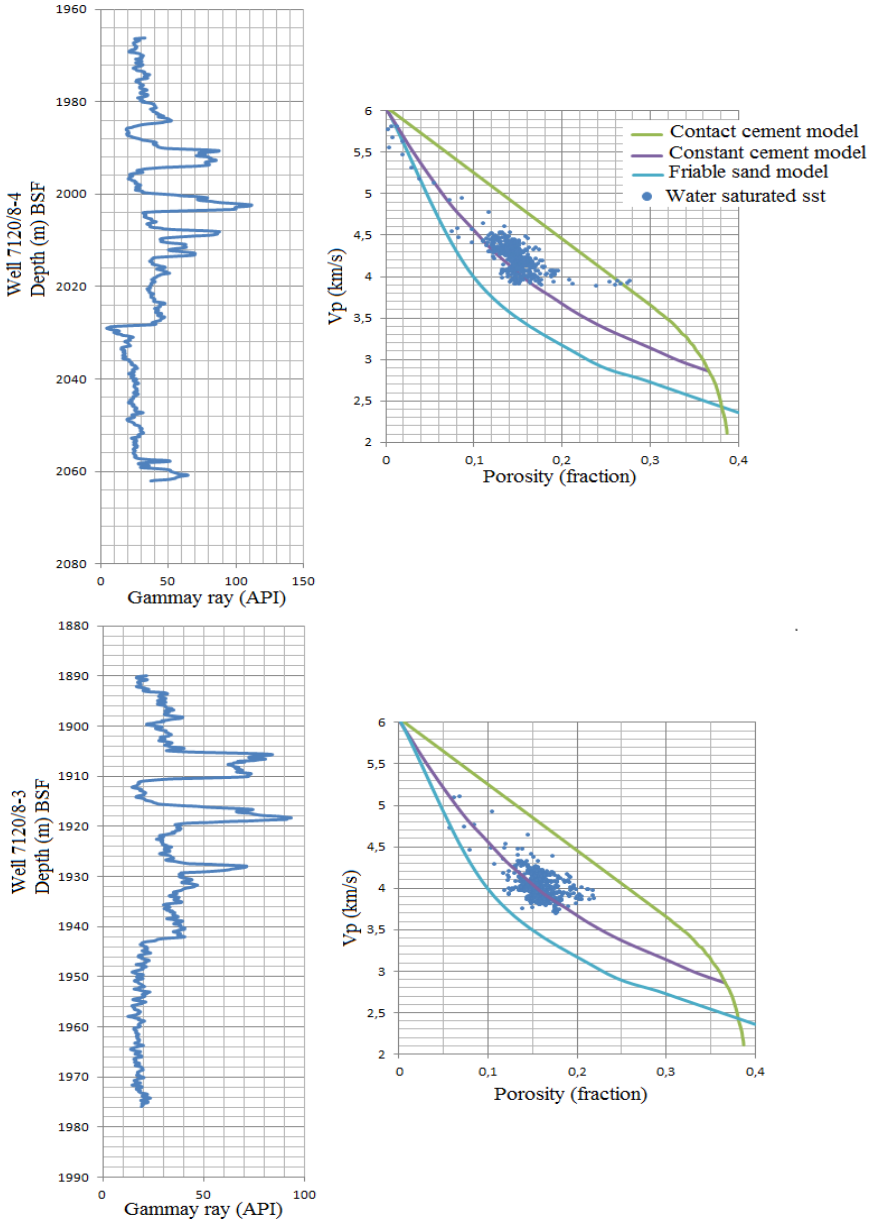

Figure 5.9: Vp-porosity cross-plot of the Stø Formation in the well 7120/8-3 & 7120/8-4 compared to three cement models. The gamma ray response of the Stø Formation as a function of depth is also known.

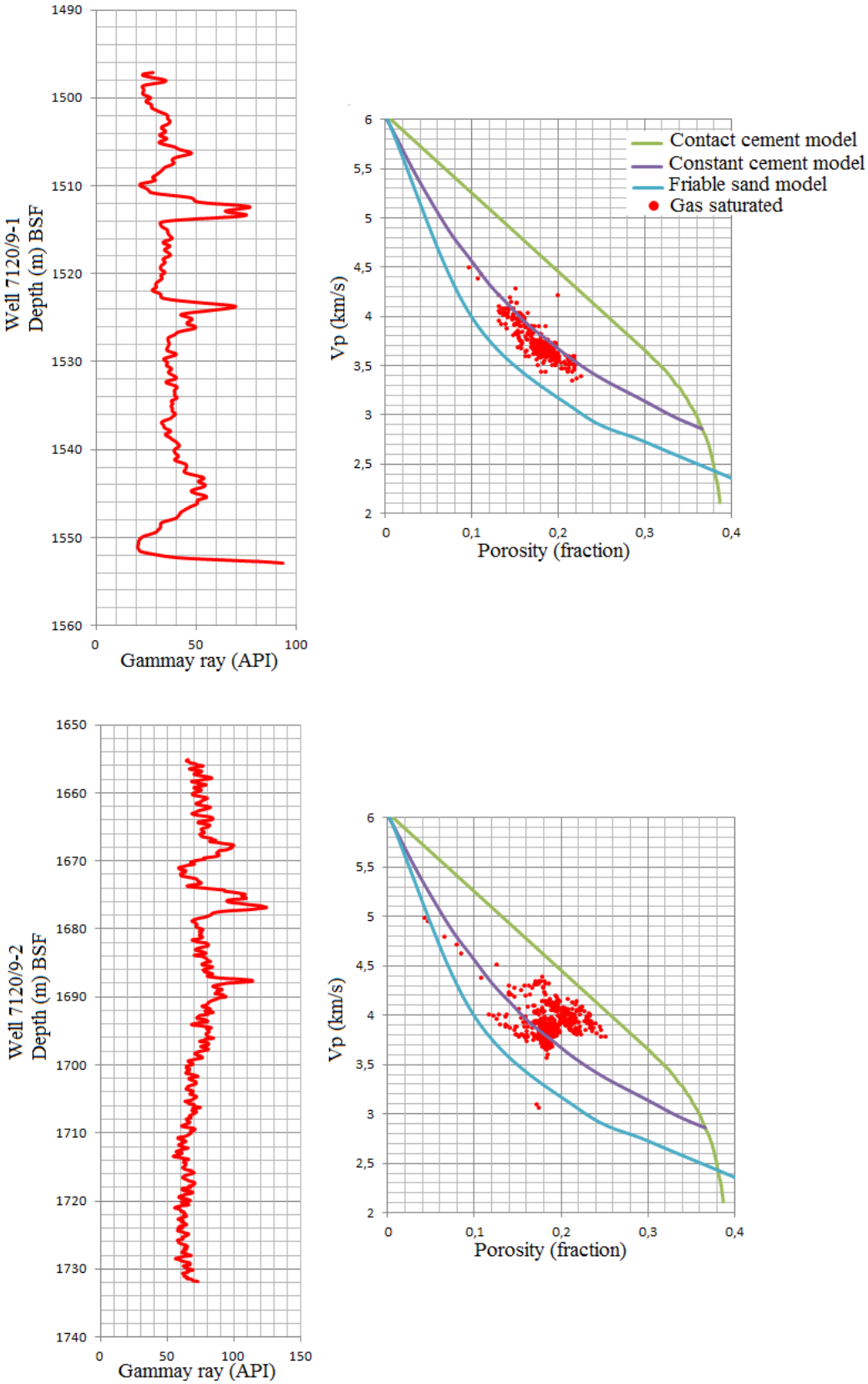

Figure 5.10: Vp-porosity cross-plot of the Stø Formation in the well 7120/9-1 & 7120/9-2 compared to three cement models. The gamma ray response of the Stø Formation as a function of depth is also known.

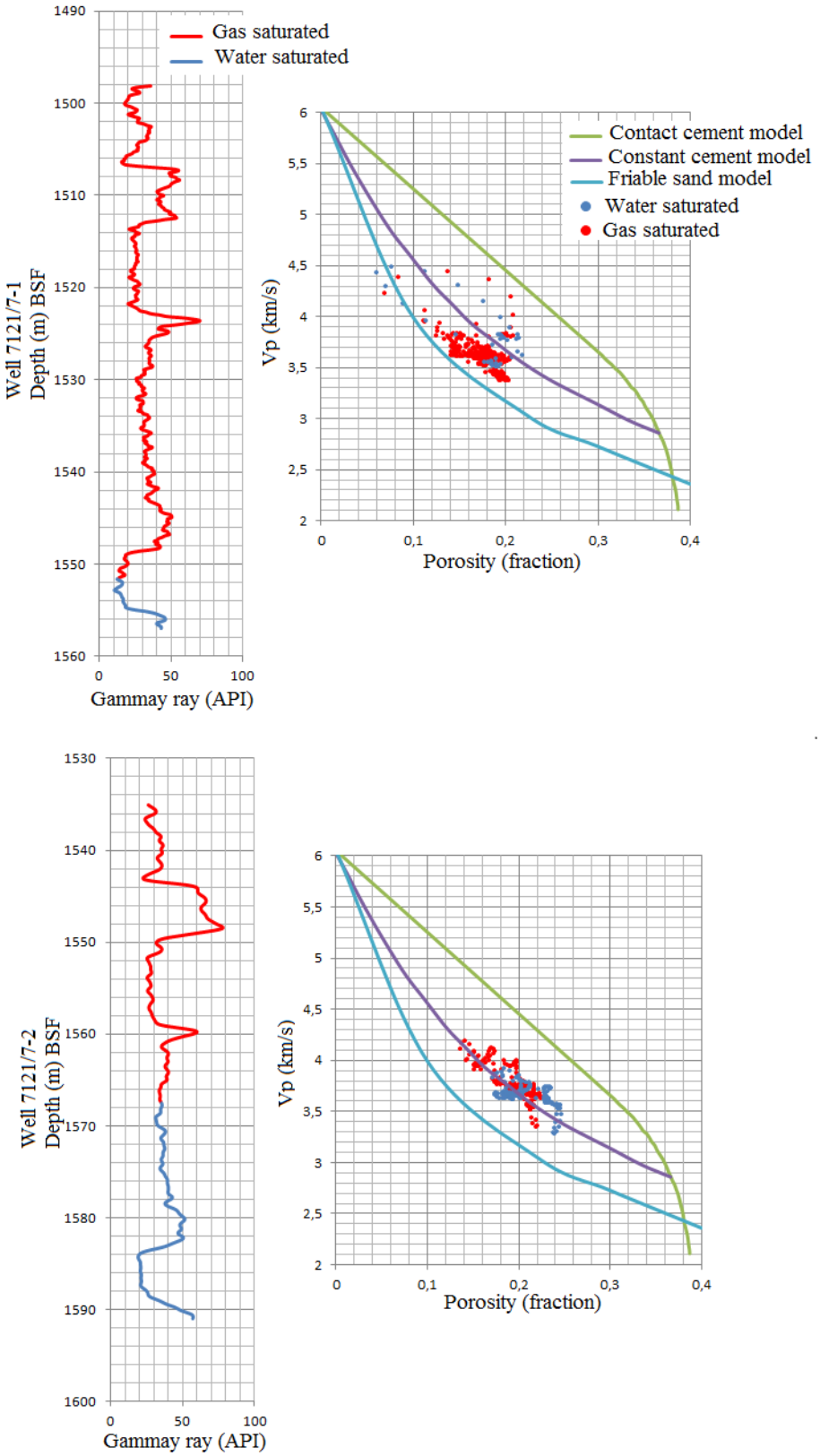

Figure 5.11: Vp-porosity cross-plot of the Stø Formation in the well 7121/7-1 & 7121/7-2 compared to three cement models. The gamma ray response of the Stø Formation as a function of depth is also known.

The well 7120/8-3 contains only a trace of hydrocarbon whereas the well 7120/8-4 is a dry well; both the wells represent western wells whereas all the remaining eastern wells (7120/9-1, 7120/9-2, 7121/7-1 & 7121/7-2) are gas saturated wells.

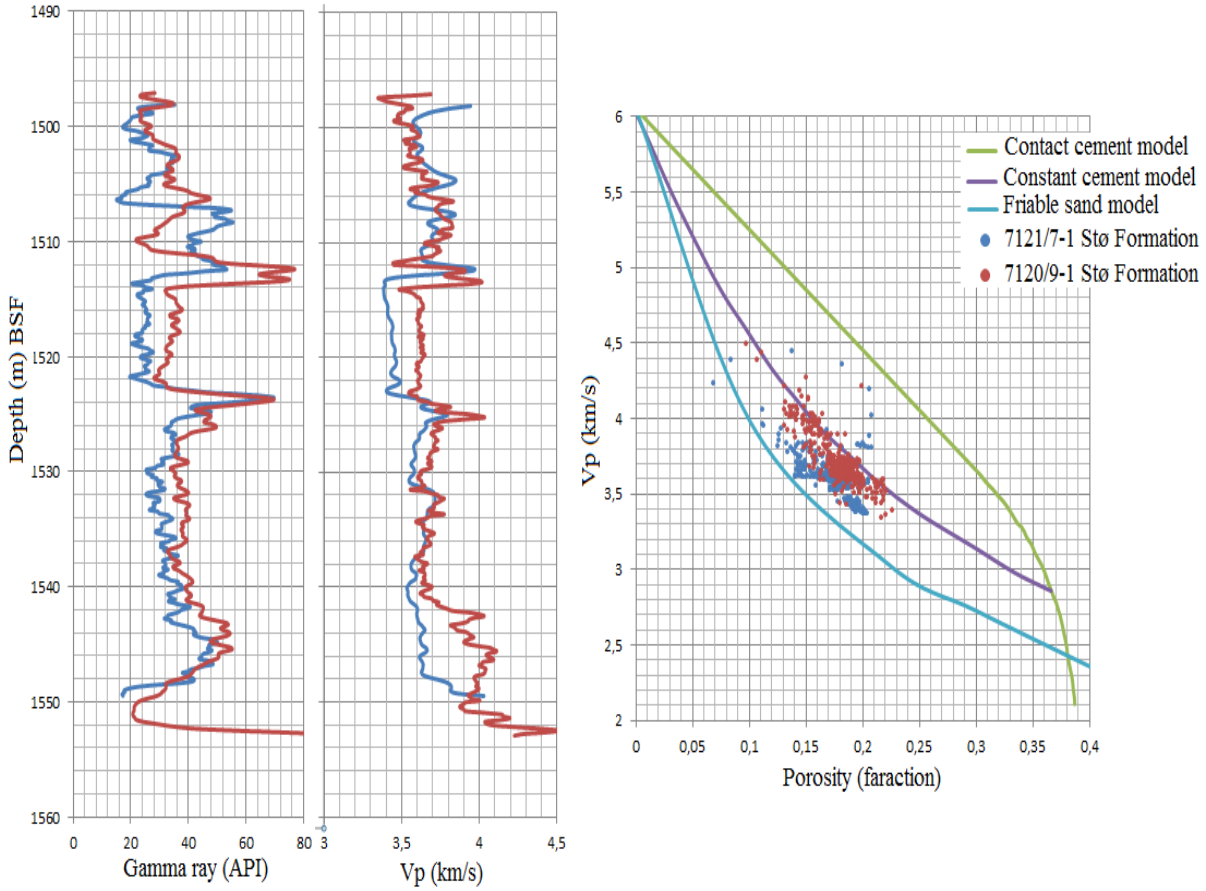

Figure 5.12: The Stø Formation of the wells 7121/7-1 & 7120/9-1 is showing different velocity, gamma ray and cement models.

The similar diagnostics also run to compare dry and gas saturated wells. The wells 7121/7-1 & 7120/9-1 are gas saturated and have similar depth for Stø Formation indicating similar history of overburden stress. Geographically both the wells are close to each other but in different blocks. The geothermal gradient for both the wells is more or less similar (30 & 31.48 ^{0}C/km) (Ch. 1, Table 1.1). The gamma ray log trends of these wells are also nearly similar but the Vp response is different depending on the mineralogical composition of the Stø Formation. The gamma ray reading fall in the range of 16 to 56 (API) and 24 to 76 (API) for the wells 7121/7-1 and 7120/9-1 respectively. Although both wells have experienced same type of compaction behavior (mechanical and chemical) due to similar depth level. The well 7121/7-1 has low gamma ray reading compared to the well 7120/9-1 (Fig. 5.12) and the Vp value for the former one is in between 3.4 to 4 km/sec and later one has a value between 3.5 to 4.2 km/sec. Due to lithological dissimilarity, owing to different sub environments within the same formation and different velocity values, the cementation history is different. The well 7121/7-1 is in between constant and friable cement models whereas the well 7120/9-1 is slightly below the constant cement model (Fig. 5.12). Both the wells follow the constant

cement model but the percentage of cement for both wells is different. The porosity ranges for both the wells fall between 12-20% which is almost similar.

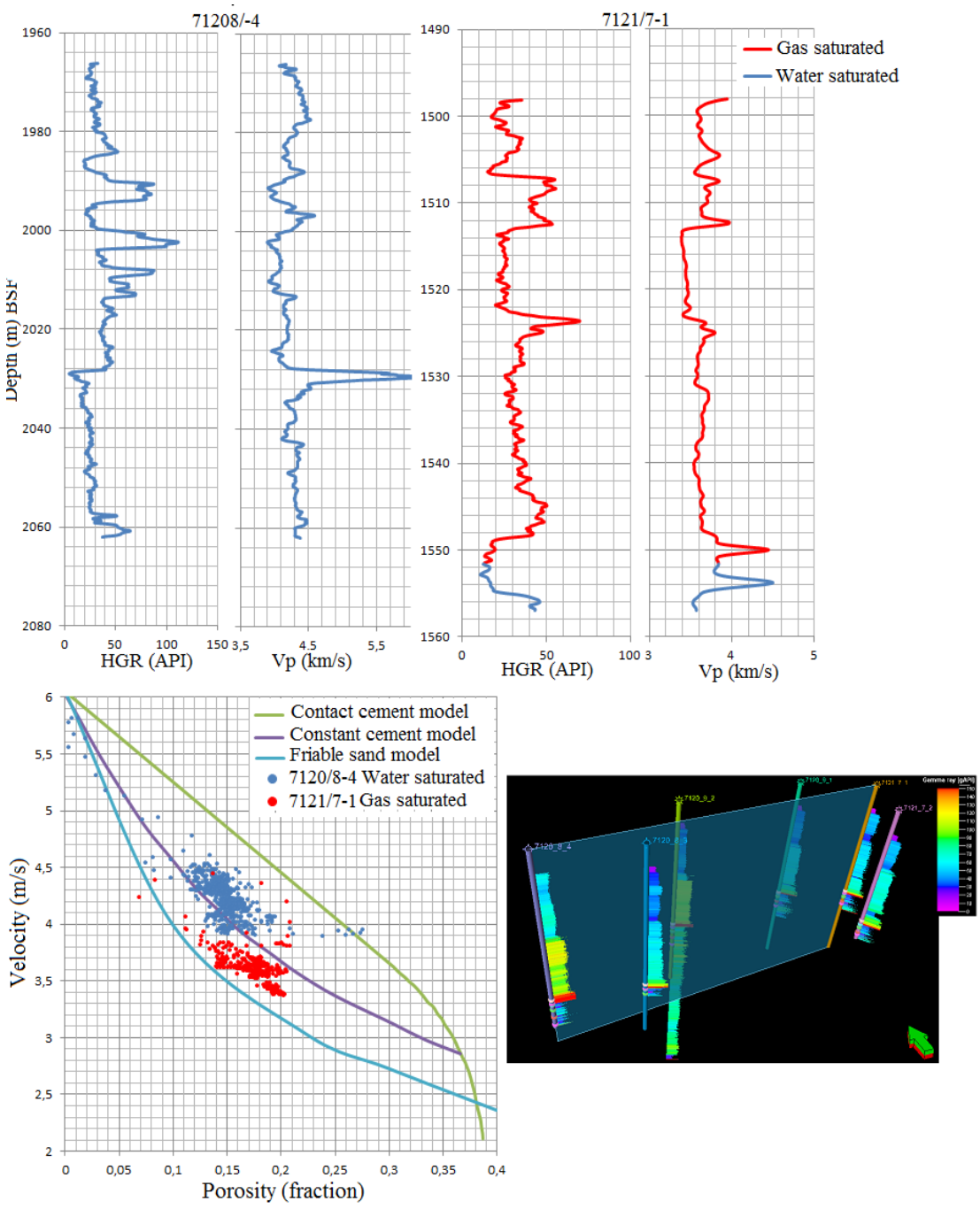

Figure 5.13: The gamma ray and velocity versus depth and velocity-porosity cross-plot with three cement models for the wells 7120/8-4 & 7121/7-1 are showing different scenario. Well fencing is showing the location of wells used.

The western well 7120/8-4 has been compared to the eastern well 7121/7-1. In other words, the comparison has been made between water saturated and gas saturated Stø Formation using different cement models (Fig. 5.13). The gamma ray reading in the well 7120/8-4 ranges from 5 to 100 API, which is higher than the well 7121/7-1, which has low gamma ray reading (10-

70 API) (Fig. 5.13). The Vp depth trends for both of the wells are also different. The middle part of the Stø Formation in the well 7120/8-4 is showing more velocity variation whereas the velocity variation in the well 7121/7-1 is not that much pronounced. The well 7120/8-4 has experienced the deepest penetration (Table 2.1) in Stø Formation whereas the depth for Stø Formation in the well 7121/7-1 is 1498 to 1556 (m) BSF. This means that the higher present day overburden stress is experienced by the western well 7120/8-4. The cement model of these two wells shows different response. The Stø Formation data points for the dry well 7120/8-4 fall between contact and constant cement model whereas the well 7121/7-1 is below the constant cement line. The prominent fact is that the well 7120/8-4 has higher velocity being water saturated compared to the gas saturated well 7121/7-1 and porosity values for the dry well 7120/8-4 is less than the gas saturated well 7121/7-1 (Fig. 5.13).

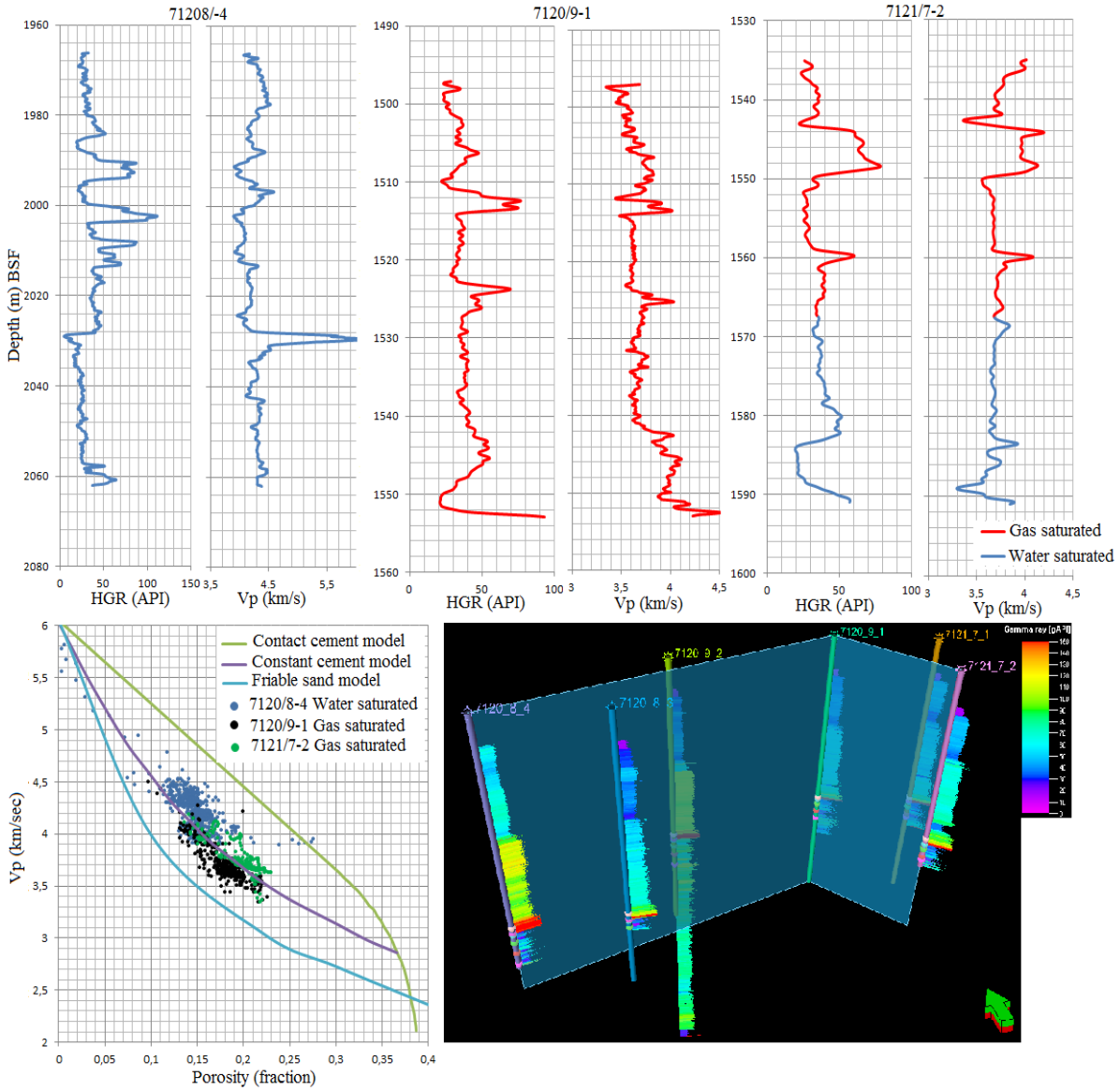

Figure 5.14: The Vp-porosity cross-plot of the Stø Formation for three wells compared with cement models along with their gamma ray and velocity log responses. Well fencing is showing the location of wells used.

Three wells have been selected for rock physics diagnostics using cement models. The eastern well 7121/7-2, the central well 7120/9-1 and the western well 7120/8-4. First two wells are gas saturated whereas the western well is water saturated. The well 7120/8-4 show higher concentration of cement compared to rest of the wells. Due to which it is showing higher Vp value. The eastern and central wells nearly follow the constant cement line. The porosity range, for the wells 7121/7-2 and 7120/9-1, is higher compared to the western well (Fig. 5.14). The Vp and gamma ray log responses versus depth are also different for all the three wells. As the thickness of the Stø Formation increases from east to west (Ch. 2, Sec. 2.4.2.1, Fig. 2.16), and thickest Stø Formation has been encountered in the western most well 7120/8-4 with a maximum burial depth (Ch. 2, Table 2.1). This point reveal the fact that present day overburden is higher in the western well due to which it has experienced the higher effective stress compared to other two wells.

5.1.7 Fluid substitution effect on rock perperties

The well 7120/8-4 has been taken as a reference well, being dry and having direct measurement of the shear velocity. The rock properties (Vp, Vs & density) are taken into account to check the rock properties variation due to the change of pore fluid and saturation.

The reservoir rock properties are changed due to the variation in the pore fluid saturation. The change of pore fluid saturation (S_w = 90 % & S_{gas} = 10 %) has a strong effect in decreasing Vp. These effects are less profound in S_w = 50 % as compared to S_w = 10 % although the concentration of gas is increasing. In general, Vs has no fluid effect but a slight increase in Vs could be observed whereas decrease in density has been observed with increasing gas saturation from 10 to 90 %.

The rock properites can be different for same rock with brine compared to saturation. After introducing 10 % gas in the water saturated quartz sands, there is decrease in the Vp (Fig 5.15a). In the same saturation conditions, there is slightly decrease in the density curve but the shear wave velocity remained unaffected. The decrease in the Vp at 50% gas saturation conditions is less compared to 10% gas saturation but the decrease in the density and increase in the Vs is more profound (Fig. 5.15b). With the further increase in the gas saturation (90%), the drop in Vp is less compared to 10% gas saturation but the density decreases dramatically and Vs also increases (Fig. 5.15c).

When data points related to water saturated Stø Formation in the well 7120/8-4 was compared with 90% gas saturated Stø formation of the same well after fluid substitution using rock physics template of water, oil and gas saturated lines. It was found that the gas saturated Stø Formation data points have low value of AI compared to water saturated data points but Vp/Vs values for both the formations are same (Fig. 5.15d). But according to the assumption, the gas saturated Stø Formation should follow the gas saturated line model.

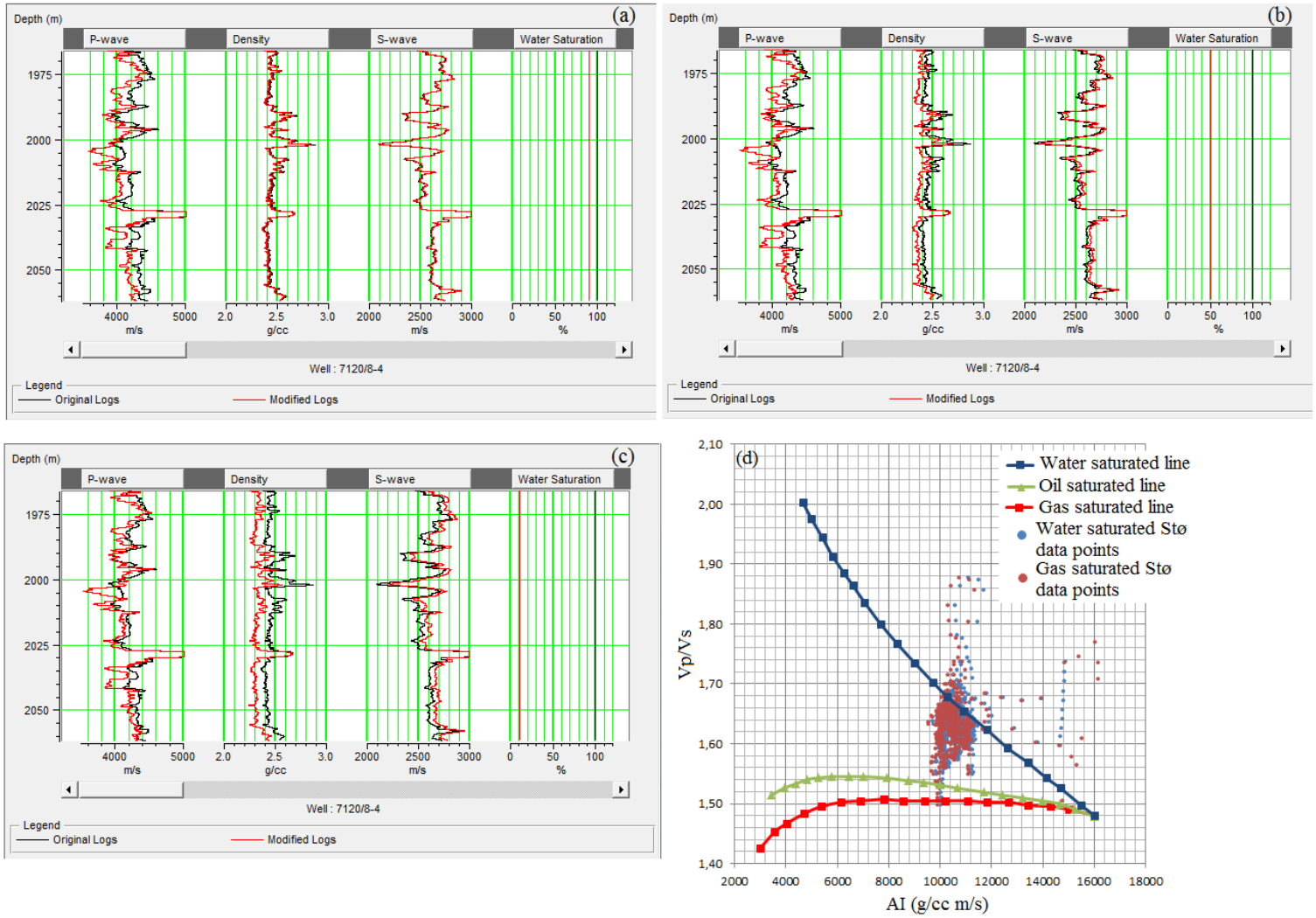

Figure 5.15: Comparision of Vp, Vs & density logs by adding (a) 10% (b) 50% and (c) 90% gas saturation in the water saturated Stø Formation of the well 7120/8-4. (d) Compasrion between warter and fluid substituted gas saturated Stø Formation using RPT.

5.1.8 Diagnostics of other reservoir rocks in the Kapp Toscana group

The Kapp Toscana group from the well 7120/8-4 has been taken into account among them the Stø Formation has good reservoir quality. The Kapp Toscana group of this well has been diagnosed by using rock physics templates. The four formation in the Kapp Toscana group have been plotted in the Vp-porosity cross plot as a background trend (Fig. 5.16). Only sand data points ($V_{sh} \leq 0.25\%$) from all the formations are plotted in these cross-plots. Then the individual formation has been analyzed based on background trend with the help of different cement models. All the formations lie between contact and constant cement model (Fig. 5.16) but the cement fraction is varying for all the formations.

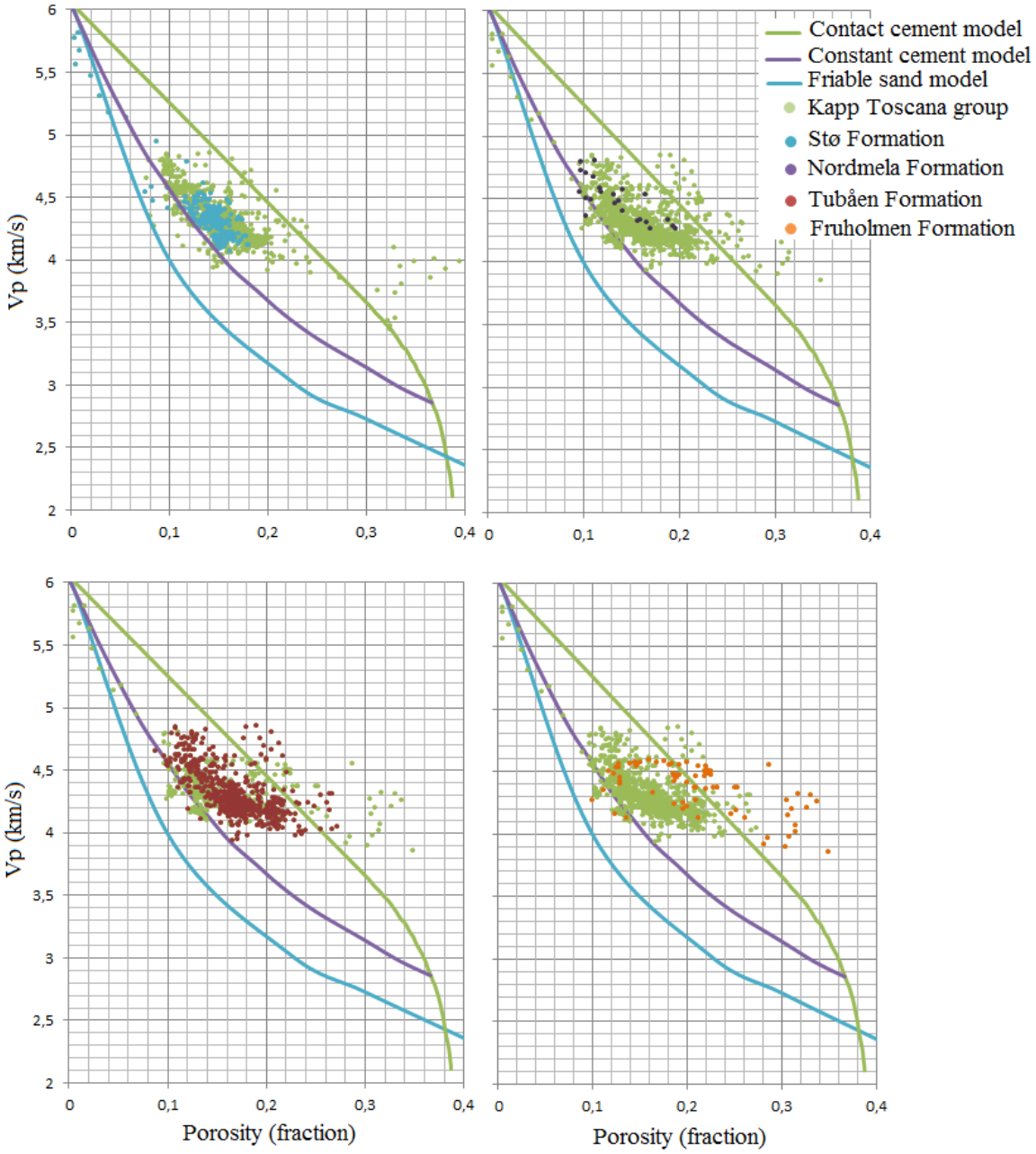

Figure 5.16: Vp-porosity cross-plot of Kapp Toscana group in the well 7120/8-4 is plotted with different cement models.

The porosity range for all the formations is varying due to which the velocity variation can be seen among them. The Stø Formation has the least porosity among them whereas the Fruholmen Formation is showing the more porosity variation.The Tubåen Formation, being the thickest among all, has a higher velocity range compared to rest of the formations and porosity in this formation ranges from 24 to 10%.

The Vp/Vs is cross plotted against AI using whole Kapp Toscana group as a background trend from the well 7120/8-4 and also three saturation models have been used in this cross plot; brine saturated line, oil saturated line and gas saturated line (Fig. 5.16). Only sand data points ($V_{sh} \leq 0.25\%$) from all the formations are plotted in these cross-plots. All the formations in the Kapp Toscana group follow the water saturated line. AI value for all the formations is almost same but Vp variation could be observed.

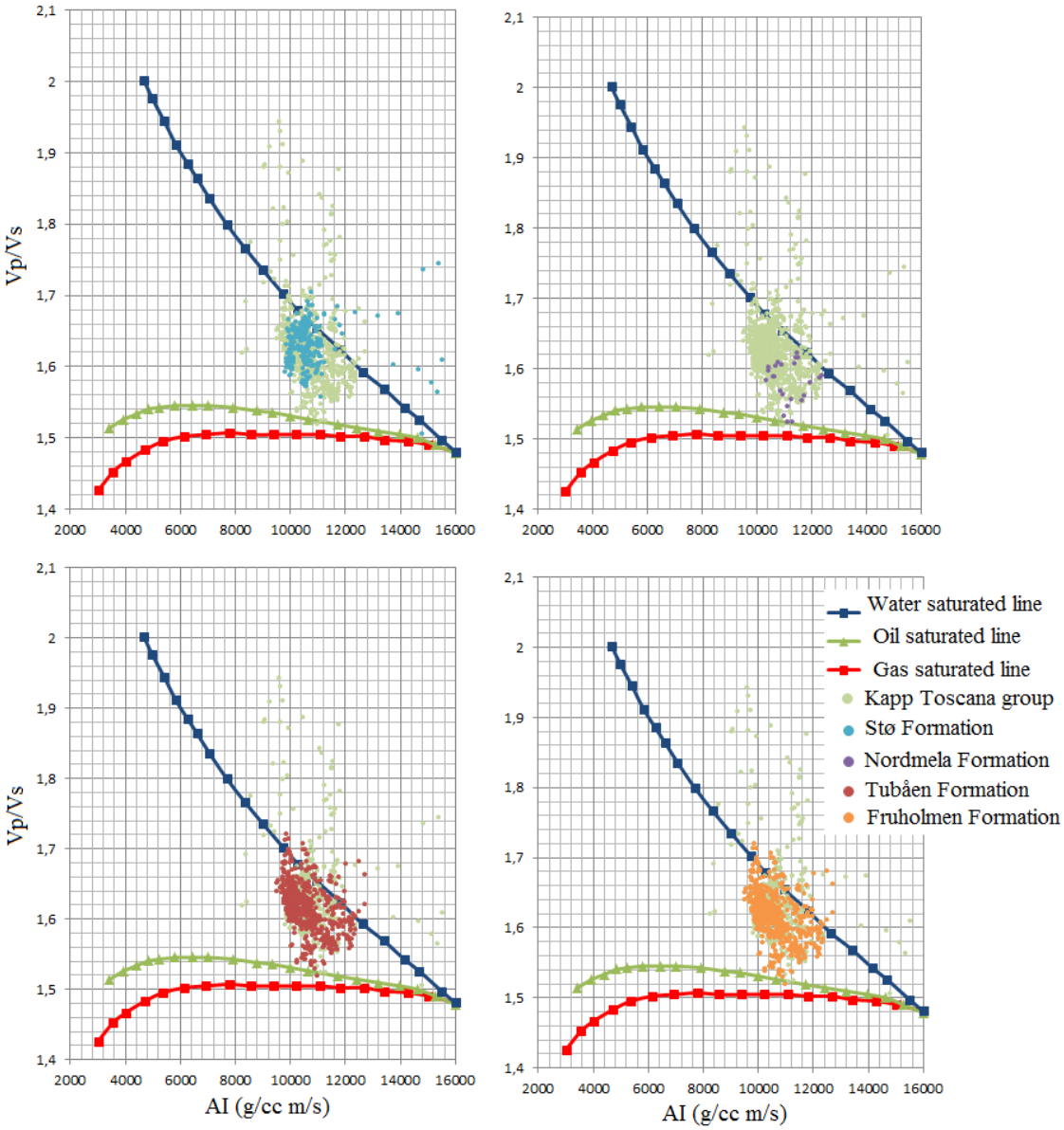

Figure 5.17: The Vp/Vs versus AI cross-plot for four formations with the Kapp Toscana group in the background of the well 7120/8-4.

5.2 Discussion

5.2.1 Rock physics diagnostics

Depositional environment has significance importance with respect to well locations (Fig. 5.18) in order to perform rock physics diagnostics study. Laterally grain size distribution and grain sorting vary in the same depositional environment. This grain size distribution and sorting can change due to the effect of different degree of compaction which interns change the rock physical properties. The composition of a particular formation deposited in the particular environment could change due to provenance. This implies that the rock physical properties can be altered depending upon well location sourced by different provenance and the direction of the sediment supply. If there is more than one sediments source, the composition of the sediments could also be changed. These multiples multiple sourced sediment compositions can have different rock properties compared to the single sediments. If there is more than one sub environments exist within the same formation then the composition of the formation would be changed giving change to different rock physical properties. In order to characterize the rock, it is really important to know the depositional environment as well as the source and direction of the sediment supply.

The gamma ray log response in the study area is different due to the different provenance as well as different kind of grain size and composition. But, in general, the gamma ray values increases from east to westward up-to 7120/9-2 which has more gamma ray value compared to rest of the wells. Western most wells (7120/8-4 & 7120/8-3) have more or less same gamma ray log response as that of eastern most wells (7121/7-1 & 7121/7-2). The trend of the Stø Formation in the gamma ray log for eastern and western wells is similar reflecting same kind of paleo depositional environment. Moreover, the gradual increase in the gamma ray log response from eastern part to the western part seems to follow proximal to distal paleo-environment settings. In the proximal zone (eastern wells), due to higher energy environment, the coarser sediments have been deposited as compared to the distal zone where low energy prevails and causes inclusion of fine grained sediments (7120/9-2).

In the study area, the eastern most wells (7121/7-1 & 7121/7-2) are located in the proximal zone which is close to the shoreface, whereas the distal zone is occupied by the well 7120/9-2 (Ch. 4, Sec. 4.2.1, Fig. 4.20) (lower shoreface). The western most wells (7120/8-4 & 7120/8-3) resembles in gamma ray log response to that of eastern most wells probably explained another source of sediments from the south explained by Berglund et al. (1986) (Ch. 2, Sec. 2.4.2.1). But due to the different source and environment, the degree of sorting and size of the sediments are different. The maximum Stø Formation thickness of the study area in the western most wells could be explained by S-E directional provenance.

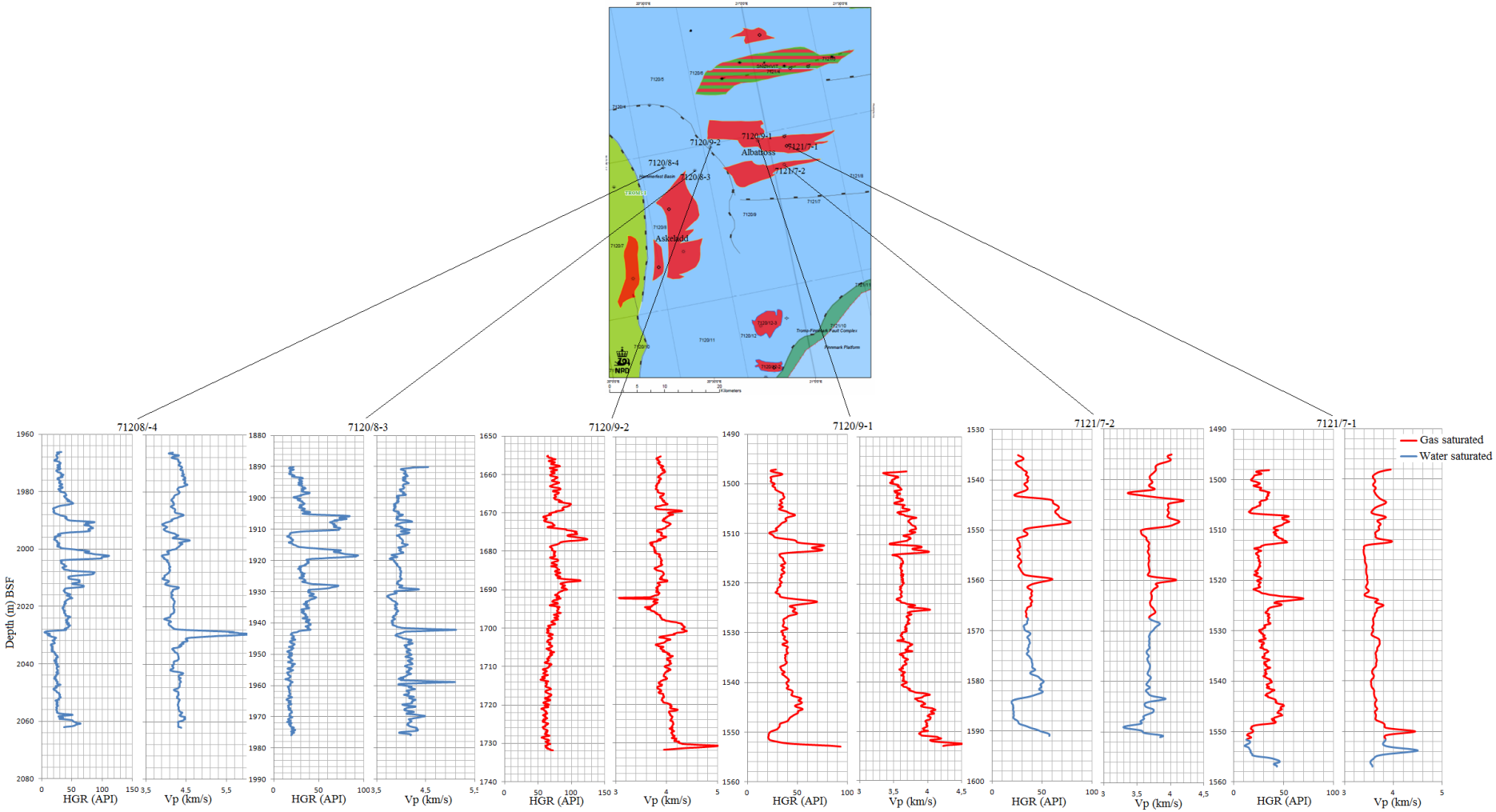

Figure 5.18: Location of the wells with their Petrophysical Vp and gamma ray log responses versus depth.

Present day depth of the Stø Formation in the wells 7120/9-1 and 7121/7-1 is similar reflecting the fact that both the wells have experienced the same overburden pressure (Fig. 5.12). Moreover the eastern well 7121/7-1 is a well sorted, coarser grained being near to the proximal zone compared to the well 7120/9-1 which consists of poorly sort fine grained material (close to distal zone) (Ch. 2, Sec. 2.4.2, Fig. 2.15). It is also cleared that the poorly sorted sandstones are mechanically more compacted than well-sorted sandstone at a similar pressure conditions (Ch. 4, Sec. 4.1.1, Fig. 4.1). Due to which the higher Vp value is experienced by the well 7120/9-1. Poorly sorted sediments in the well 7120/9-1 have more clay fraction (stylolite) hence more dissolved quartz cement compared to the well-sorted well 7121/7-1. Moreover, well-sorted, coarse-grained sandstones tend to have low surface area ratio available for quartz cement to precipitate compared to the poorly sorted sandstones, which causes the precipitation of more quartz cement making sandstones stiffer. Hence, the Stø Formation of the well 7120/9-1 is stiffer than that of the well 7121/7-1.

The eastern well 7121/7-1 has a different cement model compared to that of western well. Present day temperature gradient of eastern wells is diverse and the overburden stress is different indicating varying effective stress level experienced by these wells. Maximum exhumation was experienced by the wstern wells (7120/8-4, 7120/8-3) (Ch. 4, Sec. 4.2.3, Fig. 4.27). That's mean the sediments have experienced more time span for temperature higher than 70-80^{0}C during burial as well as uplift which is reflected by more quartz cementation in the western wells (Sec. 5.1.6, Fig. 5.13). This could be one of the phenomenons of higher velocity in the western wells keeping in view as dry wells. Another point is the different provenance due to which the rock physical properties are different and because of different provenance the grain sorting and composition is different. These could be the possible reasons which could cause different degree of cementation and porosity distribution within the wells. The thickness variation could also affect the rock properties (Fig. 5.19). In the chemical compaction, the thickness disparity could cause the stylolite spacing and the distance from each stylolite (Ch. 3, Sec. 3.2.7, Fig. 3.17) (Walderhaug and Bjørkum, 2003). Thickness of the Stø Formation in the western well 7120/8-4 is more than that of eastern well 7121/7-1. The net-to-gross is comparatively low for the 7120/8-4 well than 7121/7-1. Furthermore, the pore fluid can also affect the rock properties. Western well 7120/8-4 being water saturated has a higher velocity compared to gas saturated eastern well 7121/7-1.

It could be concluded that the depositional environment is a significant factor, which change the sediments properties within the same formation. However, reservoir diagnostics has verified that rock properties are different from well to well within same reservoir units. Moreover, due to the present day structural configuration of the Hammerfest basin, the temperature distribution as well as the overburden stress is different on the reservoir rocks. Moreover exhumation of the study area sould be considered along with all above mentioned factors in reservoir characterization. These are the factors, which can transform the rock vertically and laterally. Due to all these factors, hence, it is very much complex to evaluate the rock properties.

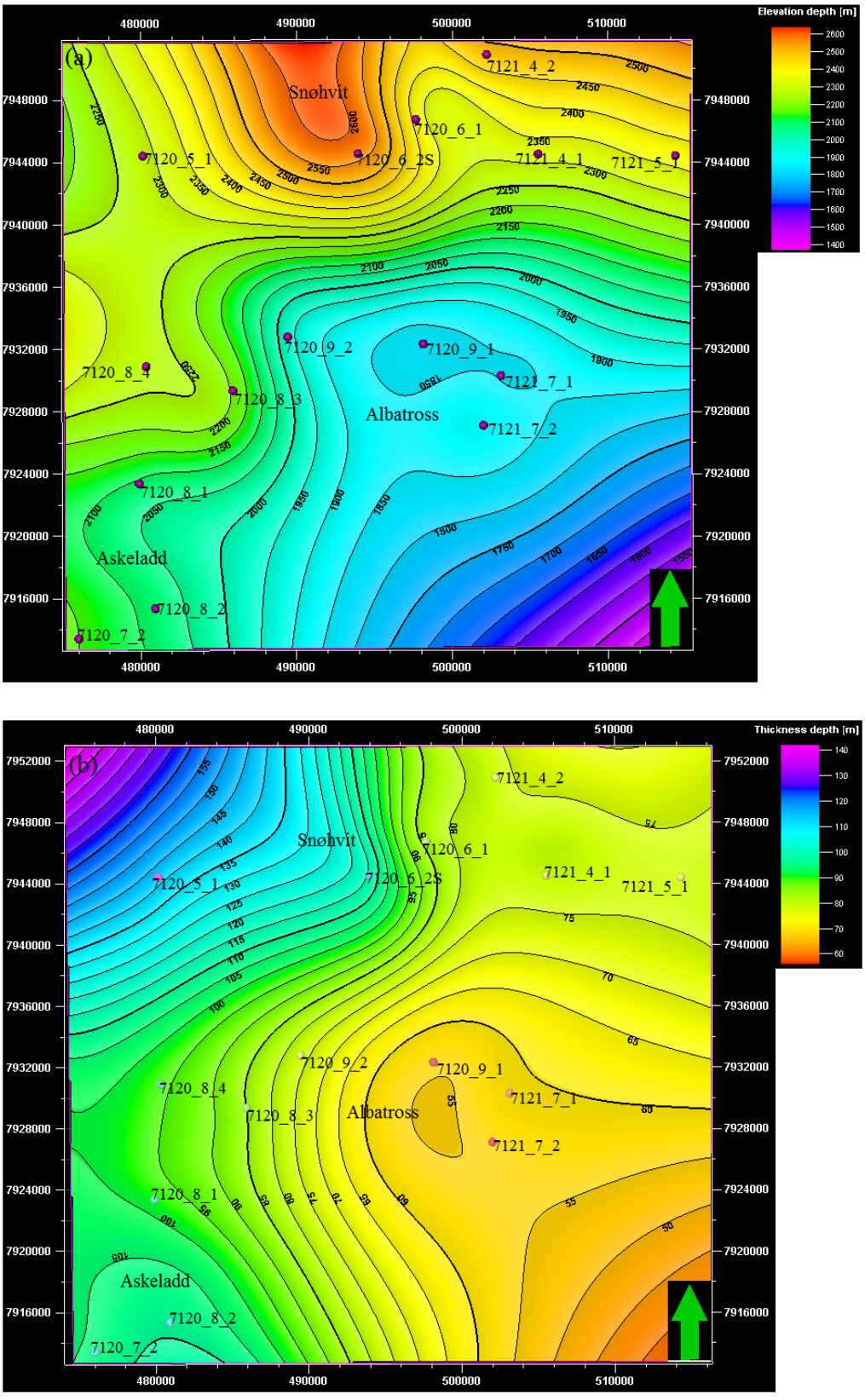

Figure 5.19: Stø Formation in the study area (Albatross discovery), (a) depth variation (b) thickness variation.

5.2.2 Fluid substitution effect on rock perperties

The rock physical properties (Vp, Vs & density) change with the variation in different pore fluid saturation (Fig. 5.15a, b, c). Vp and Vs dependent on the bulk, shear and density of the rock. Both the rock physical properties (Vp & Vs) increases with the decrease in the effective density. When percentage of gas saturation was increased from 10% to 90% there was observed a decrease in the density because the density of gas is lower than the density of water.

The fluid modulus, used as an input parameter in the fluid replacement modeling (FRM) (Ch. 3, Table 3.3), has been calculated by Hashin-Shtrikman harmonic averaging assuming homogeneous saturation. Due to the decrease in this effective fluid modulus at the 10 % gas saturation, there is a decrease in Vp. Increase in the gas saturation (10 to 90%) show relatively low decrease in Vp but the decrease in density is remarkable. With the decrease in density, change of Vs has been observed in the FRM Vs log.

Moreover, saturation affect with different mineralogical composition depends on the porosity. The porosity of clean sandstone (100%) is higher than than porosity of quartz-clay (79:21), which affects the density. With increasing gas saturation, there would be a greater difference in density in these two mineralogical settings. Furthermore, the well selected for fluid substitution has a higher proportion of cementation. Hence, these two factors: reduced net-to-gross ratio and increased cementation will reduce the fluid sensitivity of the sandstone reservoir (Fig. 5.15d).

5.2.3 Diagnostics of other reservoir rocks in the Kapp Toscana group

Surface area is an important parameter for quartz cementation to precipitate depending upon the depositional environment of sediments like mineralogy, grain size, grain shape, grain sorting and diagenetic alteration like time, temperature and different kind of cement coating (Walderhaug, 1994; Walderhaug and Bjørkum, 2003). With the increasing temperature due to the geothermal gradient, precipitation rate of quartz cement increases. Quartz cementation also depends on the degree of sorting and grain size of the formation. Coarser grains have less surface area as compared to the finer grains for quartz cement to precipitate due to which the percentage of quartz cement is less in the coarser grained particles. For quartz cement to precipitate there should be a continuous source of dissolved quartz. The formation of stylolites (Ch. 3, Sec. 3.2.7) is the source of quartz cement from the pressure dissolution which destroys the porosity in the sandstones and causes grain framework stiffening (Bjørlykke and Jahren, 2010). Hence, the sandstone body containing more shaley particles tends to have more quartz cementation because for the generation of stylolites, clay particles play an important role. The clay fraction is higher in the western wells (7120/8-3, 7120/8-4) and in the well 7120/9-2 compared to rest of the wells (7120/9-1, 7121/7-1, 7121/7-2) (Fig. 5.9 to 5.11). This clay volume fraction could be caused in the higher cementation by generating more stylolits.

Bottom hole temperature for the well 7120/8-4 is 98^0C (NPD, personal communication) and the maximum depth has been experienced by the Stø Formation in this well. Temperature, depth and effective overburden stress could be the main factors behind the reason that the Kapp Toscana group of this well has more constant cement (Fig. 5.14). Reduction in the

porosity of Tubåen Formation is the result of poorly sorted sandstone due to more clay percentage and could be the result of more quartz cement. The percentage of quartz cement is higher than constant cement but less than contact cement (Fig. 5.16) in the Tubåen Formation reflecting higher velocity variation within narrow porosity changes.

The Vp/Vs versus AI cross plot of the Kapp Toscana group in the well 7120/8-4 follow the water-saturated model (Fig. 5.16). The presence of diagenetic quartz cement could move the water saturated sandstones in this crossplot to an area of low Vp/Vs values where we could expect hydrocarbon saturated sandstone to plot. The Nordmela Formation has a higher percentage of shale due to which the sand percentage ($V_{sh} \leq 0.25$) is very low and fall between oil and water saturated model. The Tubåen Formation which is more cemented with high velocity and low porosity range show lower Vp/Vs ratio. Reduction in net-to-gross ratio as well as increase in the cementation could result in the higher value of AI which affects the fluid sensitivity of the sandstone reservoir results in the ambiguity for lithology/fluid discrimination.

Chapter 6
Summary and Conclusion

This research focuses mainly on Albatross discovery located in the southwestern part of the Hammerfest basin. It was discovered in 1982 by the exploration well 7120/9-1. The Albatross area contains four exploration wells which are 7120/9-1, 7120/9-2, 7121/7-1 and 7121/7-2. The two other wells 7120/8-3 and 7120/8-4 part of the Askeladd gas field (Askeladd Nord), have been included in this research to get a broader overview of the study area. The wells 7120/9-1, 7120/9-2, 7121/7-1 & 7121/7-2 are gas saturated and the other two wells 7120/8-4 & 7120/8-3 are dry and shows only traces of hydrocarbon. In addition, 9 more exploration wells from the Snøhvit and Askeladd discoveries have also been taken into account in order to analyze the exhumation of the greater Snøhvit development. The well data from Snøhvit and Askeladd have been considered only for comparison purpose. The data of Snøhvit and Askeladd have taken from two previous master theses (Fardi, 2012 and Rahman, 2012). In order to perform characterization of sandstone reservoirs using rock physics dignostics this work lays main emphasis on Stø Formation compared to three other reservoirs of Nordmela, Tubåen and Fruholmen Formatiuons.

Compaction trends and properties of the rocks in the Albatross discovery have been analyzed by comparing six well log data and published compaction trends. Different clay-clay and clay-silt experimental compaction curves have been used. Vp and density logs as a function of depth have been used in order to distinguish between mechanical (MC) and chemical compaction (CC). A sharp increase in Vp but nearly constant density have been observed within the same lithology (inferred from the gamma ray log) at transition from mechanical to chemical compaction in Knurr Formation. The transition zone from mechanical to chemical compaction has been identified on the basis of several techniques. .Vp-density cross plot has been taken into account in order to confirms the depth at which this transition occurs. The transition from mechanical to chemical compaction occurred within the Knurr Formation at different depth in different wells. The bottom hole temperature has been used to calculate the present day temperature at the transition point. Using shear modulus-density crossplots constrained the temperature at the transition zone.

The present day temperature at the transition zone is not in accordance with the expected temperature. When Vp-depth trends of six well compared with the published compaction trends, there was found a mismatch indicate clearly exhumation of the study area. Different published compaction trends have been used in order to find the upper and lower limit of exhumation. For lithology control, the gamma ray log has been used as a lithology indicator and Vsh has been calculated for each well. Only shale data points ($Vsh \geq 0.75$) of six studied wells and a published kaolinite-silt (50:50 percentage) (Mondol, 2009) compaction trend has been utilized for final exhumation estimate in the study area. Exhumation estimates using other published compactions trends also analyzed to see uncertanities associated with selection of published compaction trends.

The rock physics diagnostics were carried out using the well 7120/8-4 containing direct Vs measurement. A series of Rock Physics Templets (RPT's) has been used to analyse rock properties and to examine physical and acoustic properties of Stø Formation and sandstones of three other formations in the Kapp Toscana Group. The effect of cementation on the

reservoir rocks has been evaluated by using different cement models. On the other hand, the evaluation of fluid effect on the rock properties has been judged by using saturation model (VP/Vs versus AI crossplot). Three saturation models (brine, oil and gas) have been calculated for pure sandstones and utilize to see sensitivity of saturation of different sandstones and their quality has been checked with respect to each other.

Instead of number of limitations and simplistic assumptions, the following conclusions can be drawn for the study:

- Two compaction trends have been found in the study area representing mechanical and chemical compaction of silisiciclastic rocks. In the mechanical compaction zone, the Vp-depth trends in all the six studied wells follow the more or less same trend where velocity increases with depth except the organic-rich Hekkingen Formation. The systematic porosity reduction by mechanical compaction can be clearly observed in all the wells before the transition at a present burial depth. On the other hand, in the deeper part the chemical compaction controls mostly the porosity reduction by quartz cementation depended on time and temperature (Sec. 4.2.1, Fig. 4.1).

- The transitions from mechanical to chemical compaction in different wells were marked due to the abrupt change in the velocity within the same Knurr Formation may exclude the lithologic debate where the gamma ray logs show more or less constant values (Sec. 4.2.2, Fig. 4.4 to 4.6)

- It is clear from the study that the present day temperature at the transition zone depth is not sufficient enough to produce the chemical compaction. When correction for exhumation was applied to the data, the temperature was found to be agreeable with the published literature for the transition (Sec. 4.2.2).

- The calculated exhumation estimates differs for Snøhvit, Albatross and Askeladd discoveries depending upon the structural configuration. The exhumation for Snøhvit field is from 300 to 800 m increasing from west to east whereas in the Albatross discovery it increases in opposite direction ranging from 700 to 1000 m. In the Askeladd discovery it ranges from 300 to 1000 m and decreasing from south to north. This exhumation estimates is in accordance with the published literature (Sec. 4.2.2, Fig. 4.22 to 4.27).

- The sandstone and shale compaction gradients show difference in two different compaction domains where sandstones shows higher compaction gradient in the mechanical than shale whereas this is the opposite in case of chemical compaction (Sec. 4.1.6, Fig. 4.13).

- The transformation of biogenic silica has observed in the study are but restricted within the western wells. The conversion from Opal A to Opal CT in the western well 7120/8-4 has occurred at a shallow depth of 1500 (m) BSF giving rise to abrup increase in velocity (Sec. 4.2.4, Fig. 4.16, 4.17, 4.29).

- On the basis of Vp-porosity plot, it is inferred that the amount of cementation in the western wells is higher than the eastern wells. Different grain size and sorting within the reservoir could be the reason for different cementation (Sec. 5.1.6, Fig. 5.13, 5.14).

- The reservoir quality of sandstones in the Stø Formation decreases from eastern wells to westerns wells in different depth levels. This change in the reservoir quality of Stø sandstones is due to the lithological variations within the formation. Moreover, the eastern wells are close to the shoreline (proximal zone) than western wells (distal zone), controlling the deposition of coarser and well sorted sediments causing decrease in velocity. Hence, the impact of compaction (mechanical and chemical compaction) is lower in the east than west.

- Present day temperature gradient of the eastern wells (7121/7-1 & 7121/7-2) is higher than the western wells (7120/9-1 & 7120/9-2). Due to the different grain sorting and geothermal gradient, the observed composition may differs reflects different degree of cementation and, hence, different rock physical properties. Overconsolidation of reservoir rock of Stø Formation due to quartz cementation results in higher AI of reservoir sandstones and so ambiguity to discriminate fluid effect (Sec. 5.1.7, Fig. 5.16).

- Although the fluid has no influence on Vs still saturation changes by lighter fluids compared to brine may change the Vs due to the density effect. Because of cementation and low net-to-gross, the fluid sensitivity of the reservoir sandstones may also be reduced (Sec. 5.2.3, Fig. 5.15).

References

Abercrombie, H. J., I. E. Hutcheon, J. D. Bloch, and P. de Caritat, 1994, Silica activity and the smectite-illite reaction: Geology, v. 22, p. 539–542.

Asquith, G. and Krygowski D. (2004). Basic well log analysis. AAPG methods in Exploration Series 16, 224 pp.

Athy, L.F., 1930. Density, porosity, and compaction of sedimentary rocks. American Association of Petroleum Geologists Bulletin 14 (1), 1–24.

Avseth, P., Dvorkin J., Mavko G. and Rykkje J. (2000). Rock physics diagnostic of North Sea
sand: Link between microstructure and seismic properties. Geophysics, v. 27, p. 2761-2764.

Avseth, P., Mukerji T. and Mavko G. (2005). Quantitative seismic interpretation: Applying rock physics tools to reduce interpretation risk. Cambridge University Press, New York.

Avseth, P., 2008. Shale rock physics and implications for AVO analysis A North Sea demonstration. Leading edge, 27, 788.

Avseth, P. 2009. Rock physics estimation of cement volume, sorting, and net-to-gross in North Sea sandstones. Leading edge, 28, 98.

Avseth, P., Mukerji T., Mavko G. and Dvorkin J. (2010). Rock-physics diagnostics of depositional texture, diagenetic alterations and reservoir heterogeneity in high porosity siliciclastic sediments and rocks-A review of selected models and suggested work flows. Geophysics, v. 75, p. 131-147.

Avseth, P. (2010). Exploration rock physics- The link between geological processes and geophysical observables. In: Bjorlykke, K. (eds), Petroleum Geoscience: from Sedimentary Environments to Rock Physics, Berlin, Heidelberg, Springer-Verlag Berlin Heidelberg, p. 403 – 426.

Batzle, M. and Wang, Z., 1992, Seismic properties of pore fluids, Geophysics, 42, 1369-1383.

Berglund, L. T., Augustson J., Færseth R., Gjelberg J. and Ramberg-Moe H. (1986). The evolution of the Hammerfest basin. Norwegian Petroleum Society, p. 319-338.

Bjørlykke, K. 1983. Diagenetic reations in sandstones. In: A. Parker & B. W. Sellwood (Editors). Sediment diagenesis. D. Reidel, London, pp. 169-213.

Bjørlykke, K., Aagaard, P., Dypvik, H., Hastings, D.S., Harper, A.S., 1986. Diagenesis and reservoir properties of Jurassic sandstones from the Haltenbanken area, offshore mid Norway, Habitat of Hydrocarbons on the Norwegian Continental Shelf. In: Proceedings of an International Conference. Graham & Trotman, London, UK.

Bjørlykke, K. (1998). Clay mineral diagenesis in sedimentary basins - a key to the prediction of rock properties. Examples from the North Sea Basin. Clay Minerals 33(1), p. 15-34.

Bjørlykke, K., Chuhan F., Kjeldstad A., Gundersen E., Lauvrak O. and Høeg K. (2004). Modelling of sediment compaction during burial in sedimentary basins in Stephansson O., Hudson J. and King L. (eds.), Coupled Thermo-Hydro- Mechanical-Chemical Processes in Geo-Systems. Elsevier, Amsterdam, pp. 699–708.

Bjørlykke, K. 2010, Sandstones and Sandstone reservoirs. In: Bjørlykke, K. (eds), Petroleum Geoscience: From Sedimentary Environments to Rock Physics, Springer Verlag, p. 329-337.

Bjørlykke, K. and Jahren J. (2010). Sandstones and Sandstone reservoirs in Bjorlykke K. (2010), Petroleum Geoscience: from Sedimentary Environments to Rock Physics, Berlin, Heidelberg, Springer-Verlag Berlin Heidelberg, p. 113 – 140.

Bjørlykke, K. Høeg, K. and Mondol, N. H. (2010). Introduction to geomechanics: stress and strain in sedimentary basins. In: Bjorlykke, K. (eds), Petroleum Geoscience: from Sedimentary Environments to Rock Physics, Berlin, Heidelberg, Springer-Verlag Berlin Heidelberg, p. 281 – 298.

Brown, A. R., Dahm, C. G., and Graebner, R. T., 1981, A stratigtraphic case history using three dimentional seismic data in the Gulf of Thailand. Geophys Prospecting, 29, 327-349.

Brown, A. R., 1992, Interpretation of Three-Dimentional Seismic Data. AAPG Memoir 42, 3rd edn.

Buland, A., Landroe, M., Anderssen, M., and Dahl, T., 1996, AVO inversion of the Troll field data. Geophysics, 61, 1589-1602.

Bugge, T., Elvebakk G., Fanavoll S., Mangerud G., Smelror M., Weiss H. M., Gjelberg J., Kristensen S. E. and Kåre N. (2002). Shallow stratigraphic drilling in hydrocarbon exploration of the Nordkapp Basin, Barents Sea. Marine and Petroleum Geology, 19, p. 13-37.

Breivik, A. J., Gudlaugssin, S. T., & Faleide, J. I. (1995) Ottar Basin, Sw Barents Sea : a major Upper Paleozoic rift basin containing large volume of deeply buried salt. Basin Research 7, 299-312.

Carmichael, R.S., 1989. Practical Handbook of Physical Properties of Rocks and Minerals. Boca Raton, FL: CRC Press.

Castagna, J. P., Batzle M. L. and Eastwood R. L. (1985). Relationships between Compressional-Wave and Shear-Wave Velocities in Clastic Silicate Rocks. Geophysics, v. 50, p. 571-581.

Castagna, J. P., Batzle M. L. and Kan T. K. (1993). Rock physics - The link between rock properties and AVO response, in offset-dependent reflectivity - Theory and practice of AVO analysis, ed. J. P. Castagna and M. Backus. Investigation in Geophysics, No. 8, SEG, Tulsa,

Oklahoma, p. 135-171.

Chi, X. G. and Han D. H. (2009). Lithology and fluid differentiation using rock physics template. The Leading Edge, p. 1424-1428.

Chuhan, F.A., Kjeldstad A., Bjørlykke K. and Høeg K. (2002). Porosity loss in sand by grain crushing. Experimental evidence and relevance to reservoir quality. Marine and Petroleum Geology, v. 19, p. 39–53.

Chuhan, F.A., Kjeldstad, A., Bjørlykke, K., Hoeg, K., 2003. Experimental compression of loose sands; relevance to porosity reduction during burial in sedimentary basins. Canadian Geotechnical Journal 40 (5), 995–1011.

Dalland, A., Worsley D. and Ofstad K. (1988). A lithostratigraphic scheme for the Mesozoic and Cenozoic succession offshore mid and northern Norway. Norwegian Petroleum Directorate Bulletin, v.4, p. 65.

Dengo, C. A., & Rossland. K. G., (1992) Extensional tectonic history of the western Barents Sea. In: Structural and Tectonic Modeling and its applications to Petroleum Geology, R. M. Larsen, H. Brekke, B. T. Larsen & E. Talleraas (Eds). Norwegian Petrol. Soc. Spec. Publ. No. 1 (pp. 91-107). Amsterdam: Elsevier.

Dore, A. G. (1995). Barent Sea Geology, Petroleum Resources and commercial potential. Arctic, v. 48(3), p. 207-221.

Dore, A. G. and Jensen L. N. (1996). The impact of late Cenozoic uplift and erosion on hydrocarbon exploration: offshore Norway and some other uplifted basins. Global and Planetary Change, v. 12(1–4), p. 415-436.

Dræge, A. (2011). "A diagenetic rock physics approach for siliciclastics." Leading edge 30(12): 1368.

Dvorkin, J., Nolen-Hoeksema R. and Nur A. (1994). The squirt-flow mechanism: macroscopic description. Geophysics, v. 59, p. 428-438.

Dvorkin, J. and Nur A. (1996). Elasticity of high-porosity sandstones: Theory for two North Sea data sets. Geophysics, v. 61, No. 5, p. 1363-1370.

Enachescu, M. E., 1993, Amplitude interpretation of three dimensional reflection data. The Leading Edge, 12, 678-685.

Faleide, J. I., Gudlaugsson S. T. and Jacquart G. (1984). Evolution of the western Barent Sea. Marine and Petroleum Geology, v. 1.

Faleide, J. I., S. T. Gudlaugsson, et al. (1991). "Deep seismic transects across the sheared western Barents Sea-Svalbard continental margin." Tectonophysics 189(1–4): 73-89.

Faleide, J. I., Vagnes, E. & Gudlaugsson, S. T. 1993a. Late Mesozoic-Cenozoic evolution of the south-western Barents Sea in a regional rift-shear tectonic setting. Marine and Petroleum Geology, 10, 186-214.

Faleide, J. l., Vlignes, E. & Gudlaugsson, S. T., 1993b, Late Mesozoic-Cenozoic evolution of the southwestern Barents Sea. In: J. R. Parker (Ed). Petroleum Geology of Northwest Europe: Proceedings of the 4th conference, The Geological Society London, p. 933- 950.

Faleide, J. I., Solheim A., Fiedler A., Hjelstuen B. O., Andersen E. S. and Venneste K. (1996). Late Cenozoic evolution of the western Barents Sea-Svalbard continental margin. Global and Planetary Change, v. 12, p. 53-74.

Faleide, J.I., Tsikalas, F., Breivik, A.J., Mjelde, R., Ritzmann, O., Engen, O., Wilson, J. And Eldholm, O., 2008, Structural and evolution of the continental margin of Norway and Barents Sea, Episodes 31, 82-91.

Fawad, M., Mondol N. H., Jahren J. and Bjørlykke K. (2011). Mechanical compaction and ultrasonic velocity of sands with different texture and mineralogical compositon. Geophysical Prospecting, v. 59, p. 697-720.

Gabrielsen, R. H. (1984). "Long-lived fault zones and their influence on the tectonic development of the southwestern Barents Sea." Journal of the Geological Society 141(4): 651-662.

Gabrielsen, R. H. and Faerseth, R. B. (1989). The inner shelf of North Cape, Norway and its implications for the Barents Shelf-Finnmark Caledonide boundary: a comment Norsk Geol. Tidsskr. v. 69, pp. 57-62.

Gabrielsen, R., H,., Farseth, R., B,., Jensen, L., N,., Kalheim, J., E. & Riis, F. 1990. Structural elements of the Norwegian continental shelf, Part I: The Barents Sea Region. Norwegain Petroleum Directorate Bulletin, 6, 47.

Gardner, G. H. F. (1974). "Formation velocity and density; the diagnostic basics for stratigraphic traps." Leading edge 39(6): 770.

Gassmann, F., 1951, Uber die elastizitat poroser medien. Vier. Natur Gesellschaft, 96, 1-23.

Glørstad-Clark. E.. J. I. Faleide. et al. (2010). "Triassic seismic sequence stratigraphy and paleogeography of the western Barents Sea area." Marine and Petroleum Geology 27(7): 1448-1475.

Gudlaugsson, S.T., Faleide, J.I., Johansen, S.E., and Breivik, A.J., (1998), Late Paleozoic structural development of the south-western Barents Sea: Marine and Petroleum Geology, v. 15, pp. 73-102.

Han, D., Nur A. and Morgan D. (1986). Effect of porosity and clay content on the wave velocities in sandstones. Geophysics. v. 51(11), p. 2093-2107.

Hashin, Z. and Shtrikman S. (1963). A variation approach to the elastic behavior of multiphase materials. J. Mechanical physics. Solids, v. 11, p. 127-140.

Henriksen, E., Ryseth A. E., Larssen G. B., Heide T., Rønning K., Sollid K. and Stoupakova A. V. (2011). Tectonostratigraphy of the greater Barents Sea: implication for petroleum systems. Geological Society, London, Lyell collection, v. 35, p. 163-195.

Hower, J., E. V. Eslinger, M. E. Hower, and E. A. Perry, 1976, Mechanism of burial metamorphism of argillaceous sediment: Mineralogical and chemical evidence: Geological Society of America Bulletin, v. 87, p. 725– 737.

Jackson, H. R., J. I. Faleide, et al. (1990). "Crustal structure of the sheared southwestern Barents Sea continental margin." Marine Geology 93(0): 119-146.

Japsen, P. & Chalmers, J. A. 2000. Neogene uplift and tectonics around the North Atlantic: overview. Global and Planetary Change, 24, 165-173.

Johansson, Å., Meier M., Oberli F. and Wikman H. (1993). The early evolution of the Southwest Swedish Gneiss Province: geochronological and isotopic evidence from southernmost Sweden. Precambrian Research, v. 64, p. 361-388.

Johansen, T. A., B. O. Ruud, and M. Jakobsen, 2004, Effect of grain scale alignment on siemic and isotropy and reflectivity of shales: Geophysical Prospecting, 52, no. 2, 133-149.

Krief, M., Garat J., Stellingwerff J. and Ventre J. (1990). A petrophysical interpretation using the velocities of P and S waves. The Log Analyst, p. 355-369.

Larionov, V. V., 1969, Borehole radiometry, Nedra, Moskowa.

Larssen, G. B. 2002. Upper Palaeozoic lithostratigraphy of the southern Norwegian Barents Sea, [S.l.], [s.n.].

Leith, T. L., Weiss, H. M., Mørk, A., Århus, N., Elvebakk, G., Embry, A. F., Brooks, P. W., Stewart, K. R., Pchelina, T. M., Bro, E. G., Verba, M. L., Danyushevskaya, A., & Borisov, A. V. (1993). Mesozoic hydrocarbon source-rocks of the Arctic region. In T. O. Vorren, E. Bergsager, Ø. A. Dahl-Stamnes, E. Holter, B. Johansen, E. Lie & T. B. Lund (Eds.), Arctic geology and petroleum potential. Norwegian Petroleum Society (NPF) Special Publication 2 (pp. 1-25). Amsterdam: Elsevier.

Lindseth, R. O. (1979). "Synthetic sonic logs; a process for stratigraphic interpretation." Leading edge 44(1): 3.

Linjordet, A. and Olsen R. G. (1992). The Jurassic Snohvit gas field, Hammerfest basin, Offshore Northern Norway. AAPG Bulletin M 54, p. 349-370.

Lippard, S.J. & Roberts, D. 1987: Fault systems in Caledonian Finnmark and southern Barents Sea. Norges geologiske undersøkelse Bulletin 410, 55-64.

Loertzer, G. J. M., and Berkhout, A. J., 1992, An integrated approach to lithologic inversion: Part 1, Theory. Geophyscis, 57, 233-244.

Mackenzie, F. T., 2005, Sediments, diagenesis and sedimentary rocks: Treatise on Geochemistry, Volume 7: Elsevier.

Magara, K., 1980. Comparison of porosity–depth relationships of shale and sandstone. Journal of Petroleum Geology 3 (2), 175–185.

Magoon, L. B, and W. G. Dow, eds., 1994, The petroleum system- from source to trap: AAPG Memoir 60.

Marcussen, Ø., Thyberg B. I., Peltonen C., Jahren J., Bjørlykke K. and Faleide J. I. (2009). Physical properties of Cenozoic mudstones from the northern North Sea: Impact of clay mineralogy on compaction trends. AAPG Bulletin, v. 93, p. 127-150.

Marcussen, Ø., Maast T. E., Mondol N. H., Jahren J. and Bjørlykke K. (2010). Changes in physical properties of a reservoir sandstone as a function of burial depth - The Etive Formation, Northern North Sea. Marine and Petroleum Geology. In press.

Marion, D. (1990). Acoustic, mechanical and transpoprt properties of sediments and granular materials. Ph.D. dissertation, Stanford University.

Marion, D., Nur A., Yin H. and Han D. (1992). Compressional velocity and porosity in sandclay mixtures. Geophysics, v. 57, p. 554-563.

Mavko, G., Mukerji T. and Dvorkin J. (2009). The rock physics handbook: Tools for seismic analysis of porous media. Cambridge University Press, New York.

Md Jamilur, Thesis 2012: Compaction, rock properties evaluation, rock physics diagnostics, avo modeling and seismic inversion in the snøhvit field, SW Barents Sea, University of Oslo, Norway.

Middleton, G. V., 1973, Johannes Walther's Law of the correlation of the facies, Geol. Soc. AM. Bull., 84, 979-988.

Milovak, J., (2009). Rock physics modeling of an unconsolidated sand reservoir, Masters Thesis, University of Houston.

Mohsen Fardi Golyan, Thesis 2012: Compaction, rock properties evaluation and rock physics diagnostics of Askeladd discovery, Norwegian Barents Sea, University of Oslo, Norway.

Mondol, N. H., Bjørlykke K., Jahren, J. and Hoeg K. (2007). Experimental mechanical compaction of clay mineral aggregates - Changes in physical properties of mudstones during burial. Marine and Petroleum Geology, v. 24, p. 289-311.

Mondol, N. H., Bjørlykke, K., Jahren, J. 2008. Experimental compaction of kaolinite Aggregates: Effect of grain size on mudrock properties. EAGE Extended Abstract, 1037.

Mondol, N. H. (2009). Porosity and permeability development in mechanically compacted siltkaolinite mixtures. SEG Houston International Exposition and Annual Meeting.

Murphy, W. F. (1982). Effects of microstructure and pore fluids on the acoustic properties of granular sedimentary materials. Ph.D. dissertation, Stanford University.

Myhre, A. M., Eldholm, O. & Sundvor, E., (1982) The margin between Senja and Spitsbergen Fracture Zones - Implications from Plate Tectonics: Tectonophysics, v. 89, pp. 33-50.

Mørk, A., Embry, A.F., and Weitschat, W (1989) Triassic Transgressive-Regressive cycles in the Sverdrup Basin, Svalbard and the Barents Shelf. In: Collinson, J.D. (Editor) Correlation in hydrocarbon exploration. Graham & Trottman, London, pp. 113-130.

Mørk, A. & Smelror M. 2001. Correlation and non-correlation of high order circum-Arctic Mesozoic sequences. Polarforschung 69, 65–72.

Nobes, D. C., R.W. Murray, S. Kuramoto, K.A. Pisciotto, and P. Holler, Impact of silica diagenesis on physical properties variations, in Proc. ODP, Scl. Results, 127/128, K.A. Pisciotto, J.C. Ingle, Jr., M.T. von Breymann, J. Barron, et al., pp. 3-32, Ocean Drilling Program, College Station, Tx, 1992.

Nyland, B., Jensen L. N., Skagen, J., Skarpnes, O., Vorren, T., 1992. Tertiary uplift and erosion in the Barents Sea: magnitude, timing and consequences, in Larsen, R. M., Brekke, H., Larsen, B. T., Talleraas, E., (eds). Structural and Tectonic modeling and its application to petroleum geology. Amsterdam, Elsevier, 153-162.

Norwegian Petroleum Directorate (NPD) Factpages and Factmaps (www.npd.no). Latest visited 3rd of December.

Nyland, B., Jensen L. N., Skagen, J., Skarpnes, O., Vorren, T., 1992. Tertiary uplift and erosion in the Barents Sea: magnitude, timing and consequences, in Larsen, R. M., Brekke, H., Larsen, B. T., Talleraas, E., (eds). Structural and Tectonic modeling and its application to petroleum geology. Amsterdam, Elsevier, 153-162.

Nøttvedt, A., Cecchi M., Gjelberg J. G., Kristensen S. E., Lønøy A., Rasmussen A., Skott P. H. and Veen P. M. (1993). Svalbard–Barents Sea correlation: a short review in T.O. Vorren et al. (eds.): Arctic geology and petroleum potential: proceedings of the Norwegian Petroleum Society Conference, 15–17 August 1990, Tromsø, Norway. p. 63–375. Amsterdam: Elsevier.

Oelkers, E. H., P. A. Bjørkum, and W. M. Murphy, 1992, The mechanism of porosity reduction, stylolite development and quartz cementation in North Sea sandstones, in Y. K. Kharaka and A. S. Maest, eds., Proceedings— International Symposium on Water-Rock Interaction, Rotterdam, Balkema, v. 2, p. 1183– 1186

Oelkers, E. H., P. A. Bjørkum, and W. M. Murphy, 1996, A petrographic and computational investigation of quartz cementation and porosity reduction in North Sea sandstones: American Journal of Science, v. 296, p 420– 452.

Oelkers, E. H., P. A. Bjørkum, et al. (2000). "Making diagenesis obey thermodynamics and kinetics: the case of quartz cementation in sandstones from offshore mid-Norway." Applied Geochemistry 15(3): 295-309.

Ohm, S. E., Karlsen D. A. and Austin T. J. F. (2008). Geochemically driven exploration models in uplifted areas: Examples from the Norwegian Barents Sea. AAPG Bulletin, v. 92, pp. 1191-1223.

Ostanin, I., et al., Identification of a large Upper Cretaceous polygonal fault network in the Hammerfest basin: Implications on the reactivation of re..., Mar. Geol. (2012), doi:10.1016/j.margeo.2012.03.005

Peltonen, C., Marcussen O., Bjørlykke K. and Jahren J. (2009). Clay mineral diagenesis and quartz cementation in mudstones: The effects of smectite to illite reaction on rock properties. Marine and Petroleum Geology 26(6), pp. 887-898.

Palciauskas, V.V., 1991, Primary migration of petroleum, in R. K. Merril, ed., Source and migration processes and evaluation techniques: AAPG Treastise of Petroleum Geology, Handbook of Petroleum Geology, pp. 13 – 22.

Pepper, A. S. and Corvi, P. J. 1995. Simple kinetic models of petroleum formation. Part III: Modelling an open system. Marine and Petroleum Geology, 12, 417-452.

Philippi, G. and Cordell, R. 1974. Depths of oil origin and primary migration: a review and critique. AAPG bulletin 56 2029.

Raymer, L. L., Hunt E. R. and Gardner J. S. (1980). An improved sonic transit time-toporosity transform. Trans. Soc. Prof. Well log Analyst, 21st Annual Logging Symposium, paper P.

Rijks, E. J. K., and Jauffred, J. C. E. M., 1991, Attribute extraction: An important application in any detailed 3-D interpretation study. The Leading Edge, 10, 11-19.

Roberts, D., & Sturt, B. A., 1980, Caledonian deformation in Norway: Journal of the Geological Society of London, v. 137, p. 241-250.

Roufosse, M. C., 1987, The formation and evolution of sedimentary basins in the Western Barents Sea. In: J. Brooks & K. Glennie (Eds.), Petroleum Geology of North West Europe , Graham & Trotman, London, p. 1149-1161.

Ryseth, A., Fjellbirkeland, H., Osmundsen, I, K., Skålnes, A., and Zachariassen, E., 1998, High-resolution stratigraphy and seismic attribute mapping of a fluvial reservoir; Middle Jurassic Ness Formation, Oseberg Field. AAPG Bull., 82, 1627-1651.

Rønnevik, H.C., Bergsager, E.I., Moe, A., Øvrebø, O., Navrestad, T. and Stangenes, J. (1975) The geology of the Norwegian continental shelf, Petrology and continental shelf of northwestern Europe, Vol. 1., Geology Applied Science Publishers, 8, 117-129.

Rønnevik, H.C., Beskow. B. & Jacobsen. H.P. 1982: Evolution of the Barents Sea. In Embry. A.F. & Balkwill. H.R. (eds.): Arctic Geology and Geophysics. 432-440. Canadian Society of Petroleum Geologists Memoir 8.

Rønnevik, H. and Jacobsen H. P. (1984). Structural highs and basins in the western Barents Sea, in Petroleum Geology of the North European Margin: Norwegian Petroleum Society, p. 98-107.

Seldal, J. 2005. Lower Cretaceous: the next target for oil exploration in the Barents Sea? Petroleum Geology: North-West Europe and Global Perspectives – Proceedings of the 6th Petroleum Geology Conference.

Selley, R. C., 1998, Elements of Petroleum Geology (2.ed.), no. 2. ed. Sheriff, R., and Robert, E., 1995, Exploration seismology.

Smelror, M. (2001). "Middle Jurassic-Lower Cretaceous transgressive-regressive sequences and facies distribution off northern Nordland and Troms, Norway Sedimentary Environments Offshore Norway — Palaeozoic to Recent, Proceedings of the Norwegian Petroleum Society Conference." Special publication - Norwegian Petroleum Society, NPF 10: 211.

Smelror, M., Petrov O.V., Larssen, B.B. and Werner, S., 2009. Atlas Geological History ofthe Barents Sea. Geological Survey of Norway, Trondheim.

Spencer, A. M., Birkeland, Ø., and Koch, J.O. (1993). Petroleum geology of the proven hydrocarbon basins, offshore Norway. First break v. 11, No. 5.

Spencer, A. M., Briskeby P. I., Christensen L. D., Foyn R., Kjølleberg M., Kvadsheim E., Knight I., Rye-Larsen M. and Williams J. (2008). Petroleum geoscience in Norden - exploration, production and organization. Episodes, v. 31, No. 1, p. 115-124.

Srodon, J., 1999, Nature of mixed-layer clays and mechanisms of their formation and alteration: Annual Review of Earth and Planetary Sciences, v. 27, p. 19–53.

Stainforth, A. & Reinders, J. E. A. 1990. Primary migration of hydrocarbons by diffusion through organic-matter networks, and its effect on oil and gas generation. Organic Geochemistry, 16, 61-74.

Steel, R. J., & Worsley, D. (1984) Svalbard's post-Caledonian strata an atlas of sedimentological patterns and paleogeographic evolution. In: A. M. Spencer (Editors), Petroleum Geology of the North European Margin (pp. 109-135).

Stewart, D. J. K. Berge. et al. (1995). Exploration trends in the Southern Barents Sea. Norwegian Petroleum Society Special Publications. S. Hanslien. Elsevier. Volume 4: 253-276.

Storvoll, V., Bjorlykke K., Karlsen D. and Saigal G. (2002). Porosity preservation in reservoir sandstones due to grain-coating illite: a study of the Jurassic Garn Formation from the Kristin and Lavrans fields, offshore Mid-Norway. Marine and Petroleum Geology 19(6), p. 767-781.

Storvoll, V., Bjørlykke K. and Mondol N. H. (2005). Velocity-depth trends in Mesozoic and Cenozoic sediments from the Norwegian shelf. AAPG Bulletin, v. 89, p. 359-381.

Storvoll, V. and Brevik I. (2008). Identifying time, temperature and mineralogical effects on chemical compaction in shales by rock physics relations. The Leading Edge, p. 750-756.

Sturt, B. A., Pringle, I.R., and Ramsay, D.M., (1978) The Finnmarkian phase of Caledonian Orogeny: Journal of Geological Society, v. 135, pp. 597-610.

Thyberg, B. I., Jordt, H., Bjørlykke, K., Faleide, J. I., 2000. Relationship between sequence startigraphy, mineralogy and geochemistry in Cenozoic sediments of northern North Sea. Geological Society of London, Special Publication 167, 245-272.

Thyberg, B., Jahren J., Winje T., Bjørlykke K., Faleide J.I. and Marcussen Ø. (2010). Quartz cementation in Late Cretaceous mudstones, northern North Sea: Changes in rock properties due to dissolution of smectite and precipitation of microquartz crystals. Marine and Petroleum Geology 1–13.

Townsend, C., (1987) Thrust transport directions and thrust sheet restoration in the Caledonides of Finnmark, North Norway: Journal of Structural Geology, v. 9, pp. 345-352.

Vadakkepuliyambatta, S., S. Bünz, J. Mienert & S. Chand, Giant Gas Chimneys and Gas Hydrate Occurrence in the Southwestern Barents Sea. Extended Abstract, 74th EAGE Conference & Exhibition, 4-7 June 2012, Copenhagen, Denmark, 4pp.

Varsek, J. L., 1985, Lithology prediction and discrimination by amplitude offset modeling. Geophysics, 50, 1377.

Vernik, L. and Liu, X. Z. 1997. Velocity anisotropy in shales: A petrophysical study. Geophysics, 62, 521-532.

Walderhaug, O., 1994, Temperatures of quartz cementation in Jurassic sandstones from the Norwegian continental shelf—evidence from fluid inclusions: Journal of Sedimentary Research, v. 64, p. 311–323.

Walderhaug, O., 1996, Kinetic modelling of quartz cementation and porosity loss in deeply buried sandstone reservoirs: American Association of Petroleum Geologists, Bulletin, v. 80, p. 731–745.

Walderhaug, O., Bjørkum, P.A., Nadeau, P. and Langnes, O. 2001. Quantitative modelling of basin subsidence caused by temperature-driven silica dissolution and reprecipitation. Petroleum Geoscience 7, 107–113.

Walderhaug, O., and Bjørkum, P. A. (2003). The effect of stylolite spacing on quartz cementation in the Lower Jurassic Stø Formation, Southern Barents Sea. Journal of Sedimentary Research, v. 73, No. 2, p. 146-156.

Weller, J.M., 1959. Compaction of sediments. American Association of Petroleum Geologists Bulletin 43 (2), 273–310.

Wennberg, O. P. (2008). "On the occurrence and formation of open fractures in the Jurassic reservoir sandstones of the Snøhvit Field, SW Barents Sea." Petroleum geoscience 14(2): 139.

Worden, R. H. and S. Morad (2009). Clay mineral cements in sandstones : IAS special symposium.

Worsley, D., Johansen, R. and Kristensen, S.E. (1988) The Mesozoic and Cenozoic succession of the Tromsøflaket. In: Alithostratigraphic scheme for the Mesozoic and Cenozoic succession offshore Mid- and Northern Norway (Eds A. Dalland, D. Worsley and K. Ofstad), Norw. Petrol. Direct. Bull. No. 4, pp. 42-65

Worsley, D. (2008). The post-Caledonian development of Svalbard and the western Barent Sea. Polar Research 27, p. 298-317.

Wyllie, M. J. R., Gregory A. R. and Gardner L. W. (1956). Elastic wave velocities in heterogeneous and porous media. Geophysics, v. 21, p. 41-70.

Zeng, H., Backus, M. M., Barrow, K. T., and Tyler, N., 1996, Facies mapping from three dimensional seismic data: Potential and guidelines from a Tertiary sandstone-shale sequence model, Powder-horn Field, Calhoun Country, Texas. AAPG Bull., 80, 16-46.

Ziegler, W. H., Doerv, R. and Scott, J. (1986) Tectonic habitat of Norwegian oil and gas. In: Habitat of Hydrocarbons on the Norwegian Continental Shelf (Ed. A. M. Spencer), Graham and Trotman, London, pp. 3-19.

Ødegaard, E. and Avseth P. (2004). Well log and seismic data analysis using rock physics templates. First break, v. 23, p. 37-43.

http://www.senergyworld.com/software/interactive-petrophysics

http://www.npd.no (last accessed 03.12.2012)

http://nhm2.uio.no/norges/litho/svalbard/intro.htm

http://www.statoil.com/en/NewsAndMedia/News/2001/Pages/PartnersAgreeSn%C3%B8hvitDevelopment.aspx